

OPTIMIZATION OF RESTRAINT SYSTEMS OF A VEHICLE ARCHITECTURE USING META MODELS

Jan-Peter Droecker
BMW Group
Germany
Paper Number 11-0110

ABSTRACT

In the coming years, car manufacturers will continue to diversify their fleet into an ever larger number of vehicle types. Cars will be developed with a focus on new special market requirements, responding to the customer's individual needs. Until now, at most 3-4 vehicles were derived from 1 backbone car (e.g. convertibles, coupes). In the future, however, there will be many different types of cars within a vehicle class (like the compact class). BMW is developing new solutions to deal with this increasing diversity. Each new derivative will be based on a uniform vehicle architecture and standardized construction kits.

In order to have sufficient functional degrees of freedom within this architecture, it is necessary to take all planned derivatives into account. Among other requirements, crash performance has a strong influence on the limitations of diversity.

This paper describes a new virtual method to optimize a frontal restraint system based on finite element vehicle models.

On the basis of a limited number of finite element simulations, response surface models were developed to identify and visualize the functional relationship between restraint system parameters and dummy responses. With these surrogate or meta-models, the optimization will be faster compared to the standard development process.

INTRODUCTION

In recent years, safety requirements on the structure and the restraint system of a vehicle have increased due to legislation and the activities of advocacy groups. This trend will continue. Adaptive restraint control systems ensure an optimal performance in different crash scenarios: the airbag pressure after inflation may be chosen appropriately according to

the passenger's size or the crash severity. Optimizing a highly adaptive restraint system with respect to all relevant load cases is already a complex task for only one vehicle type. In the case of an entire vehicle architecture, where the engineer needs to consider many vehicle types simultaneously, the developer will have to rely on additional specialized tooling.

Until recently, restraint systems were developed using rigid body simulation techniques. Now, full Finite Element (FE) simulations have become the state of art, providing better accuracy but also higher computational costs. Therefore, due to limited computational resources and the large number of required simulation runs, direct numerical optimization with these FE models is not feasible.

This paper describes how to tackle this high-dimensional and computationally expensive optimization problem. At first, the design space is scanned systematically by means of a design of experiment technique (DOE). Using this data, surrogate or meta-models (analytical nonlinear functions which approximate the relation between system parameters and dummy responses) are generated with which solutions may be computed very quickly. These substitute models are then used to run numerical simulations and to visualize complex functional relationships between system parameters and dummy responses. This is particularly valuable as it permits the user to relate the solution to his engineering intuition.

The paper is structured as follows: first, the essential mathematical methods and the basic idea of meta-modeling will be introduced. This topic includes beside the sampling method also the modeling quality measurement and a model fitting approach. The automated workflow at BMW will be explained. Afterwards, the benefit of the method will be illustrated by a practical example.

METHOD

Figure 1 shows the principle concept of a surrogate or meta-model. The FE models represent the unknown transfer functions ($Y(X)$) between the restraint system parameters (input vector X) and the dummy injury responses (output vector Y). Starting from a limited number of simulations, a surrogate model for each dummy response is built and can be used to predict various unknown design configurations without computing any further time-consuming FE runs.

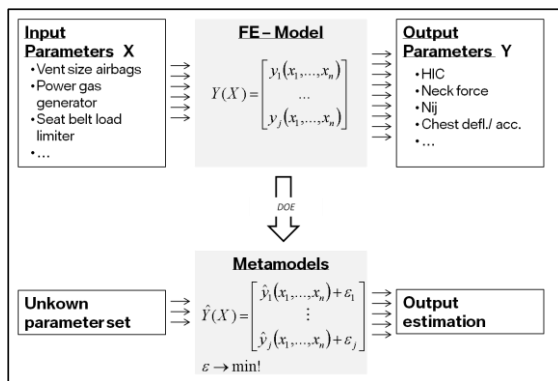


Figure 1: concept of meta-modeling

For each dummy response value j an independent mathematical surrogate model will be fitted to the sample points which were calculated using the FE model. The parameters of the meta-model will be chosen in such a way that the model error is minimized. In order to obtain an adequate accuracy for the surrogate model, a sufficient number of support points is necessary.

Design of Experiments DoE

The method Design of Experiments (DOE) is a systematic approach to get the maximum amount of information out of limited number experiments, see [5]. The available DOE methods can be classified in two main categories: orthogonal designs and random designs.

Orthogonal designs (e.g. full factorial) distribute the support points such that they are statistically independent. As a major disadvantage, the number of required experiments grows exponentially with the number of dimensions (number of input parameters). An optimization of an adaptive restraint system with approximately 10 parameters would require 2^{10} or 3^{10} simulations for a 2- or 3-level full factorial, respectively.

Random designs are commonly used in crash applications with a large number of parameters. Random means that the parameter values will be chosen by a random process. The most common method in crash applications is the so-called Latin Hypercube Sampling, which is based on the plain Monte Carlo method. A Latin Hypercube Sampling is constructed as follows: Let n be the number of designs that you are intend to simulate. Each parameter dimension will be divided into n equidistant levels. Within these subspaces, the parameter values are chosen randomly. Each design is a random permutation of design levels. This ensures that each level is probed in the design [5]. Furthermore, the limited number of sample points will be distributed over the design space in an optimal way. Practical experience in optimization of frontal restraint systems shows that 100 – 150 designs are typically enough to obtain predictable meta-models.

Modeling

A separate FE Simulation is performed for each design of the DOE (i.e. a particular set of restraint system parameters). Each simulation takes approximately 5-7h on a HPC Cluster with 12CPUs (depending on the level of detail of the FE-Model). The sample points and the computed results are used to generate the approximation functions:

$$Y(X) \rightarrow \hat{Y}(X) \quad (1)$$

In technical literature there is a wide range of approximation methods available. A commonly used method is regression analysis. Usually, the approximation function is a first or second order polynomial which is fitted to the support points. In case of smooth problems, the accuracy of the surrogate model improves with increasing number of support points. Depending on the order of the used polynomials, it may be possible to fit the approximation function exactly to all support points. However, for noisy data (e.g. data from crash analysis) there is a risk of overfitting. Figure 2 and 3 show the regression of a 2-D and 3-D problem. In addition to standard regression analysis, BMW uses also the following approximation methods:

- Moving least square approximations (advanced polynomial regression)
- Fuzzy models
- Support Vector Machines
- Neural Networks

Further information about the mathematical background is available in [2] and [3].

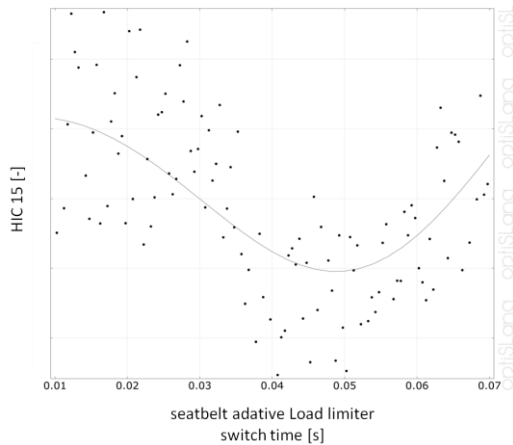


Figure 2: HIC 15 Regression Analysis 2-D

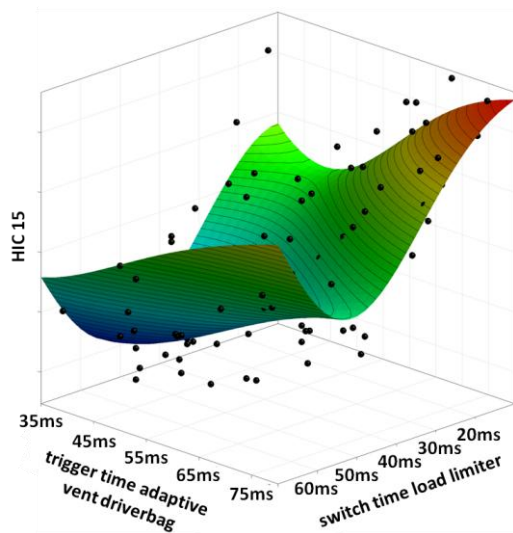


Figure 3: Regression Analysis 3-D

Figure 4 shows the problem of overfitting with advanced polynomial regression (moving least square).

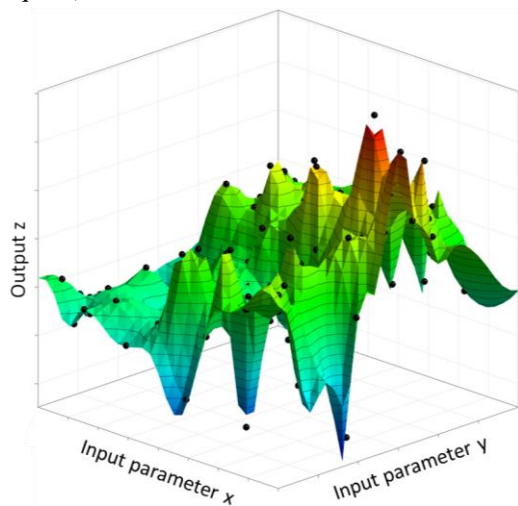


Figure 4: moving least square with noisy data

Model Quality

The accuracy of the approximation function with respect to the real problem has to be checked and verified. Appropriate error measures are necessary to assess the quality of fit. The most common value is the so-called **Coefficient of Determination R^2** or **COD**. The COD describes the ratio between the variance of the model and the total variance of the observed data:

$$R^2 = 1 - \frac{\sum_{i=1}^n (y_i - \hat{y}_i)^2}{\sum_{i=1}^n (y_i - \bar{y})^2} \quad (2)$$

where $y_i (i=1, \dots, n)$ represents the true output values of the support points, \hat{y}_i the predicted output values by the model approximation and \bar{y} the mean value of y_i . If the variance between the predicted data and the real data is very small compared to the total variance of the sampling data, R^2 is close to 1, i.e., nearly 100% of the total variance of the problem can be explained by the meta-model.

Another measure is the mean squared error which is closely related to R^2 :

$$MSE = \frac{1}{n} \sum_{i=1}^n (y_i - \hat{y}_i)^2 \quad (3)$$

The root mean squared error is the square of MSE and in the dimension of y :

$$RMSE = \sqrt{\frac{1}{n} \sum_{i=1}^n (y_i - \hat{y}_i)^2} \quad (4)$$

The linear Correlation coefficient between the observed output and the fitted model may also be used:

$$Corr(y, \hat{y}) = \frac{\sum_{i=1}^n (y_i - \bar{y})(\hat{y}_i - \bar{\hat{y}})}{\sqrt{\sum_{i=1}^n (y_i - \bar{y})^2 \sum_{i=1}^n (\hat{y}_i - \bar{\hat{y}})^2}} \quad (5)$$

Model Fitting

As described above, it is always possible to get a perfect fit for a given set of values. In this case,

each calculated support point by the meta-model is equal the real physical value ($y_i = \hat{y}_i, \forall i = 1..n$). The error measures described would be 0 (*MSE*, *RMSE*) or 1 (*CORR*, R^2). A solution to this problem is the so called cross validation method. The principle idea is to estimate a model with a set of training data and then check the prediction on additional test or validation data. The error between the results of the approximation model and the true data will be used to optimize the model parameters and to compare different modeling approaches.

The selection of the validation or test data set is very important for the quality of the model. In our first approach the DOE data was separated randomly into training and test data. However, if the test data is not representative, a model with poor performance in the relevant region may be chosen. A common approach to avoid this problem is the use of cross validation: the data set will be divided randomly into, say, 10 equally sized subsets. In each loop j ($j=1-10$) the meta-model will be calculated without subset number j . This subset j is used as a test set. The 10 resulting error measures will be averaged, thus providing a reliable estimate of the model quality. In *figure 5* on loop of cross validation is shown.

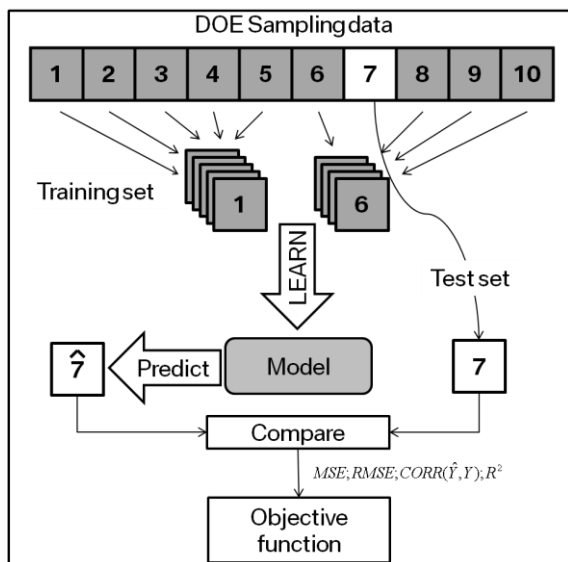


Figure 5: on step of cross-validation

Figure 6 shows the complete workflow of cross validation to calculate the best model approach.

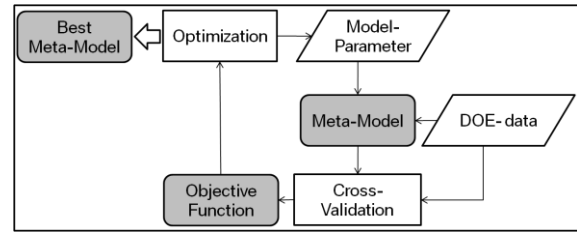


Figure 6: concept of model fit

Post processing / Optimization

The first step in post processing should be a visual check of the DOE data. This is necessary to find numerical outliers and to check the plausibility of the data. Therefore, the time history data for each injury value is analyzed. With this, it is possible to differentiate between numerical problems and outliers due to physical effects such as bottoming out of the head caused by low airbag pressure. After a manual check of the DOE data an adequate meta-model will be built in the previously described manner for each required dummy output.

Two categories of post processing are available. The first possible way is the optimization “by hand”. This means that the main dummy outputs (e.g. chest acceleration, HIC15, ...) will be plotted in 2 or 3D response surface plots. These plots are 2 or 3D cuts in the multidimensional response surface. If the number of relevant parameters is small (e.g. 2 or 3), the user can find the optimum by looking at the plots. *Figure 7* illustrates this. Both diagrams show the relationship between the head acceleration (HIC15) and 2 restraint system parameters (seatbelt: switch time adaptive load limiter; airbag: power gas generator). In addition to the seat belt and airbag generator, the HIC depends also on the vent performance of the airbag. In the diagram on the left side, the trigger time of the adaptive airbag vent is very small (35ms). In the diagram on the right side, the adaptive vent is closed. As one can see, the smallest achievable injury level of the head (which is represented by the HIC 15) depends on the vent performance. These plots are particularly valuable, as they permit the engineer to visualize the potential of restraint system components and to relate the solution to his engineering intuition.

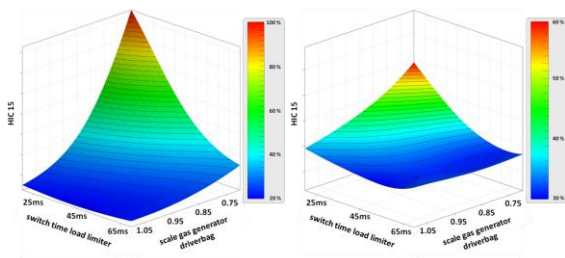


Figure 7: visual post-processing with response surface plots (e.g. HIC 15)

In case of parallel investigation of more than 1 vehicle it might be impossible to get an overview over the complete optimization problem. Therefore, it is possible to use standard numerical optimization methods to find the optimum. A common method is the Evolutionary Algorithm (EA). The optimizer uses the surrogate models to calculate individual parameter sets. Compared to a complete FE run a design calculation on the surrogate model takes only a few seconds. With this, it is possible to run a numerical optimization with multiple vehicles and load cases in an acceptable time (< 1h).

This approach, however, is limited: The optimization result is only as good as the prediction quality of the meta-model. This implies that the optimum is normally not better than the best DOE design. Therefore local optima of the approximation functions will always be in regions of DOE points. But nevertheless, the numerical optimization helps the user to find very fast the best solution with respect to additional constraints. When an optimum is found the last step should always be the recalculation of the parameter set by an additional FE run.

Process Automation

To integrate the meta-model method into the standard development process, it was necessary to create specific software. The goal was to create a tool which allows the user to optimize their occupant models without requiring deeper knowledge of the described mathematical methods. The complete process workflow from the FE simulation model to the resulting meta-model is shown in figure 8. The user can control all steps very easily by means of a specific Graphical User Interface.

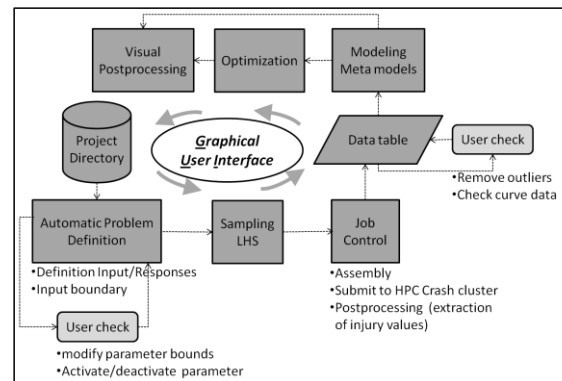


Figure 8: Workflow Process

The occupant simulation models have to be built in a particular structure, which is shown in figure 9. With this data management, we are able to optimize the restraint system simultaneously for multiple vehicle configurations of one architecture.

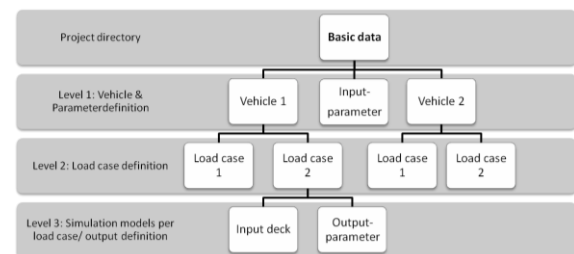


Figure 9: Project structure

EXAMPLE

The following example shows the practical benefit of using the meta-model technique in the development process of a restraint system for 2 different vehicles (driver side only). Three main load cases from FMVSS208 were investigated simultaneously:

- 35mph Hybrid-III 50% (AM50) belted, rigid barrier 0°
- 35mph Hybrid-III 5% (AF05) belted, rigid barrier 0°
- 25 mph Hybrid-III 50% (AM50) unbelted, rigid barrier 0°

The differences in the vehicle geometry are shown in figure 11. Derivate 1 (red) contains a classical sedan seating position with a flat steering column. The second vehicle (black) is a small SUV with a higher seating position (command position) and a larger angle of the steering column. Both vehicles have different crash pulses.

In Table 1, the considered restraint system parameters are shown and classified. Some

parameters like the airbag generator power are equal for both vehicles in all load cases. Other parameters can be chosen independently for each load case.

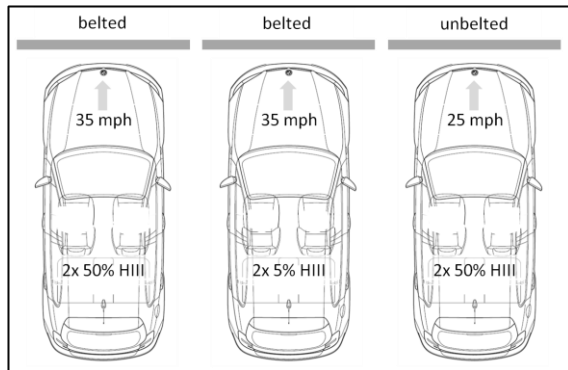


Figure 10: test condition system optimization

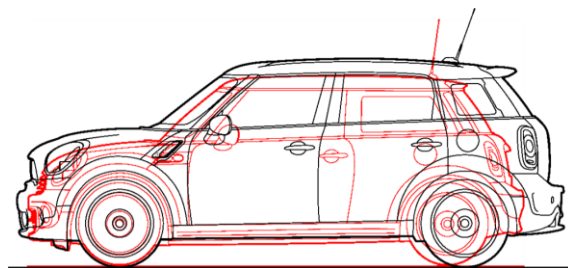


Figure 11: geometrical range in derivatives

Table 1: overview system parameter

Restraint System parameter	Vehicle 1 / 2 driver side		
	HIII AM50 35 mph belted	HIII AM50 25 mph unbelted	HIII AF05 35 mph belted
*Driver airbag generator power	X	X	X
*Driver airbag Vent size	X	X	X
**Driver airbag switch time adaptive vent	X		X
*Kneebag Generator power	X	X	X
*Seatbelt load limiter Load level 1	X		X
*Seatbelt load limiter Load level 2	X		X
**Seatbelt load limiter switch time load level	X		X
**Steering column Force level crash deformation element	X	X	X

*) parameter equal for all vehicles (standard construction kit)

***) independent parameter adjustable for load case or vehicle

Data base

The results of this study are based on validated occupant crash simulation models of both cars. As an example, one of which is shown in figure 12.

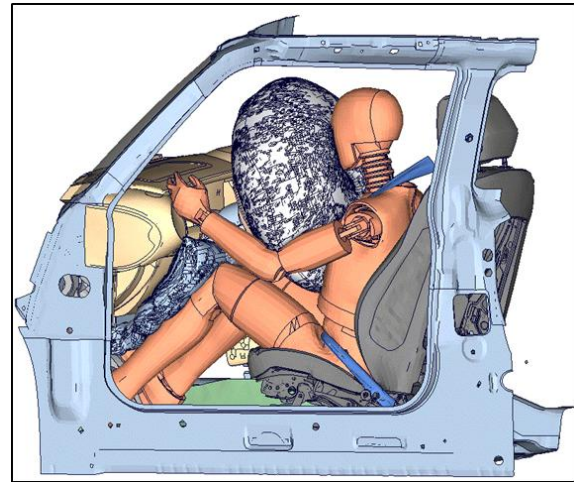


Figure 12: CAE model driver side

The evaluation of the simulation models includes the common injury values of the Hybrid III dummy which are specified in the FMVSS208. Therefore, every configuration has at least 11 injury values from different dummy regions (head, neck, chest, femur). In addition to the legal injury values, also the US-NCAP limits were considered for the optimization.

The resulting DOE table contains 11-15 dummy responses and 5-8 system parameters per load case. Therefore, approximately 85 meta-models were built. A DOE with 120 designs (6 load cases per design = 720 FE simulations) was automatically calculated on a HPC crash cluster.

Results

To reduce the complexity of the optimization problem, the range of response values of the DOE was checked and compared to the legal limits. As an example, figure 13 illustrates the results for one load case of vehicle 1. In this load case (AF05 35mph belted), 6 injury measures were close to the allowed limits. The most critical quantity is the chest acceleration which is in some configurations higher than the critical value (i.e. >80% of the legal limit). For this output, the meta-model was checked in more detail. In addition to the trigger time of the adaptive load limiter (when the force level is switched from high to low), the acceleration

depends also on the generator power of the driver airbag. All other system parameters have no significant influence on the acceleration level.

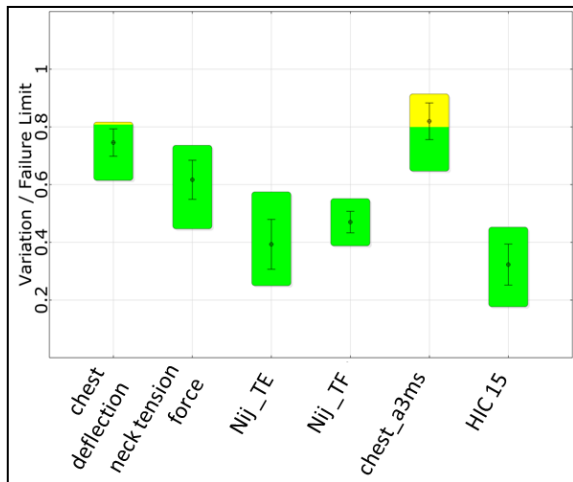


Figure 13: most critical injury values vehicle 1 Hybrid-III AF05 35mph belted

Figure 14 shows the relationship between the chest acceleration and the 2 relevant system parameters. The blue and light green area of the response surface represents the feasible area where any choice of parameters will yield a subcritical response. Note that the generator power of the driver airbag will affect several load cases, however, the trigger time only this one. Therefore, the choice of generator power has to take all load cases into account.

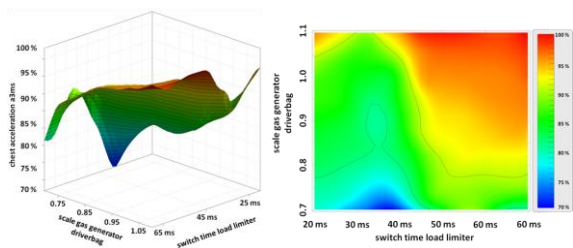


Figure 14: relationship between chest acceleration, driver airbag and adaptive seatbelt load limiter for AF05 35mph belted in Vehicle 1

To identify the most cross-linked restraint system parameters (i.e. having relevant influence on several load cases), all meta-models for the critical quantities were checked step by step. The conclusion is shown in table 2. The airbag generator has a strong influence on the chest acceleration in all load cases considered, and, additionally, on the HIC15 in the AM50 belted configuration. The influence of input parameters on

the various load cases is shown in figure 15, illustrating the level of interdependency.

Table 2: relevant restraint system parameter for most critical injury values

Restraint System parameter	Hybrid III AF05 35mph belted		Hybrid III AM50 35mph belted		Hybrid III AM50 25mph unbelted	
	chest defl.	chest accel. 3ms	femur force	chest accel. 3ms	chest accel. 3ms	HIC
*Driver airbag generator power	++	++		++	++	++
*Driver airbag Vent size				++		
**Driver airbag switch time adaptive vent						++
*Kneebag Generator power	+		+++	++		
*Seatbelt load limiter Load level 1	+					
*Seatbelt load limiter Load level 2						
**Seatbelt load limiter switch time load level	++	++			++	++
**Steering column Force level crash deformation element						

*) parameter equal for all vehicles (standard construction kit)
 **) independent parameter adjustable for load case of vehicle

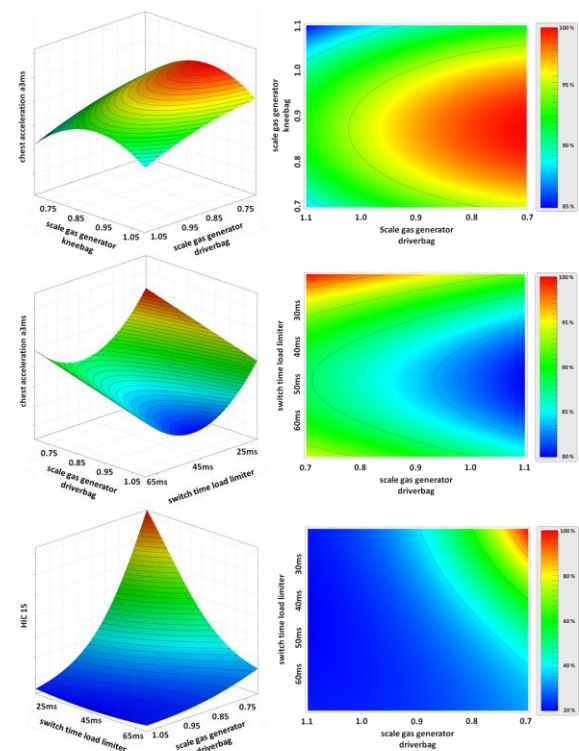


Figure 15: relationship from generator power driverbag to chest acceleration (AM50 unbelted top; AM50 belted middle) and HIC 15 (AM50 belted bottom)

The response surface of the other relevant load cases shows that the chosen gas generator power must not be too low. Especially for the HIC15 the

meta-model shows a risk for bottoming out of the head in combination with an early switch time of the adaptive seatbelt load limiter. Therefore a compromise for the choice of the generator power is necessary.

In addition to the manual optimization of the restraint system a numerical optimization of the meta-models was performed. The objective was minimizing the probability of injury according to the US-NCAP rating:

$$P_{jo\ int} = 1 - (1 - P_{head})(1 - P_{neck})(1 - P_{chest})(1 - P_{femur})$$

The injury risk values were calculated with the functions shown in *Table 3*:

Table 3: injury risk curves for frontal impact AM50 [4]

Injury Criteria	Risk Curve
Head (HIC ₁₅)	$P_{head}(AIS\ 3+) = \Phi\left(\frac{\ln(HIC_{15}) - 7.45231}{0.73998}\right)$ where Φ = cumulative normal distribution
Chest (deflection in mm)	$P_{chest_defl}(AIS\ 3+) = \frac{1}{1 + e^{10.5456 - 1.568 * (ChestDefl)^{0.4612}}}$
Femur (force in kN)	$P(AIS\ 2+) = \frac{1}{1 + e^{5.795 - 0.5196 * Femur_Force}}$
Neck (Nij and tension/compression in kN)	$P_{neck_Nij}(AIS\ 3+) = \frac{1}{1 + e^{3.2269 - 1.9688 * Nij}}$ $P_{neck_Tens}(AIS\ 3+) = \frac{1}{1 + e^{10.9745 - 2.375 * Neck_Tension}}$ $P_{neck_Comp}(AIS\ 3+) = \frac{1}{1 + e^{10.9745 - 2.375 * Neck_Compression}}$ $P_{neck} = \max(\min(P_{neck_Nij}, P_{neck_Tens}, P_{neck_Comp}))$

To find a solution which also fulfills the legal limits of the FMVSS208, additional constraints were considered. Based on the meta-models, a numerical optimization with an evolutionary algorithm method (EA) was carried out. With 5000 runs (100 generations, population size 50) of the meta-models (total calculation time < 15min on a Linux workstation) the best value for the relative risk score was found. With the identified parameter combination, all considered constraints derived from FMVSS208 (chest acceleration, HIC, etc) were satisfied. The convergence curve of the optimizer is shown in *figure 16*.

After the optimization an additional FE run was done with the identified parameter configuration. The differences between the predictions of the meta-models and the true FE values are illustrated in *Table 4*. As one can see the predicted probability values were nearly the true values calculated by the FE simulation. A slightly higher delta is observed

for the femur probability. The reason for that is a very low level of the femur forces caused by the use of a knee airbag. But the influence of this delta on the total probability is very small.

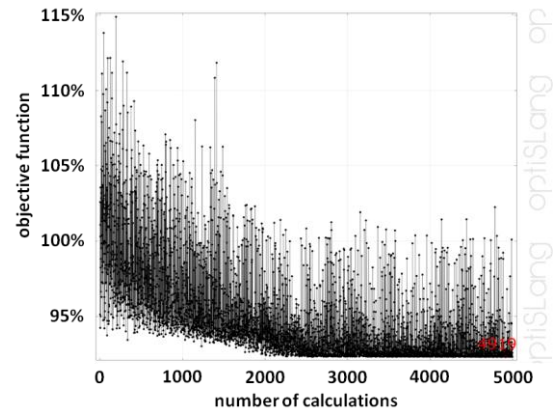


Figure 16: convergence of the objective function (probability of injury)

Table 4: optimization result with meta-models and comparison to FE-simulation

	Δ FE simulation to meta-model	Contribution to P_{joint}
Probability of injury	+7%	-
Probability of head	+3%	2%
Probability of neck	+1%	45%
Probability of chest	+13%	46%
Probability of femur	+30%	7%

CONCLUSIONS

The described meta-model approach is very useful for optimizing restraint systems. Especially in the simultaneous optimization of more than 1 vehicle, the method helps to identify the important relationships. The influences of relevant system parameters (e.g. airbag performance) can be checked visually in different load cases. Thus, the method enables the user to find the best compromise satisfying all legal requirements and those of consumer tests.

Additionally, the method presented requires significantly less work than the standard development method without applying DOEs, meta-models and visualization tools (pre-/post-processing of FE-simulations).

REFERENCES

- [1] T. Most, J. Will 2008
“Meta-model of Optimal Prognosis - An automatic approach for variable reduction and optimal meta-model selection”

- [2] Optislang Documentation Rev. 3.2.0

- [3] ClearVu Analytics Manual Rev. 2.0

- [4] DEPARTMENT OF TRANSPORTATION
NHTSA [Docket No. NHTSA-2006-26555]:
Consumer Information - New Car Assessment
Program. 2008

- [5] Optimus Theoretical Manual Rev. 9.0

DEVELOPMENT OF BODY STRUCTURE FOR CRASH SAFETY OF THE NEWLY DEVELOPED ELECTRIC VEHICLE

Hayata Uwai
 Atsushi Isoda
 Hideaki Ichikawa
 Nobuhiko Takahashi
 NISSAN MOTOR CO., LTD.
 Japan
 Paper Number 11-0199

ABSTRACT

An electric vehicle (EV) is promising as clean energy powered vehicle, due to increased interest in fuel economy and environment in recent years. However, it requires to meet unique safety performance such as electric safety and cabin deformation although mass increase of the high-voltage battery compared with the fuel tank.

Nissan has developed a new electric vehicle which achieves electric safety and occupant protection performance in addition to maintaining enough cruising distance and cabin space. This was achieved by the development of an all-new platform for electric vehicles.

The electric safety was enhanced by the protection of high-voltage components based on consideration of component layout and body structure, high-voltage shutdown by impact sensing system and prevention of short circuit by fuse in the battery. As an example of the protection of high-voltage components, the battery which locates under the floor was protected by elaborative packaging and multi-layer protection structure.

In addition, the same cabin deformation as the internal-combustion engine vehicle similar in size in frontal crash was achieved by developing an efficient layout and structure for the motor compartment.

INTRODUCTION

The concern in oil price rising and global warming is rising in recent years, and manufacturers are expected to improve fuel efficiency and reduce carbon dioxide emission [1]. Therefore, development of vehicles such as HEV (Hybrid Electric Vehicle), PHEV (Plug-in Hybrid Electric Vehicle), EV (Electric Vehicle) and FCV (Fuel cell vehicle) has become more active as new technology for energy efficiency and environment. EV is remarkably considered as one of the promising future energy vehicle because of great reduction in carbon dioxide emission.

In general, high-voltage components such as the battery and the motor are equipped on EV instead of a fuel tank and an engine on internal-combustion engine (ICE) vehicles. Therefore, new safety performance must be considered in addition to safety performance of the existing vehicles.

First is to ensure electric safety to prevent an electric shock in the crash accident due to high-voltage components. Upgrade of electric safety standards for electric powered vehicles are accelerated globally due to the sales growth of them which include EV (See Table 1) [2],[3],[4],[5]. Car manufactures are expected to develop new technology to address this situation.

Table 1.
Global electric safety standards

	Electric Safety	
	Prevention of electric shock	
	Normal use	Post crash
Japan	Technical standards Attachment101,110	Technical standards Attachment111
EUR	ECE R100	ECE R12,R94, R95
USA	-	FMVSS305

Second is to control the cabin deformation and the body deceleration for occupant protection in the frontal impact. It is often necessary to mount a battery which is heavier than a fuel tank of ICE vehicle to secure enough cruising distance. Therefore, the energy absorption by body structures during the crash increases due to the increased mass of the battery. Namely, additional energy absorption is required to achieve the same cabin deformation as ICE vehicles.

Nissan's new EV which is five-seater passenger car was developed by considering the items above with enough cruising distance and cabin space with an all-new platform for the EV.

In this paper, an approach of electric safety performance and occupant protection performance of the newly developed EV in the crash are explained.

OUTLINE OF THE NEWLY DEVELOPED EV SYSTEM AND COMPONENT PARTS

In this chapter, outline of the high-voltage system is introduced.

High-voltage system and components of the EV are shown in Figure 1. Firstly, DC flows from the battery to the inverter. Then it converts DC to AC, and finally AC is supplied to the motor and it rotates.

Following is an outline and function of the high-voltage system and its components.

•High-voltage battery

The high-voltage battery supplies the electric power to the drive system and auxiliary system. It stores the electric power when charging and regeneration during deceleration. The nominal voltage is 360 V.

•Inverter

The inverter converts battery DC into three-phase AC to supply to the motor. It controls input/output torque of the motor.

•Motor

The motor generates the driving force using the electric power of the battery. It generates braking force during deceleration and regenerates the electric power to transmit to the battery.

•Charger

The charger converts AC electric power from a commercial power source into DC electric power to supply to the battery.

•DC/DC converter

The DC/DC converter reduces the high voltage from the battery to supply the electric power to 12 V loads.

•Vehicle control module (VCM)

The VCM is a unit which controls vehicle integration.

•Service disconnect switch (SDSW)

The SDSW is a switch which cuts off the high-voltage circuit for safety work at the time of maintenance or rescue.

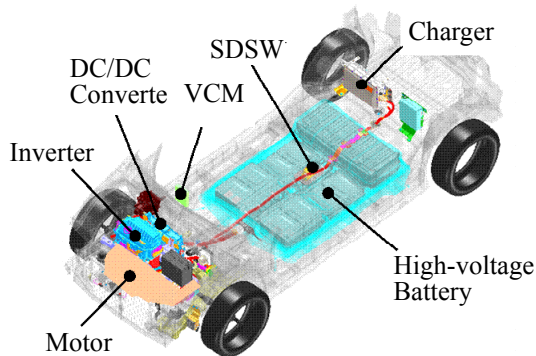


Figure 1. High-voltage system and components of the newly developed EV.

CONCEPT OF ELECTRIC SAFETY

This chapter describes concept of electric safety. The concept consists of two types of protections which are against direct and indirect contact to avoid electric shock [6].

Protection against direct contact

The first concept of protection is against direct contact. Purpose is to protect human from electric shock by not to be able to touch the high-voltage cable directly. One example is covering the components by layers or isolating by structure.

In case of covering by conductive body, energizing components have to be insulated from electric conductor.

Protection against indirect contact

The other protection is against indirect contact. This structure is to avoid electric shock by ensuring equipotential between high-voltage components and a vehicle body in case of the direct contact protection failure. One example is to connect between each high-voltage components and the vehicle body by bonding wire or earth it.

It is important to secure both the direct and the indirect protection during and after the crash for EV.

ELECTRIC SAFETY DESIGN OF THE EV

In this chapter, details of the protection against direct contact in the crash are explained.

The details consist of two parts. One is about EV packaging and the other is about protection structure of high-voltage components.

EV packaging

Firstly, high-voltage components of the EV are placed outside of the passenger compartment (See Figure 2) and inside of framework structures such as side members and body sills. In other words, it protects from electric shock in the crash by preventing direct contact to the high-voltage components. Additionally the components are protected by the structures.

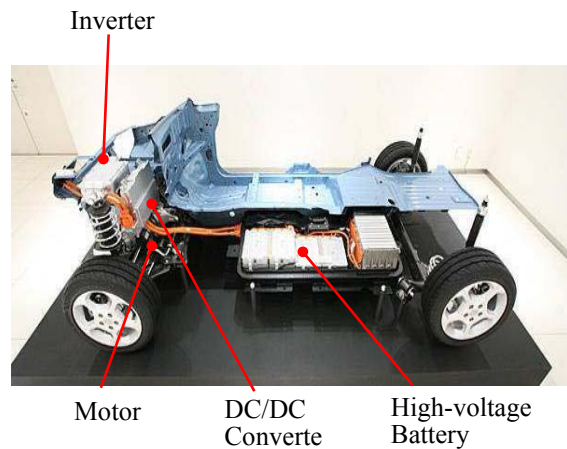


Figure 2. EV packaging.

Multiple protections of high-voltage components

Secondly, multiple protection system is applied to high-voltage components outside of the passenger compartment. In particular, electric shock due to direct contact between occupants and high-voltage components is prevented by the following.

- 1) Component layout and body structure.
- 2) High voltage shutdown device with sensing system.
- 3) Fuse in the battery pack.

Example for 1) and 2) are explained.

The high-voltage battery protection The battery is protected by consideration of layout and multi-layer protection structure in the EV.

a) Layout

The battery was placed under front and rear seats outside of the cabin by considering floor shape. Namely, the location is farther away from common front and rear crash impact zones, so the battery is protected by the zone body structure as shown in Figure 3.

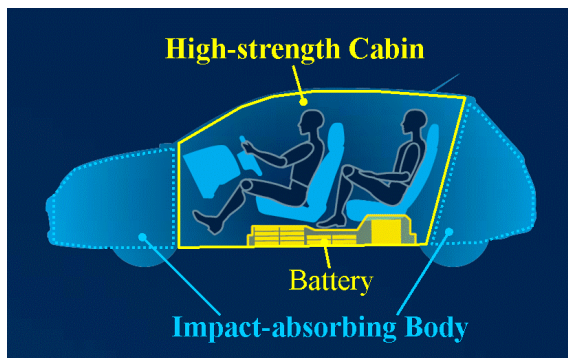


Figure 3. High-voltage battery layout.

b) Multi-layer protection structure

In addition to the considered layout, the battery was protected by multi-layer protection structure (See Figure 4).

In side impact, using not only the body sill but also fore-aft member as load path enabled the high energy absorption by small crushable space (See Figure 5-(a)).

Also, structure of floor cross members was studied for battery protection. In case of ICE vehicles, impact energy is often absorbed by floor cross members which is fixed to the body sills in side impact. However, the battery may be deformed by the force from the body sills to floor cross members when it is mounted between the body sills. Therefore, floor cross members were separated from the body sills in the EV as shown in Figure 5-(b). In the result, this design reduced the amount of force transferred through the floor and floor cross members to the battery during side impact.

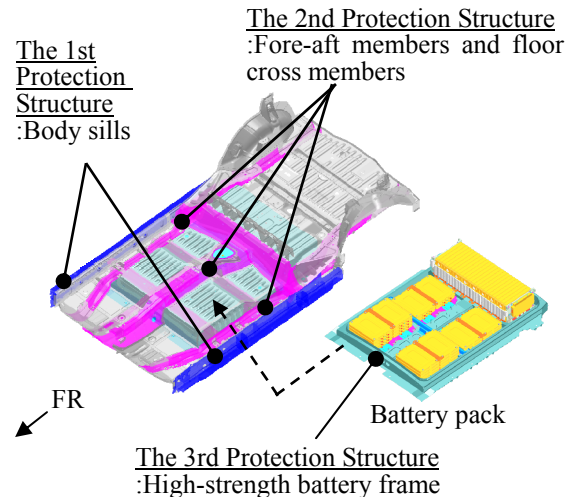


Figure 4. Multi-layer protection structure for the high-voltage battery.

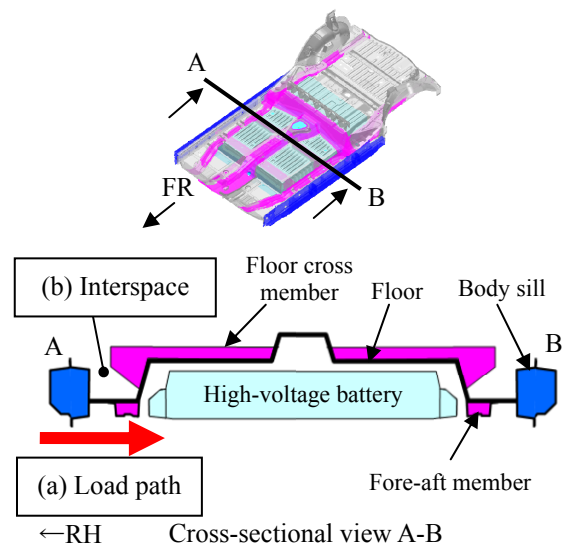


Figure 5. Body structures for the high-voltage battery protection in side impact.

c) Vehicle crash test configuration for evaluation of high-voltage battery protection and the results

Vehicle crash test with various modes of collisions designed to mimic real-world crashes were conducted for evaluation of high-voltage component protection including the battery (See Figure 6).

Photographs of batteries after each vehicle crash tests are shown in Figure 7. The battery frame was not deformed. The electric isolation between body and high-voltage system remained intact. Figure 8 shows force-deformation curve of the EV and the ICE vehicle similar in size in side impact pole test. The body deformation was reduced by control of the body reaction force.

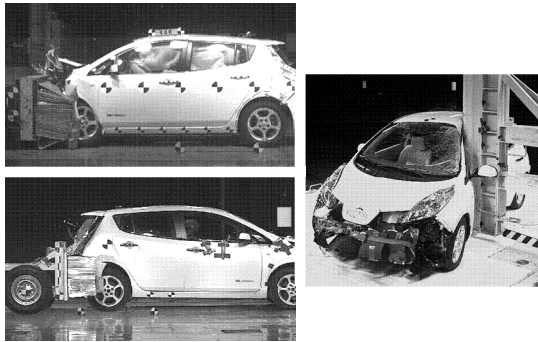


Figure 6. Vehicle crash test configuration for evaluation of high-voltage component protection.

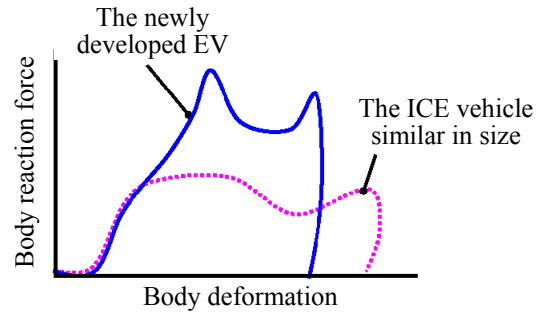
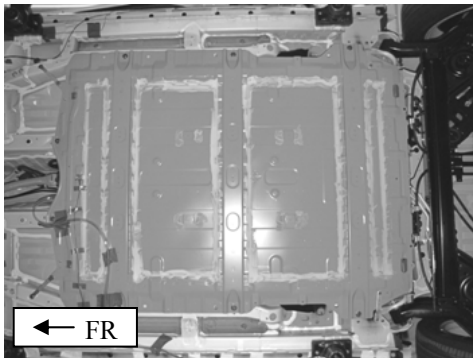
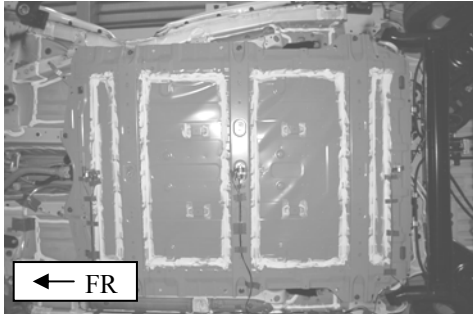


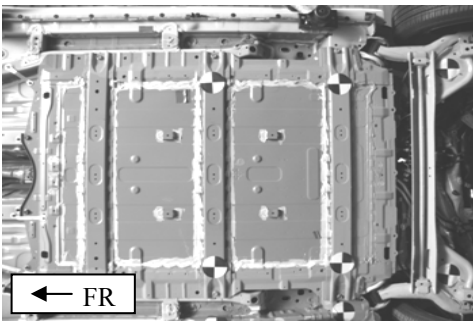
Figure 8. Comparison of force-deformation curve in side impact pole test.



(a) 64 km/h left-side frontal offset deformable barrier test (bottom view)



(b) 32 km/h left side impact pole test (bottom view)



(c) 80 km/h right-side rear moving deformable barrier test (bottom view)

Figure 7. Photographs of high-voltage batteries after vehicle crash tests.

High voltage shutdown system In addition to protection against direct contact explained in the previous section, electric shock prevention after the crash performs even better by adopting shutdown system.

The high voltage shutdown system is described by the block diagram shown in Figure 9. Firstly, an airbag control unit (ACU) detects frontal, side or rear impact using airbag sensors. Secondly, ACU send signal to VCM which controls electric system. Finally, VCM judges to shutdown the relay in the battery.

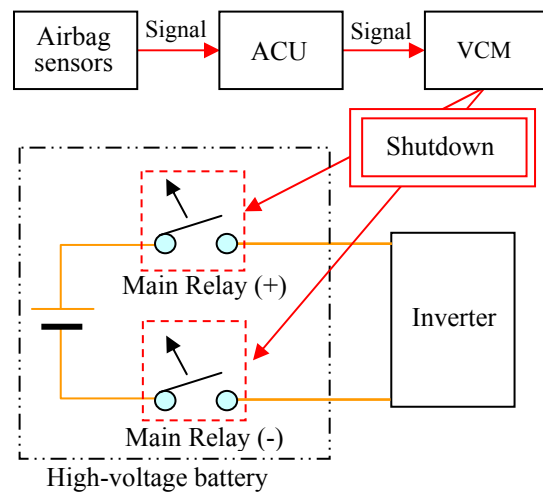


Figure 9. The block diagram of high voltage shutdown system.

OCCUPANT PROTECTION PERFORMANCE OF THE EV

This chapter describes the idea about occupant protection performance of the EV. At first, the unique consideration about occupant protection performance of the EV is explained. Secondly, details of the idea are described below.

The unique consideration about occupant protection performance of the EV

Curb weight of the EV increases from the ICE vehicle similar in size due to mass increase of the battery compared with the fuel tank as shown in Figure 10. Furthermore the additional mass is added to the floor. Therefore, the additional energy absorption by the body is required to achieve the same cabin deformation as the ICE vehicle in frontal impact.

In general, there are two ways to increase the energy absorption by the body. One is to reinforce the body to reduce the body deformation. The body deformation consists of deformation of the motor compartment and the cabin. The other is to increase crushable space of the motor compartment and the motor compartment deformation. However, there is a limit to increase the space because of some reasons such as vehicle size.

On the other hand, it is an advantage for occupant protection performance to increase the motor compartment deformation in frontal impact. Kinetic energy of an occupant is absorbed by the body deformation and restraint system which includes seatbelts and airbags etc. in frontal impact. As a consequence, larger energy absorption by the body deformation means smaller absorption by restraint system. That is an advantage for occupant protection performance since it is flexible to design restraint system.

For these reasons, it is an advantage to increase deformation of the motor compartment in occupant protection performance point of view in frontal impact.

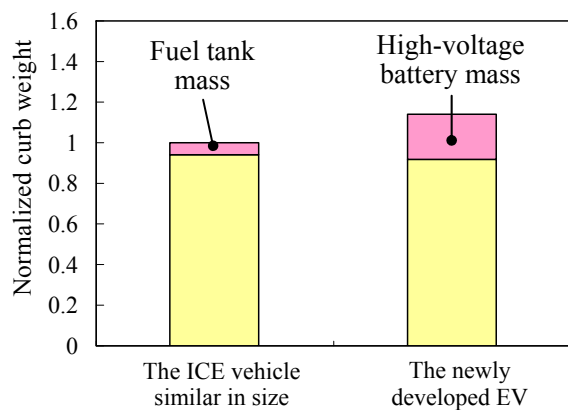


Figure 10. Comparison of vehicle curb weight.

Details of the idea to increase energy absorption of the motor compartment in frontal impact

Efficient crushable motor compartment structure was studied to increase the motor compartment deformation and reduce the cabin deformation in frontal impact. In particular, two detail ideas are explained below. One is to increase crushable length

of front side members. The other is to increase crushable space of the motor compartment.

Study of crushable length of front side members At first, additional energy absorption in frontal impact was considered by mounting the motor on the front suspension member.

A power source is generally mounted on front side members by mounting brackets in the ICE vehicle of a front-engine/front-drive configuration (See Figure 11). One of the reasons is NVH (Noise, Vibration and Harshness) performance. The mount brackets may prevent the front side members from crushing. As a result, the energy absorption by the front side members may decrease.

On the other hand, the motor of the EV can be mounted on front suspension member due to the different frequency character from an ICE vehicle (See Figure 12). That resulted in increasing crushable length of front side members.

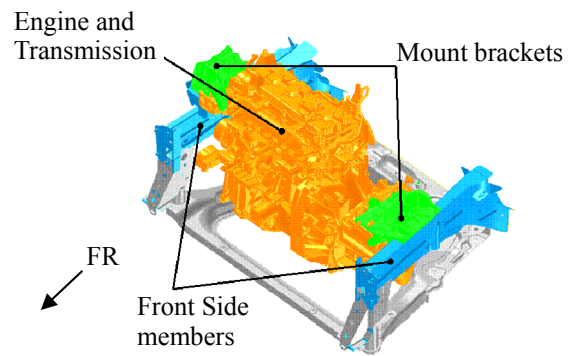


Figure 11. Mounting system of the engine in ICE vehicle.

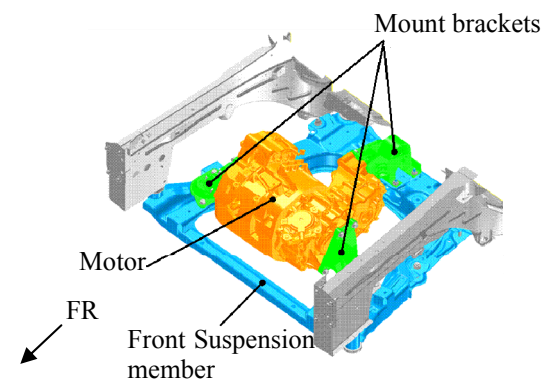
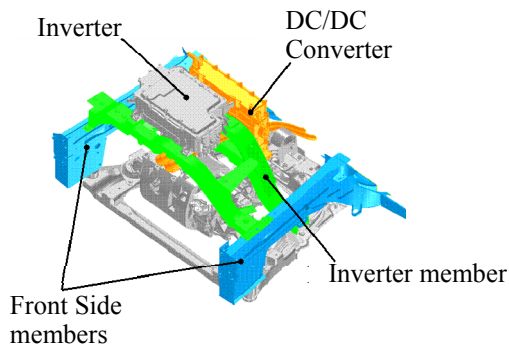


Figure 12. Mounting system of the EV motor.

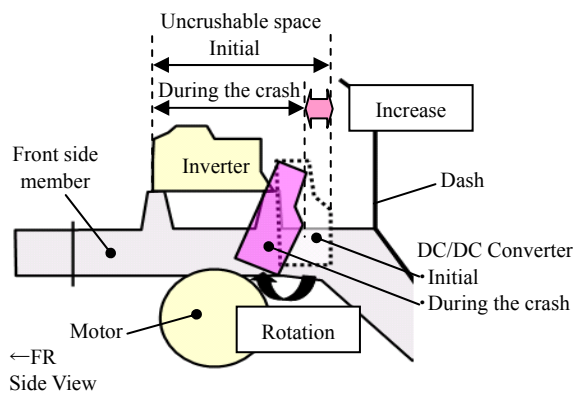
Study of motor compartment crushable space In addition, crushable space of motor compartment was increased by the optimization of motor compartment layout, considering dynamic behavior of DC/DC converter.

As shown in Figure 13-(a), DC/DC converter is mounted on an inverter member which is fixed with front side members. By controlling the fracture

between front side members and inverter members, DC/DC converter could rotate during the crash and resulted in motor compartment crushable space increase (See Figure 13-(b)).



(a) Mounting system of DC/DC converter on the body



(b) Dynamic behavior of DC/DC converter

Figure 13. Optimization of motor compartment layout.

The body characteristic of the EV in frontal vehicle crash tests In these ways, the EV achieved the same cabin deformation as the ICE vehicle in frontal impact. Cabin deformation of the EV and the ICE vehicle in vehicle frontal crash tests is described in Figure 14. The motor compartment deformation of the EV increases by about thirty percent from the ICE vehicle and the cabin deformation of the EV is the same as the ICE vehicle. Also, energy absorption by the body deformation in kinetic energy of an occupant was compared between the EV and the ICE vehicle. Ratio of energy absorption by the body deformation to kinetic energy of an occupant was calculated by the method as shown in Figure 15. The ratio for the case of driver-side HybridIII dummy in 56 km/h full-lap frontal test is shown in Figure 16. Energy absorption by the body deformation in the EV was increased by about twenty percent compared to the ICE vehicle similar in size.

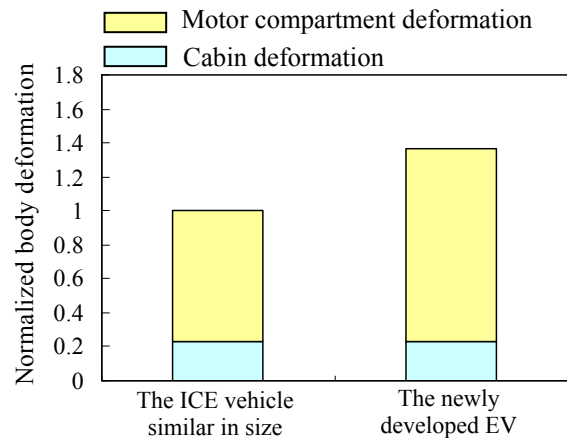
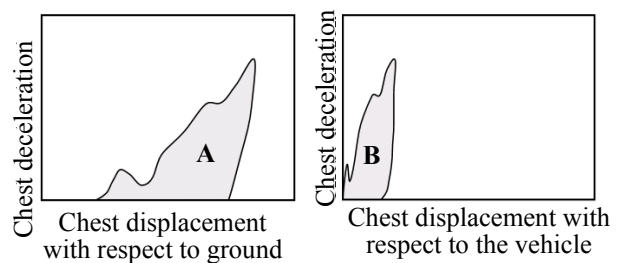


Figure 14. Body deformation of the EV and the ICE vehicle in 64km/h offset deformable barrier frontal test.



Ratio of energy absorption by the body deformation to occupant kinetic energy = $(A-B) / A$

Area A: Occupant kinetic energy

Area B: Energy except energy absorption by the body deformation

Figure 15. Calculation method of ratio of energy absorption by body structures to occupant kinetic energy in frontal impact.

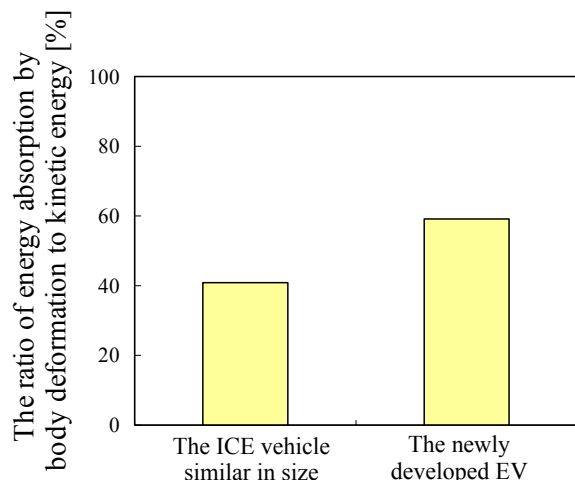


Figure 16. Comparison of the ratio of energy absorption by body deformation to kinetic energy for the case of driver-side HybridIII dummy in 56km/h full-lap frontal test.

CONCLUSIONS

Automotive Engineers of Japan, Vol. 63, No. 9, 67-72, 2009 (in Japanese).

In this paper, electric safety and occupant protection performance of the newly developed EV was explained and the following points were shown,

- It was shown that 1) layout and body structure offers protection of the high-voltage components; 2) high voltage shutdown is achieved by the impact sensing system; 3) electric shock is prevented by fuses which prevent short circuits.

- As an example of high-voltage components protection, multi-layer protection structure was presented. Vehicle crash tests were conducted and the protection of the battery was confirmed.

- Cabin deformation of the EV in frontal impact was the same as the ICE vehicle similar in size even with mass increase of the battery compared with the fuel tank. This was achieved by optimization of efficient motor compartment structure and layout.

Areas of future study are as follows.

- In order to achieve longer cruising distance, it is important to further reduce the total mass without compromising the electrical system safety and occupant protection performance.

REFERENCES

[1] Nissan Motor Co., LTD, "NISSAN GREEN PROGRAM", http://www.nissan-global.com/EN/ENVIRONMENT/GREENPROGRAM_2010/index.html

[2] Federal Register, "Federal Motor Vehicle Safety Standards; Electric-Powered Vehicles; Electrolyte Spillage and Electrical Shock Protection", Vol. 75, No. 113, 2010, <http://edocket.access.gpo.gov/2010/pdf/2010-14131.pdf>

[3] ECE/TRANS/WP29/2010/119, "Proposal for the 04 series of amendments to Regulation No. 12 (Steering mechanism)", <http://www.unece.org/trans/doc/2010/wp29/ECE-TRANS-WP29-2010-119e.pdf>

[4] ECE/TRANS/WP29/2010/122, "Proposal for the 02 series of amendments to Regulation No. 94 (Frontal collision protection)", <http://www.unece.org/trans/doc/2010/wp29/ECE-TRANS-WP29-2010-122e.pdf>

[5] ECE/TRANS/WP29/2010/123, "Proposal for the 03 series of amendments to Regulation No. 95 (Lateral collision protection)", <http://www.unece.org/trans/doc/2010/wp29/ECE-TRANS-WP29-2010-123e.pdf>

[6] Kazuya, O., et al., "The View of the High-voltage Safety of Electric Vehicles, and the Outline of the Technical Regulations", Journal of Society of

MODEL-BASED ANALYSIS OF SENSOR-NOISE IN PREDICTIVE PASSIVE SAFETY ALGORITHMS

Tobias Dirndorfer

Robotics and Embedded Systems, Technische Universität München

Michael Botsch

Department for Active and Passive Safety, AUDI AG, Ingolstadt

Alois Knoll

Robotics and Embedded Systems, Technische Universität München

Germany

Paper Number 11-0251

ABSTRACT

The introduction of environment perception sensors into the automotive world enables further improvement of the already highly optimized passive safety systems. Such sensors facilitate the development of safety applications that can act in a context sensitive manner concerning the protection of vehicle occupants. Hereby the quality of the provided information is decisive for the usability and effective range of such sensors within integrated safety systems. In this paper noise effects in sensors and their implications on the prediction of collision parameters are analyzed. The focus lies on sensors that can measure distances but not velocities or accelerations of the objects surrounding the car. For such sensors a noise model is presented as well as a tracking algorithm aiming to estimate the velocities and to compensate the effects of noise. This information is used by a trajectory-based algorithm to predict relevant collision parameters like time-to-collision, relative velocity at collision time etc. Monte Carlo simulations show the influence of noise on the accuracy of the predicted collision parameters. The described model-based study allows the systematic deduction of sensor requirements and represents a new way for the evaluation of the robustness of predictive passive safety systems.

INTRODUCTION

Modern cars provide a high level of safety due to the optimization of bodywork, seat-belts or airbags in the last decades. Conventional passive safety applications for the activation of occupant restraint systems work on established sensor concepts, e.g., acceleration and pressure sensors, and have already reached a high level of adaptivity and robustness. The introduction of environment perception sensors leads to a further improvement of security, since safety systems can be developed that act in a context sensitive manner [1, 2, 3, 4]. First applications like the proactive reversible belt-tensioner can already be found in new cars, e.g., in the Audi A7 [5], and the adap-

tation of airbags and other passive safety systems to the specific crash situation are in the focus of current development. Future cars will combine all available information—including those gained by Car-to-X (<http://www.simTD.de>, <http://www.car-to-car.org>) technologies—concerning the environment to increase the effectiveness of vehicle safety in an integral sense.

The number of sensors that are and will be integrated in new vehicles is increasing since applications have various requirements concerning the range, aperture, sensitivity or other properties. Typical applications using such sensors are mainly located in the field of advanced driver assistance systems like automatic cruise control, lane assist, heading control, etc. In the vehicle safety domain requirements on such sensors are high, i. e., a very small false positive rate and a very high true positive rate in the detection of objects in the environment of the car. Not only the detection of an object's existence is of high interest but also its exact location, velocity and geometry. Such pre-crash information allows the estimation of collision parameters before a collision occurs. This information can be used to optimize the activation of adaptive restraint systems. However, the pre-crash prediction of the collision parameters is subject to a couple of disturbance effects, e.g., inexact measurements as well as time delays caused by tracking algorithms or the communication between different electronic control units. These factors can affect

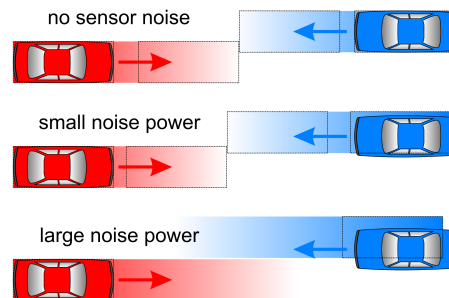


Figure 1. Effects of sensor noise on the collision prediction

the required precision of predictive crash severity estimations and therefore the effectiveness of integrated safety systems. The example from Figure 1 illustrates that a large noise power of the predictive sensor can lead to a wrong prediction of how a scenario will develop in the future. Assuming that the dynamic parameters like velocities or accelerations do not change during the prediction interval a small noise power disturbs the prediction marginally, whereas a large noise power can lead to a completely wrong estimation of the scenario. The first illustration in Figure 1 shows a prediction with no measurement noise, the second illustration the same scenario but under the assumption that small noise power disturbs the measurement and the third illustration the same scenario but under the assumption that a large noise power disturbs the measurement. Therefore, it is necessary to quantify the effect of noise on predictions that are used to adapt restraint systems by taking into account the whole signal processing chain. This paper focuses on such a model of disturbance effects and their influence on the computation of relevant collision parameters like the time-to-collision, the relative velocity at collision time, the collision angle and further geometric parameters. On the one hand the noise caused by sensors describing the state of the ego vehicle and on the other hand the noise caused by predictive sensors detecting the vehicle environment are considered. Whereas a stationary white noise Gaussian random process is assumed for the noise disturbing the ego-state, for the predictive sensor a more sophisticated model is applied. The focus lies on sensors able to measure the position and geometry of objects but not their velocity and acceleration. The velocity must be estimated based on position changes which is accomplished here using a Kalman filter. Thus, the noise process describing the inaccuracy of the position measurement determines the noise process for the velocity. The model for position inaccuracies takes into account a distance based noise power. On the basis of such a noise model Monte Carlo simulations are performed for four predictive sensor variants to analyze the effects on the computed collision parameters. The four sensor variants were chosen to represent sensors with different performances.

The chapter “MEASUREMENT DATA” introduces the relative dynamics model and the sensor noise model that are used in the Monte Carlo simulations later on. Chapter “COLLISION PREDICTION ALGORITHM” focuses on the tracking model and on the trajectory-based prediction module used to calculate the collision parameters. In Chapter “MONTE CARLO SIMULATION” three traffic scenarios are analyzed in detail and the ef-

fects of noisy measurements are presented. The general outline of the paper is illustrated in Figure 2.

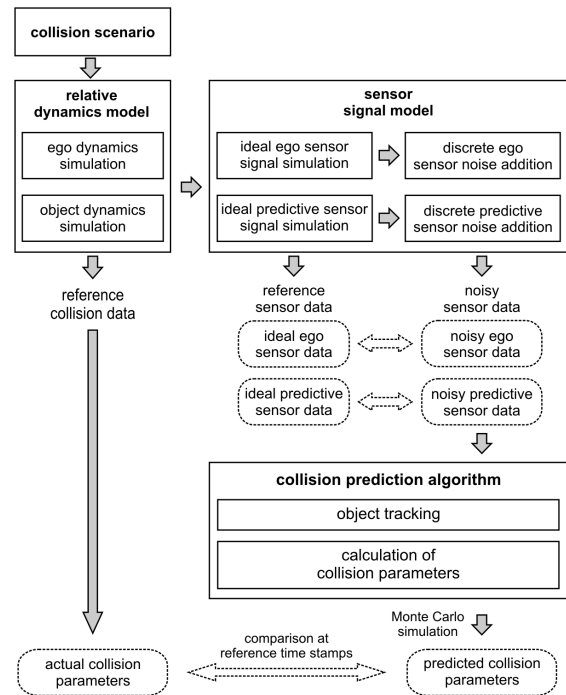


Figure 2. Outline of the paper

Throughout the paper vectors and matrices are denoted by lower and upper case bold letters. A $M \times N$ zero matrix is denoted by $\mathbf{0}_{M \times N}$.

MEASUREMENT DATA

In this chapter the model-based generation process of noisy measurements as input data for a collision prediction algorithm is described. Firstly the two-dimensional relative dynamics model used for the simulation of ideal sensor data concerning the ego vehicle and an ego-mounted predictive sensor measuring relative position data is explained. Afterwards the application of sensor noise to the simulated exact reference data is depicted.

Relative dynamics model

For the motion simulation of the ego and opponent vehicle in specific collision scenarios a nonlinear single track model with a Pacejka tire force approach as described in [6] was applied (see Figure 3). This model offers a good two-dimensional description of the global vehicle movement in stationary as well as dynamic driving scenarios disregarding effects of pitch and roll. As only the global vehicle trajectory over ground and not the exact knowledge of internal system state variables such as wheel rota-

tion speeds or forces was of interest the model was regarded as sufficient for this study. In the following, as shown in Figure 3 the capital letters X and Y denote an earth-bound coordinate system, the lower case letters x and y a vehicle-bound coordinate system that is rotated with the yaw angle ψ with respect to the X -axis, and the lower case letters x_v and y_v a vehicle-bound coordinate system that is rotated with the slip angle β with respect to the x -axis. Vectors with the subscripts XY , xy or $x_v y_v$ represent values in the corresponding coordinate systems.

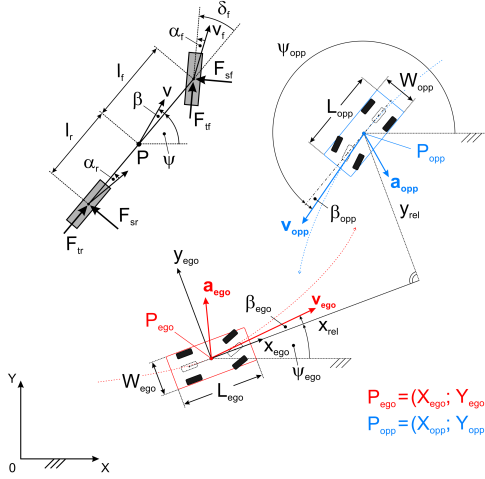


Figure 3. Relative dynamics simulation based on a nonlinear single track model

In the relative dynamics simulation environment the flat projection of each vehicle body was regarded as rectangular and symmetric to the longitudinal axis of the single track model. The basic single track model equations are summarized in the following. The tire slip angles α_f and α_r at the front (subscript f) and rear (subscript r) wheel are given by the subsequent kinematic relations containing the frontal steering angle δ_f , the yaw rate $\dot{\psi}$, the velocity v , the vehicle slip angle β and the center of mass distances l_f from the frontal and l_r from the rear end of the vehicle [7]:

$$\alpha_f = \delta_f - \arctan\left(\frac{l_f \cdot \dot{\psi} + v \cdot \sin\beta}{v \cdot \cos\beta}\right) \quad (1)$$

$$\alpha_r = \arctan\left(\frac{l_r \cdot \dot{\psi} - v \cdot \sin\beta}{v \cdot \cos\beta}\right). \quad (2)$$

The vehicle center of mass acceleration a_{lon} and a_{lat} in longitudinal (x_v) and lateral (y_v) trajectory direction can be calculated on the basis of the principle of linear momentum as a function of δ_f , β , the vehicle mass m as well as the tangential and side

tire forces F_t and F_s at the front and rear tire:

$$\mathbf{a} = \begin{bmatrix} a_{lon} \\ a_{lat} \end{bmatrix}_{x_v y_v} = \begin{bmatrix} v \cdot (\dot{\psi} + \dot{\beta}) \\ \frac{1}{m} \cdot (F_{tr} \cdot \cos\beta + F_{tf} \cdot \cos(\delta_f - \beta) + F_{sr} \cdot \sin\beta - F_{sf} \cdot \sin(\delta_f - \beta)) \\ \frac{1}{m} \cdot (-F_{tr} \cdot \sin\beta + F_{tf} \cdot \sin(\delta_f - \beta) + F_{sr} \cdot \cos\beta + F_{sf} \cdot \cos(\delta_f - \beta)) \end{bmatrix}_{x_v y_v}. \quad (3)$$

The vehicle yaw acceleration $\ddot{\psi}$ results from the principle of conservation of angular momentum depending on the mass moment of inertia I_{zz} around the vehicle z -axis (in a right-hand coordinate system with the origin in the vehicle center of mass P and the x - and y -axis according to Figure 3):

$$\ddot{\psi} = \frac{1}{I_{zz}} \cdot (F_{sf} \cdot \cos\delta_f \cdot l_f + F_{tf} \cdot \sin\delta_f \cdot l_f - F_{sr} \cdot l_r). \quad (4)$$

The temporal change $\dot{\mathbf{r}}$ in the global vehicle center of mass position is given by the following kinematic equation:

$$\dot{\mathbf{r}} = \mathbf{v} = \begin{bmatrix} \dot{X} \\ \dot{Y} \end{bmatrix}_{XY} = \begin{bmatrix} v \cdot \cos(\psi + \beta) \\ v \cdot \sin(\psi + \beta) \end{bmatrix}_{XY}. \quad (5)$$

With the Pacejka tire forces given by [7]

$$F_{sf} = C_3 \cdot \sin(C_2 \cdot \arctan(C_1 \cdot \alpha_f - C_4 \cdot (C_1 \cdot \alpha_f - \arctan(C_1 \cdot \alpha_f)))) \quad (6)$$

$$F_{sr} = C_3 \cdot \sin(C_2 \cdot \arctan(C_1 \cdot \alpha_r - C_4 \cdot (C_1 \cdot \alpha_r - \arctan(C_1 \cdot \alpha_r)))) \quad (7)$$

as a function of the constant frontal and rear tire parameters C_{fi} and C_{ri} , with $i \in \{1, 2, 3, 4\}$, and the frontal and rear tire slip angles the presented system of differential equations can be solved by numerical integration. This allows the calculation of the global vehicle center of mass position \mathbf{r} in X - and Y -direction as well as the vehicle yaw angle ψ and slip angle β as a function of time and therefore defines the vehicle trajectory over ground.

On the basis of the single track model trajectory ideal sensor data concerning the ego vehicle state is available. For this study it is assumed that in the ego vehicle the absolute ego center of mass speed v_{ego} is known based on wheel speed measurements and the yaw rate $\dot{\psi}_{ego}$ as well as the center of mass acceleration $a_{x_{ego}}$ in x_{ego} -direction and $a_{y_{ego}}$ in y_{ego} -direction are directly measured by body-mounted sensors. The corresponding state variables can be derived from the integrated vehicle

trajectory via the following equations:

$$v_{ego} = |\mathbf{v}_{ego}| = \sqrt{\dot{X}_{ego}^2 + \dot{Y}_{ego}^2} \quad (8)$$

$$\dot{\psi}_{ego} = \frac{d\psi_{ego}}{dt} \quad (9)$$

$$a_{x_{ego}} = \cos(\beta_{ego}) \cdot \dot{v}_{ego} - \sin(\beta_{ego}) \cdot v_{ego} \cdot (\dot{\psi}_{ego} + \dot{\beta}_{ego}) \quad (10)$$

$$a_{y_{ego}} = \sin(\beta_{ego}) \cdot \dot{v}_{ego} + \cos(\beta_{ego}) \cdot v_{ego} \cdot (\dot{\psi}_{ego} + \dot{\beta}_{ego}). \quad (11)$$

The parallel simulation of two trajectories offers the possibility to calculate the relative position data $\mathbf{r}_{P_{opp}/P_{ego}}$ measured by an ideal ego-mounted predictive sensor which can be calculated for any given reference point $\mathbf{r}_{P_{opp}}$ on the opponent vehicle.

For a predictive sensor located at $\mathbf{r}_{P_{sens}}$ and mounted at a displacement of $x_{P_{sens}/P_{ego}}$ in x_{ego} -direction and $y_{P_{sens}/P_{ego}}$ in y_{ego} -direction relative to the ego center of mass $\mathbf{r}_{P_{ego}}$ the relative location measurement of the opponent reference point $\mathbf{r}_{P_{opp}}$ is given by:

$$\begin{aligned} \begin{bmatrix} x_{sens} \\ y_{sens} \end{bmatrix}_{x_{ego}y_{ego}} &:= \mathbf{r}_{P_{opp}/P_{sens}} = \mathbf{r}_{P_{opp}} - \mathbf{r}_{P_{sens}} = \\ &= \begin{bmatrix} X_{P_{opp}} \\ Y_{P_{opp}} \end{bmatrix}_{XY} - \left[\begin{bmatrix} X_{P_{ego}} \\ Y_{P_{ego}} \end{bmatrix}_{XY} + \begin{bmatrix} x_{P_{sens}/P_{ego}} \\ y_{P_{sens}/P_{ego}} \end{bmatrix}_{x_{ego}y_{ego}} \right] \\ &= \begin{bmatrix} (X_{P_{opp}} - X_{P_{ego}}) \cos \psi_{ego} \\ + (Y_{P_{opp}} - Y_{P_{ego}}) \sin \psi_{ego} - x_{P_{sens}/P_{ego}} \\ - (X_{P_{opp}} - X_{P_{ego}}) \sin \psi_{ego} \\ + (Y_{P_{opp}} - Y_{P_{ego}}) \cos \psi_{ego} - y_{P_{sens}/P_{ego}} \end{bmatrix}_{x_{ego}y_{ego}} \\ &= \begin{bmatrix} x_{rel} - x_{P_{sens}/P_{ego}} \\ y_{rel} - y_{P_{sens}/P_{ego}} \end{bmatrix}_{x_{ego}y_{ego}}. \end{aligned} \quad (12)$$

The relative position data x_{sens} and y_{sens} measured by the predictive ego sensor allows the calculation of the relative center of mass position \mathbf{r}_{rel} via the following equation in which $\mathbf{r}_{P_{opp}}$ particularly refers to the opponent center of mass:

$$\begin{aligned} \mathbf{r}_{rel} = \mathbf{r}_{P_{opp}} - \mathbf{r}_{P_{ego}} &= \begin{bmatrix} x_{rel} \\ y_{rel} \end{bmatrix}_{x_{ego}y_{ego}} \\ &= \begin{bmatrix} x_{sens} + x_{P_{sens}/P_{ego}} \\ y_{sens} + y_{P_{sens}/P_{ego}} \end{bmatrix}_{x_{ego}y_{ego}}. \end{aligned} \quad (13)$$

The derived relative center of mass position data over time also allows the determination of the relative velocity \mathbf{v}_{rel} between the ego and the opponent center of mass by:

$$\begin{aligned} \mathbf{v}_{rel} = \mathbf{v}_{P_{opp}} - \mathbf{v}_{P_{ego}} &= \dot{\mathbf{r}}_{P_{opp}} - \dot{\mathbf{r}}_{P_{ego}} \\ &= \dot{\mathbf{r}}_{rel} = \begin{bmatrix} \dot{x}_{rel} - \dot{\psi}_{ego} \cdot y_{rel} \\ \dot{y}_{rel} + \dot{\psi}_{ego} \cdot x_{rel} \end{bmatrix}_{x_{ego}y_{ego}}. \end{aligned} \quad (14)$$

The relative acceleration between the two vehicle centers of mass can then be calculated by:

$$\begin{aligned} \mathbf{a}_{rel} = \mathbf{a}_{P_{opp}} - \mathbf{a}_{P_{ego}} &= \dot{\mathbf{v}}_{P_{opp}} - \dot{\mathbf{v}}_{P_{ego}} = \dot{\mathbf{v}}_{rel} = \\ &= \begin{bmatrix} \ddot{x}_{rel} - \ddot{\psi}_{ego} y_{rel} - 2\dot{\psi}_{ego} \dot{y}_{rel} - \dot{\psi}_{ego}^2 x_{rel} \\ \ddot{y}_{rel} + \ddot{\psi}_{ego} x_{rel} + 2\dot{\psi}_{ego} \dot{x}_{rel} - \dot{\psi}_{ego}^2 y_{rel} \end{bmatrix}_{x_{ego}y_{ego}}. \end{aligned} \quad (15)$$

The simulated ideal measurement data concerning the ego vehicle and the relative position data concerning the opponent vehicle measured by a predictive sensor will be used as input for a collision prediction algorithm estimating the expected geometric and kinematic collision parameters after the noise model explained in the following section is applied.

Noise model

In order to model the effect of statistically inexact measurements by real sensors noise is applied both to the ego vehicle data and the predictive sensor data from the relative dynamics simulation. Systematic sensor errors are regarded as compensable and therefore not taken into account. As Gaussian random distributions offer a good means to model measurement scattering the measurement errors are assumed to be normally distributed with a given standard deviation σ around the mean measurement value μ , see Figure 4. As the area of $\pm 4\sigma$

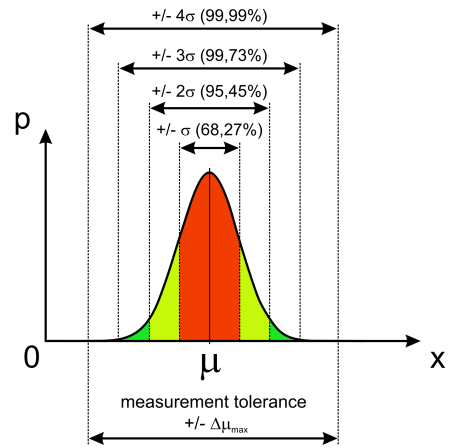


Figure 4. Normal distribution with a given standard deviation

around the mean value μ in a Gaussian normal distribution contains more than 99,99 percent of the noisy measurement values the standard deviation for the applied noise process was defined on the basis of a given measurement tolerance $\pm \Delta\mu_{max}$ via:

$$\sigma := \frac{\Delta\mu_{max}}{4}. \quad (16)$$

The following equations show the noisy measurements for the ideal ego state variables velocity v_{ego} , yaw rate $\dot{\psi}_{ego}$ and the accelerations $a_{x_{ego}}$ and $a_{y_{ego}}$:

$$v_{ego}^{noisy} = v_{ego} + \eta_{v_{ego}}(0, \sigma_{v_{ego}}) \quad (17)$$

$$a_{x_{ego}}^{noisy} = a_{x_{ego}} + \eta_{a_{x_{ego}}}(0, \sigma_{a_{x_{ego}}}) \quad (18)$$

$$a_{y_{ego}}^{noisy} = a_{y_{ego}} + \eta_{a_{y_{ego}}}(0, \sigma_{a_{y_{ego}}}) \quad (19)$$

$$\dot{\psi}_{ego}^{noisy} = \dot{\psi}_{ego} + \eta_{\dot{\psi}_{ego}}(0, \sigma_{\dot{\psi}_{ego}}), \quad (20)$$

where $\eta(\mu, \sigma)$ denotes a Gaussian random variable with mean μ and variance σ^2 .

The noisy measurements for the ideal predictive sensor data x_{rel} and y_{rel} as well as for the ideally detected opponent length W_{sens} are given by:

$$x_{sens}^{noisy} = x_{sens} + \eta_{x_{sens}}(0, \sigma_{x_{sens}}) \quad (21)$$

$$y_{sens}^{noisy} = y_{sens} + \eta_{y_{sens}}(0, \sigma_{y_{sens}}) \quad (22)$$

$$W_{sens}^{noisy} = W_{sens} + \eta_{W_{sens}}(0, \sigma_{W_{sens}}). \quad (23)$$

Figure 5 shows an example for ideal and discrete noisy measurement data over time.

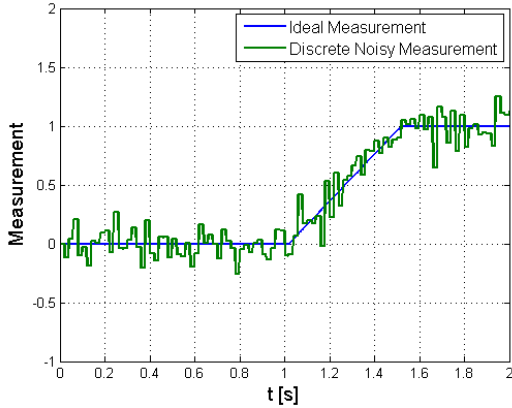


Figure 5. Ideal and discrete noisy measurement data over time

For the further analysis steps the standard deviation of the noisy ego measurements was regarded as constant over time (assumed values for σ see Table 1).

Table 1.
Assumed standard deviations
for ego sensor noise

sensor	σ
v_{ego}	0.075 m/s
$a_{x_{ego}}$	0.050 m/s ²
$a_{y_{ego}}$	0.050 m/s ²
$\dot{\psi}_{ego}$	0.005 rad/s

For the predictive sensor measurements (x_{sens} , y_{sens} and W_{sens}) a more complex model was applied. The standard deviation σ of the applied measurement noise was modeled as distance dependent via the following linear equation because the maximum resolution of the sensor element limits the detection accuracy in a decreasing manner along the measurement distance:

$$\sigma(d) = \sigma_0 \cdot (1 + c_d \cdot d). \quad (24)$$

The measurement distance d was calculated on the basis of the ideal sensor values x_{sens} and y_{sens} :

$$d = \sqrt{x_{sens}^2 + y_{sens}^2}. \quad (25)$$

The assumed basic standard deviations σ_0 for the predictive sensor are shown in Table 2.

Table 2.
Assumed basic standard deviations
for predictive sensor noise

sensor value	σ
x_{sens}	0.125 m
y_{sens}	0.0625 m
W_{sens}	0.075 m

As mentioned in the introduction four predictive sensor variants are used for the Monte Carlo analysis in this paper. The variants differ in terms of σ_0 and c_d as depicted in Table 3.

Table 3.
Analyzed predictive sensor variants

sensor variant	σ_0	c_d
1	σ	0.05 1/m
2	σ	0.10 1/m
3	$2 \cdot \sigma$	0.05 1/m
4	$2 \cdot \sigma$	0.10 1/m

The distance dependent standard deviation scaling factor is illustrated in Figure 6.

COLLISION PREDICTION ALGORITHM

Tracking Model

In order to estimate the position and the velocity of an object—as in common predictive sensors—the discrete state-space formulation

$$\mathbf{x}[k] = f(\mathbf{x}[k-1], \boldsymbol{\eta}[k], \mathbf{u}[k]) \quad (26)$$

$$\mathbf{y}[k] = h(\mathbf{x}[k], \mathbf{w}[k]) \quad (27)$$

is used, with $\mathbf{x}[k]$ being the state vector at the time instance indexed by k , $\boldsymbol{\eta}$ the system noise, \mathbf{u} the

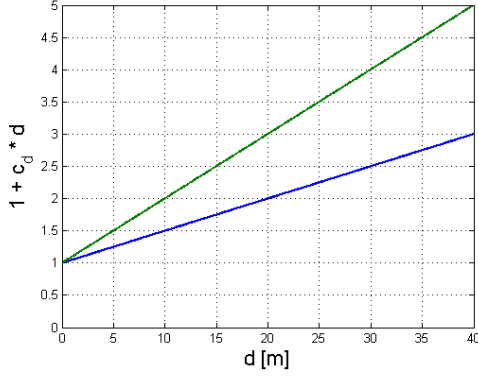


Figure 6. Distance dependent standard deviation scaling of the measurement noise

control vector, \mathbf{y} the measurement vector, \mathbf{w} the measurement noise, and f and h denote the mappings describing the dynamic model and the sensor model. In order to use the well-known notation [8] from (27)—unlike in the rest of the paper—a position vector $[x, y]^T$ is notated as $\mathbf{r} = [r_x, r_y]^T$ in this section. The coordinate system used in the following is a right-hand coordinate system that has its origin in the center of gravity of the ego car and the x -axis points to the front. Since the ego car is moving over ground also the location of the origin of the coordinate system is fixed only for one sample time T and then it is updated. Figure 7 visualizes the movement of the ego car and an object between two time stamps. The coordinate system at time $t_0 - T$,

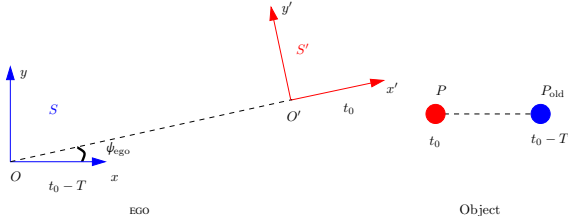


Figure 7. Movement of ego car and object in a sample interval T

having the index $k - 1$, is denoted with S , its origin with O and the coordinate system at time instance t_0 with S' and its origin with O' . During the time T the coordinate system rotates with the yaw angle ψ_{ego} and the object moves from the point P_{old} to the point P . In the following the time instance t_0 has the index k . Since the sensor type that is in the focus of this paper measures only positions but additionally also the velocities of the objects in the environment of the car are important, the following state vector will be used

$$\mathbf{x}[k] = \left[r_{x,S'}^{O'P}[k], r_{y,S'}^{O'P}[k], v_{x,S'}^{OP}[k], v_{y,S'}^{OP}[k] \right]^T, \quad (28)$$

where $r_{x,S'}^{O'P}[k]$ is the relative distance in x -direction between the object and the ego car at time instance t_0 expressed in the coordinate system S' , $r_{y,S'}^{O'P}[k]$ the relative distance in y -direction, $v_{x,S'}^{OP}[k]$ and $v_{y,S'}^{OP}[k]$ the components of the velocity vector over ground but rotated in the coordinate system S' . The advantages of implementing the tracking using the velocity over ground instead of the relative velocity are described in [9].

To find a suitable model for the mapping h in the dynamic equation (26) firstly the position and then the velocity of ego car and object must be expressed in S' based on the values in the coordinate system S .

The position $[r_{x,S}^{OO'}[k], r_{y,S}^{OO'}[k]]^T$ of the ego car at t_0 expressed in the coordinate system S is

$$r_{x,S}^{OO'}[k] = v_{x,S}^O[k-1]T + \eta_{a_{x,S}}^O \frac{T^2}{2} \quad (29)$$

$$r_{y,S}^{OO'}[k] = v_{y,S}^O[k-1]T + \eta_{a_{y,S}}^O \frac{T^2}{2}, \quad (30)$$

with $v_{x,S}^O[k-1]$ and $v_{y,S}^O[k-1]$ being the vector components of the velocity over ground rotated in the coordinate system S , and $\eta_{a_{x,S}}^O$ and $\eta_{a_{y,S}}^O$ representing noise terms which take into account that during an time interval T the acceleration of the car is neglected.

The position $[r_{x,S}^{OP}[k], r_{y,S}^{OP}[k]]^T$ of the object at time instance t_0 expressed in the coordinate system S is

$$r_{x,S}^{OP}[k] = r_{x,S}^{OP_{\text{old}}}[k-1] + v_{x,S}^{OP_{\text{old}}}[k-1]T + \eta_{a_{x,S}}^{OP_{\text{old}}} \frac{T^2}{2} \quad (31)$$

$$r_{y,S}^{OP}[k] = r_{y,S}^{OP_{\text{old}}}[k-1] + v_{y,S}^{OP_{\text{old}}}[k-1]T + \eta_{a_{y,S}}^{OP_{\text{old}}} \frac{T^2}{2}, \quad (32)$$

where $[r_{x,S}^{OP_{\text{old}}}[k-1], r_{y,S}^{OP_{\text{old}}}[k-1]]^T$ is the position of the object at time $t_0 - T$ expressed in S , $[v_{x,S}^{OP_{\text{old}}}[k-1], v_{y,S}^{OP_{\text{old}}}[k-1]]^T$ the components of the object's velocity vector over ground at time $t_0 - T$ expressed in S , and $\eta_{a_{x,S}}^{OP_{\text{old}}}$ and $\eta_{a_{y,S}}^{OP_{\text{old}}}$ noise terms taking into account that the acceleration of the object during a sample interval T is neglected.

With equations (29), (30), (31), and (32) the relative position $[r_{x,S}^{O'P}[k], r_{y,S}^{O'P}[k]]^T$ between ego car and object at time instance t_0 expressed in S can be computed as

$$\begin{aligned} r_{x,S}^{O'P}[k] &= r_{x,S}^{OP}[k] - r_{x,S}^{OO'}[k] \\ &= r_{x,S}^{OP_{\text{old}}}[k-1] + v_{x,S}^{OP_{\text{old}}}[k-1]T + \eta_{a_{x,S}}^{OP_{\text{old}}} \frac{T^2}{2} \\ &\quad - v_{x,S}^O[k-1]T - \eta_{a_{x,S}}^O \frac{T^2}{2} \end{aligned} \quad (33)$$

$$\begin{aligned}
r_{y,S}^{O'P}[k] &= r_{y,S}^{OP}[k] - r_{y,S}^{OO'}[k] \\
&= r_{y,S}^{OP\text{old}}[k-1] + v_{y,S}^{OP\text{old}}[k-1]T + \eta_{a_{y,S}^{OP\text{old}}} \frac{T^2}{2} \\
&\quad - v_{y,S}^O[k-1]T - \eta_{a_{y,S}^O} \frac{T^2}{2}. \tag{34}
\end{aligned}$$

To express the relative distances $r_{x,S'}^{O'P}[k]$ and $r_{y,S'}^{O'P}[k]$ in the state vector $\mathbf{x}[k]$ a transformation to S' is necessary, i. e., a rotation with the yaw angle $\psi_{\text{ego}}[k]$:

$$r_{x,S'}^{O'P}[k] = \cos(\psi_{\text{ego}}[k])r_{x,S}^{O'P}[k] + \sin(\psi_{\text{ego}}[k])r_{y,S}^{O'P}[k] \tag{35}$$

$$r_{y,S'}^{O'P}[k] = \cos(\psi_{\text{ego}}[k])r_{y,S}^{O'P}[k] - \sin(\psi_{\text{ego}}[k])r_{x,S}^{O'P}[k]. \tag{36}$$

The velocity of the object over ground but rotated into the coordinate system S is

$$v_{x,S}^{OP}[k] = v_{x,S}^{OP\text{old}}[k-1] + \eta_{a_{x,S}^{OP\text{old}}} T \tag{37}$$

$$v_{y,S}^{OP}[k] = v_{y,S}^{OP\text{old}}[k-1] + \eta_{a_{y,S}^{OP\text{old}}} T. \tag{38}$$

In order to express the velocity of the object over ground at time instance t_0 in S' a rotation with $\psi_{\text{ego}}[k]$ must be performed

$$v_{x,S'}^{OP}[k] = \cos(\psi_{\text{ego}}[k])v_{x,S}^{OP}[k] + \sin(\psi_{\text{ego}}[k])v_{y,S}^{OP}[k] \tag{39}$$

$$v_{y,S'}^{OP}[k] = \cos(\psi_{\text{ego}}[k])v_{y,S}^{OP}[k] - \sin(\psi_{\text{ego}}[k])v_{x,S}^{OP}[k]. \tag{40}$$

All relations required to express the mapping h in (26) are now given by (33), (34), (35), (36), (37), (38), (39) and (40). Since only the yaw rate is measurable in cars, the yaw rate is approximated by $\dot{\psi}_{\text{ego}}[k] = \dot{\psi}_{\text{ego}}[k] \cdot T$. Also it is assumed that the sampling interval T is small so that the noise terms $\eta_{a_{x,S}^O}$ and $\eta_{a_{y,S}^O}$ corresponding the the ego car can be neglected in (33) and (34). The following vectors and matrices are introduced to find an expression for h that can be used in a Kalman filter

$$\tilde{\mathbf{R}}[k] = \begin{bmatrix} \cos(\dot{\psi}_{\text{ego}}[k]T) & \sin(\dot{\psi}_{\text{ego}}[k]T) \\ -\sin(\dot{\psi}_{\text{ego}}[k]T) & \cos(\dot{\psi}_{\text{ego}}[k]T) \end{bmatrix},$$

$$\mathbf{R}[k] = \begin{bmatrix} \tilde{\mathbf{R}}[k] & \mathbf{0}_{2 \times 2} \\ \mathbf{0}_{2 \times 2} & \tilde{\mathbf{R}}[k] \end{bmatrix}, \quad \tilde{\mathbf{F}} = \begin{bmatrix} 1 & 0 & T & 0 \\ 0 & 1 & 0 & T \\ 0 & 0 & 1 & 0 \\ 0 & 0 & 0 & 1 \end{bmatrix},$$

$$\tilde{\mathbf{G}} = \begin{bmatrix} T^2/2 & 0 \\ 0 & T^2/2 \\ T & 0 \\ 0 & T \end{bmatrix}, \quad \mathbf{x}[k-1] = \begin{bmatrix} r_{x,S'}^{O'P\text{old}}[k-1] \\ r_{y,S'}^{O'P\text{old}}[k-1] \\ v_{x,S'}^{OP\text{old}}[k-1] \\ v_{y,S'}^{OP\text{old}}[k-1] \end{bmatrix}$$

$$\boldsymbol{\eta}[k] = \begin{bmatrix} \eta_{a_{x,S}^{OP\text{old}}} \\ \eta_{a_{y,S}^{OP\text{old}}} \end{bmatrix}, \quad \tilde{\mathbf{u}}[k] = \begin{bmatrix} -v_{x,S}^O[k-1]T \\ 0 \\ 0 \\ 0 \end{bmatrix}.$$

The second component in $\tilde{\mathbf{u}}[k]$ is zero since $v_{y,S}^O[k-1] = 0$. Now the dynamic equation (26) can be written as

$$\mathbf{x}[k] = \mathbf{F}[k]\mathbf{x}[k-1] + \mathbf{u}[k] + \mathbf{G}[k]\boldsymbol{\eta}[k], \tag{41}$$

with

$$\mathbf{F}[k] = \mathbf{R}[k]\tilde{\mathbf{F}}, \quad \mathbf{u}[k] = \mathbf{R}[k]\tilde{\mathbf{u}}[k], \quad \text{and} \quad \mathbf{G}[k] = \mathbf{R}[k]\tilde{\mathbf{G}}. \tag{42}$$

Since the sensor type that is considered in this paper measures only the relative position the measurement vector is $\mathbf{y}[k] = [r_{x,S'}^{O'P}[k], r_{y,S'}^{O'P}[k]]^T$ and (27) can be expressed as

$$\mathbf{y}[k] = \begin{bmatrix} 1 & 0 & 0 & 0 \\ 0 & 1 & 0 & 0 \end{bmatrix} \mathbf{x}[k] + \mathbf{w}[k] = \mathbf{H}\mathbf{x}[k] + \mathbf{w}[k]. \tag{43}$$

With the dynamic equation (41) and the measurement equation (43) it is straightforward to apply a Kalman filter [8] in order to estimate the state vector $\mathbf{x}[k]$.

Computation of collision parameters

A collision prediction algorithm has to anticipate the prospective motion of the ego vehicle and surrounding objects on the basis of realistic movement assumptions and estimate the expected collision parameters under the given premises. The prediction may both depend on kinematic ego state data and relative object measurement data provided by a predictive sensor mounted on the moving ego vehicle. The prediction process is necessary because a predictive sensor is usually not able to measure the geometric and kinematic impact conditions in adequate precision right before the collision. This results from limitations in the sensor field of view as well as the necessary time interval for the object creation and the movement tracking algorithms.

For an online estimation of the collision effect in the ego vehicle the geometric and kinematic initial conditions of the impact have to be described explicitly by the predicted collision parameters. Therefore the following parameters defining the relative position and movement of the ego and opponent bounding boxes at the time of collision were selected, see Figure 8.

The relative geometric and kinematic movement state of the two vehicle bounding boxes is described

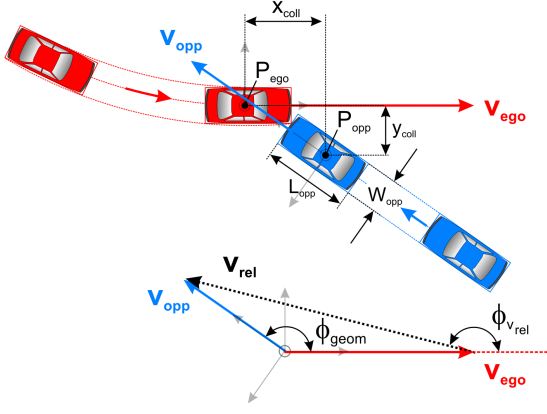


Figure 8. Predicted collision parameters as initial conditions of the mechanical impact

by the relative reference point position x_{coll} in x_{ego} -direction and y_{coll} in y_{ego} -direction as well as the geometric angle ϕ_{geom} between the vehicle longitudinal axes (in Figure 8 the slip angles of both vehicles are chosen negligibly small) in combination with the ego width W_{ego} , the ego length L_{ego} , the opponent width W_{opp} and the opponent length L_{opp} . As a real predictive sensor will mostly not be able to detect the complete opponent length the parameter L_{opp} may also refer to the current length of the detected part of the opponent vehicle. The impact direction is specified by the angle ϕ_{vrel} between the relative velocity vector and the ego velocity vector as well as the absolute value v_{rel} of the relative velocity vector. Furthermore the expected time to collision (TTC) is estimated on the basis of the underlying assumptions. For this study the collision parameters were calculated on the basis of a no change assumption concerning the current movement state of the ego vehicle and the opponent in two dimensions over ground. The assumption no change extrapolates the actual moving state of the ego vehicle and the opponent sensor object on the basis of a Taylor series for kinematic state variables. The closer the collision comes the better the no change assumption is able to predict values that fit the real development of the accident scenario.

The ego and object trajectories are calculated on the basis of the following correlations concerning the predicted movement state at t_0 defined by the velocity v , the yaw angle ψ and the slip angle β along the prediction time t_{pred} :

$$\begin{aligned} v(t_{pred}) &= v(t_0) + \frac{dv}{dt}(t_0) \cdot t_{pred} \\ &+ \frac{1}{2} \cdot \frac{d^2v}{dt^2}(t_0) \cdot t_{pred}^2 + \dots \\ &\approx v(t_0) + \frac{dv}{dt}(t_0) \cdot t_{pred} \end{aligned} \quad (44)$$

$$\begin{aligned} \psi(t_{pred}) &= \psi(t_0) + \frac{d\psi}{dt}(t_0) \cdot t_{pred} \\ &+ \frac{1}{2} \cdot \frac{d^2\psi}{dt^2}(t_0) \cdot t_{pred}^2 + \dots \\ &\approx \psi(t_0) + \frac{d\psi}{dt}(t_0) \cdot t_{pred} \end{aligned} \quad (45)$$

$$\begin{aligned} \beta(t_{pred}) &= \beta(t_0) + \frac{d\beta}{dt}(t_0) \cdot t_{pred} \\ &+ \frac{1}{2} \cdot \frac{d^2\beta}{dt^2}(t_0) \cdot t_{pred}^2 + \dots \\ &\approx \beta(t_0) + \frac{d\beta}{dt}(t_0) \cdot t_{pred}. \end{aligned} \quad (46)$$

On the basis of the movement state variable approximations at each prediction time step the vehicle velocity vector \mathbf{v} can be calculated by:

$$\mathbf{v}(t_{pred}) = \begin{bmatrix} v(t_{pred}) \cdot \cos(\psi(t_{pred}) + \beta(t_{pred})) \\ v(t_{pred}) \cdot \sin(\psi(t_{pred}) + \beta(t_{pred})) \end{bmatrix}_{xy}. \quad (47)$$

The absolute vehicle position \mathbf{r} along the predicted trajectory can then be calculated by integration:

$$\mathbf{r}(t_{pred}) = \int_{t_0}^{t_{pred}} \mathbf{v}(\tilde{t}_{pred}) \cdot d\tilde{t}_{pred} = \begin{bmatrix} x(t_{pred}) \\ y(t_{pred}) \end{bmatrix}_{xy}. \quad (48)$$

The absolute acceleration \mathbf{a} along the trajectory is given by:

$$\begin{aligned} \mathbf{a}(t_{pred}) &= \frac{d}{dt_{pred}} \mathbf{v}(t_{pred}) = \\ &= \begin{bmatrix} \dot{v}(t_{pred}) \\ v(t_{pred}) \cdot (\dot{\psi}(t_{pred}) + \dot{\beta}(t_{pred})) \end{bmatrix}_{xvyv} \\ &= \begin{bmatrix} a_{lon}(t_{pred}) \\ a_{lat}(t_{pred}) \end{bmatrix}_{xvyv}. \end{aligned} \quad (49)$$

The resulting trajectory on the basis of a given and numerically extrapolated working point of the ego vehicle movement is shown in the Figure 9. In this case the ego slip angle β_{ego} is assumed to be known with a diminishing slip rate $\dot{\beta}_{ego}$ so that it remains constant during the prediction. Both the ego vehicle state as well as the opponent vehicle movement are predicted on the basis of the described no change trajectory extrapolation, see Figure 10. Whereas for the ego vehicle the acceleration, yaw rate and the slip angle are assumed to be known for the opponent vehicle detected by the predictive sensor only the velocity in x_{ego} - and y_{ego} -direction is used for the prediction but not its acceleration, yaw or slip rate. This assumption is

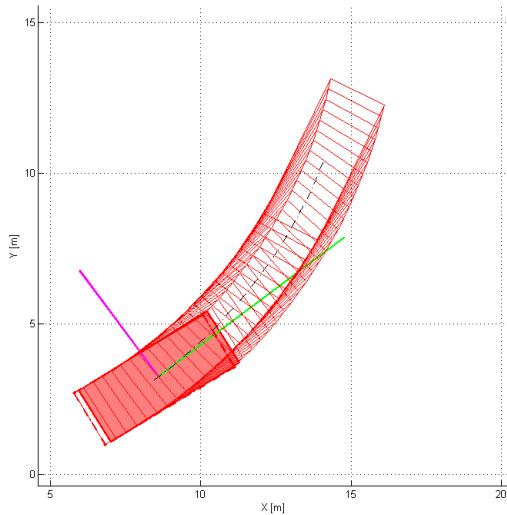


Figure 9. No change prediction on the basis of the current moving state

based on the fact that these variables are very hard to estimate with a sensor only directly measuring the position and not the relative velocity. Furthermore a diminishing slip angle is supposed for the opponent vehicle which is a good approximation for stable driving maneuvers considering the increasing number of ESP systems limiting the slip angle in modern vehicles. The resulting collision param-

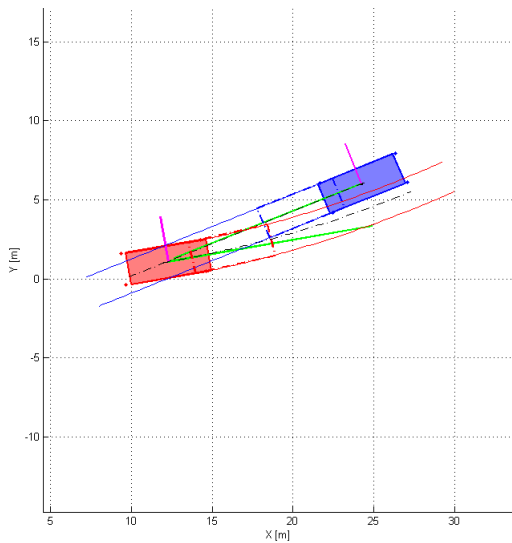


Figure 10. No change prediction of the expected collision constellation and parameters

ters described above are calculated on the basis of an analysis concerning the overlap of two rectangular bounding boxes around the vehicle contours at each point of the prediction time along the trajectories. Therefore the precision of the TTC-prediction is limited by the integration time interval during the discrete prediction process. The smaller the

prediction time interval is selected the more exact the kinematic and geometric collision parameters can be calculated.

MONTE CARLO SIMULATION

On the basis of the described measurement data generation and the collision prediction algorithm Monte Carlo simulations were performed to analyze the effect of the noisy measurement input data on the predicted collision parameters in three selected car2car-collision scenarios.

Simulation scenarios and process

In the following three critical traffic situations each resulting in a car2car-collision are presented. The scenarios will be analyzed concerning the sensitivity of the predicted collision parameters on the basis of noisy input data in this chapter. The accident scenarios are illustrated in Figures 11, 12, and 13.

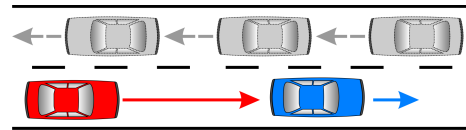


Figure 11. Scenario 1: straight rear-end collision with full overlap

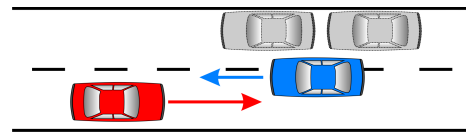


Figure 12. Scenario 2: straight frontal collision with partial overlap

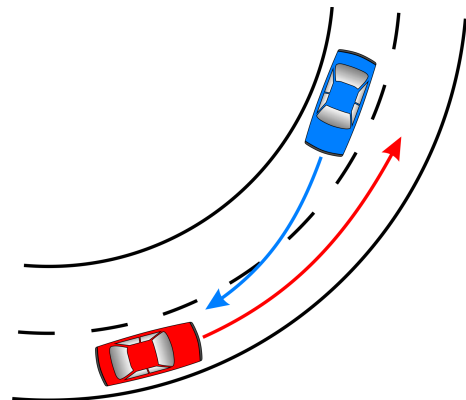


Figure 13. Scenario 3: curved frontal collision with partial overlap

In the first scenario the ego vehicle driving at a speed of 50 km/h hits the back of an opponent vehicle at a velocity of 10 km/h with full overlap. The second scenario represents a straight frontal impact

with an overlap of 40 percent within which the ego vehicle at a velocity of 50 km/h collides with the opponent vehicle driving at a speed of 40 km/h. In the last scenario the opponent vehicle driving at 57.4 km/h leaves its lane on a curved road segment and collides frontally with the oncoming ego vehicle with a velocity of 56.2 km/h. For simplicity concerning the further analysis steps the selected scenarios are all stationary concerning velocities, yaw and slip rates. Of course dynamic scenarios with sudden break or steering inputs can also be evaluated with the proposed method. For the simulation process both vehicles are assumed to be equally dimensioned with a length of 5 m and a width of 2 m.

For the sensitivity analysis of the collision parameter calculation on the basis of the Monte Carlo method for each collision scenario 1000 simulation runs were performed with MATLAB/Simulink [10] at a sample time of 1 ms for a sufficiently exact dynamics simulation. In each scenario Gaussian noise with the assumed standard deviation (see Chapter “Noise Model”) was added to the ideal measurements at a discrete measurement sample time of 20 ms modeling the processing cycle for ego and predictive sensor data. For every scenario two reference time stamps in relation to the actual time of collision (TOC) at TOC - 400 ms and TOC - 100 ms were selected. The reference collision parameters were calculated on the basis of the ideal dynamics data. At every reference time step of a scenario the predicted collision parameters on the basis of the noisy input values for the collision prediction module as well as the corresponding reference values were logged. The resulting differences between the prediction outputs and the reference values were analyzed concerning the statistical mean and standard deviation as well as the minimum and maximum values. The input values for the collision prediction module at each time step over all the 1000 simulation runs per scenario were all normally distributed with the given (distance dependent) standard deviation around the nominal value and a noise value limitation to the $\pm 4\sigma$ interval. The simulation runs were performed with constant ego sensor noise parameters and the four predictive sensor noise variations according to section “Noise model”.

Simulation results

In the following the results of the Monte Carlo simulation process are illustrated. For each of the three simulated collision scenarios introduced in the last section the noisy predictive sensor data as input for the collision prediction module as well as the resulting differences ΔTTC , Δv_{rel} , $\Delta \phi_{v_{rel}}$, $\Delta \phi_{geom}$, Δx_{coll} and Δy_{coll} between the prediction outputs and the reference values are presented for two ref-

erence points of time (TOC - 400 ms and TOC - 100 ms). The noisy ego vehicle sensor data is only illustrated for scenario 1 at TOC - 400 ms, see Figure 14, because each of the four ego sensor signals was disturbed with a Gaussian noise of constant standard deviation over all scenarios and reference points of time. The generated plots show the mean, minimum and maximum values (continuous lines, left y-axis) as well as the standard deviation (dashed line, right y-axis) at the regarded reference point of time for the four analyzed sensor variants (concerning all performed simulation runs under the given sensor noise). Figure 14 illustrates

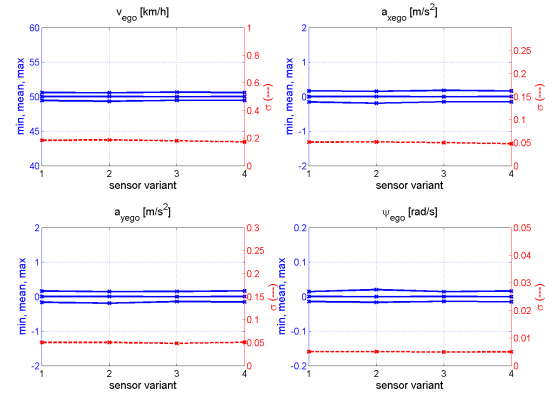


Figure 14. Scenario 1: Noisy ego sensor signals at TOC - 400 ms

the ego sensor data values in scenario 1 at TOC - 400 ms for the four presented (predictive) sensor variants in scenario 1. As the ego sensor data values were disturbed with constant noise parameters the mean, minimum and maximum sensor values over all the four sensor variants at TOC - 400 ms approximately remain constant with the chosen standard deviation. In this scenario the measured ego speed v_{ego} varies in an interval of about ± 1 km/h around the nominal value of 50 km/h, the acceleration measurements $a_{x_{ego}}$ and $a_{y_{ego}}$ in an interval of approximately ± 0.2 m/s² and the yaw rate $\dot{\psi}_{ego}$ in a range of about ± 0.02 rad/s. The effect of the distance dependent predictive sensor noise over the four variants at TOC - 400 ms in scenario 1 is shown in Figure 15. The standard deviation at that reference point of time increases from sensor variant 1 to sensor variant 4 along with the interval between the maximum and minimum values of the measured relative position x_{rel} in x_{ego} - and y_{rel} in y_{ego} -direction and the opponent width W . TOC - 400 ms is related to a mean x_{rel} -value of about 9 m and a mean y_{rel} -value of 0 m concerning the rear-end collision. The predicted collision parameters at TOC - 400 ms in scenario 1 scatter as a result of the given noisy input, see Figure 16. The differ-

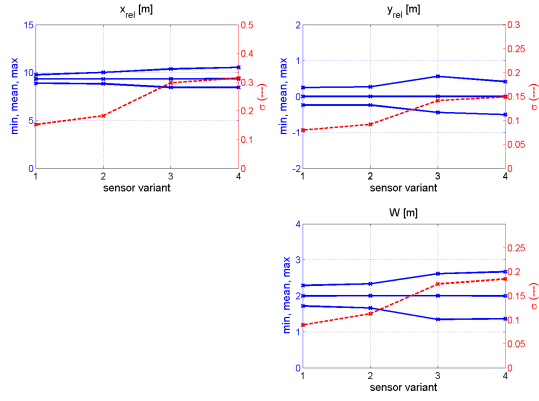


Figure 15. Scenario 1: Noisy predictive sensor signals at TOC - 400 ms

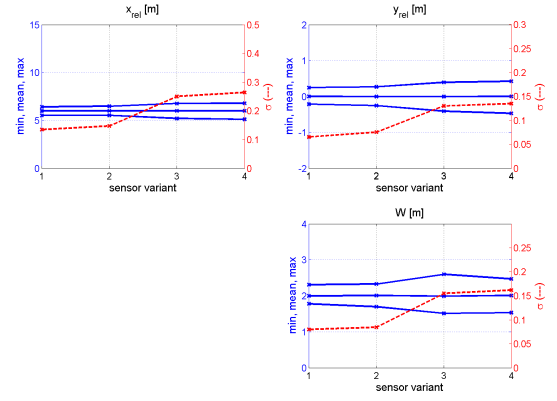


Figure 17. Scenario 1: Noisy predictive sensor signals at TOC - 100 ms

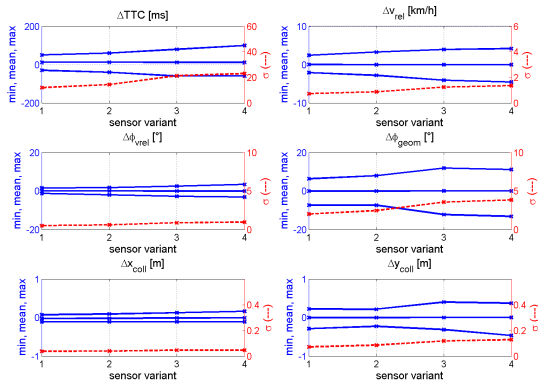


Figure 16. Scenario 1: Predicted collision parameters at TOC - 400 ms

ence between the predicted and the reference value varies between a resulting minimum and maximum value for each collision parameter. In this case for every parameter the difference increases along with the sensor variant. The predicted TTC varies in an interval smaller than ± 100 ms around the reference value for all the considered sensor variants. The mean ΔTTC -value is not exactly 0 ms because of the prediction tolerance due to the discrete prediction time interval of 10 ms. The relative velocity v_{rel} was predicted with a tolerance better than ± 5 km/h decreasing from sensor variant 4 down to 1. The predicted geometric collision angle ϕ_{geom} is more diffuse than the relative velocity angle ϕ_{vel} . Both parameters were estimated with an accuracy better than $\pm 14^\circ$ concerning the reference in all sensor variants. The predicted relative collision location parameter x_{coll} only varies in a quite small range of about ± 0.2 m. The predicted lateral collision opponent location y_{coll} scatters in a wider range of up to approximately ± 0.5 m. At the examined point of time the accuracy of the pre-

diction decreases from sensor variant 1 to sensor variant 4 for all collision parameters. At TOC-100 ms in scenario 1 the predicted TTC varies in a decreased interval of about ± 50 ms around the reference value in all sensor variants based on smaller predictive input parameter variations, see Figures 17 and 18. The relative velocity v_{rel} is predicted with an accuracy of approximately ± 4 km/h. As seen above the predicted relative velocity angle ϕ_{vel} again doesn't scatter as much as the geometric collision angle ϕ_{geom} . Both parameters remain in an interval smaller than about $\pm 12^\circ$ over all sensor variants. The relative collision location is predicted relatively exact in x_{ego} -direction (± 0.20 m) and doesn't exceed an interval of ± 0.25 m in y_{ego} -direction. As a result of the decreasing predictive sensor input noise at TOC - 100 ms compared to TOC - 400 ms the collision parameters are estimated with a better (or at least identical) accuracy for all sensor variants.

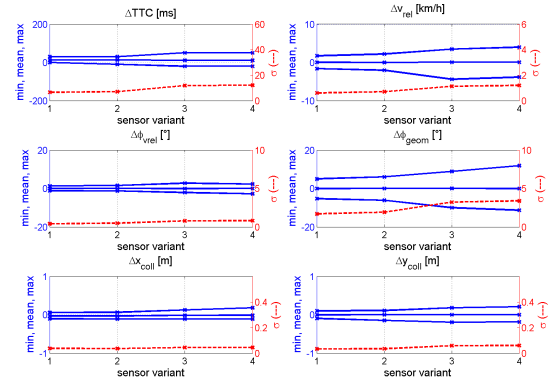


Figure 18. Scenario 1: Predicted collision parameters at TOC - 100 ms

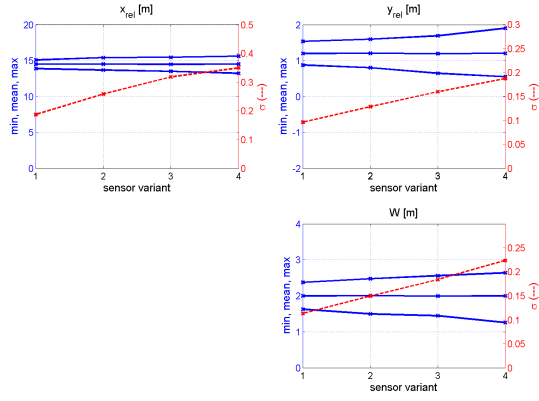


Figure 19. Scenario 2: Noisy predictive sensor signals at TOC - 400 ms

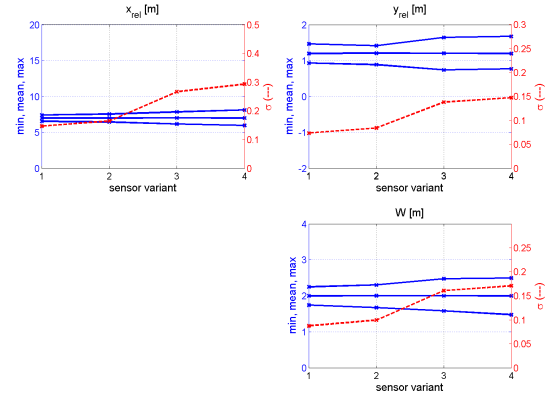


Figure 21. Scenario 2: Noisy predictive sensor signals at TOC - 100 ms

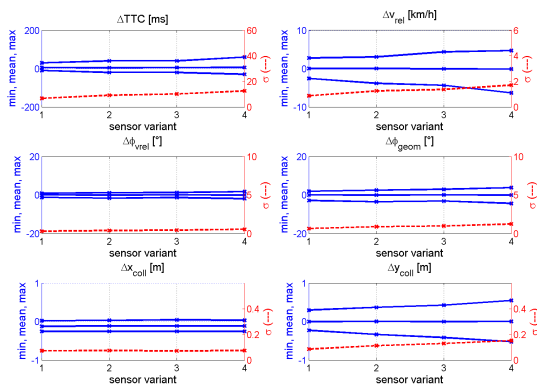


Figure 20. Scenario 2: Predicted collision parameters at TOC - 400 ms

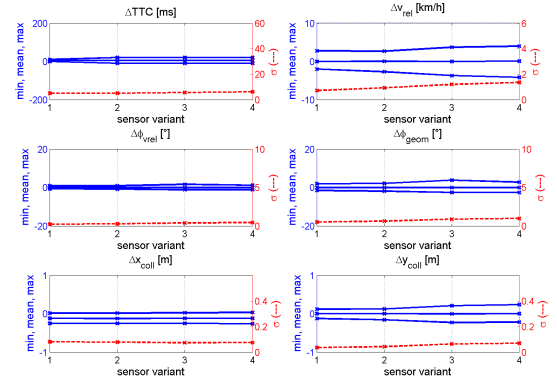


Figure 22. Scenario 2: Predicted collision parameters at TOC - 100 ms

In scenario 2 at TOC - 400 ms, see Figures 19 and 20, the predicted TTC varies in a maximum interval of about ± 60 ms around the reference value in an increasing manner along the predictive sensor variant due to the growing sensor noise at that point of time. The relative velocity v_{rel} is predicted with a minimum accuracy of approximately ± 6 km/h. Again the predicted relative velocity angle $\phi_{v_{rel}}$ doesn't vary as much as the geometric collision angle ϕ_{geom} . Both parameters remain in an interval smaller than about $\pm 5^\circ$ over all sensor variants. The relative collision location x_{coll} is predicted in a range of about ± 0.3 m in x_{ego} -direction and doesn't exceed an interval of ± 0.6 m in y_{ego} -direction. At TOC - 100 ms in scenario 2 the TTC variation interval decreases to approximately ± 20 ms due to the significantly smaller predictive sensor noise, see Figures 21 and 22. Whereas the prediction scatter intervals for the relative velocity v_{rel} , the geometric angle ϕ_{geom} , the relative velocity angle $\phi_{v_{rel}}$ and the x_{coll} -location parameter do not change significantly compared to the values at

TOC - 400 ms, the prediction of the y_{coll} -parameter gets significantly better. This results both from the less scattering y_{rel} -values at TOC - 100 ms as well as the decreasing effect of errors in the movement prediction direction with a decreasing distance.

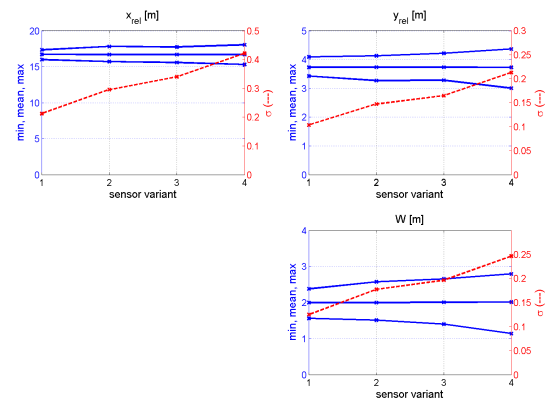


Figure 23. Scenario 3: Noisy predictive sensor signals at TOC - 400 ms

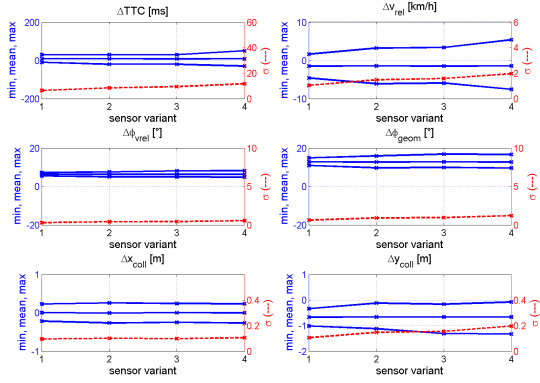


Figure 24. Scenario 3: Predicted collision parameters at TOC - 400 ms

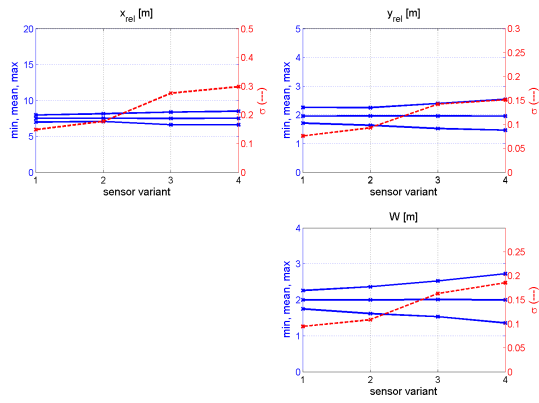


Figure 25. Scenario 3: Noisy predictive sensor signals at TOC - 100 ms

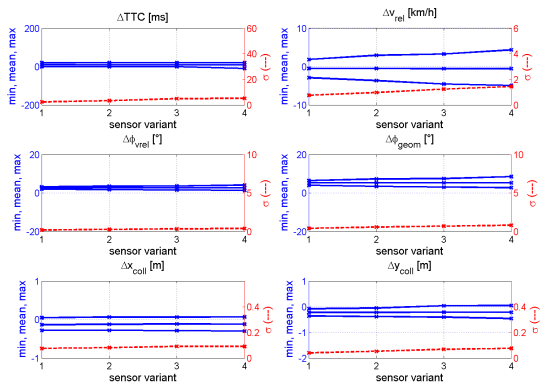


Figure 26. Scenario 3: Predicted collision parameters at TOC - 100 ms

In collision scenario 3 the predictive measurement scattering monotonically increases over all sensor variants at each reference point of time and decreases from TOC - 400 ms to TOC - 100 ms, see Figures 23 to 26. As both vehicle trajectories are

curved and the yaw and slip rate of the opponent vehicle are not estimated in the collision prediction module the no change prediction assumes a straight opponent trajectory that doesn't take into account the lateral opponent vehicle movement. This results in a visible difference of the mean prediction values for the relative velocity v_{rel} and the collision angles $\phi_{v_{rel}}$ and ϕ_{geom} as well as the lateral collision location y_{coll} in y_{ego} -direction from the reference values. The depicted difference between the mean values for the predicted collision angles and the y_{coll} -location parameter gets smaller from TOC - 400 ms to TOC - 100 ms because the effect of the inexact movement assumption decreases with a smaller distance. In this case the inexact collision parameter prediction is not only influenced by the measurement value scattering but also by the inexact movement assumption in the opponent trajectory generation. The measurement scattering effects on the predicted collision parameters are similar to those observed in scenarios 1 and 2.

CONCLUSIONS

The optimization of passive safety applications by the use of predictive sensor data requires a sufficiently exact prediction of collision parameters characterizing the type and severity of a collision. Ego vehicle state sensors as well as predictive sensors only measure with a given tolerance and resolution so that predicted geometric and kinematic collision parameters always scatter depending on the characteristics of the applied sensors as well as the sensor signal processing steps. In this paper a method for the model-based evaluation of sensor noise effects on the predicted collision parameters along the whole signal processing chain with a predictive sensor able to measure distances but not velocities was presented. On the basis of the developed method a study on the effects of measurement scattering concerning the predicted collision parameters was accomplished. Therefore fixed noise parameters for the ego vehicle sensors and two different basic noise levels for the predictive sensor combined with two noise dependencies along the measurement distance were assumed. Their effects on the collision parameter prediction were analyzed in three selected collision scenarios. Whereas in the straight collision scenarios the mean values of the predicted collision parameters based on noisy input data fitted the reference values very accurately in curved scenarios the collision prediction algorithm assuming a straight trajectory for the opponent vehicle (as opponent yaw rates are very hard to estimate) resulted in a time-dependent mean value in the geometric parameter prediction. Depending on the sensor noise parameters the geometric

collision parameters in all analyzed scenarios scattered in a specific range representing the accuracy of the prediction under the given premises. For the three analyzed scenarios under the made assumptions the TTC prediction scattering at TOC - 400 ms and TOC - 100 ms didn't exceed a range of ± 100 ms around the reference value, the relative velocity angle prediction was always in an interval of $\pm 9^\circ$ and the predicted geometric angle varied in a maximum interval of $\pm 18^\circ$. The relative reference point position in longitudinal ego vehicle body direction scattered in a range of ± 0.30 m at most and the relative reference point position in lateral ego body direction differed in a maximum range of ± 0.60 m (at TOC - 400 ms) respectively ± 0.25 m (at TOC - 100 ms) in straight scenarios and in a range from -0.10 m to -1.30 m (at TOC - 400 ms) respectively -0.50 m to 0.10 m (at TOC - 100 ms) in the curved scenario. The results show the challenge of collision predictions in the case of small vehicle overlaps and in curved scenarios. For the reliable detection and prediction of the collision parameters in these scenarios the sensor noise parameters have to be kept low in combination with an adequate dynamic object tracking with ego-compensation even in areas close to the ego vehicle. The effect of dynamic scenarios with sudden steering or brake inputs concerning the parameter prediction was not yet analyzed and has to be observed in future studies.

REFERENCES

- [1] Eichberger, A., Wallner, D., Hirschberg, W. 2009. "A situation based method to adapt the vehicle restraint system in frontal crashes to the accident scenario." Proceedings of the 21st ESV Conference; International Conference on the Enhanced Safety of Vehicles, 2009.
- [2] Moritz, R. 2000. "Pre-crash sensing - functional evolution based on short range radar sensor platform." SAE Technical Paper Series, 00IBECD-11, 2000.
- [3] Skutek, M., Linzmeier, D.T., Appenrodt, N., Wanielik, G. 2005. "A precrash system based on sensor data fusion of laser scanner and short range radars." IEEE 8th International Conference on Information Fusion, 2005.
- [4] Gietelink, O., Ploeg, J., De Schutter, B., Verhaegen, M. 2006. "Development of advanced driver assistance systems with vehicle hardware-in-the-loop simulations." Technical report, Delft University of Technology, 2006.
- [5] Pudenz, K. 2010. "Der Audi A7 Sportback: Sicherheitssysteme." ATZonline, July 2010.
- [6] Karrenberg, S. 2008. "Zur Erkennung unvermeidbarer Kollisionen von Kraftfahrzeugen mit Hilfe von Stellvertretertrajektorien." Technical report, Technische Universität Carolo-Wilhelmina zu Braunschweig, 2008.
- [7] Mitschke, M., Wallentowitz, H. 2004. "Dynamik der Kraftfahrzeuge." Springer, 2004.
- [8] Bar-Shalom, Y., Li, X. R., Kirubarajan, T. 2001. "Estimation with Applications to Tracking and Navigation." John Wiley & Sons, July 2001.
- [9] Altendorfer, R. 2009. "Observable dynamics and coordinate systems for automotive target tracking." IEEE Intelligent Vehicles Symposium, 2009.
- [10] MATLAB 2009b, Copyright © 1984-2009 The MathWorks Inc.

IS THE STEERING-WHEEL AIRBAG THE BEST SOLUTION FOR PROTECTING THE DRIVER IN FRONTAL IMPACTS?

Gustavo Zini

School of Engineering – University of Buenos Aires
Argentina
Paper Number 11-0163

ABSTRACT

“È sbagliato partire cercando immediatamente una soluzione. È necessario prima definire completamente il problema.” (Bruno Munari, Italian designer).

When considering future airbags it can be argued that their performance should be tailored considering occupant, vehicles and crash characteristics. Yet, this will increase the automobile weight, affecting in a negative way fuel economy and Ecology. Furthermore, to accomplish the target of tailoring the airbag performance, a variety of sensors and actuators should be developed and installed, as so new software to control the embedded control units. These elements add complexity and costs to an already complex and expensive solution. Therefore, this paper explores the problem of protecting the driver from the very beginning.

The purpose of the steering-wheel airbag is to prevent the driver’s head hitting the steering-wheel (which is inevitable since the head will continue its movement, unrestrained). Yet, and taking into consideration the problem from a different point of view it can be argued that another way of performing this protective action is to move away the steering-wheel from the driver. On the one hand, this proposed solution needs drive-by-wire technology to be implemented. On the other, fewer sensors and actuators, and simpler software and embedded control units will be needed.

The feasibility of both solutions will be analyzed from a general and synergistic point of view, taking into consideration both the cost and the effectiveness of each system. A theoretical approach will be predominant, pointing out some aspects that should be developed thoroughly within the corresponding settings and using appropriate resources.

INTRODUCTION

“The process of ‘reengineering’ involves the breaking of old, traditional ways of doing business and finding new and innovative ways. And from the redesigned processes, new rules will emerge that will determine how the processes will operate. The re-

engineering process is an all-or-nothing proposition, the results of which are often unknown until the completion of its course”. (Michael Hammer, "Reengineering Work: Don't Automate, Obliterate").

Airbags save many lives on a daily basis. But, in some cases, they also provoke injuries, even fatal ones.



Figure 1. An example of a circumstance where the steering-wheel airbag which may cause more damage than good.

Altogether it can be stated that airbags are by far more beneficial than potentially harmful. Therefore, they have not only become mandatory in most countries, but also their presence in automobiles is becoming greater and greater, and even small cars bear several airbags that are intended to protect the passengers in various circumstances.

At the same time, the average mass of vehicles has dramatically increased. The weight increase is basically due to more stringent legislative requirements and changing customer demands (growing vehicle size, extra comfort and safety devices, etc) that, in turn, have caused an increase weight of other components to reach the desired performance level. Heavier cars mean larger kinetic energies and bigger damage potentials.

Furthermore, airbags are still in a developing stage, since they lack many features that could mini-

mize the damages, namely a larger array of sensors, multi-stage actuators. Smarter airbags will surely protect passengers in a better way but they will also mean more complicated, heavier and costlier devices.

Therefore, the scope of this paper arises: is there a simpler, more effective way to protect the driver? Is it possible to rethink its function and purpose, and get better results with less complex solutions?

These questions will be answered in the next paragraphs, starting from the very beginning.

WHY IS THE STEERING-WHEEL AIRBAG NECESSARY?

Basically, because the steering-wheel airbag prevents the driver's head from hitting the steering-wheel (which is inevitable since the head will continue its movement, unrestrained):



instant t_0 : the car hits an object.



instant t_1 : the driver's knees hit the steering-wheel.



instant t_2 : the driver's head hits the steering-wheel.

Figure 2. Sequence for a restrained driver during an impact [1].

Its own technical name, SRS (Supplementary restraint System), gives a hint on their function and purpose: complementing the restraining action performed by the seatbelt. Since the head moves independently from the rest of the body, the steering-wheel airbag restrains its movement to prevent the head from hitting the steering-wheel.

OPERATION PRINCIPLES

Nevertheless, rather than a restraining action, the frontal airbags exerts an opposite movement to "halt" the head. While a seatbelt restrains, an airbag opposes a pressure to a kinetic energy:

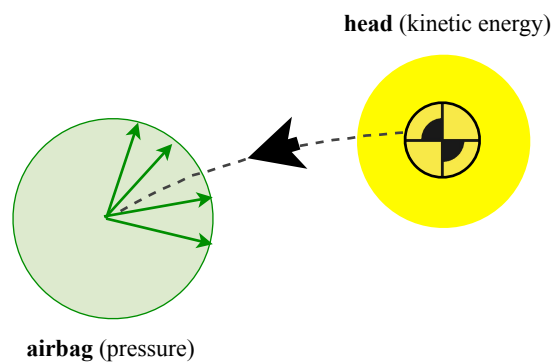


Figure 3. An airbag stops the head by opposing a certain pressure that will counteract the kinetic energy, dissipating it while the gas inside the bag is released.

Therefore, the function of the airbag is relatively more complex than the one of the seatbelt. Since it faces these two critical dilemmas:

1. if the pressure is lower than the kinetic energy, the head will still hit the steering-wheel.
2. if the pressure is higher than the kinetic energy, the head will rebound backwards, probably generating serious damages both to head and neck.

So, how important is this fact? How different maybe the kinetic energies involved and how many different responses do airbags provide?

First of all, everything that was said before must be restated, since it is inaccurate from a physical point of view that a pressure opposes a kinetic energy (since they are two different physical entities). The exact mechanism is the one where a force –rather than a pressure– decelerates a moving object which is moving in an opposite sense. Pressure is a measure of the force exerted in a given area, therefore, and considering that the area of an airbag remains relatively constant, the larger the pressure, the larger the force,

the larger the deceleration of the head. This deceleration must be within safety ranges, as explained above (otherwise or the head will hit the steering-wheel or it will rebound).

To further explain this issue a few calculations will be done. It is assumed that a driver's head weights around between 3 and 5 kilograms. Thus, its kinetic energy at the moment of the impact can be obtained:

$$K = \frac{1}{2}mv^2$$

where K = kinetic energy of the head [joule]

v = impact speed [km/h]

m = mass of the head [kg]

Assuming impact speeds between 30 km/h and 100 km/h, the range of kinetic energies is the following:

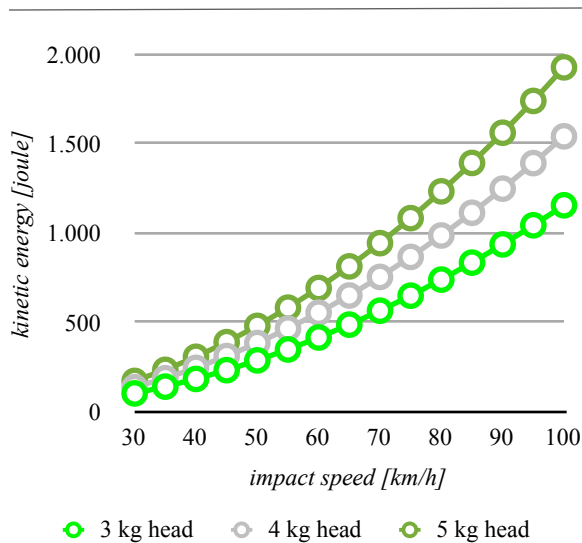


Figure 4. Range of kinetic energies developed by the driver's head during an car impact.

It is very important to notice that the difference of kinetic energy when comparing a 30 km/h impact versus a 100 km/h impact is –indeed– enormous:

- ➔ a 3 kg head at 30 km/h has a kinetic energy of nearly 100 joule.
- ➔ a 5 kg head at 100 km/h has a kinetic energy of nearly 2.000 joule (20 times higher).

Hence, an airbag should consider these differences, and respond using different pressures. Nevertheless, it can be stated that even the most advanced airbags are capable of releasing the gasses in two stages, offering two responses:

1. high speed impacts: fast response (10/20 milliseconds; higher pressure).
2. low speed impacts: less fast response (20/30 milliseconds; lower pressure).

In other words, and considering a “typical” airbag, since each car manufacturer develops different devices, while there is a need of a continuous response to a continuous range of probable kinetic energies developed by the driver's head, only two answers are given.

And, as said, this is the case of the most advanced airbags, known as “multi-stage” airbags, which are not standardly provided in the vast majority of the automobiles that are been produced.

The kinetic energies developed by the driver's head and the airbag counteraction can be compared in the following figure:

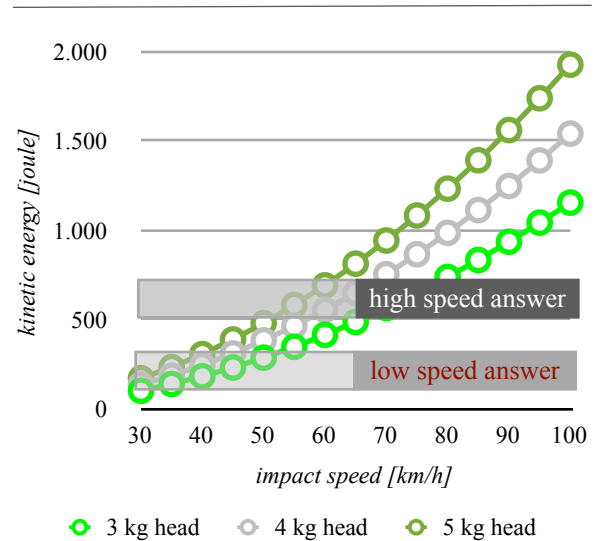


Figure 5. Range of kinetic energies developed by the driver's head during an car impact and a sophisticated airbag response.

Consequently, even the most advanced airbags offer a protection that is very limited in comparison to the range of kinetic energies developed by the driver's head. On top of that, most of the crashes with fatal injuries to the drivers take place at speeds where the kinetic energy of the head is higher than the pressure opposed to it by the airbag.

Proving this last statement exceeds the aim of this paper, but a hint of the explanation can be obtained by taking a look into NHTSA's FARS (Fatality Analysis Reporting System) data. A query was done to determine the frequency of deaths for drivers during head-on impacts where the airbag deployed [2].

The FARS query details were the following:

- (I) Year: 2009
- (II) Crashes:
 - i) manner of collision: front-to-front (includes head-on).
- (III) Person:
 - i) airbag deployed: deployed-front.
 - ii) injury severity: fatal injury.
 - iii) seating position: front seat-left side (driver's side).

The results of the query are shown in the following graph:

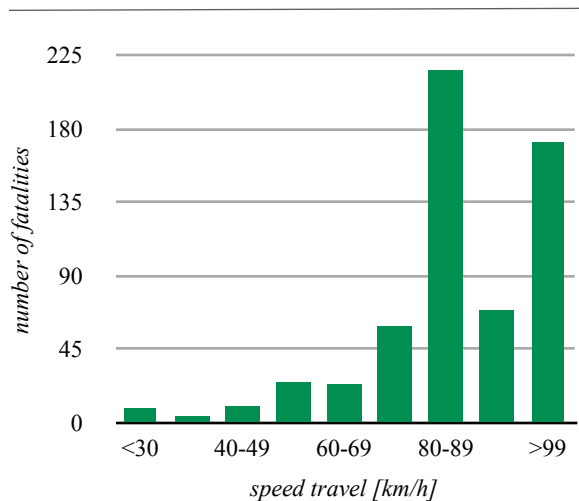


Figure 6. Number of fatalities in 2009 in the United States according to NHTSA FARS data base, for drivers suffering a head-on collision where the frontal airbag deployed [2].

As it can be clearly seen, most fatalities (88%) take place at impact speeds higher than 70 km/h. This does not necessarily mean that the airbag is the cause of these deaths, but it has to be pointed out that airbag's pressures are not set to absorb the kinetic energy of the driver's head at these speeds (as shown in figure 5).

It is most likely that these deaths are rather caused by direct impacts of other parts of the car against the driver's body instead of just the steering-wheel against the head. But when it comes to the airbag, everything indicates that, at the speed where most fatalities occur, higher pressures are needed to prevent the head from hitting the steering-wheel.

TIME

Up to this point most of the discussion involved kinetic energies and pressures, but very little has been

said about the time of the response. It was mentioned that the most sophisticated airbags have two different modalities of acting: the one with a lower pressure reacts in 20/30 milliseconds, the one with a higher pressure reacts in 10/20 milliseconds. So, is this fast enough for preventing the head from hitting the steering-wheel?

To answer this question one of the components of an airbag will be analyzed. An airbag is managed by an embedded ECU (Electronic control unit) which controls an array of devices (namely accelerometers, impact sensors, side door pressure sensors, wheel speed sensors, gyroscopes, brake pressure sensors, seat occupancy sensors).

Airbags are designed to deploy in frontal and near-frontal collisions bearing more severe threshold than the ones defined by regulations. Real-world crashes typically occur at offset angles, and the crash forces usually are not evenly distributed across the front of the vehicle.

Consequently, the relative speed between a striking and struck vehicle required to deploy the airbag in a real-world crash can be much higher than an equivalent barrier crash. Because airbag sensors measure deceleration, vehicle speed is not a good indicator of whether an airbag should deploy. Airbags can deploy due to the vehicle's undercarriage striking a low object protruding above the roadway due to the resulting deceleration.

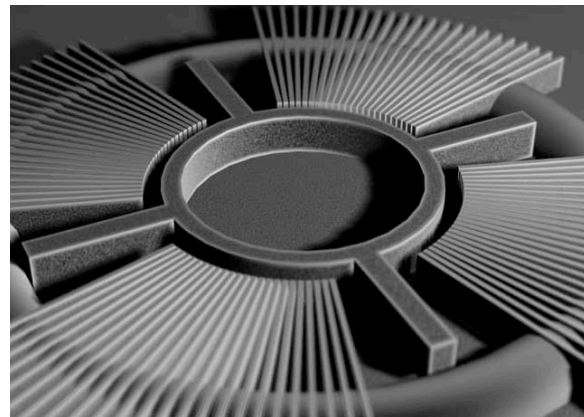


Figure 7. A microscopic photograph of a MEMS accelerometer used in airbag-triggering decision.

Therefore, the triggering algorithm must face several complex calculations and finally, when everything indicates that it is necessary, inflate the airbag. So the important issue to highlight is, how much time does it take the ECU to trigger an airbag? Typically, around 20 milliseconds.

But is this fast enough?

For low-speed impacts it surely is. But is it enough for high-speed impacts?

How much time does the driver's head travel from the moment of the impact until it eventually hits the steering-wheel?

To answer this it will be assumed that the distance from the drivers's head to the steering-wheel is around 50 cm. After this, Newton's second law is applied to calculate the time travel for different impact speeds:

$$x(t) = v_0t - \frac{1}{2}at^2$$

where x = position of driver's head (0,5 m)

v_0 = impact speed [km/h]

t = time [milliseconds]

a = acceleration = 0 (the head is unrestrained)

since acceleration is zero, the equation results in the simpler one:

$$x(t) = v_0t$$

Using the above equation, the time period in which the driver's head travels before hitting the steering-wheel, for the usual range of impact speeds is the following:

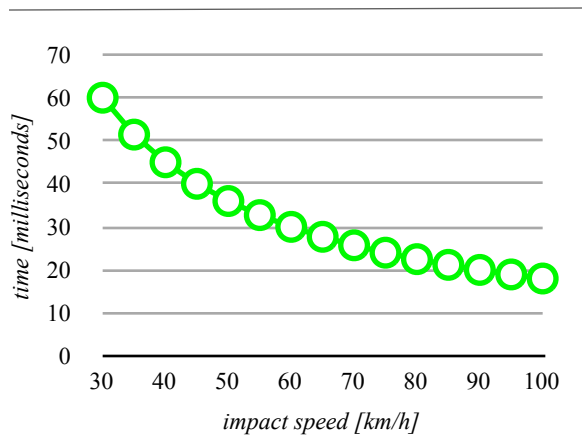


Figure 8. Time period in which the driver's head travels before hitting the steering-wheel assuming 50 cm of initial distance.

As said before, a typical ECU triggers an airbag in around 20 milliseconds. After this triggering, the time bag is inflated in around 10 milliseconds. For the most sophisticated airbags, the inflation takes places immediately after the ECU decides the triggering for high-speed impacts, and it takes place 20/25 milliseconds after the decision for low-speed impacts. If these

numbers were to be combined with figure 8, the result would be the one shown in the following graph:

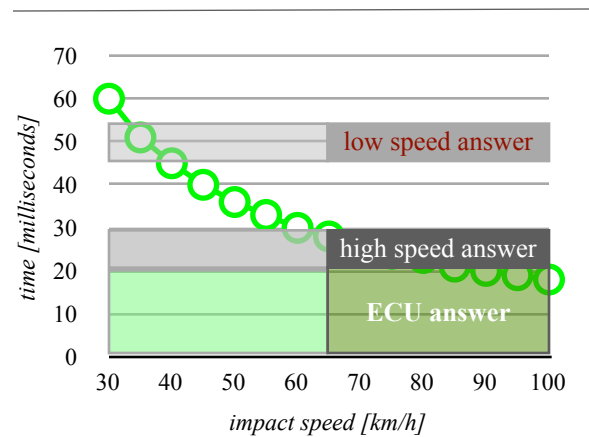


Figure 9. Time period in which the driver's head travels before hitting the steering-wheel, ECU triggering time and airbag inflating time.

It must be highlighted that at speed impacts over 70 km/h the head reaches the steering-wheel before the airbags inflates (even for the ones with two stages of inflation). Furthermore, at speed impacts over 85 km/h not even the ECU answer is fast enough to decide whether to trigger the inflation or not.

Thus, as in the case of the pressure opposing the kinetic energy, a discrete (in mathematical sense) answer is given to a continuous phenomenon. In both cases, two possible responses are given, and they are probably inefficient at high-speed impacts.

3D MOVEMENTS



Figure 10. Real-world head-on collision expose passengers to 3D movements.

To make matters worse, real-world head-on collisions (which account the vast majority of fatal crashes) include a rotation in three axes. Figure 10 shows an example of a lateral and vertical rotation. This deviation of the cockpit affects directly the area where the head hits the airbag. If there is too much offset between the relative movement of the head and a straight line, the airbag could force the head to move out, even making it hit the side window or a cockpit structure. The next figure demonstrates how the airbag is pushing the head rather than stopping it.



Figure 11. If there is a relatively large rotation, the steering-wheel airbag may push the head sideways instead of stopping it.

To prevent this, a very precise mapping of the movement of the head must be made, and eventually the geometry of the airbag must be adapted to the exact trajectory. This obviously means adding several sensors, and a complete redesign of the steering-wheel airbag, which can be stated that is mainly design for a full frontal impact, where the driver's head will hit it more or less in the middle.

Bottom line, to enhance the protecting capabilities of the steering-wheel airbag a series of improvements must be made. **Not only in terms of real-world 3D movements, but also, as stated in the above paragraphs, in terms of their capability to act more quickly, in an almost continuous range of time, and delivering an almost continuous range of pressures.**

ENHANCEMENTS

The following enhancements can be considered an incomplete list of potential modifications that steering-wheel airbags needs in order to protect the driver in a much better way:

- ➔ the ECU's triggering answer must be a lot quicker, preferable below 5 milliseconds.

- ➔ the airbag must produce several pressures, in a multi-stage mode, transforming its actual response in a "semi-continuous" one:

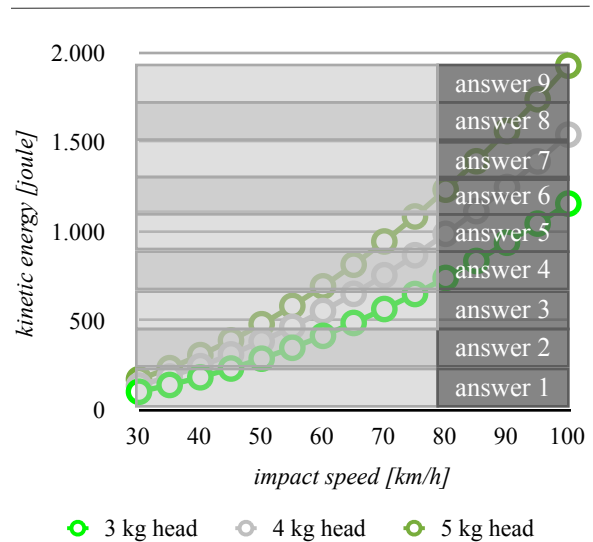


Figure 12. Example of a multi-stage airbag which provides a "continuous" response.

- ➔ the quantity of sensors must be exponentially augmented, to evaluate several information that will help enhance the efficaciousness of the airbag (namely, and not exclusively, the speed of the object the car is hitting, the direction and sense of the movement of the cockpit and of the driver's head, the distance from the driver's head to the steering-wheel, the speed of the driver's head, the latter's weight and size).
- ➔ the quantity of cavities that hold the gasses inside the airbag must also be augmented, in order to deliver different amount of gasses that will produce a relatively "continuous" pressure response.
- ➔ the geometry of the cavities of the airbag must also be controlled, so that if offset impacts take place, the driver's head will still be stopped rather than pushed away.

THE COST OF THE ENHANCEMENTS

The first question that must be answered is whether the proposed enhancements are feasible. And not only in economical terms, but also in technological and even in physical terms. Anyhow, and since this paper intends to deliver a theoretical approach, pointing out some aspects that should be developed thoroughly within the corresponding settings and us-

ing appropriate resources, a very general and approximate rule-of-thumb will be used to estimate the cost of the eventual enhancements.

It was said that even the most sophisticated airbags provide a two-stage response, and that, according to figure 12, 9 or 10 stages should be provided. This means developing a much more complex system of cavities that must occupy approximately the same volume that is filled today. This may mean new materials, new gasses, new triggers; a whole array of new components. If we take into consideration the fact that new ECUs and algorithms must be developed, and that no less than 15 to 20 sensors must be added, it can be said that the estimation of the cost of the enhancements is more of a guess than certainty.

Still, and only to make a point and to continue with the logic of this paper, it will be said that a more efficacious steering-wheel airbag could cost between 5 to 20 times more that a current one. But it must be considered as a very approximative figure.

REENGINEERING THE STEERING-WHEEL AIRBAG

Bruno Munari was an Italian designer who didn't like to solve a problem from the very beginning. In his book "*Da cosa nasce cosa*" (3) he says that there is a tendency to find a solution immediately afterwards a problem arises:

Problem → **Solution**

Yet, he proposes another method, a method where the solution gets farer and farer from the problem, and only when a whole series of vital issues are pondered comes the time to finally find the solution. The two-step sequence mentioned above, is then transformed into the following:

Problem →
→ Definition of the Problem →
→ Components of the Problem →
→ Gathering of Data →
→ Data Analysis →
→ **Creativity** →
→ Choice of Materials and Technologies →
→ Experimentation →
→ Construction of Models →
→ Assessment of Models →
→ Final Specifications →
→ **Solution**

Therefore, it is herein proposed not to follow the complete Munari's method, but at least consider the first and second steps. That is to say:

Which is the problem?

(Going back to a former question) why is the steering-wheel airbag necessary?

This was answered before. The steering-wheel airbag is necessary because it prevents the driver's head from hitting the steering-wheel (which is inevitable since the head will continue its movement, unrestrained).

Bottom line, the problem is to find a way to prevent the driver's head from hitting the steering-wheel.

Therefore, is the frontal airbag the only solution to this problem? Are there any other ways to solve the same problem?

For instance:

- What if the steering-wheel just gets away from the driver's head path?
- Why not move the steering-wheel forward?

A solution of this type would need drive-by-wire technology, which has been already developed and is used in complex and sensitive devices such as Airbus airplanes.

An most important of all, a solution of this type would mean that a better steering-wheel airbag than the current one is not an airbag.



Figure 13. The interior of the 2002 General Motors' Hy-wire concept car.

Figure 13 shows a relatively old concept-car. Moreover, it is a type of automobile that is very different from present-day ones. Yet, its drive-by-wire technology will probably be widely used as electrical cars start replacing internal combustion-engine cars. The interesting issue about the concept car is that it shows in a graphical way that, in the event of a frontal impact, the steering-wheel column could be very rapidly tumbled down, moving the steering-wheel away from the driver's head.

Furthermore, this kind of answer is surely simplest than the one the current steering-wheel airbag has to provide. In mathematical terms its only a binary problem, a go or non-go one. A tumbling steering-wheel should only get as far away and as quickly as possible, no matter which is the trajectory of the driver's head, or its kinetic energy. Its ECU's algorithm should only decide if a crash has happened with broader restraints and should need fewer sensors.

However, and as said before, the feasibility of both solutions (a more efficacious steering-wheel airbag and a tumbling steering-wheel column) are only analyzed from a general and synergistic point of view. So, the complete solution of a tumbling steering-wheel column will not be developed. This must be considered as a hint, a way of "laterally" thinking, a way of reengineering an already complex and expensive solution to make it simpler and –desirably– better.

To conclude, and regarding the cost of this proposed alternative, it can be stated that it would be much lower than the current steering-wheel. On top of that, the cost of setting the system to its original state would be almost insignificant when compared to the cost of repairing a triggered airbag.

CONCLUSIONS

"Entia non sunt multiplicanda praeter necessitatem (Entities must not be multiplied beyond necessity)." (allegedly, William of Ockham, c. 1285–1349)

"Ockham's razor", often incorrectly summarized as "the simplest explanation is most likely the correct one", suggests that we should tend towards simpler theories until we can trade some simplicity for increased explanatory power.



Figure 14. Simplicity.

Going back once more to the beginning, the purpose of the steering-wheel airbag is to prevent the driver's head hitting the steering-wheel (which is inevitable since the head will continue its movement, unrestrained). Yet, and taking into consideration the problem from a different point of view it can be argued that another way of performing this protective action is to move away the steering-wheel from the driver. On the one hand, this proposed solution needs drive-by-wire technology to be implemented. On the other, fewer sensors and actuators, and simpler software and embedded control units will be needed.

This papers proposes to replace the steering-wheel airbag with a completely new device that could be both more efficacious and less costly. In terms of reengineering it is proposed not to continue the path of continuous improvements, but finding new, innovative, completely different ways of solving a problem.

Nevertheless, the following can be stated:

- ➔ maybe the alternative solution herein proposed is not better than the current one.
- ➔ drastic changes in the automotive industry are as deeply desired as fiercely feared.
- ➔ engineers have a secondary role in designing an automobile, and generally they must follow the restraints imposed by designers.

Therefore, and to conclude, this paper performed a theoretical approach to a complex problem, pointing out some aspects that should be developed thoroughly within the corresponding settings and using appropriate resources. But more than that, this papers gives a hint about the necessity of some drastic changes in the design of automobiles that must be conducted by engineers, with no design restraints.

In this way, hopefully, things could be simpler and better. And, again hopefully, more lives could be saved.

ACKNOWLEDGMENTS

Professore Bruno Riccò, Facoltà d'Ingegneria, Università di Bologna.

REFERENCES

- (1) Hyde, Alvin. 1992. "Crash injuries: how and why they happen."
- (2) <http://www-fars.nhtsa.dot.gov>
- (3) Munari, Bruno. 2006. "Da cosa nasce cosa".

Actual Restraint Systems: Reached their limits!?

Analyses of Accident data of frontal impacts, compared to consumer test results

Volker Sandner

Thomas Unger

ADAC

Germany

Paper Number 11-0351

ABSTRACT

In the last 25 years the safety systems, such as seat belt, airbag, and a stable body shell saved thousands of people lives in traffic accidents. New test requirements from local road administrations and consumer protection programs (NCAPs) give the information of the performance of modern cars to the consumer and the way to improve safety to the automobile industry. So a lot of work has been done to implement safety systems in the complete vehicle fleet. This was the first and very efficient step to reduce the number of fatal injured passengers involved in a vehicle accident..

In Europe the number of killed people in traffic accidents decreased enormously. The number of victims in 2008 was 28.4% lower than 2001. In Germany the figures show a reduction of the fatalities in the same time period of 35.8%.

The new requirements on vehicle safety lead to very complex restraint systems and to very stiff passenger compartments, In case of an accident very stiff vehicle compartments are raising the deceleration of the vehicle body and the restraint systems had to working on a high level of pretension force at a very short time. Systems which were implemented to save lives could now be contra productive and become a problem for persons who are not able to withstand such high loads according their stature, age or mass.

On the background of the demographic change the number of elderly people driving cars is increasing. This issue is getting more and more important in the near future, because in the case of an accident their body is not able to withstand those high loadings induced by the restraint systems and the high deceleration. Multiple fractures of the chest with following injuries of internal organs and accelerations injuries of inner organs and soft tissue are the result of this high deceleration and loadings. Also smaller and even younger passengers will be affected by this dynamic behaviour due to the belt routing and positioning of the passenger according the vehicle interior. The data evaluation of the GIDAS [1] and ADAC [2] accident data base is showing a lot of real life crashes were injuries could be detected which are more severe than seen in consumer crash tests, while the accident parameters are comparable with those of the crash tests. Especially women, small and elderly

people have a higher risk of injuries. New test methods and smarter restraint systems could help to indicate problems and safe lives in accidents.

INTRODUCTION

Starting in the 90's, a lot of efforts were done to push the safety of passenger cars. Under the pressure of tests done by consumer test houses, mandatory crash tests were introduced by the government all over the world to make sure that only cars with basic safety behaviour will be sold. Consumer crash test programs raised the bar on the requirements of the test results. Nowadays several NCAP's (New Car Assessment Program) are established all around the world. Even in mid and low income countries safety is an aspect which is addressed by new programs such as the Latin NCAP. The following paper uses accident data for Germany, addressing the chest injuries in frontal impact crashes. but the results could be transferred to other Centre European countries, too.

The data evaluation of the accident data base of the ADAC accident research showed several accidents with passenger cars involved causing severe injuries of the vehicle passengers or even killed passengers while the performance of the car showed good results in consumer crash tests. With nearly the same boundary conditions, than in a consumer crash test, in impact velocity and overlap, the difference between the rated injuries and the real ones were significant.

With **GIDAS data** a deeper investigation was done on this issue using both data bases as source of information. GIDAS (German In-Depth Accident Study) is the largest accident study in Germany.

The data collected in the GIDAS project is very extensive, and serves as a basis of knowledge for different groups of interest. Representativity compared to the federal statistic is guaranteed due to several processes.

Since mid 1999, the GIDAS project collects about 2000 accidents in the areas of the cities Hanover and Dresden per year. The project is supported by the Federal Highway Research Institute (BAST) and the German

Association for Research in Automobile Technology (FAT). "

The ADAC Accident Research Project

The "Yellow Angels" of the ADAC air rescue service (HEMS) give medical care to those injured in road accidents which is an essential part of their rescue missions.

Since June 2005, data of nine ADAC HEMS (Helicopter Emergency Medical Service) bases of road accidents is collected and have been closely examined.. Approx.1,600 road accidents per year are investigated. Each case is analysed retrospectively. The study is based on several pillars (Figure 1). With the information gathered from various sources, accidents can be accurately analysed and evaluated.

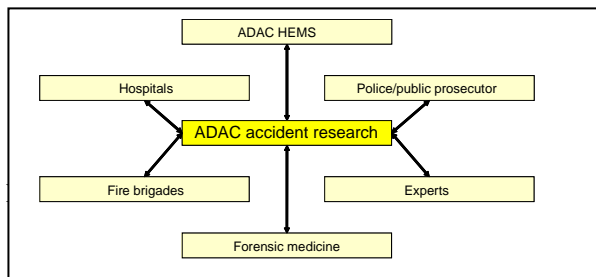


Figure 1. Structure of ADAC Accident research

Despite the fact that details, such as reason of the accident, injury patterns vehicle specifications are well known and medical data is available, this project has restrictions due to the fact that helicopters only work by daylight, on urban areas, seldom in cities and are called for severe accidents.

The combination of the results of both research activities delivers a very good data basis including representative accident data and a lot of accidents on urban roads were the more severe injuries occur.

ACCIDENT DATA ANALYSES

A detailed analysis of frontal impacts was carried out using data from the German In-Depth Accident Study, GIDAS including accidents from 1999 to 2010.

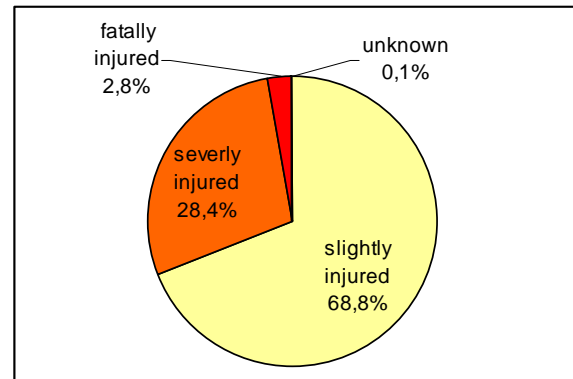


Figure 2. (GIDAS) Severity of accidents with passenger car involvement – Official classification, n=12967

Figure 2 shows a percentage of 2,8% fatal injuries in the last decade, while 28% were severely injured, expressed in MAIS, 19,3% had MAIS 2, 4,6% MAIS 3, 1,4% MAIS 4, 10% MAIS 5 and 0,6% MAIS 6 injuries. Focused on the life threatening and fatal injuries the related number of the ADAC database shows a comparable result, while the number of severely injured persons is quite higher depending on the scaling and the focus on severe accidents.

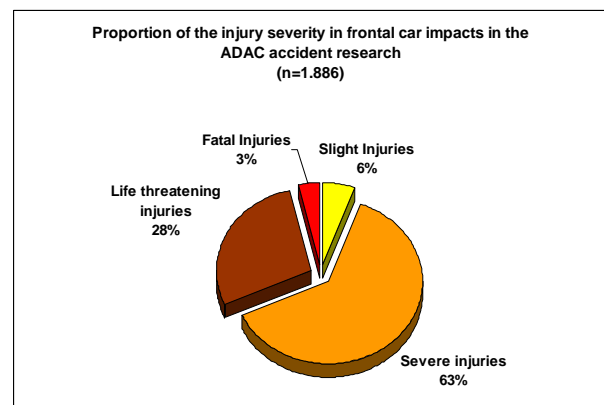


FIGURE 3. (ADAC) Severity of accidents with frontal car impacts – ADAC Classification, n=1886)

Both databases are showing a higher number of fatal injuries than the federal statistic, where the percentage of fatal injuries is close to 2%.

The issue to be investigated is the frontal impact and the restrain systems activated in this kind of accident, with the main focus on the seat belt and its function. The distribution of impact types of passenger cars is listed in Figure 4. in 28% a single front accident occurs (n=5475) and in 73% the opponent is an other passenger car.

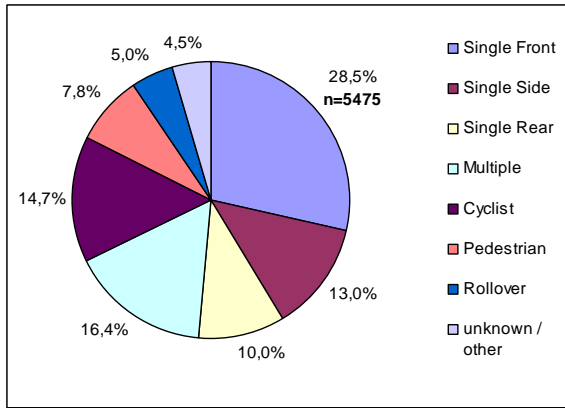


Figure 4 (GIDAS) Impact types of passenger cars, n=19195

While the percentage of the single front accidents with 45% is higher in the ADAC Database than in GIDAS the percentage of 77% in the car to car is quite close in comparison.

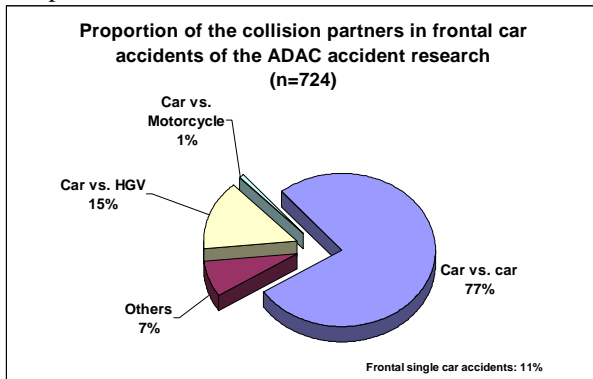


Figure 5 (ADAC) Constellation of impacts, n=724

A more detailed view on the type of cars involved in single frontal accidents with another vehicle show in 76% a kerb weight from 750 to 1500kg, respectively 84% in the ADAC database, so the compact, lower mid class and the mid class are the cars to be involved most common in a traffic accident. These cars will be deeper analysed in the chapter of Euro NCAP test evaluation.

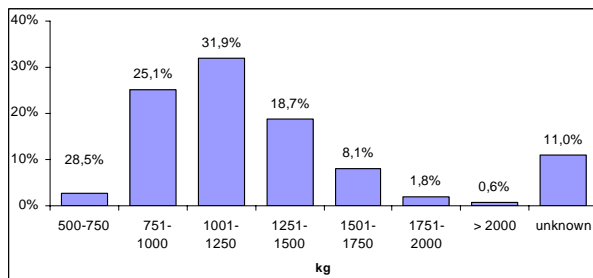


Figure 6. (GIDAS) Kerb weight of passenger cars in single frontal impacts, n=5475

A further interesting detail of the cars involved in a frontal impact is the year of first registration to take the safety standard into account. The distribution of first registration is shown in Figure 7. More than 50% of the cars involved in single frontal car to cars impacts are

first registered after 1996 and even 15,8% are not older than 10 years and 58% are equipped with a frontal airbag in the GIDAS database.

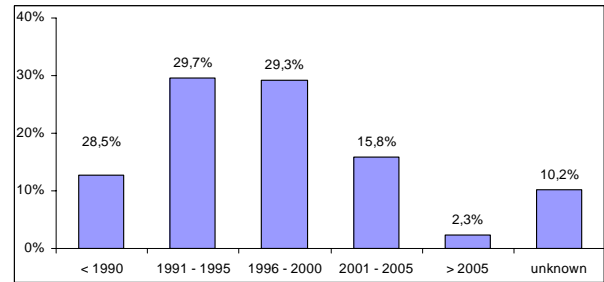


Figure 7. (GIDAS) Year of first registration of passenger cars in single frontal impacts, n=5475

In fact the numbers of fitment rate differs between the two databases. Instead of 58% fitment rate of frontal airbags the percentage in the ADAC database is 70% which is higher and maybe an indication of a newer vehicle fleet which is detected. The first registration is not captured by the research team of ADAC.

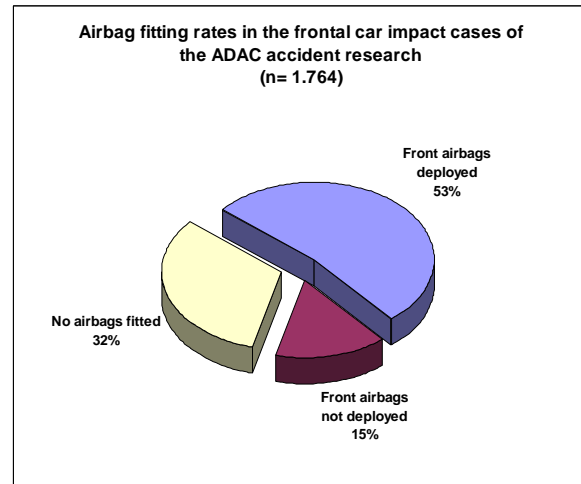


Figure 8. (ADAC) Airbags in passenger cars in frontal impacts

The MAIS distribution in the single frontal impact of belted occupants reflects a picture seen from the national accident statistics, were the number of severe and deadly injured car occupants is decreasing over the last decade. Most of the belted occupants have very minor injuries MAIS 0 or MAIS 1. MAIS 2 and MAIS 3+ representing the more severe injuries is only registered by 6.6% respectively 2%.

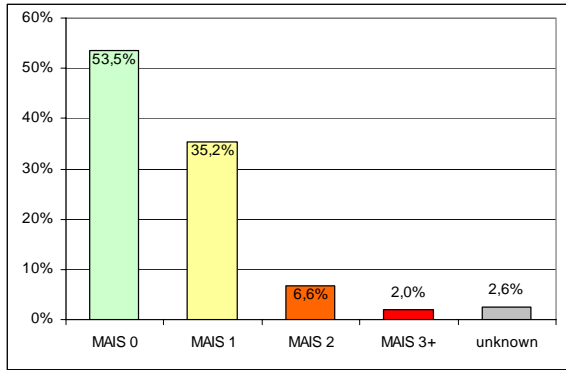


Figure 9. (GIDAS) MAIS distribution of belted front seat occupants in passenger cars in single frontal impacts, n=6102

Dividing up the MAIS 1 and MAIS 3+ into the year of registration and the age of the injured occupants the following graphs show some different tendencies. Figure 10 is showing the trend of less MAIS 1 injuries according the built level of the cars. The younger the vehicles built level the less percentage of minor injuries occurs. This trend could be seen for all injured occupants not depending on the age. All specific age groups are showing the same trend lines.

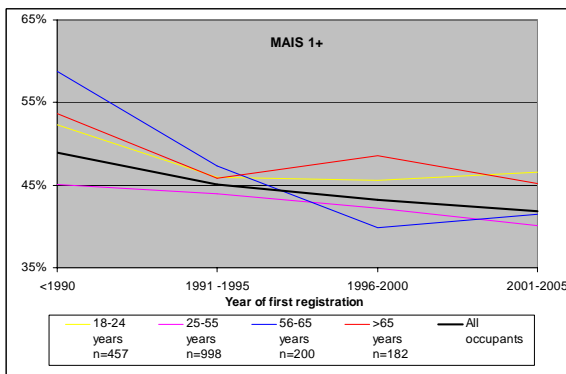


Figure 10. (GIDAS) Share of MAIS 1+ injured belted front seat occupants of passenger cars in single frontal impacts

This picture changes with the MAIS 3+ injuries divided up into the built level of the car and the age of the injured occupants. For the 25 to 65 year olds the trend of the reduction of MAIS3+ injuries seems so be equally to the MAIS 1+ injuries, but for young persons and especially for persons over the age of 65 the risk of a MAIS 3+ injury in a car of the built level 2000 and later is increasing. The trend of all MAIS 3+ injuries is therefore constant, with tendency of slightly rising than decreasing.

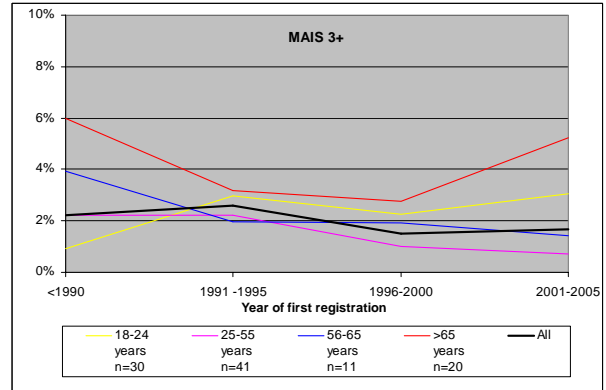


Figure 11.(GIDAS) Share of MAIS 3+ injured belted front seat occupants of passenger cars in single frontal impacts

A similar situation is documented in the ADAC database. While a decreasing number of life threatening injuries could be recognized in vehicles from 1991 till 2000 in comparison to vehicles of the model year before 1990, the number of severe injury increased. So the injury severity could be reduced over all. The fatality rate was also reduced at the same time. But this positive trend could not be seen in the following model years from 2001 to 2005 and from 2006 to 2010 were a stagnation of the severe injuries could be recognized and on the other hand a slightly increase of the life threatening injuries could be also recognized. The percentage of fatalities is constant in that situation; taking into account the number of cases for the brand new car is less than the model year from 2001 to 2005. This effect seems to be caused by the more stable vehicle cells, which were an improvement in the mid end of the 90's. Deeper investigation will be done later in this paper.

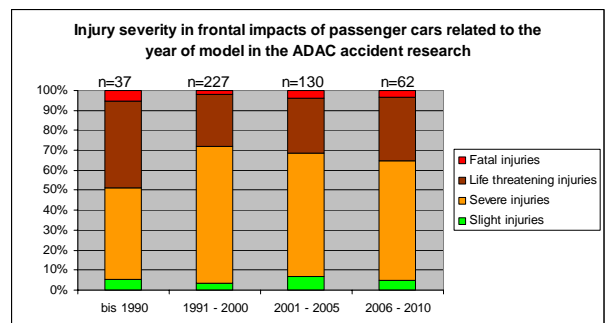


Figure12. (ADAC) injury severity in frontal impacts according the year of production

A more detailed look into the accident data dividing up the occupants according their age show that elderly people have a higher risk of fatal, life threatening and severe injuries, starting at the age of 30, were the numbers of injuries is increasing especially of severe injuries (04). From 70 years onwards the percentage of life threatening injuries is increasing as the fatal number does. This development is caused by the physical condition of the occupant due to his age, were the

skeleton, muscles etc. are not resisting in the same way than in the age of 20 to 30. The classification of the ADAC accident data is the following:

The classification of the injury severity bases on 7 steps with:

- 01 = Slight Injury
- 02 = Ambulatory Treatment
- 03 = Stationary Treatment
- 04 = Possible imminent mortal danger
- 05 = Imminent mortal danger
- 06 = Sufficient cardiopulmonary resuscitation
- 07 = Exitus, insufficient cardiopulmonary resuscitation

This classification gives details about the overall situation of the accident victim comparable to MAIS.

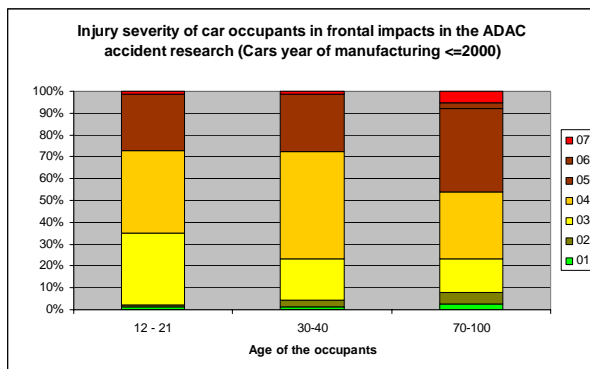


Figure13 (ADAC) injury severity in frontal impacts with cars of MY <=2000, related to the age of occupants,

But this fact seems to get a bigger problem in cars of model year 2001 onwards, where the percentage of fatal and life threatening injuries is increasing for the passengers of 70 years plus. The occupants of the age of 30 to 40 are still protected quite well and even better protected than in a car of an earlier built level. The number of no or only slightly injured young occupants is developing in a positive way, but at the same time the fatalities from occupants from 12 to 21 are increasing in the cars of a newer built level.

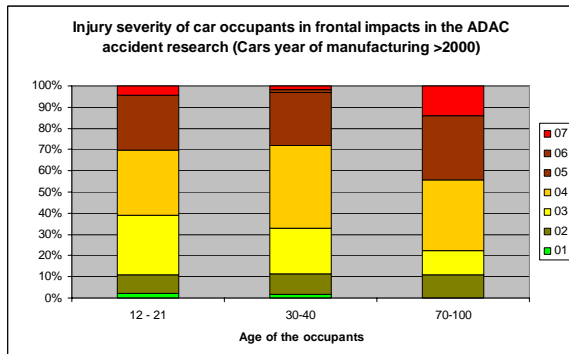


FIGURE14. (ADAC) injury severity in frontal impacts with cars of MY >2000, related to the age of occupants

The following data evaluation is focused on the Thorax area, because this area was seen the demanding one for higher injury risk, while the test results show nearly no problem at that area at all. The maximum thorax injury could be seen in the GIDAS data evaluation of Figure 15. The highest percentage of AIS 0 is fixed to the occupants of the age of 18 to 24, but up to the age of 18 and from 24 onwards the risk of an AIS 1 and AIS3+ injury is increasing. This might be transferred to the stress capacity of a human depending on the age. So a deeper look inside this data is needed to differentiate according to the age and sex of the occupant and the age of the cars to deliver a better picture

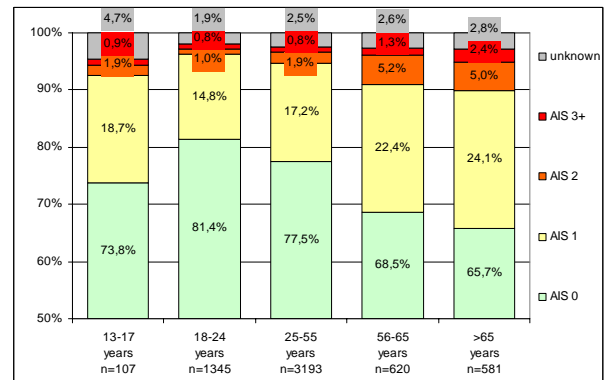


Figure 15 (GIDAS) Maximum thorax injury severity of belted front seat occupants of passenger cars in single frontal collisions by occupant age, n=5846

In accidents with cars of a built level before 1990 in comparison to cars younger than 2005 a continuous decrease of AIS 1,2 and 3+ for chest injuries could be seen for the group of occupants <=55 years. This is a positive trend and shows the capability of modern cars compared to cars from an earlier decade. For elder occupants from 55 onwards the trend of a reduction of AIS 1, 2 and 3+ is obvious for cars with built level up to the end of the 90's. The discrepancy between elderly and younger people is rising in cars of a built level from 2000 onwards.

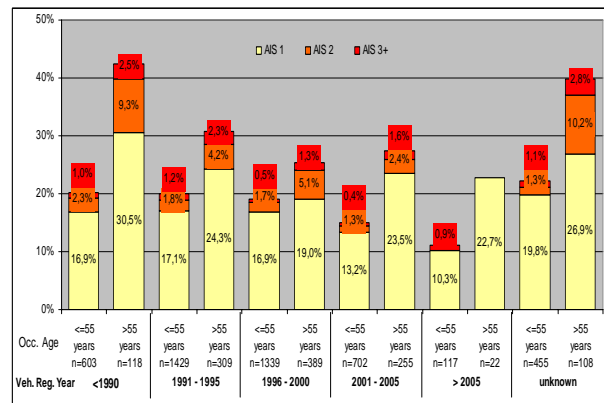


Figure 16.(GIDAS)Maximum thorax injury severity of elderly compared to younger belted front seat occupants of passenger cars in single frontal collisions, n=5846

A comparison on the same basis, built level of vehicles in accordance with the gender of the occupants show that there is a difference in the thorax injury between male and female. Starting at the built level of cars in the 90's and younger the number of AIS 1 injuries for male is continuous decreasing and halved from 14.4% to 7.1% for cars of the built level 2005 and younger. At the same time the AIS 2 injures were reduced from 3.1% to 0.7%, while the AIS 3+ injuries are nearly constant or slightly increasing. Contrary to the male the females' numbers show no significant reduction of thorax injuries of the last decades. Neither the AIS 1 Injuries nor the AIS3+ injuries were reduced significantly with the younger built level of cars.

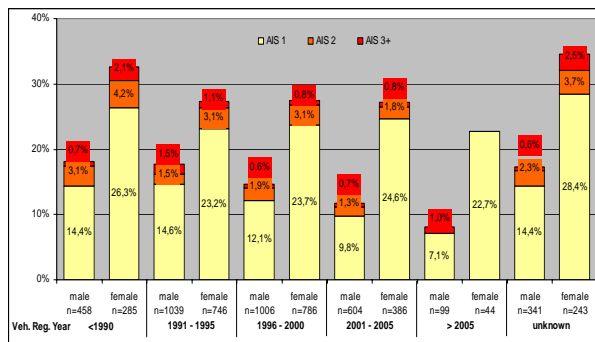


Figure 17 (GIDAS) Maximum thorax injury severity of male compared to female belted front seat occupants of passenger cars in single frontal collisions; N=6037

Comparable data could be found in the ADAC accident data. There the risk of severe, life threatening and deadly Thorax injuries is 30% higher for female than for male, while the percentage for deadly injuries is 4 times higher for male than for female. The AIS 1 Thorax injuries have nearly the same percentage for each gender.

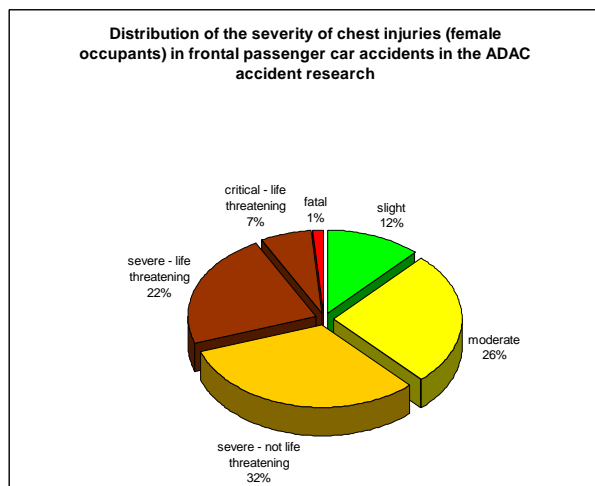


Figure 18. (ADAC) Thorax injury severity of female belted front seat occupants of passenger cars, n=80

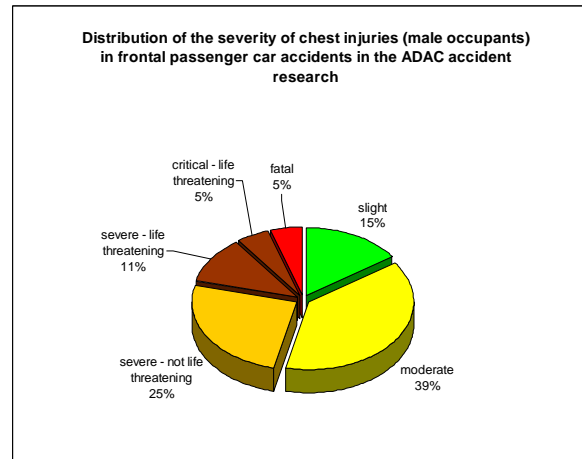


Figure 19 (ADAC) Thorax injury severity of male belted front seat occupants of passenger cars, n=99

A further comparison between the time of first registration and the height of occupants should give answer if there is a trend that young, mid-sized male occupants will have less risk of injuries in a frontal impact accident than other people of the population. A constant decrease of AIS 1 injuries could be realized for persons below 165cm while the AIS 1 injuries for persons > 165cm are nearly constant up to a slightly decrease which is also the case for AIS 2 while AIS 3+ is decreasing over the building periods. This counts for vehicles of a built level up to the year 2000. But from the built level 2000 onwards the injury risk for smaller persons is increasing. So overall a higher risk for smaller occupants of Thorax injuries could be realized in cars of a younger built level.

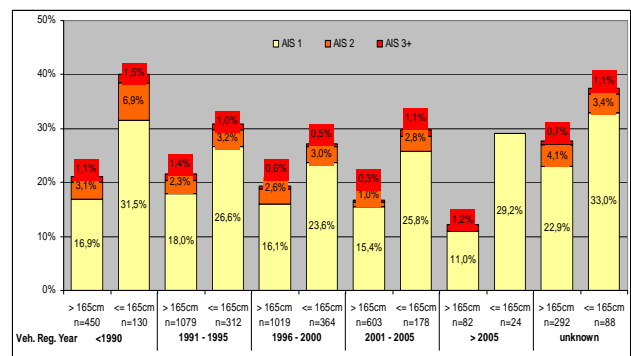


Figure 20 (GIDAS) Maximum thorax injury severity of tall (>165cm) compared to small (<=165cm) belted front seat occupants of passenger cars in single frontal collisions, n=4621

EVALUATION OF EURO NCAP TEST RESULTS COMPARED TO REAL LIFE ACCIDENTS

A stable vehicle body is the first and important step toward a safe vehicle. To minimize intrusions and deformation was a big step forward in the early 90's and nowadays nearly 100 of the tested cars in Euro NCAP show no problems with cell stability at all. This trend could also be seen in the ADAC database, where nearly 70% of all frontal impacts have no deformation of the vehicle cell. The following figure shows the distribution in CDC level of deformation while deformation of the zones 1 to 6 will not affect the passenger cell.

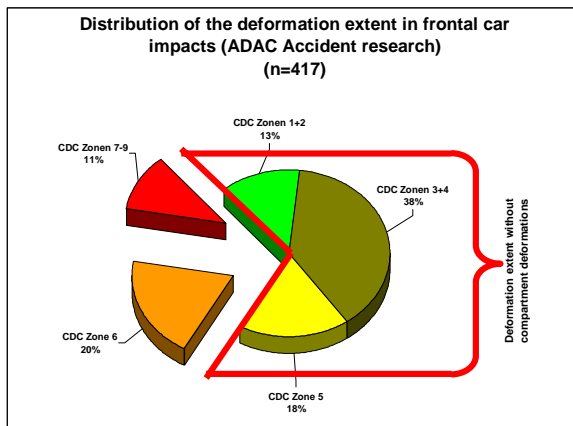


FIGURE 21 (ADAC), CDC LEVEL OF DEFORMATION IN FRONTAL IMPACT OF CARS

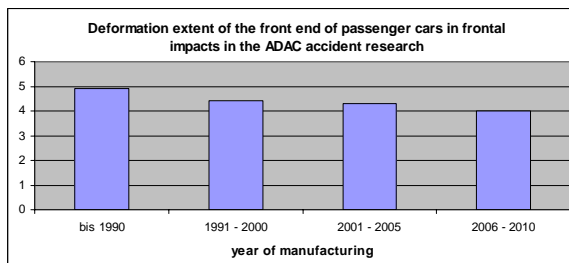


FIGURE 22 (ADAC), CDC LEVEL OF DEFORMATION ACCORDING THE BUILT LEVEL

The result of stable passenger compartments and no intrusion in the vehicle interior is the reduction of the crumple zone to the vehicle front, while the length of the zone is limited towards the A-pillar.

The overall result out of this reduction of deformation area is a higher deceleration of the cars during an impact. This could also be found while analysing the vehicle decelerations of cars tested by Euro NCAP, especially the vehicles of the compact class and the vehicles of the small sized cars and SUV's show higher decelerations of the latest model than the earlier built level ones. Not only the maximum deceleration rises, also the mid deceleration is higher.

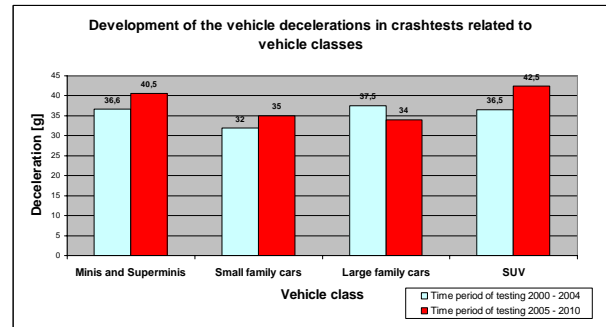


FIGURE 23 (ADAC), SHIFT OF VEHICLE ACCELERATIONS OVER THE YEARS

A more detailed look on several cars of this classes show a rising deceleration with the introduction of the new model.

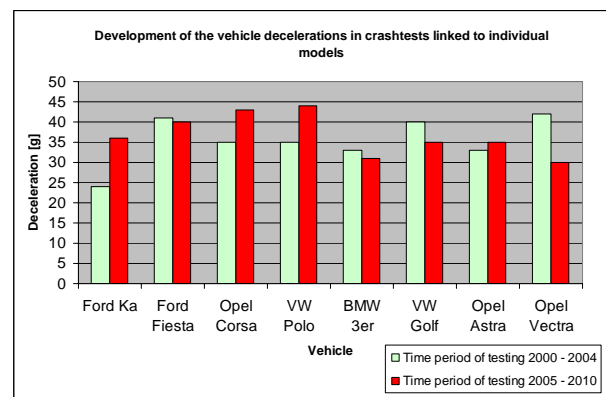


FIGURE 24 (ADAC), EXAMPLES OF THE SHIFTING OF ACCELERATION OF NEW MODELS

High accelerations could cause severe injuries. The analyses of the accidents including the reports from the medical rescue services and the hospitals are showing internal haemorrhaging due to injuries of the inner organs in the abdominal, lung and pelvic area. There are several reasons responsible for this kind of injuries. The most important point of all is the deceleration, which is responsible for the shifting of the inner organs. Only the blood vessels and the nerve fibres prevent them of further movement, resulting in damages of the nerves and the possibility of destruction of the arteries and veins this could cause the inner bleedings which could not be observed quite fast but in those cases very fast help is necessary.

Another mechanism of the deceleration is affecting the tissue fluids, such as water, blood etc. which is resulting in a higher intercellular pressure causing ruptures and other injuries of the tissue structures.

Figure 25 shows a comparison of chest acceleration of new cars tested in 2004 and before and after 2005.

It is obvious, that the accelerations measured in the chest area are significantly higher for superminis and SUV's of a later built level.

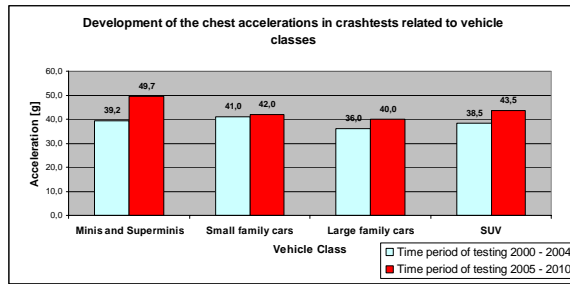


FIGURE 25 (ADAC), SHIFTING OF CHEST ACCELERATION OVER THE YEARS

The higher level of accelerations in the chest area seems to be responsible of the higher injury rate especially of elderly people.

But there is also an increase of risk for younger, smaller people, see Figure 13 and 14. This may be the result of safety systems working not perfect for all kind of humans. An adaption and optimization of the restraint systems to a certain group may be the reason for his findings. The loading of the chest could be reduced by the load limiter, which is used in nearly every new car. Over the last years the limitation force in Euro NCAP tests is between 4 and 5 kN. In only a few cases the limitation force is higher, then up to 6kN or lower down to 3,5kN.

But even with the use of the limitation of 4 to 5kN the chest acceleration raised over the years causing acceleration injuries and fractures. A logical correlation between the belt forces, chest acceleration and chest deflexion could not be seen in the Euro NCAP data.

The following risk curves are showing the correlation between the forces, age and the risk of an AIS 3+ injury.

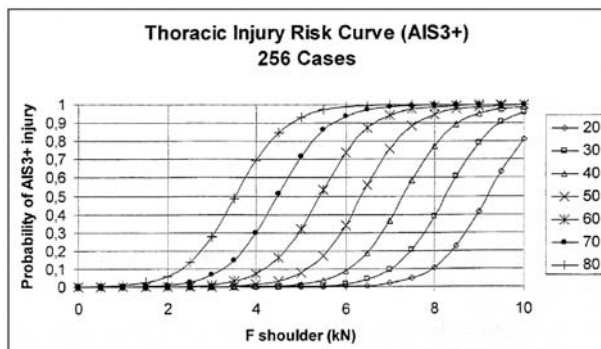


Figure 4. Probability of severe thoracic injuries (AIS3 or more severe) depending on the shoulder belt force and the occupant's age [7]

FIGURE 26 THORACIC RISK CURVES DEPENDING ON SHOULDER FORCE AND AGE [3]

CONCLUSIONS

The study of German accident data and accident statistics are showing a positive trend in reducing traffic accidents and also in the reduction of killed people in traffic accidents.

This numbers could also be seen in the European accident data.

So in general the injury severity of belted front seat occupants is on a very low level right now. The implication of consumer tests such as Euro NCAP is showing a positive effect in the development of passive safety over the last decade.

So the share of injured occupants decreased from 50% in vehicle models registered before 1990 down to 40% in models registered after the year 2000.

But a deeper look in the accident data and the injured body regions are showing problems in the thorax area. In those cases the injuries of the occupants in the real life accidents were not comparable with the tests conducted for consumer test programs, even when the vehicle and the kind of impact were comparable. Especially for elderly occupants, which are in general more frequently injured, independent from the vehicle age, seems to exist a slightly increased risk.

The risk for female occupants to suffer thoracic injuries however this is only observable on minor injury levels AIS 1-2 [1], while the ADAC data is showing a risk of 1.4 times higher for life threatening injuries.

For smaller persons <165cm there is also in increasing risk of thorax injuries at the level of AIS 1-2.

Future developments in consumer test programs should take this development into account. The actual test condition and the actual dummy is not able to reflect the injuries in the Thorax area. Investigation should be put in the development of new test tools to address this issue. A short term solution would be the use of results of the Thorax project and an update of the actual dummy and injury criteria.

Consumer Test/Accident Research

T. Unger, ADAC
V. Sandner, ADAC

Acknowledgement: Ford kindly provided the GIDAS data to ADAC

REFERENCES

- [1] GIDAS German In-Depth Accident Study,
- [2] ADAC Accident Research
- [3] Zellmer et al.; Optimized pretensioning of the belt system, 2004

Method to estimate the field effectiveness of an automatic braking system in combination with an adaptive restraint system in frontal crashes

Anja, Reßle
Markus, Lienkamp
TU Munich
Germany
Franz, Fürst
Audi AG
Germany
Paper Number 11-0281

ABSTRACT

Current passive safety standards have already achieved a very high level of occupant protection. This is confirmed year by year through declining numbers of traffic related fatalities. This trend is assumed to continue because more and more vehicles on the road are designed to fulfill strong safety requirements especially in high speed crashes.

In order to further improve frontal crash protection active safety systems like automatic braking systems are introduced to the market. These systems are designed to mitigate the crash severity and they are expected to have a great impact in further reducing the number of injured persons in traffic accidents.

This paper will discuss a method to estimate field effectiveness of an automatic braking system in combination with an adaptive restraint system in frontal crashes.

The method is based on the German In-Depth Accident Study GIDAS. Accidents are clustered in relevant car-to-car scenarios. In each scenario the effect of an automatic braking system and of an adaptive restraint system on the injury outcome is analyzed. The sum of all the injury risks is weighted with the relevance of each scenario and the expected value of MAIS3+ injured persons is calculated with and without the integrated safety system.

INTRODUCTION

In the year 2009 more than 35.000 fatalities occurred in the EU in traffic accidents and more than 1.5 million persons were injured. The cost for society of these accidents including physical and psychological damage to the victims and their families represent approximately 130 billion € in 2009. Based on that societal burden the European

commission proposes to continue with the target of reducing the overall number of road deaths by half in the European Union by 2020 starting from 2010. In order to achieve this strategic goal the European commission has identified seven objectives for the next decade. Two of these objectives are safer vehicles and promoting the use of modern technology such as advanced driver assistance systems [1].

During the last decades also in the U.S. a great success in increasing road safety was achieved as Figure 1 shows.

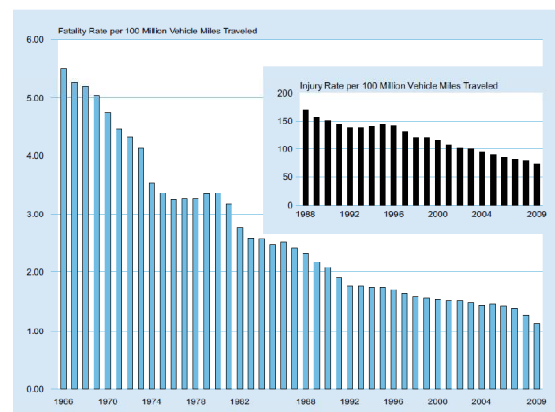


Figure 1. Motor Vehicle Fatality and Injury Rates per 100 Million Vehicle Miles Traveled, 1966-2009 in the US [2]

From 2008 to 2009 fatal crashes decreased by 9.9 percent, and the fatality rate reduced in 2009 to 1.13 fatalities per 100 million vehicle miles of travel. Furthermore, the injury rate per 100 million vehicle miles traveled decreased by 6.3 percent from 2008 to 2009. The decreased numbers of fatalities certainly are a result of common efforts in the fields of regulatory and traffic laws, enforcement, infrastructure, traffic education, post accident care and vehicle technology. Regarding vehicle technology a lot of new safety technologies within the last 50 years have contributed to this positive trend. Although passive safety systems are

nowadays well-engineered there is still room for improvements. Moreover, the trend in car safety is towards integrated and adaptive safety systems.

Active safety systems like automatic braking systems are designed to mitigate crash severity. These systems have already been introduced to the market, because they are expected to be very effective in reducing the injury outcome of traffic accidents. The most current efforts in development of restraint systems tend towards adapting the restraint performance to different crash parameters. In order to realize such an adaptive restraint performance new components like adaptive airbags and adaptive load limiters have been developed and already found their way to the market.

Therefore, the largest benefit for reducing the injury outcome in traffic accidents is expected by combining active and passive safety systems to an integrated system. Such an integrated safety system is not only effective during the accident. In general it assists the driver in the complete accident causation process (see Figure 2).

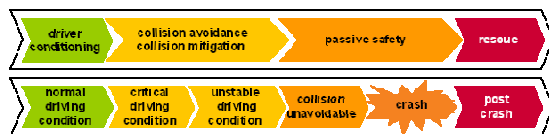


Figure 2. Process of accident causation and operating scheme of integrated safety systems [3]

In regular driving situations, condition safety of the driver should be assisted. That means that a good physical and psychological condition of the driver has to be assured. To this category belong all activities and systems supporting the reduction of the driver's workload and thus hold the probability for errors as low as possible. An example of such a system is driving comfort, air conditioning or seat design. In critical and instable driving situations, an integrated safety system helps to avoid an accident or to mitigate the accident severity via adequate countermeasures of the driver or an automatic system like an emergency braking system. If the collision cannot be avoided, passive safety measures will mitigate the accident outcome. The main issue is the evaluation of the efficiency of such an integrated safety system.

Benefits of passive safety systems can be evaluated by means of crash tests. These crash tests are

crucial and an indisputable method to develop cars which provide maximum protection for vehicle occupants as well as pedestrians and other road users. Repeatability is an important requirement in crash tests which can be achieved by standardized test configurations, the test itself and the instrumentation. Crash tests enable a view into higher accident severities compared to real world accident databases.

Active safety systems intervene before the collision and therefore modify the entire accident sequence.

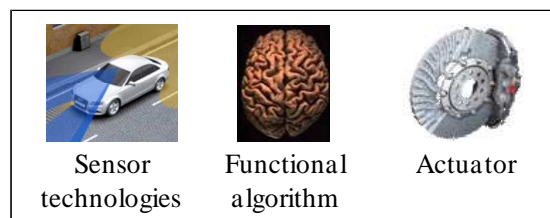


Figure 3. Components of an active safety system [4]

Figure 3 shows the components of an active safety system. An example of such a system is a crash imminent braking system. A sensor monitors the environment in front of a vehicle. If a critical situation occurs an algorithm determines whether a driver has already applied full braking power or not. If he has not and the collision is unavoidable, a braking actuator is activated and mitigates the accident severity. But how efficient is such an active safety system? Nowadays there are only a few methods available for evaluating the efficiency of an active safety system.



Figure 4. Estimated benefit of integrated safety systems [3]

Figure 4 shows the expected benefits of active and passive safety measurements. Passive measurements have already reached a very high level and a good market penetration. For the future active safety systems are expected to have a large

potential for improving safety system benefits, but their market penetration is still poor. So the maximum efficiency is expected through combining active and passive measurements in an integrated safety system.

Therefore, the objective of this paper is the presentation of a method enabling the computation of the efficiency of such an integrated safety system based on real accident data.

STATE-OF-THE-ART

Busch [5] developed an assessment methodology for the prediction of safety benefits of a driver assistance system such as brake assist or an emergency braking system. Figure 5 shows the schematic process of the automated individual case analysis.

The required data is taken from GIDAS (German In-Depth Accident Study) [6]. At first the real accident scenario sequence from GIDAS is simulated without any active safety systems. Second, a kind of virtual prototype is generated, i.e. accident scenarios are simulated with an active safety system. The simulation requires the change of each single scenario when an active system like an emergency brake is available. At first a safety benefit is calculated based on changes of physical measurements, e. g. reduced collision speed.

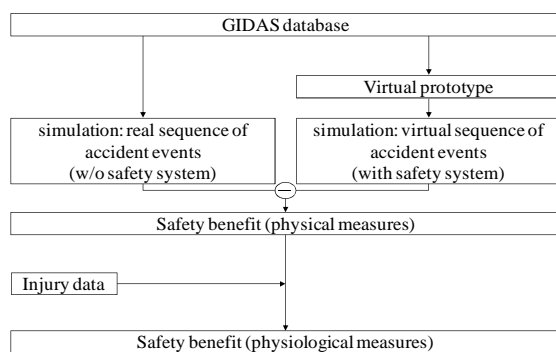


Figure 5: Schematic process of the automated individual case analysis [5]

Besides the information on accident circumstances, GIDAS also includes information on injuries of persons involved in the accident. These injury data are used to establish the so called injury-risk-functions. These functions describe the relationship of physical measurements such as collision speed and the injury risk. By using this relationship the

calculation of a safety benefit of an active system in terms of injury reduction is possible.

For the first time, this method provided an assessment of active safety systems based on real world accident data for all kinds of road traffic participants such as car occupants, vulnerable road users etc. This method is useful if the effects of an active safety system on the changes of a crash scenario outcome are easy to model. But if the complexity of an integrated safety system grows a new procedure to evaluate the effects has to be developed. That means that in each discrete time step the changes in the environment and in the decision making module of the active safety system is necessary to be analyzed. Therefore, the methodology from [5] had been revised and enlarged in [7].

The assessment method, PreEffect-iFGS, presents a procedure to assess the real-world safety benefit of integrated pedestrian protection safety systems (IPPSS). The schematic procedure is depicted in Figure 6. Initially, the real-world accident data from GIDAS are imported in a system simulation tool for reconstructing the original event of the accident into a simulation scenario. Next the changes to the original event of the accident in case of the existence of an integrated safety system is analyzed. For this each system component like sensor technology, algorithm or actuator is modeled. In an early stage of the system development general idealistic assumptions are made for these component models. Later on in the development process these component models are getting more and more realistic by using test data to validate the component models. The influence of various passive safety measures is implemented via modeling varying injury-risk-functions using the “Injury-Shift-Method” described in [8]. Depending on the location of the pedestrian impact on the vehicle, injuries will be reduced to minor injury if the passive safety system of the car shows good results at the point of impact. The effect of the safety system in the event of the accident is simulated based on the original scenario. Modified physical measures are also correlated to a risk of injury for each individual case allowing determination of the safety benefit of an IPPSS in terms of reduction of injured pedestrians for various active and passive components.

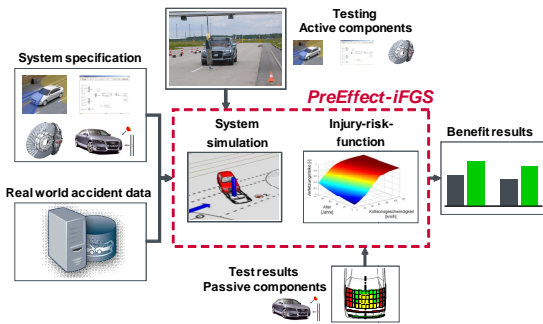


Figure 6. Method for assessment of integrated safety systems PreEffect-iFGS [7]

For the first time it is possible to model an integrated safety system for IPPSS with real components. Even real algorithms can be implemented and their effect on the real-world accident data can be determined.

The main focus of this method lies on injured pedestrians and not on occupants. However, effects of an automatic braking system on a driver or the effect of various adaptive restraint systems is not considered. Therefore, taking into account the safety benefit of integrated safety systems in car-to-car collisions, PreEffect-iFGS has to be extended.

In [9] a new method to determine the safety benefit of integrated safety systems in car-to-car collisions based on actual real-world accident data is presented. The schematic process of this method is shown in Figure 7, displaying an improved PreEffect-iFGS methodology shown in Figure 6.

The method is classified into two parts. In the first part, the database is updated to current safety standards, i.e. the reported benefit from a novel integrated safety system is achieved not only by taking into account current safety standards, but “on top” of these current standards.

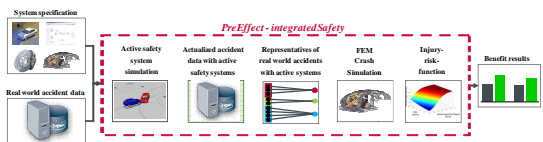


Figure 7. Method for assessment of integrated safety systems

In the second part, changes to the loads of an occupant because of the new integrated safety system are calculated via PC-Crash and occupant simulations.

METHOD

In this paper a first application of the method described in [9] on a subset of load cases with high relevance in real world accidents is demonstrated. In addition, an extension of the method towards material damage will be presented.

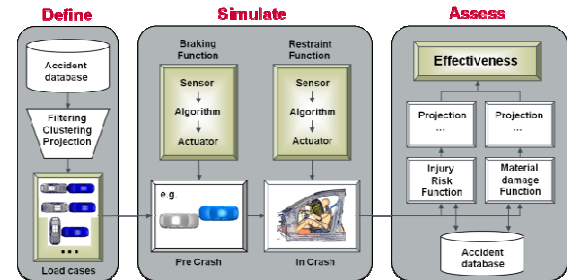


Figure 8. Three Steps to assess the effectiveness of an integrated safety system

The method is divided into three steps. First the load cases of interest are defined. Therefore, an accident database has to be chosen and analyzed for those scenarios being very relevant for real-world accidents. The major goal of this paper is the calculation of the effectiveness of an automatic braking system in combination with an adaptive restraint system in frontal crashes. Therefore, only frontal collided passenger cars will be considered. In the second step the implication of active and passive safety systems on the road users and the vehicles is simulated. To determine the changes to each impact because of an automatic braking system each scenario is simulated with PC-Crash. The effect of an adaptive restraint system in terms of changed occupant loads is simulated in an occupant simulation. In the third step for each simulated load case the changed risk of an AIS3+ injury to the occupants is calculated. Furthermore, the changed impact speed is used for estimating a reduction to material damage.

Step 1: Define

The method applies data from the In-Depth accident study GIDAS, which contains information about the accident, affected vehicles and people involved in the accident. GIDAS is the largest project on investigation of accident data in Germany. Since 1999 about 2000 accidents per year are collected in the greater areas of Hanover and Dresden according to a statistical sampling plan. GIDAS compiles only accidents with at least one injured person [6].

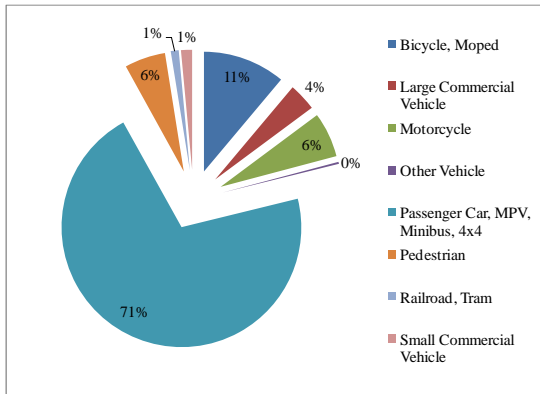


Figure 9. Distribution of the type of road users

For this study only accidents between passenger cars are relevant. In Figure 9 the distribution of the type of road users is shown. 71% of all accident participants in GIDAS are occupants of passenger cars, MPVs, Minibuses or 4x4.

The distribution of the collision opponents of these 71% involved people are shown in Figure 10. 54% of the opponents are passenger cars themselves. Another 10% of the opponents are objects like trees or road signs. For this study only the collisions between two passenger cars are considered.

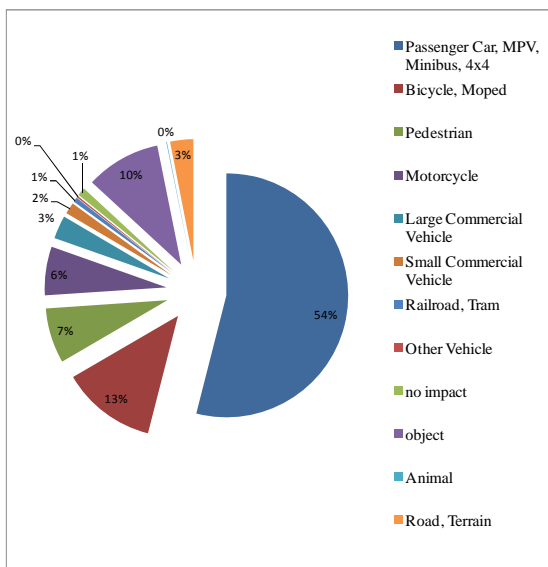


Figure 10. Distribution of collision opponents of passenger cars

Since several studies of real-world accidents have shown that accidents could be avoided if the car is equipped with an electronic stability program (ESP) the EU Parliament requires ESP system being obligatory in all new vehicles from 2013 on. In the considered database 10% of the passenger

car occupants are involved in a skidding accident. These accidents are removed from the database.

11% of the remaining occupants are involved in multiple collisions, i.e. collisions between more than two opponents. Such accidents are very complex and the effect of active and passive safety systems is limited by a lot of constraints and assumptions. In order not to overestimate the effect of such an integrated safety system only the first collision between two opponents is considered.

Figure 11 shows the distribution of the vehicle segments in the remaining database. The segments are chosen according to the coding of the German Kraftfahrtbundesamt (Federal Motor Transport Authority).

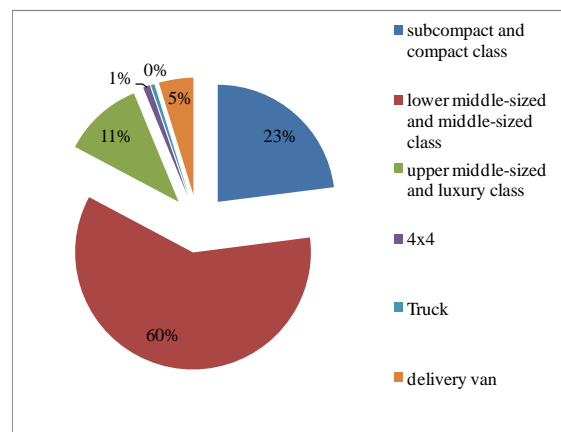


Figure 11. Distribution of the vehicle segments

In the chosen data from GIDAS about 94% of the vehicles belong to the subcompact, compact, lower middle-sized, middle-sized, upper middle-sized or luxury class. Only 6% of the persons involved in the accidents are occupants of a 4x4, Truck or delivery van. Therefore, for the following analysis these types of vehicles are no longer considered.

The distribution of the vehicle segments matches the homologation numbers of the Kraftfahrtbundesamt very well. That means that each vehicle has the same probability to collide with each other segment and therefore, no combination of vehicle segments exists, which has a larger probability of accident involvement.

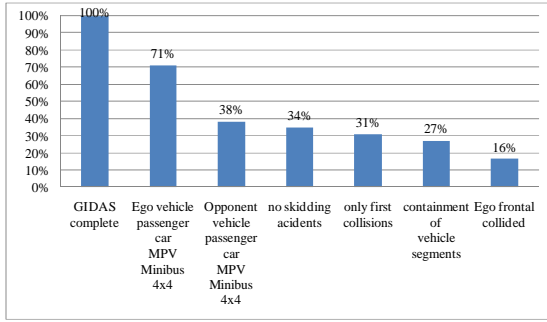


Figure 12. Summary of the filtering of the database

In Figure 12 a summary of the filter steps described above is shown. After all of these filter steps 27% of the people in the GIDAS database remain. This subset is considered for later analysis.

Next the database is analyzed concerning the impact constellations. Each impact constellation is described by the point of first impact and the angle between the longitudinal vehicle axes at the beginning of the crash.

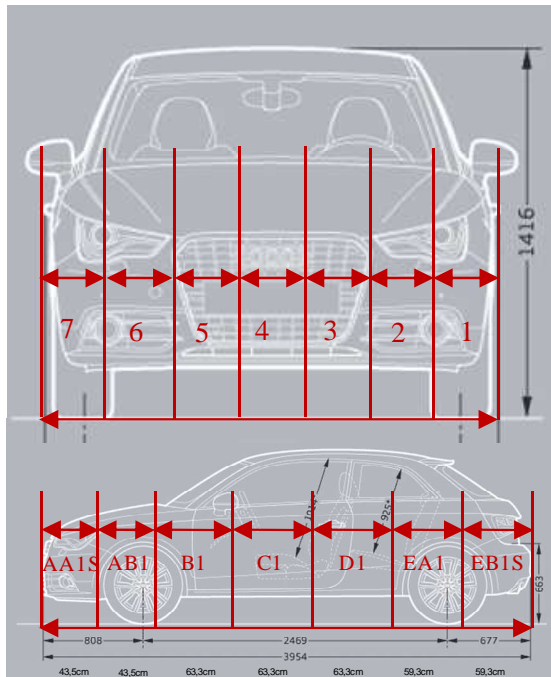


Figure 13. Clustering of the vehicle geometry

The point of first impact is defined as the distance from the foremost point of the car to the impact point towards the longitudinal vehicle axis and from the middle of the vehicle to the left or right. To determine generic impact points the width of the vehicles is sub-divided in seven equal sized parts (see Figure 13). The length of the vehicles also is divided in seven parts according to crash relevant

areas, for example A-pillar, middle of the driver's door or B-pillar.

In order to describe the point of first impact regarding the clustering as shown in Figure 13 some assumptions have to be made. The homologation statistic of the Kraftfahrtbundesamt lists all the vehicles, including make and type, and how many of this vehicle models are homologated. From each segment of interest about 50% of the homologated passenger cars are analyzed according to their geometrical partition. The segments are grouped as shown in Table 1.

Table 1. Summary of the segments

ID	Segment	Combined segment
A00	Subcompact class	Small
A0	Compact class	
A	Lower middle-sized class	Medium
B	Middle-sized class	
C	Upper middle-sized class	Large
D	Luxury class	

For each of the combined segments the mean value of the clustering shown in Figure 13 is calculated in terms of percentage of the length of the car (see Table 2).

Table 2. Clustering of the crash relevant impact areas

Cluster	Small	Medium	Large
AA	11%	11%	12%
AB	11%	12%	13%
B	17%	14%	12%
C	18%	14%	12%
D	17%	14%	12%
EA	13%	17%	19%
EB	13%	18%	20%

The combination of the points of first impact and the impact angle describes the impact constellation. Figure 14 shows an example of the clustered impact combinations. This combination describes a rear-end collision with an angle of 45° between the longitudinal vehicle axes.

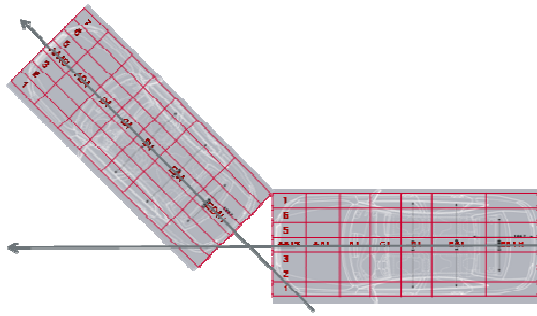


Figure 14. Generic impact constellation

This type of clustering generates 140 impact constellations which describe the selected database.

Each of these constellations can be assigned to an overall impact situation, e.g. rear-end collision.

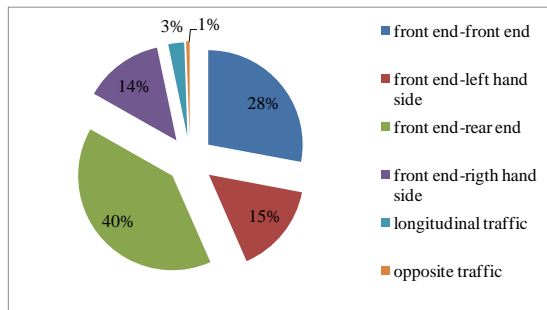


Figure 15. Distribution of overall impact types

Figure 15 shows the distribution of these overall impact types. About 40% of the selected occupants are involved in rear-end collisions. Another 28% are collisions between the front-ends of the opponents.

For the following analysis only collisions with at least one frontal collided vehicle are considered. About 61% of the involved occupants of the interesting database are passengers of frontal collided cars, i.e. 16% of all the persons in the GIDAS database according to Figure 12.

To determine the relevance of each scenario the distribution of the seat occupancy has to be analyzed (see Figure 16). 67% of the frontal collided occupants are drivers, 22% are passengers and 11% are sitting in the rear of the car.

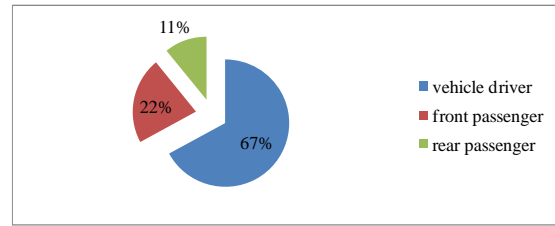


Figure 16. Distribution of seat occupancy

In order to select scenarios with a high relevance in the field, in this analysis only the driver of the frontal collided car is considered. About 66% of the drivers are male and 34% are female. In step 2 of the method (SIMULATE) the effect of passive safety systems on the occupant is simulated with HIII-dummies.

Table 3. Comparison of the GIDAS population and common dummy geometries

Percentile	Weight GIDAS	Weight HIII dummy	Height GIDAS	Height HIII dummy
5 th	52 kg	54 kg	158 cm	152 cm
50 th	74 kg	77.7 kg	173 cm	175 cm
95 th	100 kg	101 kg	188 cm	188 cm

For this, the size and weight of the occupants in the database have to be compared with the dummy geometry. Figure 17 and Figure 18 show the cumulative distributions of the height and weight of the occupants in GIDAS. In Table 3 the comparison between the occupants in GIDAS and the dummy geometries is listed. The dummy sizes and the GIDAS occupant sizes are matching very well.

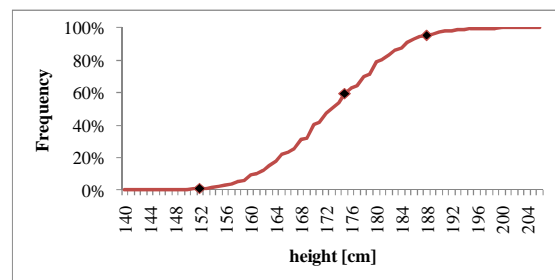


Figure 17. Cumulative distribution of the occupant height

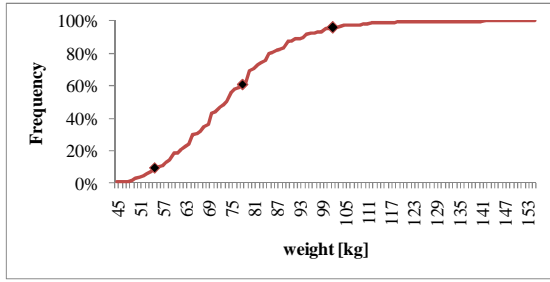


Figure 18. Cumulative distribution of the occupant weight

The goal of this paper is do determine the effect of an automatic braking system in combination with an adaptive restraint system based on real-world accidents. Therefore, different accident severities will be considered, to show the potential of the adaptive restraint system. As a measurement for the accident severity the change in velocity, Δv , due to the collision is used.

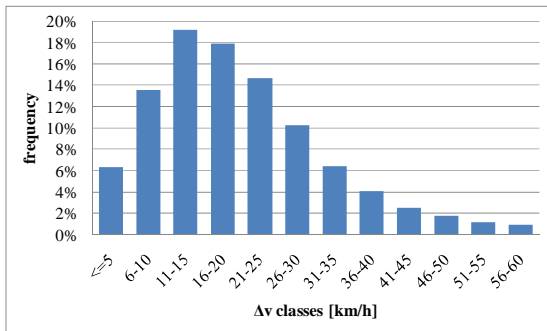


Figure 19. Distribution of the Delta-v classes

Figure 19 shows the distribution of Δv in the selected subset database. 20% of all frontal collided occupants suffered a Δv less or equal to 10km/h and another 37% of this occupants are involved in accidents with Δv between 11 and 20km/h. In summary about 57% of the frontal collided occupants are involved in relatively low accident severities.

In the next step representative accidents for all the accident severities are determined. For accident severities Δv less or equal to 40km/h (about 92% of the frontal collided cars) fully covered rear-end collisions with different relative collision velocities are chosen. The relative collision velocity v_{rel} is the velocity of the frontal collided vehicle minus the velocity of the rear end collided vehicle at the time of collision.

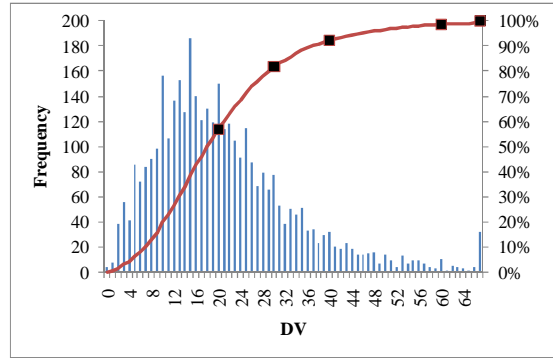


Figure 20. Cumulative distribution of Δv in the subset dataset

In Figure 20 the distribution of Δv is supplemented with the cumulative distribution. The first three black marked points are representatives for a mid-class crash severity. They are equivalent to completely covered rear-end collisions with a v_{rel} of 40, 50 and 60km/h.

As representatives for high-class crash severity with Δv greater than 40km/h two crash tests known as the Euro NCAP and the US NCAP frontal crash tests are selected (see Figure 21). These both tests cover about 99% of the accident severities in real life accidents.

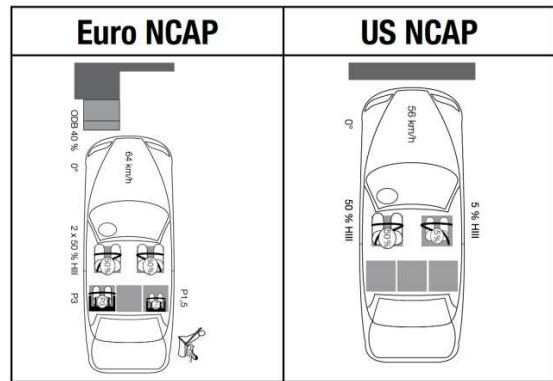


Figure 21. Load cases for $\Delta v > 40\text{km/h}$

Next the braking behavior of the driver has to be analyzed.

If the driver adjusted an average deceleration rate higher than 6m/s^2 the deceleration is boosted up by the brake assist system (BAS) to the maximum available deceleration dependent on the ground in each considered accident scenario. Because the EU decided to regulate the installation of BAS in new cars from November 2011 on, the effect of a 100% equipment rate of the BAS has to be accounted for.

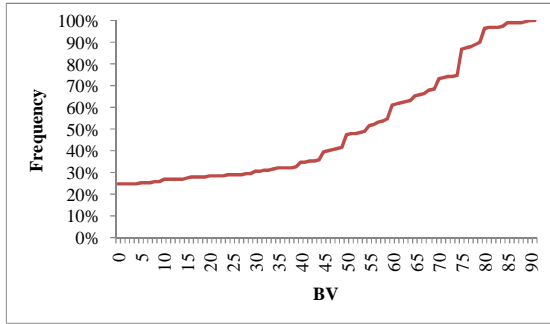


Figure 22. Cumulative distribution of the deceleration rate (BV) [10*m/s²] in the subset dataset

In Figure 22 the cumulative distribution of the deceleration rate of the driver in the subset database is shown. About 25% of these drivers are not braking at all, another 30% of the drivers adjusted a deceleration rate less than 6m/s². Therefore, in about 45% of the frontal collided accident scenarios a BAS is boosting up the deceleration to the maximum available deceleration rate. This maximum deceleration rate is only limited by the maximum transferable braking performance due to ground floor restrictions in each considered accident scenario. Based on this analysis an automatic braking system is able to reduce the collision speed in 55% of the subset database.

One possibility to account for the braking behavior of the driver in the method is to introduce weighting factors. Based on the analysis above for the automatic braking system a weighting factor of 0.55 is introduced, whereas for the adaptive restraint system a weighting factor of 1.0 is chosen, because it is able to be fully effective in each single accident.

In this section an exemplary filtering of the database towards load cases with high relevance in real life accident scenarios was conducted. In the next step the influence of an automatic braking system in combination with an adaptive restraint system on the selected load cases will be simulated.

Step 2: Simulate

Exemplarily for the mid-class crash severity accidents the influence of an automatic braking system is simulated based on three rear-end collisions from GIDAS (ANB1 - ANB3). For that these load cases are reconstructed in PC-Crash, one of the most common accident reconstruction software. In Table 4 the parameters of the original

scenarios and the changes to them, if an automatic braking system (ANB) is active, are listed.

Table 4. Parameters of the load cases ANB1-ANB3

Parameter	ANB1	ANB2	ANB3
V0	40km/h	50km/h	60km/h
BV	0m/s ²	0m/s ²	0m/s ²
available friction	8.8m/s ²	8.8m/s ²	8.8m/s ²
VK _{rel}	39km/h	50km/h	60km/h
VK _{rel} *	32km/h	39km/h	49km/h
ΔVK _{rel}	7km/h	11km/h	11km/h

Compared to the original relative collision speed VK_{rel} a reduction of 7-11km/h (ΔVK_{rel}) in these load cases is possible. Definitely, the amount of ΔVK_{rel} depends on the setting of relevant system parameters and environmental circumstances.

Next, the effect of an adaptive restraint system on the loads to the occupants is simulated. Such an adaptive restraint system consists of an adaptive belt and an adaptive airbag. The restraint behavior of these adaptive components is adaptable to specific parameters of real-world accidents. Several studies have shown that it is advantageous if the adaptive components are able to adapt their restraint behavior to the crash severity and to the anthropometry of the occupants [10].

The effect of such an adaptive restraint system on the loads on the occupants is simulated with specific simulation software, e.g. PAM Crash. Because current occupant compartments are designed for high crash severities it is assumed that the occupant compartment is still stable in the considered mid-class severity accidents. Therefore, only one occupant compartment model is used for the simulation of the different crash severities.

To determine the effect of an adaptive restraint system, the scenarios ANB1-ANB3 and both the load cases from Figure 21 are simulated three times.

First of all, the original scenario without any braking system and without an adaptive restraint system is modeled. In a second step, the scenarios, changed by a braking action, are simulated without the adaptive restraint system. In a final step, the changed scenarios with an adaptive restraint system are modeled. As a result from the occupant

simulation the different loads on the occupants are calculated.

In the second step (SIMULATE) of the method, the influence of an automatic braking system and an adaptive restraint system on the selected load cases was simulated. In the third step of the method, the effectiveness of these systems is estimated.

Step 3: Assess

In order to assess the effectiveness of an automatic braking system in combination with an adaptive restraint system the simulated changes of the load cases have to be transferred in terms of injury reduction or reduction of material damage.

For determining the influence of changed occupant loads on the injury outcome injury risk functions have to be used. In order to provide for comparability with legislation and consumerism at the best, the injury risk curves from the FMVSS 208 [11] are used. The considered injury level is the so called MAIS3+, i.e. all occupants with at least one body region injured more than AIS 2 (AIS stands for the Abbreviated Injury Scale). To calculate the overall risk of an MAIS3+ injury the assumption is made, that the injuries of each body region are independent. The combined MAIS3+ injury risk is calculated after the new US NCAP regulation for p_{joint} . For frontal collisions p_{joint} combines the injury risks for the head, the neck, the chest and the femur.

In this way a change of injury risk can be evaluated for each specific load case. The sum of all the MAIS3+ injury risks is the expected number of MAIS3+ injured persons in the specified load cases. The reduction of MAIS3+ injured occupants by a new system (like an automatic braking system and/or an adaptive restraint system) defines the field effectiveness of this system.

Besides the injury outcome also the changes to material damage are of interest.

The material damage of a vehicle in an accident depends on a lot of factors. In order to determine the influence of automatic braking systems on the material damage some assumptions have to be done. First of all, the material damage of each car is limited by the residual value of the car. An analysis of the Schwacke-list [12] suggests an exponential degeneration of the residual value over the age of

the car. Under the assumption that the residual value after three years amounts to half the original price, the residual value dependent on the age of the car can be calculated as

$$RV(t) = OV \times 2^{-\frac{t}{3}} \quad (1)$$

where RV is the residual value, t is the age of the car in years and OV is the original value of the car. Because the database contains a lot of different cars, for each combined segment an average OV is estimated (see Table 1).

Table 5.
Estimated average original value

Combined segment	Estimated average OV
Small	17.500 €
Medium	35.000 €
Large	75.000 €

In order to calculate the resulting cost of repairing depending on the crash severity several crash tests were analyzed. The analysis showed that the cost of repairing is more or less directly correlated to the crash severity Δv . Therefore, a regression analysis between Δv^2 and the cost of repairing damage (CORD) is conducted (see Figure 23).

$$CORD(\Delta v^2) = 208.82 \times \Delta v^2 - 1048.5 \quad (2)$$

Formula (2) describes the correlation of Δv^2 in m^2/s^2 and CORD in percentage of the OV.

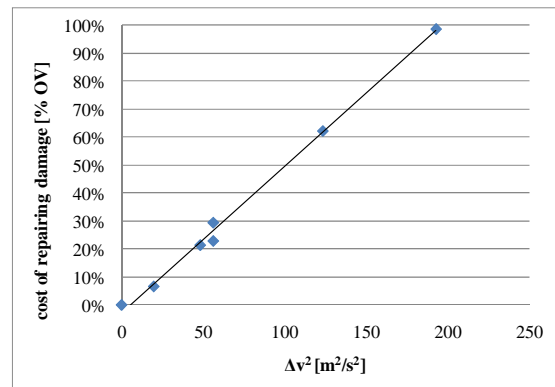


Figure 23. Regression of Δv over the cost of repairing damage

This function assumes that the cost of repairing damage does not depend on the segment of the car.

The material damage (MD) calculates out of a combination of formula (1) and (2).

$$MD(\Delta v^2, t) = \min_{\{\Delta v^2, t\}} (RV(t), \text{CORD}(\Delta v^2) \times OV) \quad (3)$$

The reduced cost of repairing is calculated out of the difference from the original MD without the braking system and the MD resulting from the reduced Δv .

As shown in this section the method allows an estimation of the changes to the injury outcome of occupants and the resulting material damage.

Summary and outlook

In this paper a method is described to calculate the effect of an automatic braking system in combination with an adaptive restraint system on the injury outcome of the occupants and on the material damage of the cars. The method is presented via some exemplary load cases with a high relevance in real-world accidents. The great advantage of this method is its modular composition.

The database can be replaced with other databases (e.g. U.S. accident statistics), whereby differences of vehicle populations or infrastructure can be accounted for. Therefore, the method allows estimating the effectiveness of integrated safety systems for arbitrary nations. For a worldwide prediction national accident databases have to be analyzed. In this regard harmonized accident databases with respect to representativeness, data structure and parameters according to the German In-Depth Accident Study GIDAS are required.

In the method the functions for determining the injury outcome and the material damage can be easily replaced by other functions. So the method is easily adoptable to the latest scientific findings, for example renewed injury risk functions. Also, the selection of the repairing cost function can depend on the specific realization of the automatic braking function components. Even if new types of dummies for the evaluation of vehicle safety are introduced into regulation and/or rating procedures the method is still valid because only the occupant simulation element and the injury risk function element have to be adjusted.

Although this method is very generic in the future a closer look to the robustness of the method is necessary. A further region of interest is the influence of the constitution of the load cases on

the calculated effectiveness. So the questions has to be answered how many and how detailed load cases must be chosen in order to get a valid prediction of the overall benefits. Also the sensitivity of the calculated effectiveness to the weighting of load cases is an interesting field of study.

Once the method is fixed in its constraints it can be applied to study the effect of integrated safety system parameters on the overall effectiveness of the system. Furthermore it is necessary to find out how strong are the relationships among relevant system parameters with respect to the largest achievable benefits and their limitations.

For example in order to study the benefits of an adaptive restraint system on the injury outcome new technologies for infinitely variable airbags and belts are desired because these components are expected to maximize occupant protection.

In the future an integration of additional elements to this method is planned to account for the latest developments in vehicle safety. Especially vehicle-to-vehicle or vehicle-to-infrastructure communication technologies are expected to have a great impact on further reducing fatalities and injured people. So we are looking forward to extend this method to assess also such kind of integrated safety systems.

Finally an extension of this method to all kind of road users has to be conducted in order to predict prospectively the changes to all the real-world accidents.

REFERENCES

1. European Commission, "Towards an European road safety area: policy orientations on road safety 2011 – 2020," Brussels, 20.7.2010
2. U.S. Department of Transportation, "Traffic Safety Facts 2009," DOT-HS-811-392
3. Gollewski, T., „Integrale Sicherheit - Herausforderungen, aktuelle Funktions- und Auslegungskonzepte aus Sicht eines OEMs,“ presented at Integrated Safety 2008, Germany, July 2-3, 2008.
4. Reßle, A., Schramm, S., Kölzow, T., „Generierung von Verletzungsrisikofunktionen für Fußgängerkollisionen,“ presented at 10th Crash.Tech, Germany, April 13-14, 2010.
5. Busch, S., „Entwicklung einer Bewertungsmethodik zur Prognose des Sicherheitsgewinns ausgewählter Fahrerassistenzsysteme,“ Ph.D. thesis, Technical University of Dresden, 2004.
6. Schramm, S., „Methode zur Berechnung der Feldeffektivität integraler Fußgängerschutzsysteme,“ Ph.D. thesis, Technical University of Munich, 2011.
7. Liers, H., „Benefit Estimation of the Euro NCAP Pedestrian Rating Concerning Real World Pedestrian Safety,“ ESV Technical Paper 09-0387, 2009.
8. Ressler, A., Fuerst, F., Heissing, B., Koelzow, T., Lienkamp, M., "Field Effectiveness Calculation of Integrated Safety Systems," 2011-01-1101 presented at the SAE 2011 World Congress, USA, April 12-14, 2011.
9. German In-Depth-Accident-Study (GIDAS), "accident investigation on the spot – Dresden and Hanover," <http://www.gidas.org/files/GIDAS.pdf>, Jan. 2011.
10. Schramm, C., Fuerst, F., Van den Hove, M., Gonter, M., „Adaptive Restraint Systems-The Restraint System of the Future,“ presented at 8th International Symposium Airbag 2006, Germany, December 04-06, 2006.
11. Department of Transportation, NHTSA, "Consumer Information; New Car Assessment Program," Docket No. NHTSA-2006-26555,
12. Schwacke, <http://www.schwacke.de>, March 2011.

1999, the GIDAS project has collected on-scene accident cases in the areas of Hanover and Dresden. GIDAS collects data from accidents of all kinds and, due to the on-scene investigation and the full reconstruction of each accident, gives a comprehensive view on the individual accident sequences and its causation. The project is funded by the Federal Highway Research Institute (BAST) and the German Research Association for Automotive Technology (FAT), a department of the VDA (German Association of the Automotive Industry). Use of the data is restricted to the participants of the project. However, to allow interested parties the direct use of the GIDAS data, several models of participation exist. Further information can be found at <http://www.gidas.org>.

ACKNOWLEDGEMENTS

GIDAS Acknowledgement: For the present study accident data from GIDAS (German In-Depth Accident Study) was used. GIDAS is the largest in-depth accident study in Germany. The data collected in the GIDAS project is very extensive, and serves as a basis of knowledge for different groups of interest. Due to a well defined sampling plan, representativeness with respect to the federal statistics is also guaranteed. Since mid

ANALYSIS OF THE PRE-CRASH BENEFIT OF REVERSIBLE BELT PRE-PRETENSIONING IN DIFFERENT ACCIDENT SCENARIOS

Mark Mages
Martin Seyffert
Uwe Class
TRW Automotive GmbH
Germany
Paper Number 11-0442

ABSTRACT

The goal of active belt systems is to reduce occupant movement in highly dynamic driving situations to increase both safety and comfort. In this paper the ability of such systems to reduce occupant displacement is quantified and the resulting increase in occupant safety is analyzed for different accident scenarios. These scenarios are characterized by the direction of occupant displacement as it results from vehicle dynamics prior to the accident such as braking or evasive steering and by the impact direction.

To identify the occupant displacement as initial condition for the chosen accident types, the inertial forces prior to the accident are reproduced in a test vehicle for the chosen scenarios. Different levels of reversible pre-pretensioning are used within these tests. A conventional belt system (no pre-pretensioning), a belt system with reactive pre-pretensioning (activation based on vehicle dynamics data) and a belt system with predictive pre-pretensioning (pre-triggered based on environmental sensors) are being compared. The occupant displacement is measured during these tests.

The results show, that a significant reduction of occupant displacement is possible using active belt systems. For instance forward head displacement during panic braking scenarios can be reduced significantly with reactive pre-pretensioning and even further with pre-triggered pre-pretensioning in comparison to the same scenario with a conventional belt system without pre-pretensioning.

The effect of reduced occupant displacement is studied using crash simulation and sled tests. In both cases the dummy is positioned according to the measured displacement values as initial condition. Characteristic injury values of these crash simulations and sled tests are compared to identify the effect of different levels of occupant displacement on injury probability.

Both simulation and sled tests demonstrate that a modified initial occupant position may result in an altered injury mechanism during the crash. The rapid deceleration in the tested panic braking situations for example leads to a forward displacement of the

occupant that in case of a subsequent front crash may result in a bag slap (caused by the reduced distance between occupant and instrument panel). The improved occupant position using an active belt could decrease the probability of a bag slap for the same scenario.

Lateral displacement with a subsequent frontal collision could have even more severe consequences on occupant injuries. The simulation results show that because of the lateral displacement of the occupant the contact with the frontal airbag may be misaligned and therefore airbag effectiveness could be reduced. As a worst case scenario the probability for a contact to the instrument panel could increase. This effect is intensified as the routing of the belt is influenced by lateral occupant displacement, which may reduce the effectiveness of the belt system in a crash. Reduced occupant displacement can avoid or mitigate the risk of such an injury mechanism.

In case of a rear impact with initial forward occupant displacement the changed occupant position results in injury rating values many times higher than those in nominal position. Again, reduced occupant displacement can mitigate this effect.

In conclusion reversible pre-pretensioning allows the reduction of occupant displacement and proves to have a direct effect on occupant safety in the examined scenarios.

INTRODUCTION

Since their introduction into premium class vehicles in 2002, reversible belt pre-pretensioning systems spread into upper-class and mid-range vehicles and it is expected that they will be available in compact cars in the near future. Unlike pyrotechnical belt pretensioners, reversible systems are activated prior to an imminent collision if the driving situation is identified as critical. As a result, seatbelt effectiveness is increased. This is especially useful in situations, in which the occupant is moving out of his initial position prior to the accident. This movement can be reduced, if the reversible belt pretensioner is activated in time, thus increasing occupant safety.

Occupant movement prior to an accident can be caused by inertial forces that result from evasion maneuvers or emergency braking. The analysis of accident data shows that for a significant number of accidents there was an attempt for counter-measures beforehand, like braking or evasive steering. In case of rear-end collisions which account for 25% of all accidents with occupant injury in Germany [1] about 40 % of the drivers of the rear vehicle initiated emergency braking with an additional 12 % that partially applied the brakes [2]. For intersection accidents, which account for about 23 % of all accidents with personal injury/fatalities in Germany [1], about 40 % of the drivers of the vehicle causing the accident and about 40 % of the drivers of the colliding vehicle with the right of way tried to avoid the accident by braking [3]. This leads to the conclusion that a substantial number of accidents occurs with occupant movement during the last seconds prior to the impact.

Based on vehicle dynamics data (e.g. provided by the sensors of the Electronic Stability Control (ESC) in case of an instable vehicle dynamics) or the data of environmental sensors (as used for collision avoidance/mitigation systems like an Automatic Emergency Brake (AEB) in case of an imminent rear-end collisions) the current driving situation can be analyzed. If potentially dangerous situations can be identified early enough, reversible belt pre-pretensioning can be activated while or even before occupant movement starts. The result would be reduced frontal (braking) or lateral (evasive steering or skidding) occupant displacement. As a result of reduced displacement the occupant's position should be closer to the nominal position as foreseen in the vehicle interior design, increasing the effectiveness of the restraint system in total.

It is important to note that reversible pre-pretensioners are no replacement for pyrotechnical pretensioners, as their activation during the pre-crash phase can not be guaranteed for all cases [4]. Furthermore, reversible pretensioners work on a much lower force level and the webbing pull-in speed is significantly lower compared to pyrotechnical pretensioners [5], [6]. Therefore the benefit of reversible pre-pretensioning is seen in activation before t_0 , while pyrotechnical units are triggered after t_0 .

MOTIVATION AND STATE OF THE ART

As most automotive components occupant safety systems are subject to continuous development. Airbags and pyrotechnical belt pretensioners are currently standard features of most passenger cars. Reversible pre-pretensioners are a relatively new advancement to improve occupant safety furthermore.

The goal of reversible pre-pretensioning is to remove belt slack before inertial forces cause the occupant to leave the nominal position. This reduces occupant displacement during pre-crash braking or evasive steering. As the restraint system is designed with respect to the nominal position (e.g. given by regulation or consumer testing) this position is expected to provide the best occupant safety. Therefore one of the major objectives of this study is to determine whether and in which scale the efficiency of the restraint system is affected negatively if the occupant is not in nominal position due to inertial forces (unlike studies regarding the effect of pre-pretensioning in secondary collisions as in [7]). A comparison of these results for conventional and active belt systems provides information on the benefit of pre-pretensioning regarding injury severity.

A parallel trend to reduce the number of fatalities and to increase traffic safety is the advancement in active safety. Collision avoidance/mitigation systems are state of the art in upper class vehicles. Based on environmental sensors using e.g. radar and video, imminent collisions may be identified in advance and an Automatic Emergency Brake (AEB) can be activated. Usually these systems also include a driver warning and autonomous braking is only initiated if braking is the only way to prevent a collision (at higher velocities the stopping distance is longer than the distance required for evasive steering [8]). Since an AEB may only be activated if there is no other option to prevent a collision, only collisions below a certain velocity can be prevented autonomously. Still, the reduction of collision velocity reduces the risk of severe or fatal injuries at higher speed). That is why depending on the accident scenario AEB activation will either reduce relative velocity at t_0 or avoid the collision.

Consumer organizations like Euro NCAP accommodate the development of active safety systems like AEB on their roadmap (e.g. beyond NCAP [9]). Dekra and BMW performed a crash test with automatic emergency braking prior to the impact to demonstrate the benefit of the reduced collision velocity in 2010 [10]. A full testing methodology for integrated safety systems is being developed in the EC-funded research project "ASSESS", including rating criteria and tools [11]. These examples can be interpreted as a first step of an adaption of current standard testing procedures to an integrated active and passive safety evaluation in future vehicles.

Current standardized crash tests are performed without braking or evasive steering and therefore do not include initial dummy displacement. On the other hand static Out-of-position (OOP) tests in which the dummy is positioned close to the airbag module are integrated

in current U.S. legislation to evaluate potential harm by the deploying airbag for non-nominal seating positions. These tests are based on the fact that especially unbelted occupants or children without proper child restraint system on the front seats might be in an unfavorable position closer to the airbag module at the time of airbag activation. However, currently there is no standard procedure available to analyze and evaluate the potentially reduced restraint system effectiveness due to pre-crash occupant displacement. The analysis of the relevance of initial occupant displacement with and without active belt systems on the efficiency of the restraint system in total provides information about the change of the injury mechanism if collision avoidance actions like evasive steering or emergency braking were attempted prior to the accident (either by the driver or by active safety systems) and thereby supports a further development and improvement of occupant safety systems.

APPROACH

The goal of this study is to analyze a potential real-world benefit of an active belt system. The study is divided into two major tasks. The first task is the analysis of the effect of active belt systems on occupant displacement. This is done in vehicle testing with real test persons. The test results can also be used as validation data for subsequent numerical pre-crash simulations with human body models (as done with similar tests within the cooperative project OM4IS [12]), but this will not be further discussed here.

Real test persons were chosen instead of test dummies because the kinematic of the dummy in the chosen scenarios turned out to be unrealistic in preliminary tests (Since the dummy is made for crash tests instead of driving scenarios it resists inertial forces in the order of 1 g stronger than the real occupant resulting in virtually no displacement). The resulting displacement values are then used as initial conditions for crash simulations and sled tests to identify the effect on occupant injury severity.

The driving scenarios chosen for the displacement analysis are examples for collision avoidance/collision mitigation maneuvers as they are attempted by the driver in critical situations if collisions are imminent: Emergency braking and evasive steering. These highly dynamic maneuvers can represent the dynamic status of a vehicle prior to an imminent crash. The deceleration or lateral acceleration of the vehicle causes inertial forces that affect the position of the occupants. The occupant position is identified during these tests using measurement equipment. All measurement is done for a test person on the passenger side as preliminary tests indicated that these values are more reproducible.

The second task is to identify the effect of occupant displacement on injury probability. For this a crash simulation is used for frontal and lateral impact while the rear impact scenario is analyzed in sled tests. In both cases the dummy or dummy model is positioned according to the measured displacement values from the vehicle tests as initial condition.

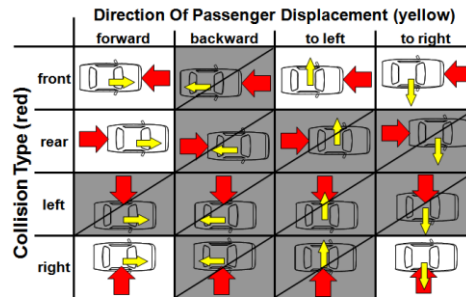


Figure 1. Combination matrix for collision type and displacement direction

As a result, major real world accident scenarios are represented by a combination of displacement direction and impact direction (See Figure 1). The accident scenarios with white background have been chosen for this study. Due to its limitation by the backrest of the seat backward displacement is not incorporated. All far side crash scenarios (impact from the left) are put aside as occupant injury is expected to be higher for a near side impact (see e.g. [13]). Rollover crashes have not been included in this matrix. Consequently the simulated or tested scenarios (passenger side) are

- Front impact with initial forward displacement
- Front impact with initial lateral displacement to the left
- Front impact with initial lateral displacement to the right
- Right side impact with forward displacement
- Right side impact with initial lateral displacement to the right
- Rear impact with initial forward displacement

The results provide information on how the injury mechanism is influenced by occupant displacement. This allows an estimation of the potential real-world benefit of reversible pre-pretensioning and offers indications for further improvement of active belt systems.

OCCUPANT DISPLACEMENT

Hypotheses

Dynamic driving as in collision avoidance maneuvers generates inertial forces which lead to a displacement

of the occupant. The goal of reversible pre-pretensioning systems is the reduction of occupant displacement to increase occupant safety. One hypothesis is that a reduction of occupant displacement can be achieved for both lateral and frontal displacement using reversible pre-pretensioning systems.

As for all safety measures, it is important to trigger pre-pretensioning as soon as possible as current pre-pretensioning systems do not provide enough force to move a displaced occupant back into position. As described earlier the intention is to preemptively remove belt slack to prevent high displacement values in the first place. That is why from the safety side point of view it is best to activate pre-pretensioning systems early (while avoiding unnecessary activations because of potentially unpleasant or even annoying reception). For rear end collisions a “predictive” activation of a reversible pre-pretensioning retractor based on e.g. radar sensors is already in series production. A second hypothesis therefore states that earlier activation improves the ability of a reversible pre-pretensioner to reduce occupant displacement.

Method and Tools

The tests were performed using one test person with weight and size similar to a 50%-dummy on the passenger seat (different persons for frontal and lateral displacement tests but no test person variation within one test scenario). As current reversible belt pre-pretensioning system the Active Control Retractor II (ACR2) was chosen, a retractor based reversible pre-pretensioner. The setup was tuned with a maximum ACR-generated belt force of up to 110 N for full retraction. The duration to reach the predefined shoulder force for full pre-pretensioning is approx. 120 ms, depending on driving situation and clothing.

Forward Displacement To measure forward displacement a vehicle equipped with a prototype Automatic Emergency Brake (AEB) was chosen. The AEB uses a 24 GHz radar sensor and a video camera. Based on these sensors the system recognizes the threat of an imminent collision and applies an emergency braking. By using an AEB instead of a driver the scenario is more reproducible regarding the brake pressure gradient (As long as the driver applies enough brake pressure to get all four tires into the Anti-lock Braking System (ABS) regulation for the duration of braking the deceleration is not influenced substantially by the driver). Also the activation time for the reversible pre-pretensioner can be adjusted gradually to identify the benefit of early activation based on environmental sensor data.

In braking tests the occupant was filmed from the driver side window using a video camera. The maximum frontal displacement for the occupants head and neck was identified from the video images using the intercept theorem and a defined scale on the vehicle as reference. Unlike the tests for lateral displacement this method only provides maximum displacement values and no progress of displacement over time. Vehicle dynamics data from the vehicle’s inertial sensors and the brake pressure sensor were used to ensure comparability of all tests as described for lateral displacement testing.

For this test scenario a comparison was done between a conventional belt system, a reactive reversible pretensioning (ACR2 triggered simultaneously with emergency braking) and a pre-triggered reversible pretensioning (ACR2 triggered 120 ms before emergency braking by the AEB control).

Due to wet road surface all tests for forward displacement were performed with a resulting maximum vehicle deceleration of about 7 m/s². Braking maneuvers on dry concrete may well provide deceleration levels of 11 m/s² and may therefore result in higher inertial forces and possibly higher forward displacement.

Lateral Displacement The tests for lateral displacement analysis were performed in a current, representative compact class vehicle. The test person was filmed using a video camera and displacement values were identified with video tracking software as shown in Figure 2. The video tracking software uses reference markers for tracking. Two markers have been placed on the test person, one on the chest and one on the forehead. In addition one marker was used on the belt to visualize the belt movement (This marker is not used for measurement; the belt movement was measured using a separate belt pullout sensor). Figure 2 also shows two reference points near the vehicle’s roof.



Figure 2. Measurement of occupant displacement using video tracking software

Using measurement sensors and the vehicles own sensors the following data was recorded in addition to the displacement values: belt force (near the shoulder), belt pullout, lateral and longitudinal acceleration, yaw rate, brake pressure, ACR2 motor current and ACR2 trigger signal. A flash is used to synchronize video and directly measured data. This way all signals (including lateral displacement) are measured over time and even complex scenarios like a double lane change can be analyzed. The measurement of vehicle dynamics data was also used to ensure that all repeated tests for one scenario are comparable and show similar values for lateral acceleration.

The first test scenario for lateral displacement analysis is the double lane change maneuver as defined in ISO 3888-2 [14]. The vehicle's velocity ahead of the course is regulated by cruise control. When entering the course the cruise control is turned off and the course is driven with engine brake. If a traffic cone is moved or knocked over during a run this run is considered invalid and repeated. Based on the recorded vehicle dynamics data all runs were checked for anomalies of velocity, lateral acceleration and yaw rate. Runs with high deviations were not used for the displacement analysis.

For the analysis the double lane change data is divided into parts to examine both sides of occupant displacement separately. Still the displacement values for left and right side are not independent from each other as the displacement during the first part of the maneuver may influence the further behavior of the test person. To allow an independent analysis of passenger displacement to both sides of the vehicle a curve with constant radius is introduced as a second maneuver.

The same curve is passed from both sides with all other parameters kept unchanged. With the exception of the course setup and the initial velocity the test procedure is identical to the double lane change maneuver, including the validation of vehicle dynamic data to ensure comparable test runs.

The occupant displacement with a conventional belt was compared to the reversible pre-pretensioner with partial and full retraction strength. In addition to a reactive system that identifies critical situations based on the vehicle dynamics a pre-triggered system is analyzed. The pre-triggering is done manually when entering the course. The pre-triggered variant provides a first impression of the potential additional benefit for further displacement reduction when integrating environmental sensors or e.g. road map data with reversible pre-pretensioners.

As driving the single curve maneuver does not create a critical situation there is no reactive activation of the belt pre-pretensioning system based on vehicle dynamics data. Therefore this scenario is only tested

with a pre-triggered pre-pretensioner and a conventional belt-system as reference.

Results

Forward Displacement For the braking maneuver no partial pre-pretensioning was used. All tests were performed with either a conventional belt system or with a full pre-pretensioning with approx. 110N maximum pre-pretensioning force. A distinction is made regarding the timing of the pre-pretensioner in relation to the emergency braking. The reactive system variant is triggered simultaneous with the AEB while the predictive variant is pre-triggered approx. 120 ms prior to AEB activation. The situation interpretation algorithm of the AEB provides a calculated time-to-collision (TTC) based on obstacle distance and relative velocity. From this TTC value the timing of the emergency braking is deducted and the timing for activation of the ACR is preponed for 120 ms.

The results are shown in Figure 3 in form of box plots. The box plots show the maximum and minimum deviation values (as dotted gray lines), the 25th and 75th percentile (represented by the "box"), the median (as dotted black line) and the mean value (as solid red line). For each variant separate plots visualize the head and chest displacement.

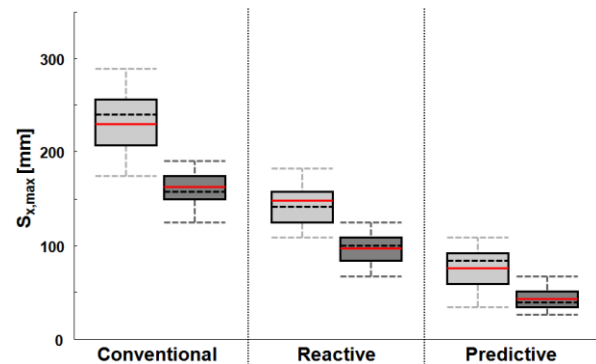


Figure 3. Maximum forward displacement in emergency braking maneuvers for head (light gray) and chest (dark gray), n=8 for each variant

Figure 3 shows that for a conventional belt system the maximum forward head displacement reaches maximum values of in average 232 mm. The corresponding chest displacement is 159 mm. This occupant displacement can be reduced significantly by the use of reversible pre-pretensioning. Simultaneous activation of the active retractor results in a displacement of 143 mm (head) and 92 mm (chest) respectively. The pre-triggered active retractor demonstrated a further reduction to 68 mm (head) and

46 mm (chest) respectively. The results of the unpaired two-sample t-test are highly significant for all variants and for both head and chest displacement. It should also be noted that the variance of displacement values is reduced by reversible pre-pretensioning.

Lateral Displacement The double lane change scenario as standardized evasive steering maneuver is divided into three parts for the analysis. This separation allows a detailed study of the displacement behavior in the different sections of the maneuver as illustrated in Figure 4.

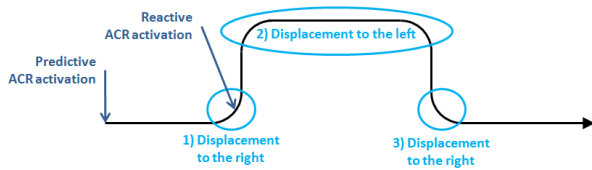


Figure 4. Illustration of the double lane change separated into three sections

The first section is characterized by the evasive steering to the left from the entry lane, resulting in occupant displacement to the right (towards the B-pillar - referring to the passenger as all data was recorded on the passenger side). The second phase includes the right curves when entering/leaving the evasive lane, resulting in occupant displacement to the left (towards the driver). The final left curve with occupant displacement to the right is considered as section three. Figure 5 shows the resulting occupant displacement (absolute values) as separate box plots for the three sections of the double lane change maneuver.

It is shown, that lateral head displacement values are consequently higher than the values for chest displacement. Also the variance of head displacement values is mostly higher than for chest displacement. That is why the following analysis primarily refers to the chest displacement because it allows higher significance levels.

For section 1 of the driving maneuver the reactive pre-pretensioner does not reduce the occupant displacement compared with the conventional belt system. This is due to the fact that the reactive system is activated near the end of section 1 (cp. Figure 4). That is why reactive pre-pretensioning may not affect lateral occupant displacement significantly in the first phase of the double lane change maneuver, while occupant displacement in the following segments 2 and 3 benefits from the reactive belt system. On the other hand, predictive (pre-triggered) pre-pretensioning showed significantly reduced occupant displacement in section 1, with an increased efficiency for the full retract with higher retraction force.

In section 2 of the double lane change reactive and predictive systems could provide a significantly improved occupant position. It can be seen that chest and head displacement values for partial pre-pretensioning with approximately 85 N can be reduced to a similar level for predictive and reactive pre-pretensioning activation. The full retraction force allows a higher reduction of occupant displacement (again for predictive and reactive triggering) with the exception of head displacement values for the pre-triggered variant.

The third chart in Figure 5 illustrates the occupant displacement towards the B-pillar in section 3 of the double lane change. A comparison of the results of the conventional seat belt with all tested active belt

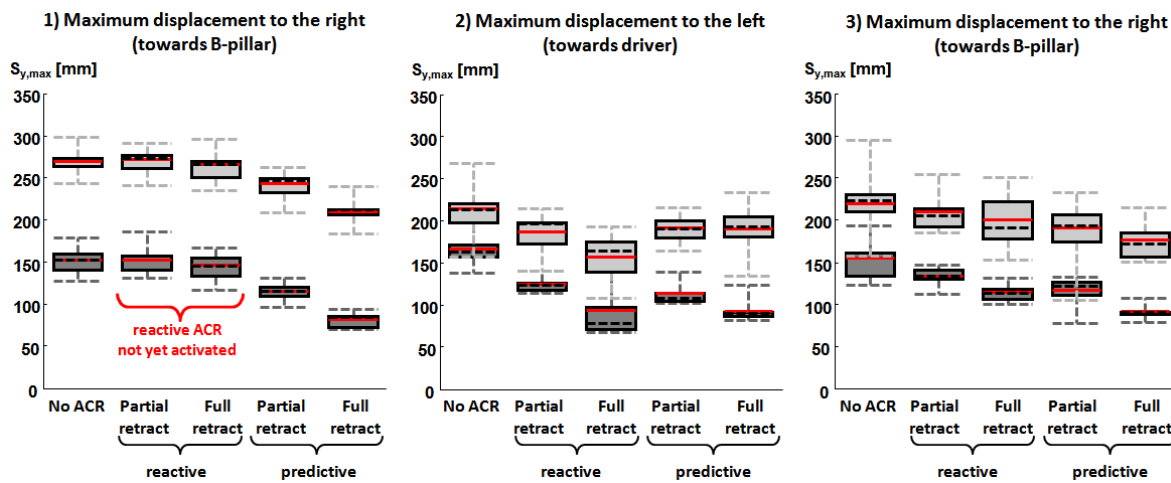


Figure 5. Maximum lateral occupant displacement for head (light gray) and the chest (dark gray), n=9

systems show a significant reduction of occupant displacement due to reversible pre-pretensioning. It can be seen that predictive triggering could further improve the occupant position compared to reactive triggering in section 3 although the displacement values for predictive and reactive systems are on a similar level in section 2 of the maneuver.

Table 1 sums up the displacement results of the double lane change maneuver for the passenger's chest, including the results of significance testing using unpaired two-sample t-test to compare displacement values for a conventional belt with the active belt variants. A significance level < 0.3 % is considered highly significant and marked with a blue background, a level < 5 % is considered significant and marked in light blue.

It can be seen that for chest displacement a significant or highly significant improvement is found for all systems except for reactive variants in section 1 as mentioned earlier.

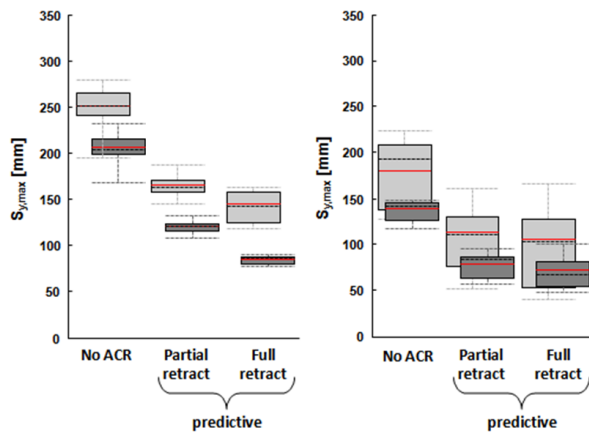


Figure 6. Maximum lateral head (light gray) and chest (dark gray) displacement for right (n=8) and left (n=9) curve

The box plots for lateral displacement for the constant curve are shown in Figure 6. The left chart shows the clockwise turn with displacement to the left (towards the driver), the right one presents the results of the counter-clockwise turn with displacement to the right

(towards the door and B-pillar). Since reactive pre-pretensioning is not activated during these maneuvers (the driving situation is not rated “critical” based on vehicle sensors as no loss of vehicle stability is detected), reactive variants have not been included in the corresponding tests and box plots.

Similar to the results for the double lane change the variance of head displacement exceeds the variance of chest displacement. It can be seen that predictive pre-pretensioning could further reduce occupant displacement significantly. The higher pretensioning force of the full retract provides an additional benefit regarding occupant displacement. This effect is higher for displacement to the left than for displacement to the right. In general, lateral occupant displacement towards the center of the vehicle seems to reach higher absolute values as displacement towards the B-pillar in this maneuver. A comparison of the lateral acceleration values shows similar levels of inertial force. The passenger door as limiting factor and the asymmetric belt geometry are assumed to be the cause of this variation.

A comparison of the average displacement values and the results of the corresponding significance test can be found in Table 2.

**Table 2
Max. lateral chest displacement in constant curve**

		Chest Displacement		
		no ACR	predictive	
			Partial retract	Full retract
Left Curve	Significance Level		0,0000%	0,0001%
	Displacement	138 mm	79 mm	72 mm
Right Curve	Significance Level		0,0001%	0,0000%
	Displacement	207 mm	122 mm	86 mm

It can be seen that the improvement of occupant position is highly significant for all of the tested variants in curve driving.

Conclusion

For all scenarios the displacement (both forward and lateral) could be reduced significantly by the use of a reversible pre-pretensioner. In conclusion the

**Table 1
Maximum lateral chest displacement in double lane change tests**

		no ACR	reactive		predictive	
			Partial retract	Full retract	Partial retract	Full retract
Segment 1	Significance Level		93,9903%	42,8243%	0,0134%	0,0000%
	Displacement	152 mm	153 mm	145 mm	115 mm	81 mm
Segment 2	Significance Level		0,0065%	0,0014%	0,0005%	0,0000%
	Displacement	165 mm	124 mm	93 mm	113 mm	92 mm
Segment 3	Significance Level		3,7909%	0,0786%	0,1490%	0,0026%
	Displacement	155 mm	134 mm	115 mm	116 mm	92 mm

hypotheses stand the test. Occupant displacement can be reduced using active belt systems.

The comparison of reactive and predictive systems shows that earlier activation improves the ability of the analyzed reversible pre-pretensioner to reduce occupant displacement. The additional benefit of the pre-triggered active retractor can be seen best in the first phase of the double lane change maneuver or in the emergency braking tests.

In addition the lateral displacement also affects the routing of the belt webbing on the shoulder of the occupant. For test driving situations with high displacement towards the interior of the vehicle (during phase 2 of the double lane change and in the right curve) the belt slipped off the occupant's shoulder if no pre-pretensioning was used. As a result the geometry of the belt would be completely changed and the restraint effectiveness of the belt system would be significantly reduced. The effect of the changed belt geometry on occupant injuries was analyzed as part of the crash simulation.

INJURY ESTIMATION

Hypothesis

Besides the displacement study it is the goal of this work to determine in which way injury kinematics and the resulting injury severity are affected by the different levels of occupant displacement in case of a subsequent crash. As basis for the injury estimation the hypothesis is defined, that occupant displacement resulting from inertial forces increases the injury severity to be expected in a subsequent accident.

Since reversible pre-pretensioners do not allow to pull the occupant into nominal position but only help to reduce occupant displacement, the final position of the occupant is still displaced compared to the nominal position. The improvement of occupant safety due to reversible pre-pretensioning is addressed in the hypothesis, that the reduction of occupant displacement by reversible pre-pretensioning reduces consequential injury severity.

These hypotheses are being tested for both lateral and forward displacement in combination with side and frontal impact.

Method and Research Tools

Simulation Based on the results of the displacement studies a crash simulation is done for the predefined front and side impact scenarios (cp. Figure 1). The mean value of the maximum occupant displacement values for each belt system setup with the system variants

- conventional belt
- reactive pre-pretensioning based on vehicle dynamics data
- predictive pre-pretensioning based on environmental sensors

is used as initial dummy position for the start of the crash simulation at t_0 (t_0 = Time of the impact). The expected occupant injury in nominal position is identified within a reference simulation run. For better comparison to standardized testing (e.g. Euro NCAP) 50% male dummy models are used for simulation (Hybrid III for front crash, ES-2 for side crash).

The dummy models are positioned according to the displacement values. For lateral displacement hip displacement was not included in the simulation as it would increase simulation effort substantially (The dummy is seated in a predefined dent in the seat cushion. As the dent is in the center of the seat, lateral hip displacement would require a modified modeling of the seat cushion including a new position of the dent). The dummy model is seated in the middle of the seat and tilted to the side to fulfill the initial displacement conditions. Since displacement values for the chest showed a lower variance than for the head, chest displacement has a higher priority than head displacement if it is not possible to position the dummy model according to both measured conditions due to the rigidity of the virtual dummy. For simulations with forward displacement the dummy model is positioned according to displacement values for hip, chest and head with higher priority for the compliance with hip and chest displacement values than for head displacement. As a simplification inertial and belt forces prior to the accident are ignored in the simulation, because the forces before t_0 are significantly smaller than the forces during the crash. Also no initial dummy velocity is introduced to the crash simulations. The dynamic situation is only represented by the displacement of the dummy. The error made due to this simplification is analyzed in [15] for a front impact while braking.

For side impact different test scenarios are used for forward and lateral displacement. Forward displacement with a subsequent side impact is regarded as a typical intersection accident with crossing traffic after attempted but insufficient emergency braking (As described earlier, the percentage of intersection accidents with attempted emergency braking is significantly higher than for accidents with attempted evasive steering). This scenario is represented using an AE-MDB side barrier model. In contrast to that a virtual pole (as in the Euro NCAP pole side impact tests) is used for side impact simulation with lateral

displacement. This represents a skidding accident in which the vehicle is e.g. striking a tree with the side.

The simulation environment for side crashes is PAMCRASH 2009.1 with the ES-2 v4.1.2 dummy model. Side and curtain airbags are activated as well as the pyrotechnical belt pretensioner. The time-to-fire (TTF) is set to 6ms for the barrier crash and 10 ms for the pole crash. For front crashes the simulation software MADYMO V621 is used with the Hybrid III 50% male dummy model. The simulated restraint system includes the passenger airbag, a torsion bar load limiter and a pyrotechnical belt pretensioner. The belt is simulated using an FE belt model. Side crash analysis is done on the driver side under the assumption that the protection against side impact is similar for both sides. Front crashes were simulated on the passenger side because of the different airbag system and since the data was measured using a test person as front passenger.

Because of the reduced degrees of freedom and the rigidity of the dummy there is an intrusion conflict for some of the modified dummy positions. One conflict results from forward displacement of the side impact ES-2 dummy model. This virtual dummy does not allow a sufficient bending angle of hip and abdominal area to reach the aimed-at displacement values if seated correctly. To allow side impact simulation with the intended forward displacement the contact between feet and vehicle structure is taken out as well as the contact between the dummy's thighs and the front edge of the seat. The resulting position for maximum forward displacement is illustrated in Figure 7.

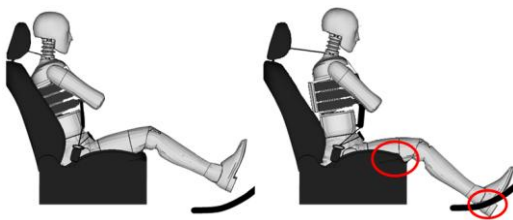


Figure 7. ES-2 dummy with/without forward displacement for side impact simulation
left: dummy in nominal position,
right: dummy with max. displacement and removed contact to seat/vehicle

To ensure that the elimination of these contacts and the resulting change in the distribution of forces does not affect the accident simulation all simulation runs in this specific scenario (including reference simulation runs with the dummy in nominal position) were also performed with cleared contact at the described areas. For side impact simulation the maximum lateral displacement towards the B-pillar measured in previous

testing could not be realized with the virtual ES-2 dummy due to the stiffness of the dummy's chest/shoulder area and because the vehicle used for testing is not the same one as used in the simulation. As a result only one position with lateral displacement is simulated for side impact to give a first impression of the change of injury kinematics in case of lateral occupant displacement.

Sled Tests For the predefined rear crash scenario with initial forward displacement (cp. Figure 1) a sled test is performed to identify the effect of occupant displacement on potential injury consequences. For this scenario the lowest crash pulse of the Euro NCAP whiplash testing protocol with a collision velocity of 16 km/h [16] was used as it represents a standardized evaluation method. The lowest pulse was chosen because the majority of cervical spine injury in rear end collisions occurs with a relative velocity less or equal to the velocity used in this pulse [17]. The crash pulse is recreated using the TRW Hy-G crash sled.

The whiplash tests are done with a BioRID dummy. The dummy is positioned with initial forward displacement as measured in the driving tests and secured with adhesive tape. A notch and the resulting notch effect ensure that the tape is torn upon impact and does not affect the dummy's behavior during the crash phase.



Figure 8. BioRID dummy in nominal position (left) and with forward displacement (center: with pre-pretensioning, right: with conventional belt) for whiplash sled tests

The initial dummy position for the three test setups representing the nominal position (Figure 8 left), forward displacement while braking with predictive pre-pretensioning (center) and forward displacement while braking with a conventional belt system (right) are illustrated.

Unlike the simulation tests the reversible pretensioner was activated during the whiplash test (only for the setup with displacement values measured with a reversible pre-pretensioner). As the belt force is reduced due to the rear impact, the pre-pretensioner can still reduce belt slack during the crash phase and therefore mitigate the rebound effect.

Results

Front crash forward displacement Forward displacement as initial condition for an impact from the front changes the injury kinematic in the simulation. Figure 9 illustrates the direct comparison of nominal position and maximum forward displacement (232/159 mm for head/chest as measured for emergency braking with a conventional belt) for a Euro NCAP forward collision simulation. The characteristics of head deceleration look less critical with forward displacement, but it has to be mentioned, that an initial bag-to-head contact during deployment (bag slap) occurs here.

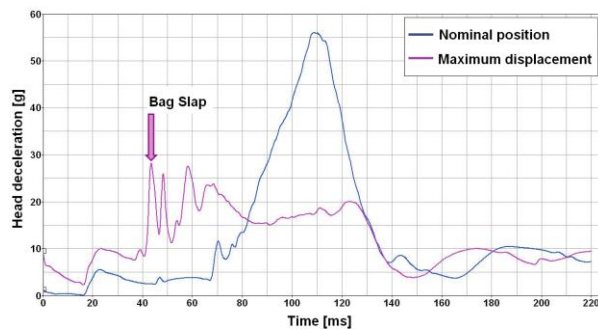


Figure 9. Comparison of nominal position and forward displacement - head deceleration over time

The peak of head deceleration at $t_0 + 40$ ms results from a bag slap, which has to be avoided completely, because it may cause additional injuries in the head and face area (It should be noted that the simulation of the unfolding phase of the airbag in the simulation environment used for these tests has limitations regarding accuracy and predictability for bag slap effects. Still the measured relative velocity of airbag and occupant head at the time of the first contact as ballpark figure allows the conclusion that the risk of a bag slap increases drastically with this level of forward displacement). The bag slap effect only occurred for the conventional belt system, the displacement measured for active belt systems did not result in a bag slap. Therefore, the potential occurrence of a bag slap for forward displaced occupants can be reduced using reversible pretensioning.

A comparison of the forward displacement values for the 50 % male with the nominal position of a 5 % female (usually the most critical standard test case regarding the bag slap) may exemplify this. While the head of the 5 % female in nominal position is approximately 138 mm more forward compared to the head of the 50 % male in nominal position (Average value of five arbitrary upper & middle class vehicles),

the maximum pre-crash forward head displacement of the male test person (similar in size and weight to a 50% dummy) reaches a value of 232 mm.

Front crash lateral displacement As seen in the displacement analyses the belt may slip off the occupant's shoulder for lateral displacement towards the interior of the vehicle without reversible pre-tensioning. This effect of the displacement study was included in the initial conditions of the simulation. The consequences are increased local belt forces for the abdominal region which could lead to a higher injury risk. Figure 10 shows the belt position for the conventional belt system (no reversible pre-tensioning) after pyrotechnical pretensioning.



Figure 10. Belt position with maximum lateral displacement after pyrotechnical pretensioning ($t_0 + 94$ ms)

The lateral displacement results in a non-central occupant to airbag contact. This limits the protection potential of the frontal airbag. During the simulation runs with initial forward displacement of the occupant in combination with the unfavorable belt position a dummy-to-IP contact was observed. In the head acceleration diagram this can be seen as a small peak in the head deceleration in Figure 11 for the curve without reversible pre-tensioning.

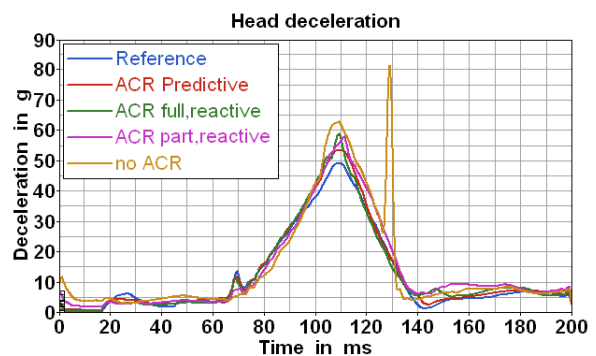


Figure 11. Head deceleration for lateral displacement towards vehicle interior

It can be seen that the head deceleration is best for nominal position and shows higher loads for higher initial forward displacement of the occupant. The simulation provides similar results for chest deflection values.

For initial displacements towards the B-pillar the belt webbing shows unfavorable routing close to the occupant's neck. When the pyrotechnical pretensioner is activated during the crash phase, this situation could lead to additional belt loads in the neck area, which would not occur for nominal seating positions. However, in the simulation model the pyrotechnical pretensioner was able to pull the occupant back and reduce the initial outboard lateral displacement (cp. Figure 12), resulting in a better restraint performance as seen for lateral displacement towards the interior.

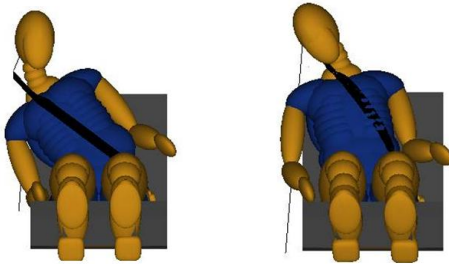


Figure 12. Belt position with maximum lateral displacement before (left) and after (right) pyrotechnical pretensioning

For these simulation runs, some injury criteria for the front crash like chest deflection show even slightly better numbers than for the nominal seating position. This is due to the fact, that the changed belt routing does not directly contact the sternum area, where the chest displacement measurement is located in the dummy and has therefore no real-world significance. But it has to be noted that the unfavorable belt routing close to the neck might lead to additional neck or spinal loadings compared to the nominal case, which do not show in standardized rating criteria for the front crash.

Side crash (barrier) with forward displacement

In this scenario the most apparent change due to forward displacement prior to a barrier crash is the changed position of the occupant in relation to the side airbag. As seen in Figure 13 the given width in x-direction of the airbag shows limited ability to cover the whole thorax area for increasing forward displacements. Therefore, the occupant is moving out of the protection zone of the airbag resulting in an increased injury potential in the thorax area.

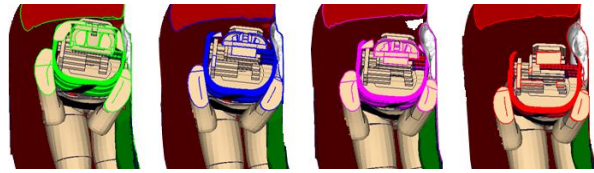


Figure 13. Section view from above – side crash with different levels of forward displacement during airbag deployment (left: nominal position, right: max. displacement).

With rising forward displacement also the abdomen load is increased. This is caused by a contact with the armrest as the occupant is moving out of the protection zone of the airbag. The direct contact with the armrest and the corresponding increase in abdomen force are shown in Figure 14.

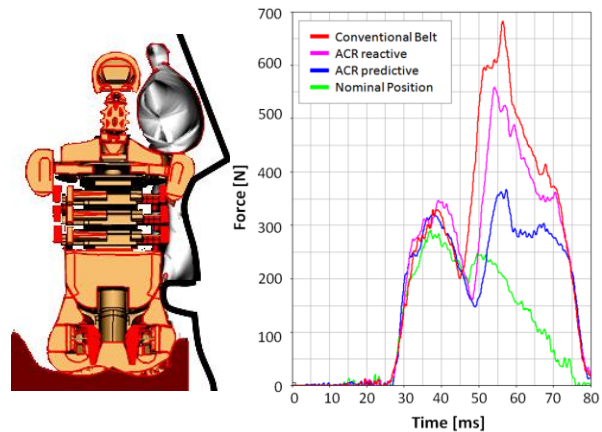


Figure 14. Contact with the armrest (left) and abdomen force for different levels of forward displacement (right)

Side crash (pole) with lateral displacement Most of the standard injury criteria show lower values in the simulation for an initial outboard displacement of the occupant due to the shoulder load path. The maximum shoulder force for the virtual ES-2 dummy is increased from 2.3 kN to 5.1 kN. However, shoulder load is not considered a standardized injury criteria in usual side impact assessment. As the shoulder load increases, some other injury criteria show lower values because of the stiffness of the simulated dummy. Therefore the standardized injury assessment criteria cannot be used to evaluate the effects for this test scenario properly. In addition it was not possible to recreate all occupant positions measured in vehicle testing with lateral displacement as mentioned earlier. That is why the nominal position as reference was only compared to the maximum of lateral displacement that could be reached using the dummy in the simulated vehicle, which is

lower than the maximum measured value. The result of this simulation is seen in Figure 15.

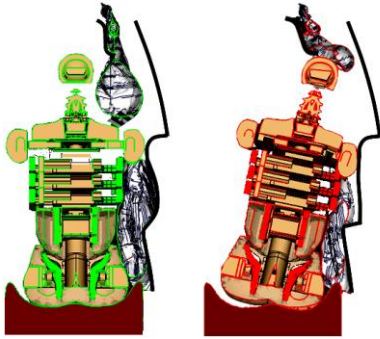


Figure 15. Side crash without (left) and with (right) lateral displacement

It can be seen that both the side airbag and the curtain airbag are not positioned properly due to lateral displacement. During deployment the curtain airbag hits the occupant's head causing a significant head-acceleration in vertical direction. This effect might be even higher with a real occupant with higher initial head displacement (the stiffness of the dummy's neck prohibits higher head displacement values as initial conditions in the simulation). The belt pressure for the side airbag (not illustrated) indicates that the deployment phase of this airbag is affected as well. It is expected that with additional hip displacement the deployment of the bag would have been hindered even more by lateral occupant displacement (Lateral hip displacement was not included in the initial conditions though inertial forces in e.g. the double lane change affect head, chest and hip position).

Rear crash with forward displacement As mentioned earlier the injury estimation for the rear impact crash scenario was done using sled tests with a pulse similar to the specifications of the Euro NCAP whiplash protocol for the lowest severity test. Therefore all whiplash test results should only be compared among each other.

The analysis shows that the values of most injury criteria used for the whiplash rating are highly increased as a result of forward occupant displacement. Figure 16 shows the resulting curve for the neck injury criterion (NIC) as an example.

In comparison to the reference value (dummy in nominal position), the NIC is increased to 240% for the dummy position representing reversible pre-tensioning and to 410% for the dummy position representing a conventional belt system. Similar tendencies (but with lower differences) are found for the criteria

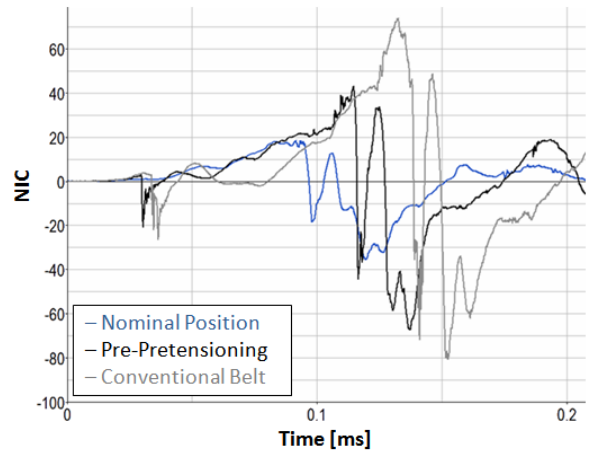


Figure 16. NIC for whiplash tests with/without forward occupant displacement.

- Rebound velocity: 115% respective 143%
- Upper Neck Shear: 142% respective 175%
- Upper Neck Tension: 160% respective 262%
- T1 acceleration: 154% respective 216%.

In contradiction to these results the Nkm values are reduced with increasing occupant displacement (95% respective 84%). The reason for this behavior is still in discussion.

Subsuming the whiplash test results show that increased forward occupant displacement as e.g. by braking in a rear crash leads to increased injury probability.

Conclusion

The results of the crash simulation using lateral and forward occupant displacement as initial conditions show how the crash phase of the accident is affected by the changed occupant position. For the simulated vehicle with maximum forward displacement a bag slap occurred in the simulated front crash. Due to the fact, that only one vehicle was studied in this study and because of limitations of the simulation this cannot be generalized for all vehicles and occupant sizes. For initial forward displacement in a front crash the potential for a bag slap is increased and the reduction of forward displacement by e.g. reversible pre-tensioning could mitigate or even eliminate this risk. Lateral displacement in a front crash affects the belt geometry. This may cause additional neck and spinal loads for initial outboard lateral displacement towards the B-pillar as the belt moves closer to the neck and may press on the neck area. For initial lateral displacement towards the center of the vehicle the changed occupant position and the changed belt geometry result in a reduced protection effectiveness of

the restraint system. As shown in the simulation results, higher loads in the abdominal area could occur. Furthermore, the potential for occupant-to-IP contacts would be increased for this scenario. The general conclusion is that a reduction of displacement reduces the tendency of unfavorable belt geometry and its subsequent consequences.

The side impact simulation with initial forward displacement shows that the occupant might move out of the protection zone of the side airbag and therefore the effectiveness of the side restraint system could be decreased. The increase in abdomen forces due to the armrest is regarded as specific for the simulated vehicle.

For initial outboard lateral displacement in side impacts the proper deployment and positioning of curtain and side airbag could be disturbed. In case of the curtain airbag the deployment could even lead to additional vertical head accelerations. Furthermore, after deployment the curtain airbag is not positioned properly, which could further reduce the protection effectiveness. These observations are not specific to the vehicle under investigation, but can be transferred to other vehicles as a general effect including the additional load in vertical direction.

The negative effect of high occupant displacement values and the potential improvement using reversible pre-pretensioning is also proven for the whiplash scenario. If the rear impact occurs, while the vehicle is still braking, the resulting forward displacement may result in load values many times higher than the stress in nominal position. This effect can be mitigated significantly using reversible pre-pretensioning.

Recapitulating the use of reversible pre-pretensioners is favorable in all the cases because the reduction of the initial occupant displacement also reduces the negative influence of initial displacements to the effectiveness of the restraint system. The potential occurrence of effects like bag slap or a contact to the instrument panel can be reduced if the occupant remains closer to the nominal seating position, as this is the reference position the restraint system can show its best protection effectiveness. This confirms the hypotheses stated earlier.

DISCUSSION AND OUTLOOK

To reduce the effort for vehicle testing and crash simulation and due to the restrictions of some of the tools some limitations apply to this study. The displacement values introduced with this paper have been measured using one male test person as a passenger and one sample vehicle with an ACR2 as reversible pre-pretensioner for each scenario. Further tests regarding the influence of varied test persons (e.g.

including test persons similar to a 5% female), different vehicles or a comparison of driver and passenger displacement would increase the transferability of the study. Similar tests are ongoing as part of the cooperative project OM4IS with the intention to develop a simulation model that is validated for both the pre-crash and the crash phase [12].

Other pre-pretensioning systems may differ from the tested one in pretensioning speed/strength, activation thresholds and basic function. For instance the Active Buckle Lifter performs pre-pretensioning at the buckle instead of the retractor, which results in a different distribution of belt force for lap and chest/shoulder area with possibly different displacement values.

Regarding the simulation results the predictability of the tools has to be taken into account. Especially, quantitative values for contact situations have limited transferability. The use of a human model is expected to allow a more realistic positioning of the occupant according to the measured displacement values and the behavior during the crash phase is expected to allow more realistic kinematics for a human model. Still the simulation data is very well able to demonstrate possible effects of reversible pre-pretensioning on injury severity. And the general effects that were identified remain valid for other vehicles and scenarios.

In case of the whiplash sled tests it has to be noted, that the pulse is similar to Euro NCAP requirements so injury values should not be used for an absolute rating, while a comparison among these tests is still valid. This comparison proves the drastic increase of the probability of potential injury with increasing forward displacement and illustrates the positive effect of reversible pre-pretensioning systems in this scenario. This constitutes a substantial finding compared to previous publications regarding the benefit of reversible pre-pretensioning [18].

Subsuming the ability of active belt systems to reduce occupant displacement and to mitigate the negative effects on potential injury has been shown. This benefit can be increased even more if the activation of such safety measures is done before vehicle dynamics cause inertial forces. E.g. the activation of the ACR2 prior to an Automatic Emergency Brake can reduce forward displacement significantly compared to simultaneous triggering. Therefore an early recognition of critical situations is an important factor to further minimize unfavorable pre-crash occupant displacement.

Rollover crash scenarios are not included in this study. Since a positive effect is assumed also for these scenarios, it is planned to include such test scenarios in further analysis regarding the benefit of active seat belt systems.

REFERENCES

- [1] Statistisches Bundesamt. 2007. "Verkehr - Verkehrsunfälle 2006, Fachserie 8, Reihe 7." Metzler-Poeschel Verlag, Stuttgart
- [2] Knoll, Peter; Schäfer, Bernd-Josef; Güttler, Hans et. al. 2004. "Predictive Safety Systems – Steps Towards Collision Mitigation." SAE 2004-01-1111
- [3] Meitinger, Karl-Heinz. 2009. "Top-Dow-Entwicklung von Aktiven Sicherheitssystemen für Kreuzungen." Fortschritt-Berichte Reihe 12, Nr. 701. VDI-Verlag, Düsseldorf
- [4] TRW Press Release. 2002. "Aktiver Eingriff "passiver" Systeme: das aktive Sicherheitsgurtsystem ACR von TRW." Livonia, Michigan
- [5] Wallentowitz, Henning; Reif, Konrad. 2006. "Handbuch Kraftfahrzeugelektronik – Grundlagen, Komponenten, Systeme, Anwendungen." Vieweg Verlag, Wiesbaden
- [6] Kramer, Florian. 1998. "Passive Sicherheit von Kraftfahrzeugen – Grundlagen, Komponenten, Systeme." Vieweg Verlag, Wiesbaden
- [7] Sander, Ulrich; Mroz, Krystoffer; Boström, Ola et. al. 2009. "The Effect of Pre-Pretensioning in Multiple Impact Crashes." In proceedings of the 21st ESV Conference, Stuttgart. 2009
- [8] Mücke, Stephan; Breuer, Jörg. 2007. "Bewertung von Sicherheitssystemen in Fahrversuchen." In proceedings of the Darmstädter Kolloquium Mensch & Fahrzeug. Ergonomia, Darmstadt, 119-129
- [9] Gelau, Christhard; Gasser, Tom Michael; Seeck, Andre. 2009. "Fahrerassistenz und Verkehrssicherheit." In: Winner, H.; Hakuli, S. und Wolf, G. (Eds.). "Handbuch Fahrerassistenzsysteme." Vieweg, Wiesbaden, 24-32
- [10] Internet-page: <http://www.atzonline.de/Aktuell/Nachrichten/1/11751>, accessed 07.10.2010
- [11] McCarthy, Mike; Fagerlind, Helen; Heinig, Ines et al. 2009 "Preliminary Test Scenarios" Deliverable D1.1 of the EU FP7 project ASSESS
- [12] Prügler, Adrian. 2010. "OM4IS – Mensch im Pre-Crash." virtual vehicle magazine Nr. 5 1-2010 Kompetenzzentrum Das Virtuelle Fahrzeug Forschungsgesellschaft mbH, Graz
- [13] Sander, Ulrich; Boström, Ola. 2010. "Analysis of Far-Side Impacts in Europe – Occurrence, Injury Outcome and Countermeasures." In Proceedings of Airbag 2010 – 10th International Symposium on sophisticated Car Occupant Safety Systems. Karlsruhe. 2010
- [14] International Organization for Standardization. 2002. "ISO 3888-2: Passenger cars – Test track for a severe lane-change manoeuvre – Part 2: Obstacle avoidance"
- [15] Woldrich, Markus. 2010. "Movement in the PRE-Crash situation – A simulation with a reversible reserach with a reversible PRE-SAFE Pulse system." In Proceedings of Airbag 2010 – 10th International Symposium on sophisticated Car Occupant Safety Systems. Karlsruhe, 2010
- [16] European New Car Assessment Programme. 2010. "The Dynamic Assesment of Car Seats for Neck Injury Protection – Testing Protocol, Version 3.0." Brussels
- [17] Langwieder, Klaus. 2002. "Perspektiven der aktiven und passiven Fahrzeugsicherheit." Verkehrsunfall und Fahrzeugtechnik Nr. 1/2003, Potsdam
- [18] Mages, Mark; Seyffert, Martin; Class, Uwe. 2010. "Benefit of Reversible Belt Pre-Pretensioning for different Pre-Crash Scenarios – Reduction of Occupant Displacement and the Effect on Injury Severity" In Proceedings of Airbag 2010 – 10th International Symposium on sophisticated Car Occupant Safety Systems. Karlsruhe. 2010

INVESTIGATION OF PRE-BRAKING ON UNBELTED OCCUPANT POSITION AND INJURIES USING AN ACTIVE HUMAN BODY MODEL (AHBM)

Bastien, Christophe

Blundell, Michael

Coventry University

England

Van Der Made, Robin

TASS

Netherlands

Neal-Sturgess, Clive

University of Birmingham

England

Paper Number 11-0296

ABSTRACT

Following intensive field research based on over 5000 vehicles [1], it was shown that 5% of the drivers still do not wear any seatbelts. New vehicles are now being fitted with active safety features which will influence the kinematics of these un-restrained drivers [2] and may have important safety implications.

The proposed study assesses the safety benefit of a pre-braking event on the occupant position, stance and injury and will review the contribution of active muscle behaviour of a 50th percentile human model [3] in comparison with a passive human model [4] and discusses the potential using active human simulation for testing driver assistance safety technologies.

INTRODUCTION

Original investigations undertaken [5] [6] backed up by physical tests, concluded that anthropometric test dummies (ATD) injuries in static FMVSS208 Out-Of-Position (OoP) load cases occurred mainly in the punch-out and membrane loading phases. Further airbag computer model improvements were developed to simulate scenarios involving occupants of different statures [7]. An initial method of assessing the effects of active safety involved the improved airbag model [7] and a constant 1.0'g' pre-braking scenario on an occupant [8]. This study showed that the Passive Human Body Model's (PHBM) spine was more flexible than the one of an ATD and that the kinematics were very different, leading to different injury levels between the two occupant models [8].

Some modelling improvements were suggested [8], especially the 1.0'g' braking pulse which did not consider the braking duration, the original stance of the occupant during the pre-braking phase, the effect of the occupant's muscle tensioning [9], as well as the airbag triggering time.

DRIVERS' KINEMATIC STUDY

Drivers' Positioning

The PRISM European project, which was completed in 2003, studied the occupant's behaviour whilst driving a vehicle. This study was conducted on 6 sites, 2 in the UK, 2 in Spain and 2 in Austria, recording information over 5000 vehicles [1]. Volunteers were tasked to follow an itinerary, in which they were filmed and photographed at set positions. The visuals were then inputted into a database for analysis. From this database, it was reported that 5% of all drivers did not wear a seatbelt (6% of all male drivers) [10], as shown in Figure 2.

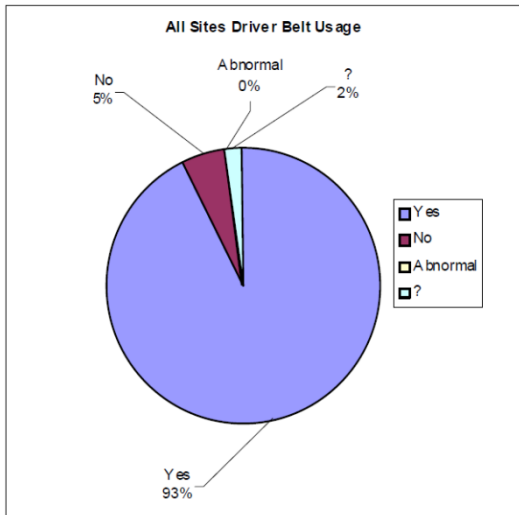


Figure 1: PRISM project. Percentage of drivers not using the seatbelt

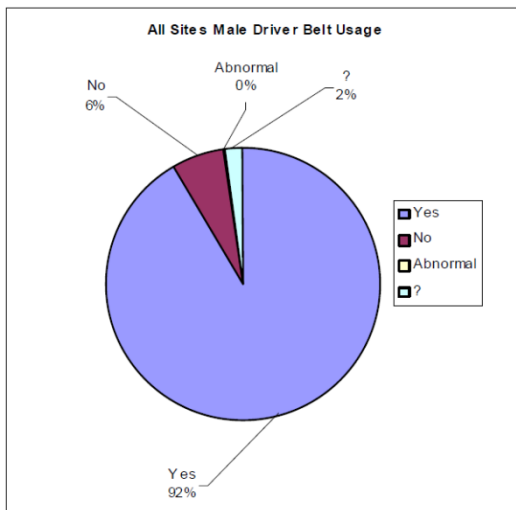


Figure 2: PRISM project. Percentage of male drivers not using the seatbelt

Most drivers were observed with both hands on the steering wheel in the FMVSS208 standard position (Figure 3) [11]. It was also observed that a large percentage of the participants adjusted the radio, as per Figure 4.

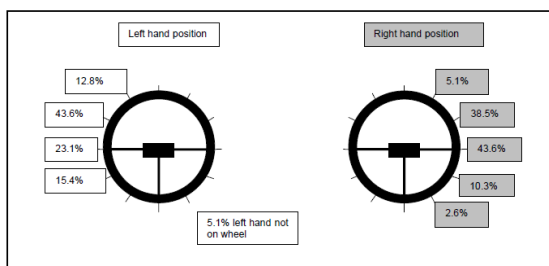


Figure 3: Volunteers preferred hand locations

Activity	Often %	Sometimes %	Seldom %	Never %
Adjust the radio	41.0	43.6	12.8	2.6
Change CDs	15.4	38.5	25.6	20.5
Arm on the waist rail	5.1	23.1	33.3	38.5
Arm on the arm rest	5.1	25.6	28.2	41.0
Hand on the grab Handle	0.0	0.0	23.1	76.9
Arm out of window	2.6	30.8	25.6	41.0
Using mobile phone	2.6	23.1	38.5	35.9
Hand on sun visor	0.0	2.6	23.1	74.4
Hand on head restraint	0.0	0.0	10.3	89.7
Fiddle with seat belt	0.0	25.6	30.8	43.6
Reach into passenger footwell	7.7	28.2	35.9	28.2
Eat/ Drink	7.7	25.6	48.7	17.9
Talk to rear passengers	2.6	12.8	33.3	51.3

Figure 4: Activities performed while driving

The stances which were chosen for the occupant kinematic study were:

1. FMVSS208: standard test position.
2. Adjusting the radio (left hand): most frequent activity.
3. Mobile phone in left hand: as it is usually illegal to use a hand-held phone.
4. Arm on armrest: activity leaving right hand free.

All other positions occurred less frequently, hence have not been included..

These positions were then modelled using the Madymo Active Human Body Model (AHBM) and positioned within a Madymo vehicle dynamic model [11] [12], able to simulate breaking scenarios as well as a brake dive.

FMVSS208's hand positioning follows the legislative requirement, which has been also verified by the PRISM project finding that 87.5% of the volunteers had a 3 and 10 o'clock right and left hand positioning (Figure 5).

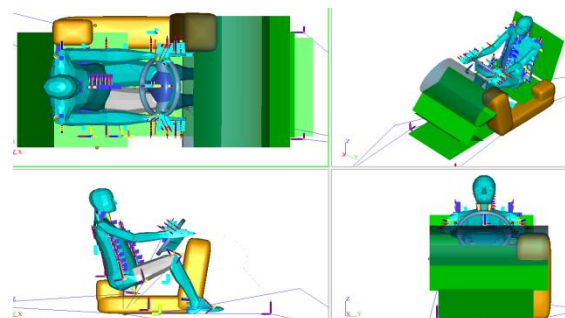


Figure 5: FMVSS208 computer model setup

Adjusting the radio's right hand positioning follows the PRISM's project finding [11] (see Figure 6). The height of the left hand had been estimated in the computer model (Figure 7).

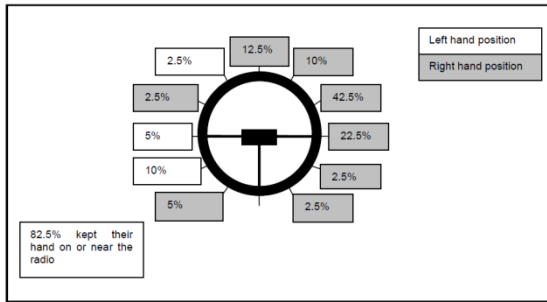


Figure 6: Right Hand position while adjusting radio

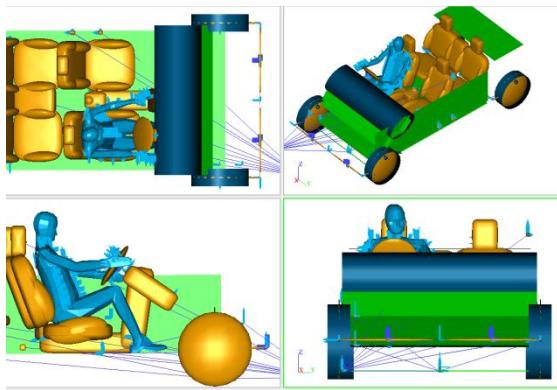


Figure 7: Radio adjustment computer model setup

The mobile phone in the left hand scenario (Figure 8) has shown that 67.5% of the volunteers who had reached their ear with the phone continued to hold it to their ear (Figure 9).

If no participant removed their right hand from the steering wheel during the event, some drivers with their right hand on the left of the steering wheel were turning it in an attempt to swerve around vehicles [11].

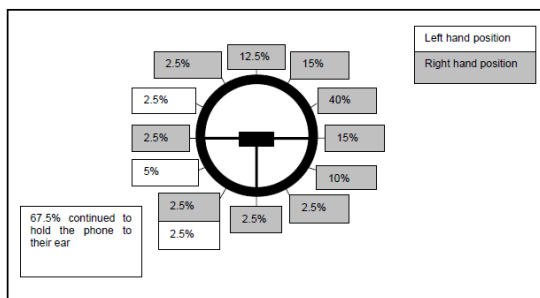


Figure 8: Right Hand position while holding a mobile phone

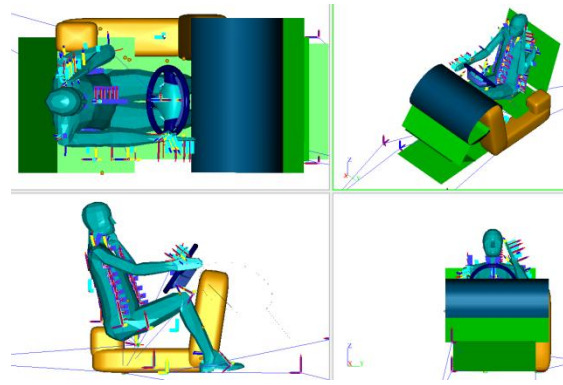


Figure 9: Mobile phone computer model setup

The right arm on the armrest scenario was chosen as a scenario considering the right hand not in contact with the steering wheel (Figure 10). It was noted that "82.5% kept their right arm on the rest and hand off the wheel" [11], as is modelled in Figure 11.

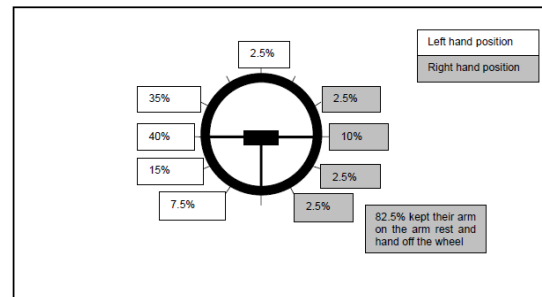


Figure 10: Left Hand position while resting on armrest

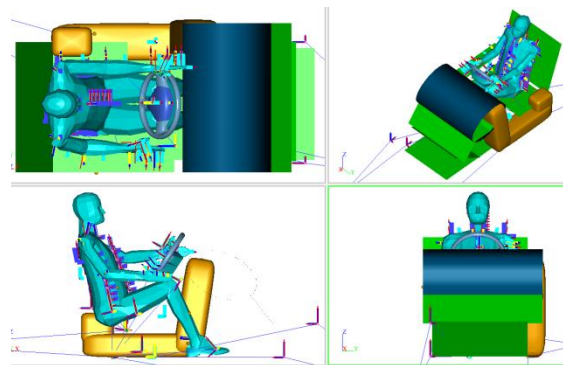


Figure 11: Armrest computer model setup

Vehicle braking extreme braking pattern

Vehicle braking deceleration cannot exceed the road coefficient of friction and is accepted to be in the interval of 1.0'g' to 1.3'g' in very rare instances [8]. Original work conducted on active safety

assumed a constant 'g' pulse ignoring the duration of braking [8].

Some occupant behaviour under extreme braking was conducted to understand their reaction [13]. These occupants were belted and, without knowing, driven by a professional driver performing extreme braking scenarios. Accelerometers at the centre of gravity of the vehicle outputted the vehicle linear deceleration, without taking the brake dive into account (Figure 12).

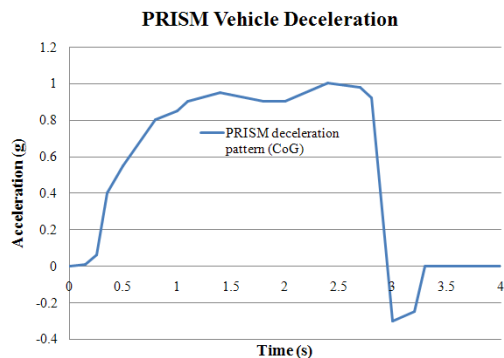


Figure 12: Straight line braking. Vehicle deceleration

From this deceleration pattern, it can be seen that the deceleration initially ramps up slowly during the first 0.3s and then abruptly to reach 0.9'g' after 1.0s (near plateau). This pulse is less severe than a constant step-function of 1.0'g' and shows that the longer the braking, the steeper the deceleration. This pre-braking pulse suggests a more gradual deceleration for the 1st second of deceleration compared to a step-function constant pre-braking value.

Modelling the occupant grip on the steering wheel

The 50th AHBM (Active Human Body Model) model designed by TNO, as seen in Figure 13, now includes a stabilized spine compared to the PHBM (Passive Human Body Model).

This 50th AHBM stabilizing spine contains 25 joint torque actuators, sensors and controllers for each of the two bending directions (25 in flexion-extension and 25 in lateral bending). The actuators are positioned between the pelvis and the L5 vertebra, between each set of vertebrae (L5-C1) and between C1 and the head. Each actuator applies a torque to the child body of the vertebra above (or of the head) calculated by the controller. The controller receives input from the sensors, which measure the

angle of each vertebra with respect to the inertial coordinate system, hence maintaining the AHBM's posture [9].

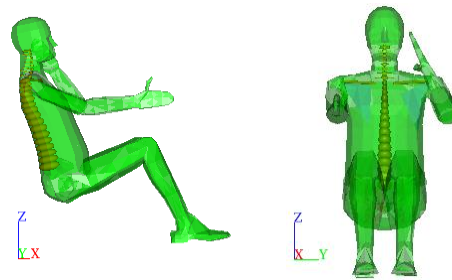


Figure 13: TNO AHBM [3]

To evaluate the gripping force, Bao [14] has performed experiments involving hand power and pinch grips among 14 subjects, using electromyograms (EMG). He has concluded that the power grip strength is approximately 300 N for women and 470 N for men. These values differ vastly from Bose [15] who has extrapolated the hand forces from the steering column loads to a maximum of 151N. Boa's tests being more applicable in the scenario of this study, an average resultant force value of 400N was chosen.

The grip was modeled using a RESTRAINT_POINT between the AHBM's hands and the steering wheel body. This feature is a spring-damper element for which stiffness has been determined to simulate the hand releasing force as well as keeping a reasonable computational timestep [9].

Table 1: RESTRAINT_POINT characteristic function

Displacement (m)	Force (N)
0	0
0.005	10000
0.010	20000
0.100	100000

The force level is monitored using a SWITCH_SENSOR command. Should the resulting force between the hand and the steering wheel body exceed 400N, the STATE RESTRAINT_REMOVE flag is activated, representing the effect of removing the hand from the steering wheel.

Comparison of AHBM and PHBM under 1.0'g' constant deceleration

Looking at this worst pre-braking scenario, an AHBM and PHBM are both compared under 1.0 'g' using the 400N hand grip threshold. The two occupants start at the same position and the simulation is stopped when the thorax impacts the steering wheel (Figure 14).

It can be noted that:

- The contact time between the thorax/ steering wheel is comparable between the two occupants.
- The kinematics between the 2 occupants is different. The PHBM tends to slouch because it does not have a stabilised spine, nor grip stiffness in its arms and hands. This can have an effect as the AHBM will stand straighter and will be more likely to impact the windscreen than the PHBM.



Figure 14: Comparison of AHBM (light) and PHBM (dark) kinematics under 1.0 'g' constant deceleration

Outputting the restraint force levels for both hands, it can be noted that in a FMVSS208 steering wheel grip, the 2 hands are subjected to a force of 90N.

The force level measured might be under-estimated due to the fact that there is no arm muscle activation included in this model yet.

Comparison of AHMB under 1.0'g' constant 'x' deceleration and PRISM deceleration pulse

Four occupant stances were considered and subjected to the PRISM deceleration and constant 1.0'g' deceleration. The results are summarised in Table 2.

Table 2: Comparison of occupant time to contact to hard points vs. Stance and deceleration pulse

Deceleration braking pulse	Driver's stance	Time thorax to steering wheel or any hard contact (ms)	Time hand not gripping the wheel anymore (ms)
PRISM	FMVSS208	720	Still gripping
PRISM	Mobile phone	750	Still gripping
PRISM	Arm on armrest	1000	Still gripping
PRISM	Left arm on radio	760	Still gripping
Constant 1'g'	FMVSS208	260	Still gripping
Constant 1'g'	Mobile phone	260	Still gripping
Constant 1'g'	Arm on armrest	260	Still gripping
Constant 1'g'	Left arm on radio	250	Still gripping

From the results obtained, it can be seen that the times for the occupant to impact the steering wheel, using the pre-braking pulse obtained in the PRISM project, are constantly longer (for every occupant's stance) than the ones obtained using a constant 1'g' pulse. The times to impact using the constant 1.0'g' pulse are almost 3 times faster.

Because the PRISM pulse is obtained from tests, it means that the assumption taken in previous studies [8] is much too severe.

Comparison of AHMB under 1.0'g' constant deceleration and vehicle braking dynamics

Original research was considering a 1.0'g' constant deceleration for a pre-braking scenario by using the MOTION_ACC command in Madymo [8] [16].

This can be observed in Figure 15, as the velocity slope of run 8 is constant.

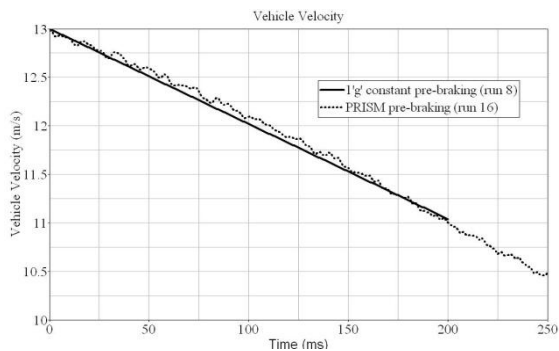


Figure 15: Vehicle velocity change under 1.0'g' constant braking

By measuring the vehicle mass (1140 kg) and applying a constant 1.0'g' deceleration would generate a braking force for the vehicle of 20307N. By splitting the braking forces at the front and the rear with a ratio of 60/40, would give a retarding force per wheel at the front of 6092N and of 4061N at the rear.

The occupant kinematics is then extracted (no dive – top, brake dive – bottom) (Figure 16, Figure 17 and Figure 18):

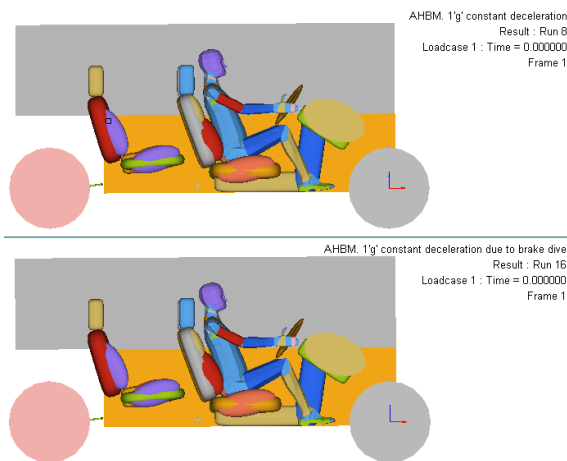


Figure 16: Brake dive estimation (time = 0ms)

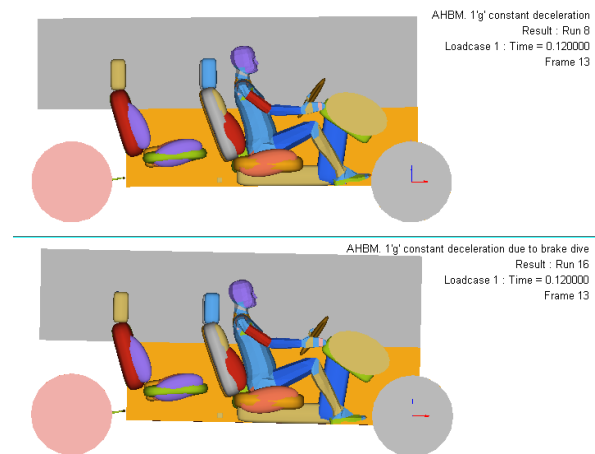


Figure 17: Time 120ms: drivers' stance and position in the cockpit is comparable.

In Figure 18 the drivers' stance and position in the cockpit is very different. The brake dive scenario delays the impact on the steering wheel compared to the 1.0'g' constant acceleration. The occupant submarines in his seat and the angle between the airbag and the occupant is wider.

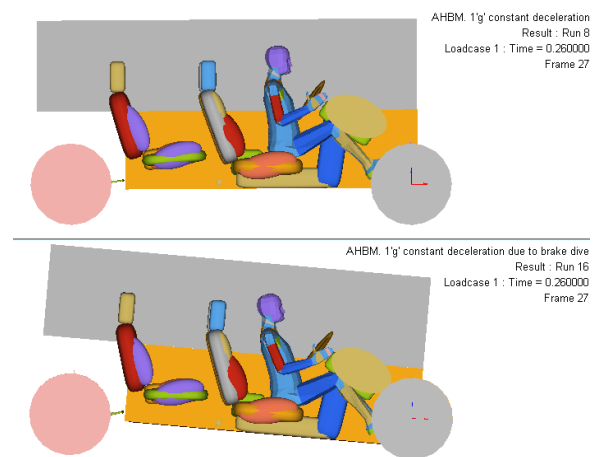


Figure 18: Time 260ms

Preliminary conclusions

The kinematics of an AHBM is different from a PHBM and tends to stay straighter because of its stabilising spine. These new AHBM kinematics suggests an increased likelihood of head contact with the windscreen as opposed to using the PHBM model, which has a more slouching behaviour.

The pre-braking kinematics modelling has been improved from previous studies, thanks to the addition of a more realistic pre-braking pulse obtained from the PRISM project as well as the grip feature from the new AHBM.

The first 120ms of an unbelted occupant kinematics subjected to a 1.0'g' constant pre-braking deceleration is not influenced by the vehicle brake dive. Looking at the PRISM test braking curve, which is much less severe than a constant 1.0'g' and knowing that all the occupants would impact the wheel around 0.7s, it would be surprising if the brake dive had any influence on an unbelted occupant's kinematics before a 1s braking duration (1.0'g' is only met around 1s braking duration). A side study could aid to find the braking/dive function which would match the PRISM deceleration pulse and demonstrate the above categorically.

For the continuation of this paper, the PRISM 'x direction' deceleration function will be used and will ignore vehicle brake dive.

ACTIVE SAFETY INJURY COMPUTATION

Active Safety Accident Scenario Proposal

A new methodology is now proposed [8] varying by the following (see Figure 19):

- The pre-braking will be provided by the PRISM braking pulse and not a constant 1.0'g' deceleration, as the former is more realistic.
- The vehicle crash pulse will be based on an FMVSS208 25mph full frontal barrier test and not a 35mph barrier test. The reason for this change is because unbelted occupant tests are performed at 25mph. This will then be useful for future injury comparisons.
- The occupant model used will be the AHBM with steering wheel grip feature

The starting point of the scenario is a vehicle driving at a constant velocity.

The vehicle is then subjected to a pre-braking pulse (from the PRISM project) with varying braking durations. When the pre-braking phase is finished, the vehicle occupant will be accelerated by a crash pulse based on a 25mph (11m/s) rigid wall impact. This acceleration will be followed shortly after by an airbag deployment (delay varying from 10ms to 20ms). The active safety scenario timeline is explained in Figure 19.

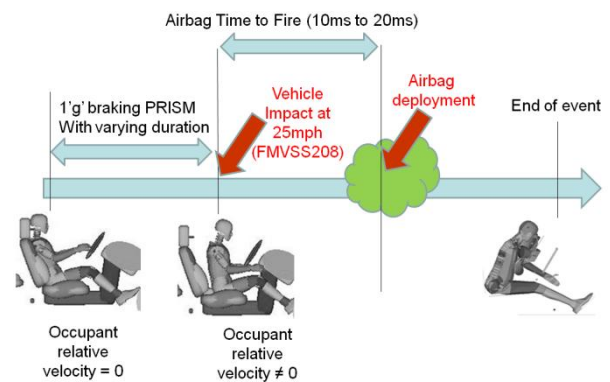


Figure 19: Updated Active safety scenario to investigate injury levels

Determination of the vehicle crash pulse and restraint systems assumptions

The airbag system provided has been validated in static positions OoP1 and OoP2 [6] [7] [8].

A simplified sled model was generated and tuned in order to meet a dynamic FMVSS208 test. This model has not been validated, but it does however allow investigation of relative analyses based upon a model meeting the legal requirements.

An LS-Dyna computer model of a Toyota Rav4 has been used [17] to simulate a 25mph rigid wall impact (Figure 20) and extract a generic low speed crash pulse.

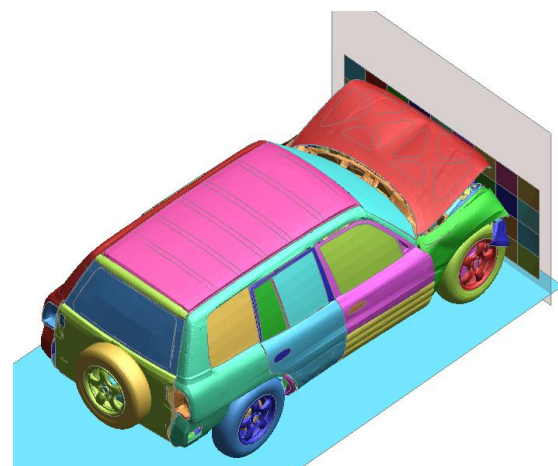


Figure 20: Toyota Rav4 impacting a rigid wall at 25mph

The pulse has been approximated to a triangular one (Figure 21). The maximum deceleration level is around 30'g'. In order for the system to meet FMVSS208, the starting value of 6'g' is chosen, whilst keeping the same pulse shape.

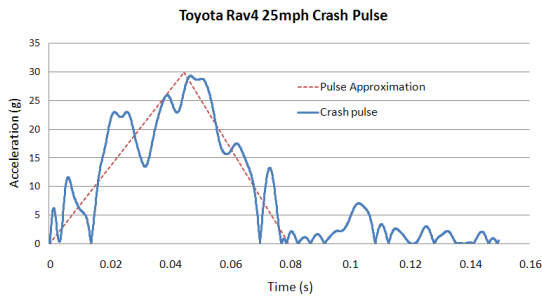


Figure 21: Approximation of Toyota Rav4 crash pulse

Determination of study parameters and permutations

The study will investigate the effect of the pre-braking duration, as well as the occupant starting stance and the airbag firing time.

Looking at the PRISM pre-braking pulse, the braking duration should be chosen before any hard contact between the occupant and the steering wheel take place.

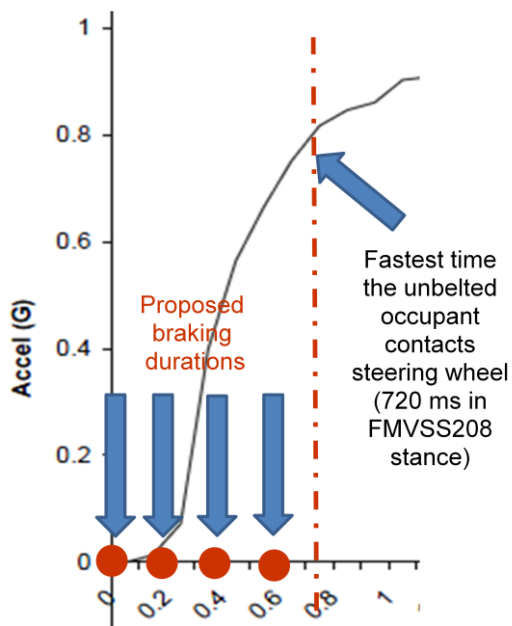


Figure 22: Proposed braking duration and occupant contact time with steering wheel

Furthermore a suitable accident time needs to be chosen for the injury investigation. Should the pre-braking phase be too small then no collision avoidance will be available. Should the pre-braking phase last too long, then the occupant will find himself in a forward position relative to the steering wheel with an initial velocity before the airbag is fired.

From the previous kinematics study, it was estimated that the contact occupant (FMVSS208) to steering wheel occurs after 720ms of pre-braking. Hence the pre-braking phase must be less than 720ms.

It is therefore proposed to split the pre-braking duration into 4 interval durations: 0ms, 200ms, 400ms and 500ms, staying within the 720ms window (Figure 22). 500ms is chosen because it is immediately before the legs start contacting the knee bolster.

The following parameters are taken into account in the study (Table 3):

Table 3
Study parameters

Occupant stance	Duration of pre-braking (ms)	Airbag TTF (ms)
FMVSS208	0	10
Left hand with mobile phone	200	20
Right arm on armrest	400	
Adjusting radio	500	

Computation of occupant initial velocities

The human_joint will be extracted for each driving stance position.

Table 4: Occupant initial velocities vs. pre-braking duration

Occupant stance	Duration of pre-braking (ms)	Velocity (m/s)
ALL STANCES	0	0
	200	0
	400	0.44
	500	0.90

Looking at Table 4, it can be seen that the first 200ms of the pre-braking have almost no effect on the occupant position and initial velocity. The ‘g’ level is very low (around 0.02’g’), which must be counter-acted by the seat friction and the occupant’s inertia.

At time 400ms, the occupant is moving forward with a linear velocity of 0.44m/s.

At time 500ms, the knees start to touch the knee bolster before the torso rotates to then touch the steering wheel.

It can be seen that all the velocities are identical in all stance cases under 500ms and will vary greatly thereafter (Figure 23).

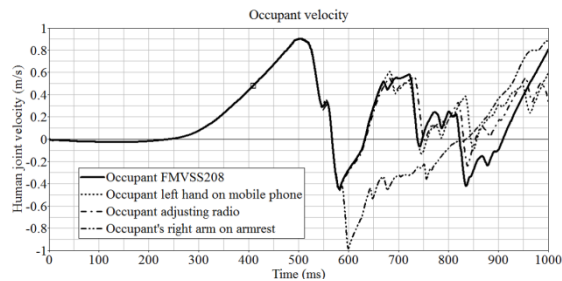


Figure 23: Occupant’s velocity during pre-braking

Also, from previous research, where a constant 1’g’ deceleration was used, the initial velocity of the occupant 250mm from the steering wheel was found to be 1.76m/s [8], which is more than twice the velocity extracted from models in which the PRISM pre-braking pulse is used.

Injury comparisons and analyses

To create a baseline for the study, the relationship between the windscreen provided by the vehicle dynamic model and the occupant was modified. This windscreen has been moved 100mm forward to prevent any hard contacts with the occupant’s head, hence allowing all the FMVSS208 criteria to be achieved.

Results are summarised in the tables below:

Table 5: 50th percentile AHBM model. Pre-braking 0ms. TTF 10ms

50th percentile AHBM model. Pre-braking 0ms TTF 10ms					
Major head neck and chest injury values		FMVSS208	Mobile Phone	Radio	Armrest
	Run number	39	31	40	41
Head	HIC (15 ms) [-]	213	448	7	12
Neck	Nij [-] Tension-Extension	0.05	0.21	0.05	0.04
	Nij [-] Tension-Flexion	0.04	0.17	0.03	0.04
	Nij [-] Compression-Extension	0.27	1.1	0.2	0.04
	Nij [-] Compression-Flexion	0.05	0.16	0.06	0.05
	Tension force [N]	376	88	249	305
	Compression force [N]	219	788	182	200
	Flexion [Nm]	33	129	29	46
	Extension [Nm]	10	49	8	7
Chest	Accel (3 ms) [g]	10	16	5	5

From the results in Table 5 (normal FMVSS208 stance situation) , it can be seen that all the figures are within the legal limit, except the case for the occupant holding a mobile phone which suggest a NIJ (Compression- Extension) above 1. Identical results have been obtained with a pre-braking delay of 0ms and 200ms respectively, in combination with airbag firing times of 10ms and 20ms.

**Table 6: 50th percentile AHBM model. Pre-braking
400ms TTF 10ms**

50th percentile AHBM model. Pre-braking 400ms TTF 10ms					
Major head neck and chest injury values		FMVSS208	Mobile Phone	Radio	Armrest
	Run number	50	56	54	52
Head	HIC (15 ms) [-]	105	65	61	110
Neck	Nij [-] Tension- Extension	0.6	0.48	0.3	0.6
	Nij [-] Tension- Flexion	0.08	0.09	0.07	0.06
	Nij [-] Compression- Extension	0.08	0.63	0.5	0.85
	Nij [-] Compression- Flexion	0.2	0.2	0.2	0.2
	Tension force [N]	967	893	838	898
	Compression force [N]	426	407	343	416
	Flexion [Nm]	102	82	67	110
	Extension [Nm]	20	18	19	19
Chest	Accel (3 ms) [g]	14	13	13	14

From the results in

Table 6, all the values in the table for a pre-braking lasting 400ms and an airbag with a time to fire of 10ms are within the legal limit.

It can be noted that, with the exception of the mobile phone case, the extreme values for tension force, compression force, flexion and extension are higher than in a normal FMVSS208 starting stance.

Table 7: 50th percentile AHBM model. Pre-braking 500ms TTF 10ms

50th percentile AHBM model. Pre-braking 500ms TTF 10ms					
Major head neck and chest injury values		FMVSS208	Mobile Phone	Radio	Armrest
	Run number	51	57	55	53
Head	HIC (15 ms) [-]	78	35	44	82
Neck	Nij [-] Tension-Extension	0.06	0.07	0.06	0.07
	Nij [-] Tension-Flexion	0.09	0.08	0.09	0.08
	Nij [-] Compression-Extension	0.6	0.35	0.18	0.67
	Nij [-] Compression-Flexion	0.2	0.09	0.11	0.13
	Tension force [N]	367	218	244	351
	Compression force [N]	131	106	145	116
	Flexion [Nm]	69	43	21	82
	Extension [Nm]	27	19	23	23
Chest	Accel (3 ms) [g]	11	9	10	11

All the values in the

Table 7 for a pre-braking lasting 500ms and an airbag with a time to fire of 10ms are within the legal limit.

It can be noted that injury values are in general less than for time 400ms with an airbag time to fire of 10ms.

Compression and tension forces tend to be less than for the starting FMVSS208 scenario, but the flexion and extension are generally higher.

Table 8: 50th percentile AHBM model. Pre-braking 400ms TTF 20ms

50th percentile AHBM model. Pre-braking 400ms TTF 20ms					
Major head neck and chest injury values		FMVSS208	Mobile Phone	Radio	Armrest
	Run number	60	66	64	62
Head	HIC (15 ms) [-]	118	90	30	65
Neck	Nij [-] Tension-Extension	0.6	0.6	0.2	0.4
	Nij [-] Tension-Flexion	0.1	0.1	0.1	0.1
	Nij [-] Compression-Extension	0.8	0.7	0.3	0.7
	Nij [-] Compression-Flexion	0.2	0.2	0.2	0.2
	Tension force [N]	974	885	811	973
	Compression force [N]	410	420	367	494
	Flexion [Nm]	105	92	44	91
	Extension [Nm]	21	17	22	19
Chest	Accel (3 ms) [g]	14	14	13	15

All the values in the Table 8 for a pre-braking lasting 400ms and an airbag with a time to fire of 20ms are within the legal limit.

It can be noted that all the injuries, for all cases, have the same magnitude as for a pre-braking lasting 400ms with an airbag with a time to fire of 10ms.

It can therefore be proposed that up to a pre-braking duration of 400ms, a usual airbag triggering time (between 10 and 20ms) does not have a major influence on occupant injuries compared to a standard unbelted FMVSS208 test.

In Figure 24, looking at the FMVSS208 driving scenario, it can be clearly seen that the injury traces have the same shape and timing regardless of the airbag firing time.

The main difference is in F_x , where the airbag strikes the occupant in the 'x' direction, as it is its primary direction of deployment. As the airbag has a pressure-time inflation characteristic, it will create a different load level according to the time it is struck.

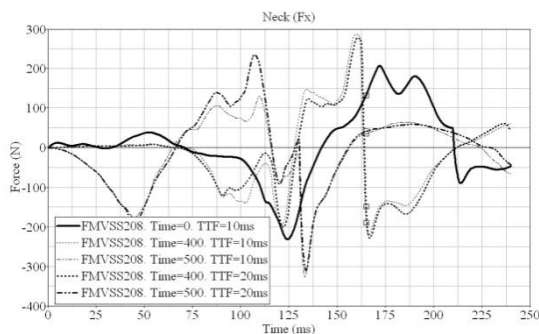


Figure 24: FMVSS208 driving stance. Neck F_x injuries

The neck tension and compression forces (Figure 24, Figure 25) in the neck are almost a perfect overlay, showing that the airbag firing time does not affect the injury patterns in FMVSS208 scenario.

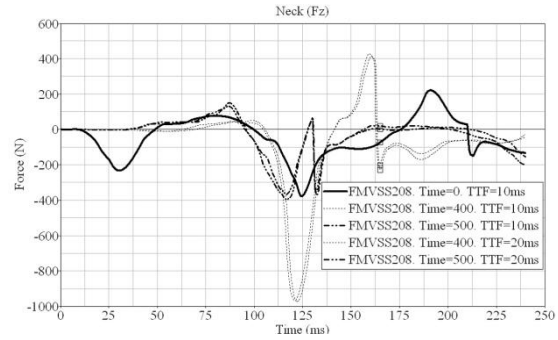


Figure 25: FMVSS208 driving stance. Neck F_z injuries

At time 130ms, 165ms and 212ms, it can be seen that the neck moments are asymptotic. This also ties up with a change of direction of the value of F_z , where neck compression is suggested.

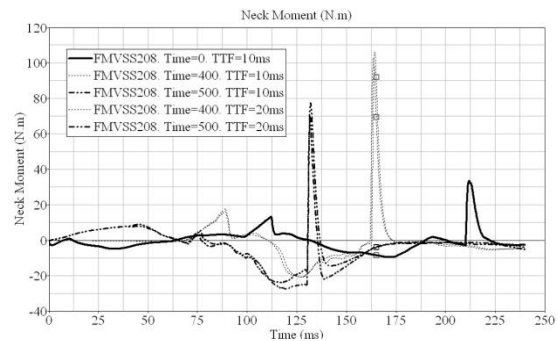


Figure 26: FMVSS208 driving stance. Neck My injuries

Simulations with asymptotic neck moments do indeed show that the occupant's head contacts the windscreen, as illustrated in Figure 26 and Figure 27.

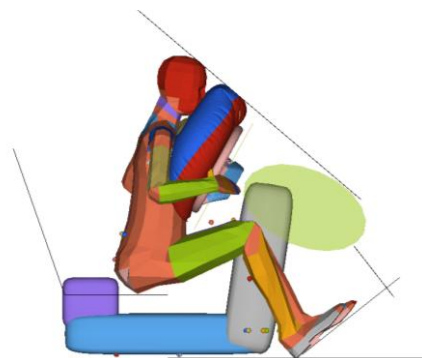


Figure 27: Occupant's head contacting the windscreen

Table 9: 50th percentile AHBM model. Pre-braking 500ms TTF 20ms

50th percentile AHBM model. Pre-braking 500ms TTF 20ms					
Major head neck and chest injury values		FMVSS208	Mobile Phone	Radio	Armrest
	Run number	61	67	65	63
Head	HIC (15 ms) [-]	85	19	26	11
Neck	Nij [-] Tension-Extension	0.1	0.1	0.1	0.1
	Nij [-] Tension-Flexion	0.1	0.1	0.1	0.1
	Nij [-] Compression-Extension	0.6	0.1	0.1	0
	Nij [-] Compression-Flexion	0.1	0.1	0.1	0.1
	Tension force [N]	397	233	187	213
	Compression force [N]	150	118	157	154
	Flexion [Nm]	75	9	8	9
	Extension [Nm]	24	27	24	30
Chest	Accel (3 ms) [g]	11	9	11	9

All the values in Table 9 for a pre-braking lasting 500ms and an airbag with a time to fire of 20ms are within the legal limit and are the same level as with an airbag firing time of 10ms.

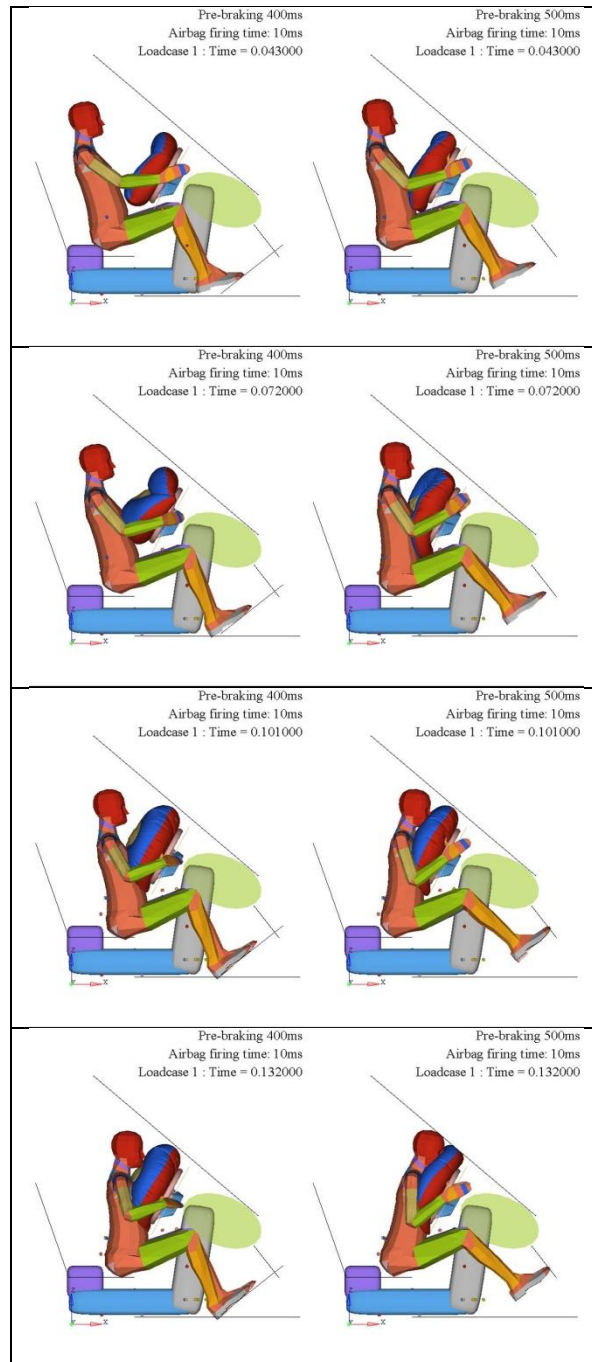
It can be noted that all injuries, for almost all cases, are less severe than the corresponding ones for a pre-braking lasting 400ms with an airbag fire time of 20ms. This is counter intuitive, as the occupant is closer to the steering wheel and moving toward the airbag at a higher speed.

Looking at the occupant kinematics (Figure 28), it can be noted that the occupant's legs are impacting the knee bolster.

Upon contact with the knee bolster, the torso rotates about the hip joint. At this point, the occupant is not sitting straight anymore and slouches on the airbag.

As the occupant is not sitting straight, its head position relative to the windscreen is different than for the scenario where the pre-braking lasts 400ms.

This is the reason why the neck moments generated by the head contact to the windscreen is less severe for a pre-braking of 500ms than for 400ms.



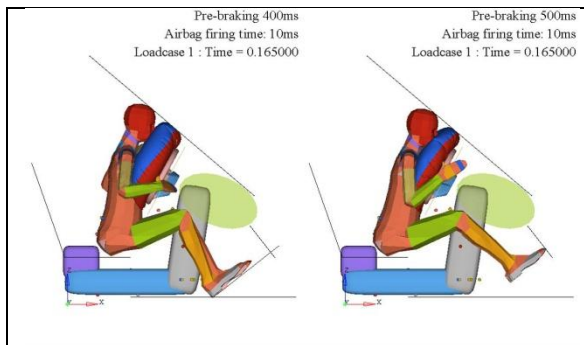


Figure 28: Occupant Kinematics Comparison between 400ms and 500ms pre-braking duration

CONCLUSIONS

This paper reviewed the kinematics and potential injury levels from different unbelted driving stances (established by the PRISM project) caused by an active safety scenario comprising of a pre-braking event followed by a 25mph FMVSS208 impact phase, using an Active Human Body Model.

It showed that using a constant pre-braking load was a too severe loadcase and that the vehicle pre-braking nose dive may have further effects on the occupant's kinematics and relationship between its position in the vehicle and the airbag system.

It was found that the unbelted driver's pre-braking kinematics were different according to the starting driving stance (FMVSS208, adjusting the radio, holding a mobile phone and driving with the arm on the armrest). It was however also found that prior to any hard contact inside the vehicle interior; the occupant's velocity was independent of the starting driving stance, as would be expected

For a standard FMVSS208 occupant starting position, subjected to a pre-braking followed by a vehicle impact phase, it has been shown that the airbag firing time (for which the extremes were set to 10 and 20ms) did not have any major influence on the shape and magnitude of the tension/compression loads and the neck moments.

It was found that the kinematics of the AHBM is the same for the first 200ms of the pre-braking phase in all models, as the braking pulse is low and is overtaken by the seat friction.

It follows that for a pre-braking lasting 500ms before vehicle impact occurs; the occupant's kinematics are modified because of the interaction

with the knee bolster, forcing the torso to rotate about the hips, hence avoiding direct head contact with the windscreen.

FURTHER WORK

Further research will consider looking into more detail in the mobile phone, armrest and radio stances and comparing their outcomes with the findings generated by the standard FMVSS208 driving stance.

Occupant injuries from accident avoidance by swerving and breaking could also be considered and compared with the ones from this paper forward pre-braking [18].

This study should be extended to look into longer duration pre-braking phase and extend the scope to duration greater than 500ms as well as including arm and leg muscle activation.

ACKNOWLEDGEMENTS

The authors would like to thank Michael Freisinger, Dr. Jörg Hoffmann for their continuous support on the realisation of this paper. Thanks goes also to Deborah Stubbs (MIRA) for her kind advice on Madymo modelling, Gabrielle Cross (MIRA) for her patience and providing PRISM project information, Mark Jones (Advanced Simtech) for his help regarding using the Madymo vehicle dynamics model and Alix Weekes/ Tony Harper (Thatcham) for their kind advice on pre-braking technology and vehicle crash pulses.

REFERENCES

- [1] Prism project. www.Prismproject.com
- [2] TRW active seatbelt and pre-braking vehicle feature. Traffic Technology Today, 17th February 2011. <http://www.traffictoday.com/news.php?NewsID=27992>
- [3] Madymo 7.2, Human Body Model user manual, Tass
- [4] Ronal de Lange, Objective Biofidelity Rating on a numerical Occupant Model in Frontal and Lateral Impact, Stapp Car Crash Journal, Vol. 49, November 2005, The Stapp Association
- [5] M. Mahangare, Investigation into the

Effectiveness of Advanced Driver Airbag Modules Designed For OoP Injury Mitigation, ESV 07-0319

[18] Accident investigation report. Advanced Simtech, Ref: 07.OF.UK.03287/MB

[6] M. Blundell, M. Mahangare, Investigation of an Advanced Driver Airbag Out-of-Position (OoP) Injury Prediction with Madymo Gasflow Simulations, Madymo User Meeting (1996)

[7] C. Bastien, Correlation of Airbag Fabric Material Mechanical Failure Characteristic for Out of Position Applications, ISMA 2010

[8] C. Bastien, Investigation into injuries of Out-of-Position (OoP) posture occupants and their implications in active safety measures, ICRASH2010 paper 2010-023

[9] R. Meijer, C. Rodarius, J. Adamec, E. van Nunen, L. van Rooij, 2007: A First Step in Computer Modelling of the Active Human Response in a Far Side Impact. International Journal of Crashworthiness, Vol. 13, No. 6, December 2008, pp. 643–652.

[10] Prism project. www.Prismproject.com. Report Reference R4A.pdf

[11] Prism project. www.Prismproject.com. Report Reference R4B.pdf, November 2003

[12] Madymo model from Advanced Simtech

[13] Prism project. www.Prismproject.com. Report Reference R4C.pdf

[14] S. Bao, Grip strength and hand force estimation, SHARP. Tech. Rep. 65-1-2000, Department of Labor and Industries, Olympia, WA, 2000.

[15] D. Bose, Influence of pre-collision occupant parameters on injury outcome in a frontal collision, Accident Analysis and Prevention 42 (2010) 1398–1407

[16] Madymo 7.2, User Reference, Tass, 2010

[17] Toyota Rav4, LS-Dyna model. NCAC. FHWA/NHTSA National Crash Analysis Center. Finite Element Model of Toyota Rav4. Model year 1997. Version 1. <http://www.ncac.gwu.edu/vml/models.html>

EFFECT OF VARIOUS PRE-CRASH BRAKING STRATEGIES ON SIMULATED HUMAN KINEMATIC RESPONSE WITH VARYING LEVELS OF DRIVER ATTENTION

Lex van Rooij

TNO

The Netherlands

Paper Number 11-0306

ABSTRACT

In this study, human kinematic response resulting from various pre-crash braking scenarios is quantified. The underlying question is what effect pre-crash braking systems have on the driver or the front seat passenger.

The vehicle deceleration pulses resulting from various pre-crash braking strategies are implemented on a vehicle interior model in a multi-body software code. The two most important strategies are based on 1) a brake assist system with modulated braking (BAS+) and 2) an autonomous braking system (AUT). In addition, simplified braking scenarios at various deceleration levels (3, 6 and 9.5 m/s²) are simulated. The driver is represented by a numerical human model incorporating, besides all passive stiffness and damping properties, algorithms that simulate active stabilising behaviour in case of an induced acceleration on the body. The lumbar and thoracic spine are stabilised by torque actuators, while the cervical spine is stabilised by Hill-type muscle segments. The level of control, bracing and reaction time delays can be varied. This allows for the simulation of various attention schemes. A parameter study is performed, in which sensitivity of the kinematic response to vehicle braking strategies and to various human reaction types are discussed and compared to findings in literature.

This study provides insight in human kinematic motion in the vehicle under various braking scenarios and human attention levels. The methods currently lack specific validation for frontal pre-crash braking, due to the lack of available volunteer testing data. Also, due to the complexity of human behaviour and the current state-of-the-art regarding its characterisation or modelling, the models are empirical of nature, however provide practical guidance to the range of possible pre-crash kinematics as a result of varying human behavioural strategies. Conclusions from this research are that driver attention plays an important role in determining the effectiveness of pre-crash braking systems in preventing severe occupant motions and in positioning the occupant in an optimum position at time of impact.

INTRODUCTION

Pre-crash braking systems

Pre-crash braking systems are being employed in vehicles on the market currently, and the performance of them is being improved with the availability of more accurate sensor technology and risk estimation algorithms. Even though these pre-crash braking systems have limited penetration in the vehicle fleet, even in developed countries, numerous studies showing their efficacy have been performed. For example, Kuehn *et al.* (2009) showed that a collision mitigating braking system (of level 2) can avoid 12.1% of all crashes if all cars would be equipped with such a system. A level 2 system is defined as a system that, based on forward environmental detection and estimation of case vehicle speed, provides a warning at Time To Collision (TTC) of 2.6 s, performs automatic partial braking of 0.4-0.6 G if the driver has not braked at TTC 1.6 s or a applies modulated braking to avoid the crash if the driver has applied the brakes at TTC 1.6 s. Schittenhelm *et al.* (2009) assessed the effectiveness of various stages of pre-crash braking systems based on comparing registered crashes with numbers of sold cars with or without such a system. The presence of Brake Assist systems resulted in 8% less rear-end collisions to occur and 13% less serious impacts against pedestrians. More advanced systems, with warning, modulated braking when the driver reacts and partial autonomous braking, similar to as defined by Kuehn as level 2, showed to be able to avoid a collision with a vehicle in front in 20% of all cases and to reduce the severity in 25% of all cases. As such, pre-crash braking systems are entering the market that act differently when the driver does or does not apply the brakes, i.e. detects the oncoming crash. In this light, Ore *et al.* (1992) indicated that roughly half of all vehicle occupants apply the brakes prior to a frontal collision.

Woldrich *et al.* (2010) presented a pre-crash braking system that attempts to position the occupant in an optimum position at the time an apparently inevitable crash occurs. Moreover, the system attempts to provide the occupant with as much as safely possible rearward velocity, in order to mitigate the consequences of a possible oncoming crash. This safety system functions

during the pre-crash braking phase by means of seat belt actuation and as such highly depends on accurate prediction of occupant kinematics in the pre-crash braking phase.

Human kinematic behaviour characterisation

As discussed in the previous section, the characterisation and quantification of human kinematic behaviour in the phase prior to the crash is of importance for optimal restraint performance and as such for mitigating fatalities and injuries in the case a crash occurs. Based on volunteer tests, Begeman *et al.* (1980) identified muscle activation reaction times of more than 200 ms when exposed to frontal impact acceleration. Choi *et al.* (2005) performed volunteer tests to assess the change in driver posture as a result of bracing for an impact that was detected by the driver. In addition, muscle activation levels were computed from EMG measurements as well as forces applied on the vehicle structures. Occupant motion as a result of acceleration was not quantified. Ejima *et al.* (2009) performed a series of tests with volunteer seated on rigid seats, restrained by a three-point belt system and subjected to a 600 ms 0.8 G constant deceleration. For a tensed volunteer, kinematic figures indicate that head forward displacement was in the order of 100 mm at 200 ms after impact, while T1 forward displacement was in the order of 25 mm and hip forward displacement around 10 mm. For a relaxed occupant restrained by a lap belt only, the head displacement was in the order of 600 mm at 600 ms after impact with T1 displacement around 400 mm. In an earlier study with tensed volunteers on simple seats and an approximate 200 ms duration 1.0 G pulse Ejima *et al.* (2007) identified that the sternocleidomastoid muscles in the neck were activated around 100-200 ms after impact at the time when the torso was moving forward more than the head, i.e. the head moved rearward with respect to T1. In a later phase, when the head/neck goes into flexion the paravertebral muscles (i.e. longus colli and longus capitis) were activated. In addition, the latissimus dorsi muscles in the torso were activated. Behr *et al.* (2010) focussed on lower extremity kinematic and muscle activation behaviour during emergency braking and established reaction times for first movement of the foot after the emergency situation was visually detected of 0.285 s (0.042 SD). Muscle activation levels were up to 57% of the maximum possible activation level for muscles in the lower extremity.

Numerical human modelling

From Crandall (2008) it can be stated that due to the breadth of variations in which collision-induced injuries occur, in order to achieve goals set in further injury and fatality reduction, numerical simulation methods allow for vehicle (restraint) design for optimising towards real-world

protection, as opposed to protection in a specific scenarios. In doing so, a concise review was presented on the state the art in numerical human modelling for injury reduction. Bose *et al.* (2008) used a numerical human model (de Lange *et al.*, 2005 & Cappon *et al.*, 1999) to study the effect of pre-impact posture, as well as levels of muscle bracing in the lower extremities and body mass and stature, on the injury risk in the event a crash was unavoidable. Pre-impact posture was shown to be the parameter affecting the injury risk the most. In an optimisation routine it was found that with a seat belt system with adaptive force limiting settings and variable pretensioner firing time, a reduction of injury risk of up to 35% could be achieved. While this study showed the necessity for the prediction of occupant kinematics, the human model used could not predict this in the pre-crash phase.

In order to develop human models that predict occupant kinematics during emergency braking manoeuvres, the active muscle response behaviour of occupants needs to be simulated. While numerous human models have been developed that simulate muscle behaviour at various levels of detail, limited models are able to predict human reactive response to an external stimuli, such as vehicle braking. Most models merely prescribe muscle activation dynamics based on electromyography (EMG) measurements in similar test environments. The first known approach to predicting human reactive response was developed by Cappon *et al.* (2007). A passive human model, validated for the crash scenarios (de Lange *et al.*, 2005) was extended with torque actuators acting on each spinal vertebrae, being controlled by a set of PID-controller, thus stabilising the spine resulting in human-like kinematics. Obviously, body internal loads as well as the stabilising algorithm were not human-like. In order to overcome this deficit, Fraga *et al.* (2009) applied similar PID controllers, however acting on Hill-type line element muscles present in a multi-body neck model. This controller approach was given a higher degree of biofidelity by developing a control algorithm that allowed for a definition of muscle recruitment strategies, provision of a level of co-contraction and uncoupled control in three main degrees of freedom of the neck, i.e. head roll, pitch and yaw motion (Nemirovsky *et al.*, 2010). Similar approaches are taken currently by Östh *et al.* (2011) and Prügler *et al.* (2010).

Objectives

The objective of this study is to predict human kinematic response resulting from various pre-crash braking scenarios, based on simulations with numerical human models that are developed to be suitable for such simulations and to study sensitivity to driver attention schemes.

METHODS

Simulation setup

For this study a human model was developed in MADYMO that was a combination of two models:

- The human model with stabilising spine (Cappon *et al.* 2007) was used for actuation of lumbar and thoracic spine
- The human neck model with Hill-type line-element muscle control (Nemirovsky *et al.*, 2010) was coupled to the above human model

This combined model is shown in figure 1.

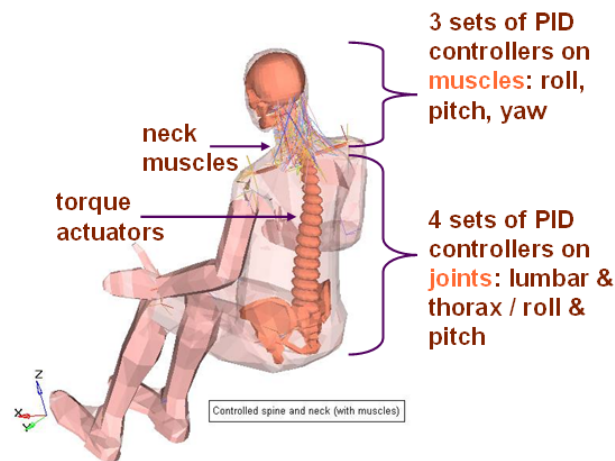


Figure 1. The MADYMO active human model with stabilising spine and neck model with line-element muscle control.

This model was positioned in a simplified vehicle interior model, in order to focus on occupant behaviour as opposed to vehicle model parameters. The human model was positioned on a rigid seat with flat surfaces at angles similar to an automotive seat. A rigid foot well surface was introduced, as well as a steering column with steering wheel. A three-point belt system with standard belt stiffness and retractor properties was fitted around the occupant. The occupant's hands were constrained to the steering wheel with a maximum force of 400 N per hand, simulating grip as based on Bao (2000). The model setup is shown in figure 2.

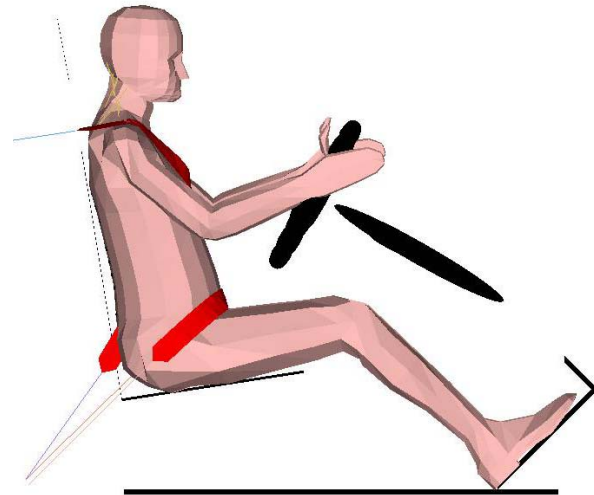


Figure 2. The MADYMO active human model in a simplified vehicle environment.

A uni-axial linear acceleration, without vehicle pitch motion, was implemented on the occupant environment in order to simulate vehicle braking. First, a set of three idealised vehicle braking pulses assuming constant deceleration from 50 km/h to 0 km/h were implemented, as shown in figure 3.

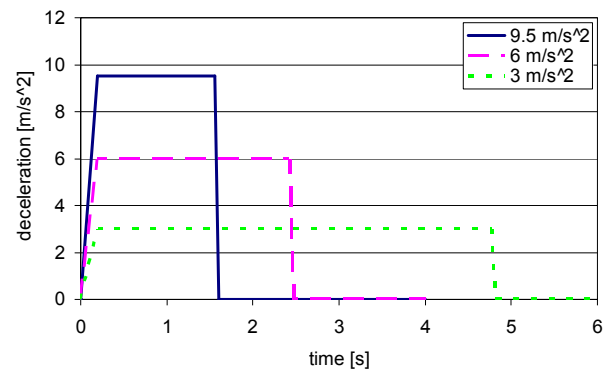


Figure 3. Idealised vehicle braking pulses at various deceleration levels, decelerating the vehicle from 50 km/h to 0 km/h.

Secondly, two pulses approximating possible responses from two types of pre-crash braking systems were implemented, as figure 4 shows:

- BAS+ is the deceleration profile arising from a Brake Assist system in which the driver applied the brake while the system applies the amount of modulated braking necessary to prevent a collision with an object in front.
- AUT is the deceleration profile from an autonomous braking system that first applies partial braking at 4 m/s², then full braking to assure collision avoidance.

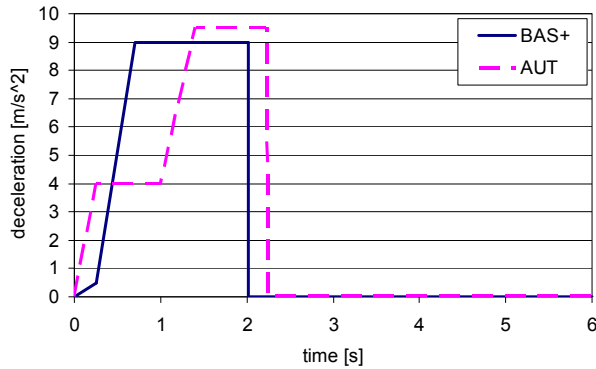


Figure 4. Pre-crash braking system pulses for Brake Assist with modulated braking (BAS+) and an autonomous braking system (AUT), both decelerating the vehicle from 50 km/h to 0 km/h.

In the human model various activation strategies or attention levels are simulated by varying settings of the controller. In table 1, three strategies are defined:

- Validated: represents the controller settings for which the human model was validated, as presented in Cappon *et al.* (2007) and Nemirovsky *et al.*, (2010). The PID controller settings for the various body parts determined through optimisation towards an experimental dataset. For the neck, frequency response perturbation tests (Keshner *et al.*, 2003) and 3.6 G rear impact tests performed by JARI (Ono *et al.*, 1999) served as validation dataset. For lumbar and thoracic spine it was based on Muggenthaler (2005)
- Attentive: originally, the controller settings for the validated strategy were believed to simulate an attentive driver due to the relatively high G level anticipated by the volunteers in the JARI laboratory tests. However, it was found that a constant level of co-contraction as high as 80% resulted in the neck locking up in a different position than the reference position due to the braking input. In order to overcome this, a co-contraction algorithm needs to be implemented that is variable for a change in head/neck pitch orientation. As such, the attentive scheme incorporated reduced co-contraction at 40% and tenfold increased PID settings in the neck. In addition, response time delay was reduced to 0 ms, since the driver is fully aware of the oncoming impact.
- The inattentive scheme presumes a person is not paying attention to the road or is even asleep. As such, the PID settings are reduced with respect to the attentive strategy. In addition, a response time of 500 ms is introduced, as well as a 10% level of co-contraction, barely able to hold the neck upright.

Table 1. Muscle activation strategies employed with varying control, delay and co-contraction (CC) settings

strategy	control	delay	CC
validated	<i>neck:</i> P: 0.4 I: 1.25 D: 0.07 <i>thorax:</i> P: 12 I: 1.1 D: 3.3 <i>lumbar:</i> P: 18 I: 1.5 D: 3.2	excitation: 30 ms activation: 10 ms response: 100 ms	80%
attentive	<i>neck:</i> P: 4.0 I: 12.5 D: 0.7 <i>thorax:</i> P: 12 I: 1.1 D: 3.3 <i>lumbar:</i> P: 18 I: 1.5 D: 3.2	excitation: 30 ms activation: 10 ms response: 0 ms	40%
inattentive	<i>neck:</i> P: 0.4 I: 1.25 D: 0.07 <i>thorax:</i> P: 0.5 I: 0.33 D: 0.33 <i>lumbar:</i> P: 5 I: 1.5E15 D: 0.32	excitation: 30 ms activation: 10 ms response: 500 ms	10%

The muscle recruitment strategy employed for this model was as commonly found in literature (Dul, 1984):

Minimise
$$\sum_j \left(\frac{F_j}{F_{MAXj}} \right)^p \quad (1)$$

Dul (1984) also proposed a value for $p=3$ to represent a minimum fatigue criterion. As such, this was adopted for this model. In order to minimise this sum, all muscles will contribute while the muscles that have the largest contribution in terms of moment in the desired direction will contribute more. The contribution of each muscle to any of the three desired head rotations (roll, pitch, yaw) is shown in table 2. Also, a division is

made for every muscle whether it contributes to head flexion or extension in the pitch direction. As such, in this model the longus colli is the strongest flexor, while the semispinalis cervicis is the strongest extensor. However, all other muscles are recruited as well only to a lesser degree (or power p).

Table 2.
Percentage contribution of each neck muscle to desired head rotation in roll, pitch and yaw direction for the MADYMO active human model.

Muscle	Total Roll	Total Yaw	Total Pitch	Type of Pitch
Hyoids	38.9%	10.0%	51.1%	Flexor
Levator Scapulae	58.9%	7.8%	33.3%	Extensor
Longissimus Capitis	56.8%	13.8%	29.3%	Extensor
Longissimus Cervicis	74.3%	4.4%	21.3%	Extensor
Longus Capitis	38.3%	13.9%	47.7%	Flexor
Longus Colli	29.0%	4.8%	66.3%	Flexor
Multifidus Cervicis	8.9%	39.5%	51.6%	Extensor
Scalenus Anterior	67.3%	18.8%	13.9%	Flexor
Scalenus Medius	83.6%	12.2%	4.2%	Flexor
Scalenus Posterior	88.0%	8.0%	4.0%	Extensor
Semispinalis Capitis	29.2%	22.9%	47.9%	Extensor
Semispinalis Cervicis	3.0%	29.3%	67.8%	Extensor
Splenius Capitis	30.8%	16.3%	52.9%	Extensor
Splenius Cervicis	40.1%	18.7%	41.1%	Extensor
Sternocleidomastoideus	49.2%	28.4%	22.4%	Extensor
Trapezius	19.3%	43.8%	37.0%	Extensor

Simulations are performed with the five braking pulses and the three muscle recruitment strategies, resulting in in total 11 simulations.

RESULTS

Attentive driver with 9.5 m/s² braking

The occupant kinematics of the attentive driver in 9.5 m/s² braking serves as a base case. The kinematic images at various phases during the braking event are shown in figures 5 to 9. At 0.2 s head and torso have moved forward. Neck flexion starts to occur after that resulting in maximum neck flexion and head forward displacement at 0.82 s. This head position slowly returns to neutral, however once the deceleration is removed, the body rebounds into the seat back, resulting in neck extension around 2.35 s.

This kinematic behaviour is a result of deceleration imposed on the occupant, the passive properties of the human model and the muscle activation time history as determined by the controller. In figure 10 the muscle activation time histories are shown for all the muscles that result in head/neck flexion. In figure 11, the same for all extensors. The flexors are all activated by 0.4 (i.e. 40% of maximum activation as given by the Hill-muscle model) due to the 40% co-contraction setting. The extensors are activated to a smaller degree (around 15%) as dictated by the co-contraction algorithm contracting all muscles without head/neck motion to occur.

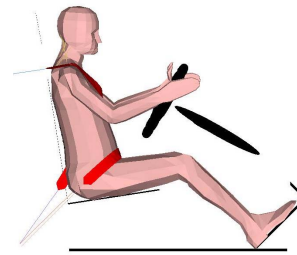


Figure 5. Attentive Active Human Model in 9.5 m/s² braking at t=0 s

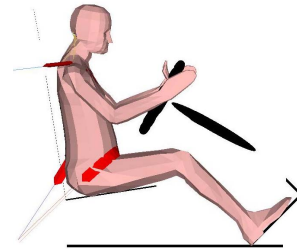


Figure 6. Attentive Active Human Model in 9.5 m/s² braking at t=0.2 s

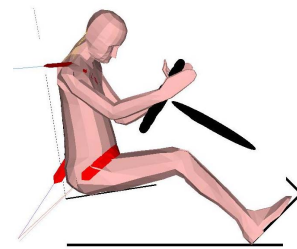


Figure 7. Attentive Active Human Model in 9.5 m/s² braking at t=0.4 s

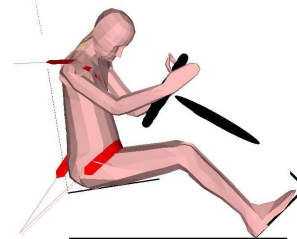


Figure 8. Attentive Active Human Model in 9.5 m/s² braking at t=0.8 s

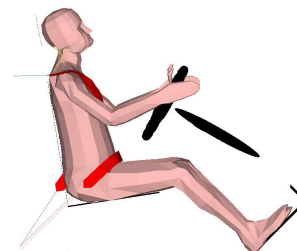


Figure 9. Attentive Active Human Model in 9.5 m/s² braking at t=2.35 s

Around 0.25 s after braking started the extensors start to activate more, attempting to overcome neck flexion observed in figure 7 and 8. The maximum activation level for the extensors is around 45% of the maximum. After 2.25 s the head is in rebound extension due to which the flexors start to activate. These figures also indicate that many muscles are activated however at different activation levels as given by the chosen muscle recruitment strategy. The flexor muscle with largest degree of activation is the longus colli, as dictated by table 2.

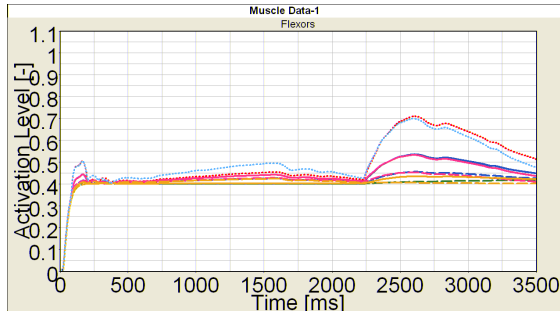


Figure 10. Flexor muscle activation signals for attentive Active Human Model in 9.5 m/s² braking.

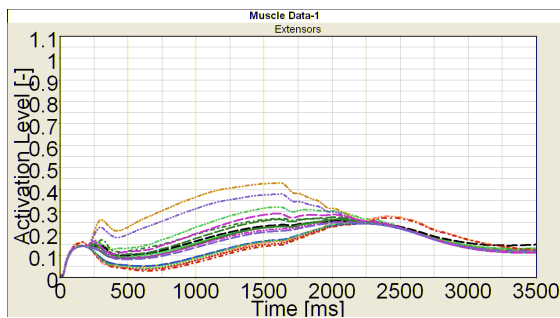


Figure 11. Extensor muscle activation signals for attentive Active Human Model in 9.5 m/s² braking.

Inattentive driver with 9.5 m/s² braking

The occupant kinematics of the inattentive driver in 9.5 m/s² braking is presented in comparison. The kinematic images at various phases during the braking event are shown in figures 12 to 15. At 0.2 s head and torso have moved forward slightly more than in the attentive scenario. Neck flexion starts to occur after that resulting in maximum neck flexion and head forward displacement at 0.78 s. The flexion is larger than in the attentive case, even resulting in the chin to contact the chest. This head position persists until the deceleration is removed and the body rebounds into the seat back, resulting in neck extension around 2.35 s.

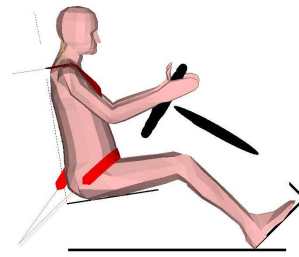


Figure 12. Inattentive Active Human Model in 9.5 m/s² braking at t=0 s

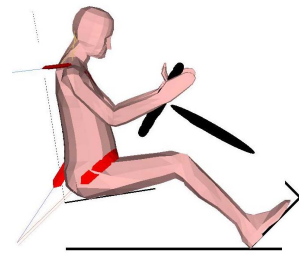


Figure 13. Inattentive Active Human Model in 9.5 m/s² braking at t=0.2 s

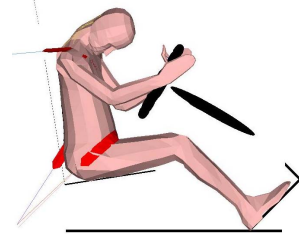


Figure 13. Inattentive Active Human Model in 9.5 m/s² braking at t=0.4 s

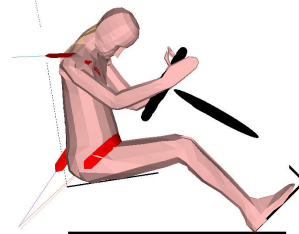


Figure 14. Inattentive Active Human Model in 9.5 m/s² braking at t=0.8 s

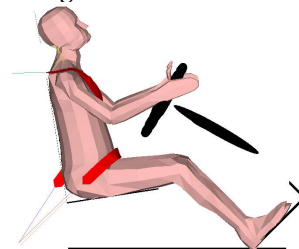


Figure 15. Inattentive Active Human Model in 9.5 m/s² braking at t=2.35 s

This kinematic behaviour is a result of deceleration imposed on the occupant, the passive properties of the human model and the muscle activation time history as determined by the controller. In figure 16 the muscle activation time histories are shown for all the muscles that result in head/neck flexion. In figure 17, the same for all extensors. The flexors are all activated by 0.1 (i.e. 10% of maximum activation as given by the Hill-muscle model) due to the 10% co-contraction setting. The extensors are activated to a smaller degree (around 3%) as dictated by the co-contraction algorithm contracting all muscles without head/neck motion to occur.

After 0.5 s, which was defined as the response time delay, the controller activates both flexors and extensors in an attempt to stabilise the neck. However, this approach is unsuccessful in counteracting the inertial load on the head as a result of braking. Only after braking has stopped and the head rebounds into extension do the flexors act to bring the head in a more neutral position.

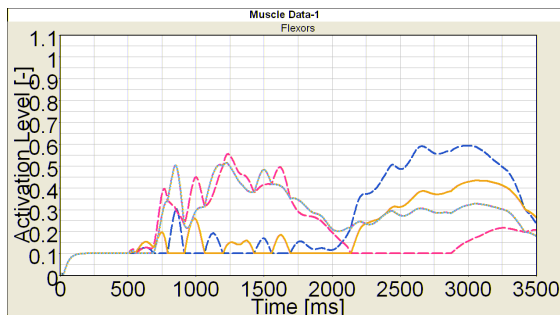


Figure 16. Flexor muscle activation signals for inattentive Active Human Model in 9.5 m/s² braking.

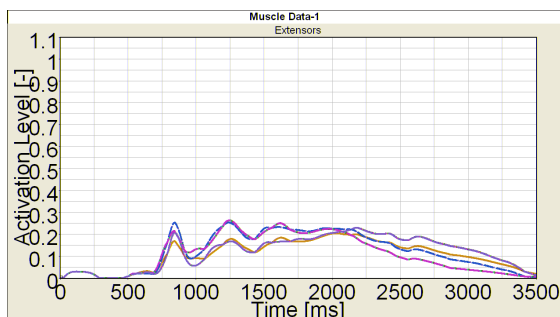


Figure 17. Extensor muscle activation signals for inattentive Active Human Model in 9.5 m/s² braking.

Parameter study

Results from the parameter sensitivity study are condensed in table 3 where maximum forward displacement of human model head centre of gravity, T1 and pelvis are shown together with the time at which this occurs. The simulation with the validated muscle recruitment strategy is shaded, as it was found not valid for braking simulations due

to the lock up of the neck in forward flexed position. For all simulations pelvis forward displacement was negligible, most likely caused by the simulated environment with optimal seat belt and rigid seat and foot well.

Table 3. Human model excursion in various braking scenarios with various muscle activation strategies

Braking accel.	Human activation	Head X[mm] t [s]	T1 X[mm] t [s]	Pelvis X[mm] t [s]
9.5 m/s ²	validated	181 <i>1.22</i>	87 <i>1.56</i>	12 <i>1.56</i>
9.5 m/s ²	attentive	157 0.82	91 1.57	10 1.56
6 m/s ²	attentive	129 0.87	68 1.69	1 0.28
3 m/s ²	attentive	93 0.93	49 1.29	0 0.0
BAS+	attentive	163 1.37	100 2.02	10 2.01
AUT	attentive	147 1.50	80 1.49	4 1.51
9.5 m/s ²	inattentive	180 0.78	90 1.56	11 1.56
6 m/s ²	inattentive	158 0.45	69 1.71	2 0.28
3 m/s ²	inattentive	146 0.49	53 0.99	0 0.0
BAS+	inattentive	291 2.03	207 2.02	6 1.88
AUT	inattentive	149 0.49	83 1.48	3 1.49

The 10 simulations with 2 muscle recruitment strategies (attentive, inattentive) and the 5 braking pulses are discussed based on figure 18 and 19 in which the results from table 3 are plotted. For the attentive scenario and simple (3, 6 or 9.5 m/s²) braking the maximum head forward displacement occurs at around 0.8 to 0.9 s with varying levels of forward displacement: 157 mm for 9.5 m/s², 129 for 6 m/s² and 93 mm for 3 m/s². For the inattentive scenario and simple braking higher head forward displacements are seen for all braking severities. In addition, timing of maximum head displacement is lower for lower braking severity.

The BAS+ system with an attentive occupant displays similar levels of head forward displacement as a 9.5 m/s² pulse however with 0.5 s delay. When referred back to figure 3 and 4, the BAS+ pulse is similar to the 9.5 m/s² pulse with a delayed start. As such, this explains the similarity.

The AUT system with inattentive occupant shows good performance since the head forward displacement is nearly identical to that of the 3 m/s² pulse, even though the deceleration level is higher up to 1.0 m/s².

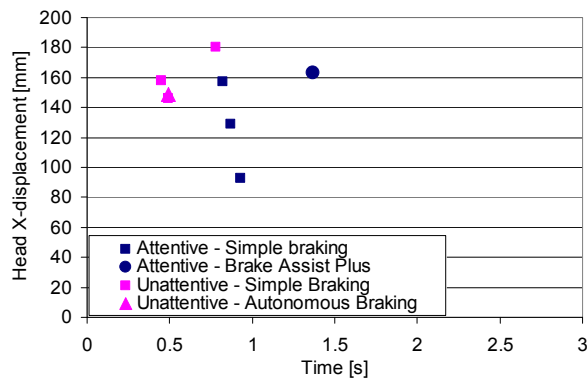


Figure 18. Head forward displacement as function of time for various combinations of braking scenarios and muscle activation strategies.

The T1 forward displacement is very similar between attentive and inattentive occupant for the simple braking cases. This indicates that the spinal stabilisation algorithm has limited influence in the simulated setup, possibly again due to the fairly optimal restraint with rigid seat. Again for BAS+ a delay is observed.

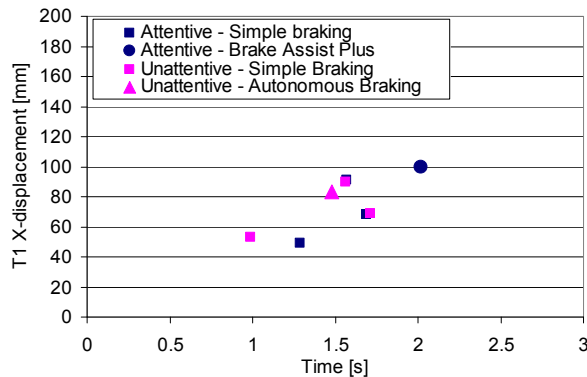


Figure 19. T1 forward displacement as function of time for various combinations of braking scenarios and muscle activation strategies.

DISCUSSION

The human model in this study was validated for specific dynamic loading conditions, such as frequency perturbations, rear impact and hub impactor tests. A first application in a braking scenario demonstrated that the validated controller settings were not valid for this application. The multi-body neck model with musculature was validated for front, rear and side impact. As such, the lack of validation in this case demonstrates that muscle control strategies of humans are more complex than currently implemented. The question

that can not be answered based on the current study, but that would need to be answered is whether the chosen controller approach can be used to result in a model that can be validated for a number of scenarios. In other words, can a PID controller with delays and co-contraction setting be tuned to represent a number of scenarios while the parameters that define the controller are known instead of need to be tuned for every specific condition?

The fact that the validated setting did not create results that were anticipated is based on empirical findings as opposed to on the availability of a specific volunteer braking validation dataset. The braking tests performed by Ejima (2009&2007) are sufficiently similar to make a quantitative comparison with the results from this study. Head forward displacement in 8 m/s² deceleration was around 100 ms in Ejima's volunteer dataset, while it would be between 129 and 157 mm based on these results. T1 displacement was around 25 mm in Ejima's tests, while it would be between 68 and 91 mm in this study. As such, this model predicts around 50 mm larger T1 and head forward displacement. Since T1 is largely influenced by the seat belt, this may cause the better restraint of the torso and resulting lower T1 and head forward displacement. Additionally, Ejima discussed the activation of the sternocleidomastoid muscle early in the braking phase, which was not observed in the current study. The activation of longus colli, one of the paravertebral muscles, to overcome extension during rebound was observed in both Ejima's study as well as in the current.

CONCLUSIONS

The developed model showed applicable and sensitive to frontal pre-crash scenarios, however specific validation for frontal pre-crash braking based on kinematics and muscle activation patterns is required for assessing the controller parameters.

REFERENCES

- Bao S., Grip strength and hand force estimation, SHARP Tech. Rep. 65-1-2000, Department of Labor and Industries, Olympia, WA, 2000.
- Begeman, P., King, A., Levine, R., Viano, D.C., 1980. Biodynamic response of the musculoskeletal system to impact acceleration. In: Proceedings of the Twenty-fourth Stapp Car Crash Conference, Society of Automotive Engineers, Warrendale, PA, pp. 477–509.
- Behr, M., Poumarat, G., Serre, T., Arnoux, P.J., Thollona, L., Brunet, C., 2010 "Posture and Muscular Behaviour in Emergency Braking:

An Experimental Approach” *Journal of Accident Analysis and Prevention* 42 (2010) 797–801

Bose, D, Crandall, JR, Untaroiu, CD, Maslen, E. (2008) Influence of pre-collision occupant properties on the injury response during frontal collision. *IRCOBI Conference on the Biomechanics of Impact*.

Cappon H.J.; Kroonenberg R.; Happee R.; Wismans J.S.H.M. (1999) An Improved Lower Leg Multibody Model, *Proceedings of IRCOBI Conference*, pp. 499-512

Cappon H.J. ; Mordaka J.; van Rooij L.; Adamec J.; Praxl N.; Muggenthaler H.(2007) “A computational human model with stabilizing spine: a step towards active safety”, *SAE paper 2007-01-1171*.

Choi, HY, Sah, SJ, Lee, B, Kang, S, Mun, MS, Lee, I, Lee, J. (2005) Experimental and numerical studies of muscular activations of bracing occupant. Paper 05-0139, *International Technical Conference on the Enhanced Safety of Vehicles (ESV), Proc. 19th ESV*.

Crandall, J., “Simulating the Road Forward: the Role of Computational Modeling in Realizing Future Opportunities in Traffic Safety” *IRCOBI Conference on the Biomechanics of Impact*.

Dul J., Townsend M.A., Shiavi R., Johnson G.E., ‘Muscular Synergism- I. On Criteria for Load Sharing Between Synergistic Muscles’, *Journal of Biomechanics*, Vol. 17 N°9, 1984, pp 663-673.

Ejima, S, Ono, K, Holcombe, S, Kaneoka, K, Fukushima, M. (2007) A Study on Occupant Kinematics Behaviour and Muscle Activities during Pre-Impact Braking Based on Volunteer tests. *IRCOBI Conference on the Biomechanics of Impact*.

Ejima, S., Zama, Y., Ono, K., Kaneoka, K., Shiina, I., Asada H., (2009) “Prediction of Pre-Impact Occupant Kinematic Behaviour based on the Muscle Activity During Frontal Collision” *International Technical Conference on the Enhanced Safety of Vehicles (ESV), Proc. 21st ESV*.

Fraga F.S., Van Rooij L., Happe R., Wismans J., Symeonidis I., Peldschus S., ‘Development of a Motorcycle Rider Model with Focus on Head and Neck Biofidelity, Recurring to Line Element Muscle Models and Feedback Control’, *ESV 09-0244*, 2009.

Keshner E. A., ‘Head-Trunk Coordination During Linear Anterior-Posterior Translations’, *Journal of Neurophysiology*, vol. 89, 2003, 1891-1901.

Kuehn, M., Hummel, T., Bende, J. 2009. “Benefit estimation of advanced driver assistance systems for cars derived from real-life accidents” *International Technical Conference on the Enhanced Safety of Vehicles (ESV), Proc. 21st ESV*.

Lange R. de, Rooij L. van, Mooi H., Wismans, J. (2005): Objective biofidelity rating of a numerical human model in frontal to lateral impact. *Stapp Car Crash Conference, SAE 2005-22-0020*, 2005.

Muggenthaler, H., Praxl, N., Adamec, J., Von Merten, K., Schönpflug, M., Graw, M., Schneider, K. (2005) The effects of muscle activity on human kinematics and muscle response characteristics – Volunteer tests for the validation of active human models. *Digital Human Conference paper 06DHM-8*.

Nemirovsky, N., Rooij, L. van 2010, “A New Methodology for Biofidelic Head-Neck Postural Control” *International Technical Conference on the Enhanced Safety of Vehicles (ESV), Proc. 21st ESV*.

Ore, LS. 1992. “Design requirements and specifications” dummy lower extremity development task. *Event Report, NHTSA*.

Ono K., Inami S., Kaneoka K., Gotou T., Kisanuki Y., Sakuma S., Miki K. ‘Relationship between localized spine deformation and cervical vertebral motions for low speed rear impacts using human volunteers’, *IRCOBI Conference 1999*.

Östh, J., Brodin, K., Carlsson, S., Wismans, J., Davidsson, J. (2011) “The Occupant Response to Autonomous Braking: A Modeling Approach That Accounts for Active Musculature” in submission

Prügler, A. 2010 “Näher am Menschen” *Virtuelles Fahrzeug, Magazine Nr. 8, IV-2010*

Schittenhelm, H. 2009. “The Vision of Accident-Free Driving – How Efficient are we actually in Avoiding or Mitigating Longitudinal Real World Accidents” *International Technical Conference on the Enhanced Safety of Vehicles (ESV), Proc. 21st ESV*.

Woldrich M. 2010. “Movement in the PRE-Crash situation - A simulation research with a reversible PRE-SAFE® Pulse system” *Airbag 2010 conference*

PRESENTATION AND DISCUSSION OF A CRASH TEST USING A CAR WITH AUTOMATIC PRE-CRASH BRAKING

Alexander Berg

Peter Rücker

DEKRA Automobil GmbH
Germany

Christian Domsch

BMW AG
Germany

ESV Paper Number 11-0318

ABSTRACT

The utilisation of passive safety systems to protect occupants has attained a very high level over the past thirty years. Although further improvements are still possible, these increasingly minor improvements are only to be had with a high degree of effort. As a result, the key question must always be their efficacy in an accident situation. If reliable information is available on the imminent collision, measures taken in the pre-collision phase can as a rule frequently exert a significantly greater influence on the accident situation. Preventive measures are the key to success here.

This paper aims to show how a preventive safety approach can contribute to lessening the serious consequences of an accident by creating an optimum interplay of active and passive safety measures. To further enhance vehicle safety, driver assistant systems are already available that warn the driver of an imminent rear-end collision, support him in his reactions or if he fails to react sufficiently, to even initiate an automatic braking, should the collision prove unavoidable.

Automatic pre-crash braking can, in an ideal situation, fully prevent such collisions or can greatly reduce the collision speed and thus the impact energy (and in turn the severity of the accident).

If a vehicle is being braked in the lead-up to the collision, the occupants are already being pre-stressed by the deceleration. The information available about the imminent accident can be used to activate the belt tensioners and likewise other passive safety systems in the vehicle before the advent of the impact. The vehicle deceleration before the crash also causes the front of the vehicle to dip. Conventional crash tests do not take this specific impact situation into consideration. This is why, for example, the influences of the pre-collision movements of the

occupants are not recorded in the test results. Furthermore, a reproducible representation of the benefit of the vehicle safety systems which prepare the occupants for the imminent impact is not possible.

In order to demonstrate the functions of automated pre-crash braking and to investigate the differences during the impact as a consequence of the altered occupant positions as well as the initiation of force and deformations of the vehicle front, DEKRA teamed up with BMW to carry out a joint crash test with the latest BMW 5 series vehicle.

It involved the vehicle braking automatically from a starting test speed of 64 km/h (corresponding to the impact speed set by Euro NCAP) to 40 km/h. The test was still run by the intelligent drive system of the crash test facility. The test supplemented the work of the vFSS working group (vFSS stands advanced Forward-looking Safety Systems]).

The paper will describe and discuss the relevant test results. In addition, the possible benefits of such systems will also be considered. The test required several modifications to be made to the test facility as well as the vehicle. The paper will also deal with that.

INTRODUCTION

Active safety systems designed to avoid accidents and passive safety systems for lessening the consequences of an accident used to be considered separately. This isolated approach was dispensed with after it was recognised that active safety systems favourably influence both active and passive safety.

One example of this is the electronic stability control ESC. It was primarily developed to prevent accidents following a loss of vehicle control (so-called skidding accidents). Analyses of real-life accidents have, however, shown that ESC not only prevents accidents, but also can mitigate unavoidable

accidents and their consequences. [1, 2, 3]. One typical example is the alteration to the impact situation of what are normally for occupants particularly severe lateral collisions to less severe frontal collisions due to the effect of ESC.

Another example is the brake assist system BAS. It supports the driver after the initiation of a hard stop by helping to reduce the speed of the vehicle by a maximum and bringing it to a halt (or until the braking is interrupted) at the highest possible level. This shortens the brake path and can avoid collisions. Where the accident cannot be avoided, it reduces the impact speed (and thus the severity of the accident) in collisions with other vehicles or pedestrians. The potential of a conventional brake assist system to prevent accidents and to lessen the consequences can be further enhanced by combining it with distance radar [4].

This led to the coining of the term "integrated safety". Here, a holistic approach is taken to the effect of vehicle safety systems both as regards active safety as well as passive safety.

By utilising information from the pre-crash phase, certain passive systems can already be influenced at an early stage. This improves the effectiveness of the safety measures overall. If the vehicle has already reached a state of dynamic instability, or if a head-on collision is unavoidable, the belts, for example, of driver and front passenger can be pre-tensioned and the seat backs straightened. This brings the occupants into a stress-decreasing position [5].

Despite these additional safety effects that have since been verified many times in findings derived from real-life accidents, passive and active safety still continue to be evaluated separately in the relevant test scenarios.

Crash tests serve to test and evaluate the passive safety of a vehicle, covering deformation zones, occupant cell as well as the seat belts and airbags. The active safety, such as the effect of ESC and BAS, for example is analysed in separate driving tests.

So far there exists no test standard that enables a reliable and comparative statement on the extended effect of active safety systems on passive systems. In order to be able to reproducibly test and evaluate the effects of relevant systems in crash tests according to the holistic approach of integrated safety, the pre-crash reactions of the vehicle must be initiated in a realistic manner well before the impact with the barrier. If, for example, automatic pre-crash braking is initiated before the impact, the vehicle front dips and a displacement of the occupants relative to the vehicle takes place. Both factors are important for the

course and the results of the crash test. However, these are not taken into account in today's standards.

VFSS WORKING GROUP

The aim of the vFSS working group (vFSS stands for advanced Forward-looking Safety Systems) is to promote the market penetration of front protection systems designed to avoid accidents and to lessen the consequences of accidents into the volume model segment and to further improve road safety. To achieve this it is necessary to stipulate test standards for preventative safety systems that reflect real-life situations. In order to attain this all the German car manufacturers joined forces with the accident database centre of the German Insurers Association, the Federal Institute for Highway Safety (BASt), and the AZT Group under the chairmanship of DEKRA and the Vehicle Test Institute Germany (KTI), set up the vFSS working group. Honda and Toyota joined the working group at a later date. Findings from accidents and definitions of system requirements are divided into three work packages "accident analysis", "pedestrian safety" and "longitudinal traffic safety systems".

The preliminary findings of the vFSS working group gave occasion for a demonstration of the efficacy of an emergency braking system in a vehicle impact with a barrier. The first crash test with such an automatic braking of the vehicle was carried out in the 2,222nd crash test at the DEKRA Crash Test Center in Neumünster.

HISTORIC DEVELOPMENT OF THE ACCIDENT SITUATION AND OBJECTIVES

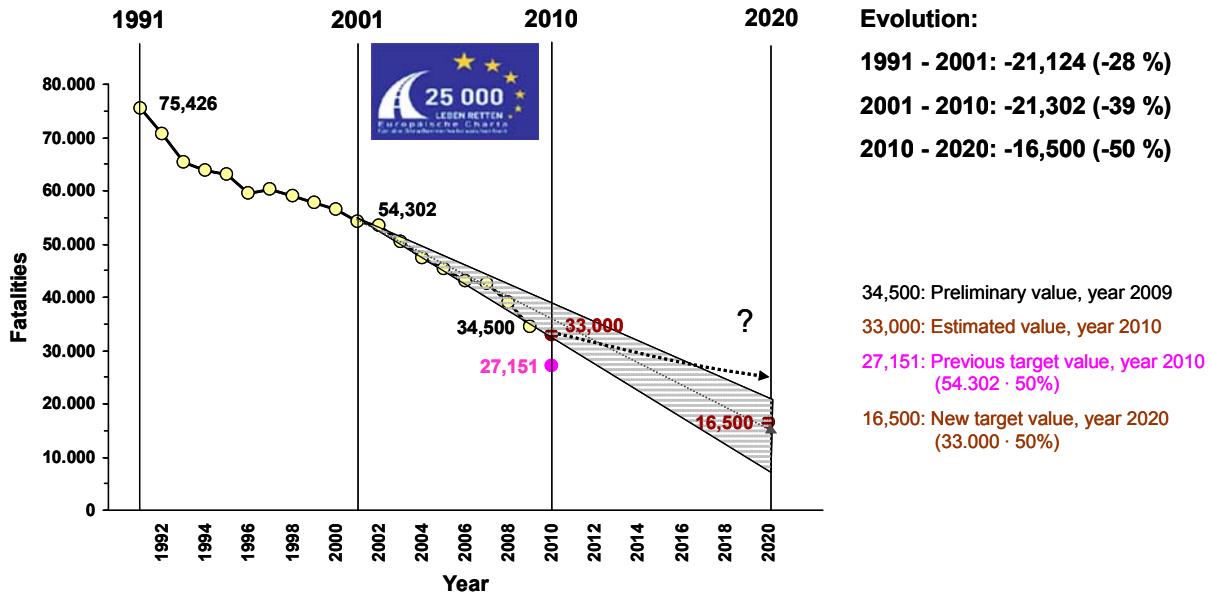
Accident statistics show that considerable advances in safety have been made over the past decades. For example, in Europe (EU-27) the number of road deaths per year fell from 1991 to 2001 by 28%, **Fig 1**. Now nearing its end, the third European road safety campaign provides preliminary figures that suggest a further reduction in the number of annual road deaths from 2001 to 2010 by 39%. The new EU guidelines for road safety until 2020 have set the objective of achieving a further reduction of 50% to approximately 16,500 road fatalities per annum.

Although a linear continuation of the past trend could possibly see this renewed and very ambitious target being met, it is also just as likely that the previous positive development will reach saturation point as an effect of the vehicles already equipped with conventional safety technology (including ESC) and

will tail away in the future. To ensure that the objective is met by 2020 it is therefore urgently

necessary to introduce new technologies with demonstrable effect to further improve vehicle safety.

Fig 1. Development of the number of road deaths in the European Union (EU-27) from 1991 until 2008 as well as previous and new objectives (source: CARE European Road Accident Database)



EXAMPLE TO DEMONSTRATE THE ENERGY POTENTIAL OF PRE-CRASH BRAKING

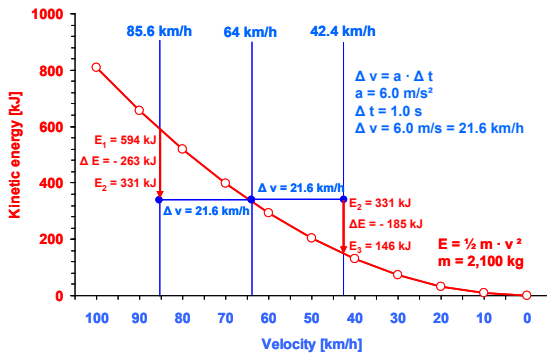
A key factor in the severity of a road accident is the kinetic energy of the vehicles involved at the start of the collision. This energy can be effectively reduced by pre-crash braking. Possible magnitudes of the relevant potential illustrate a simple calculation (see Fig 2).

Let us assume that the pre-crash braking is 1.0 s before the collision begins and the vehicle until collision is braked at a medium deceleration of 6.0 m/s². This reduces the speed of the vehicle before the collision by 21.6 km/h. So, the initial speed of 85.6 km/h is reduced to a collision speed of 64 km/h (as in a Euro NCAP crash test). An initial speed of 64 km/h would see the collision speed reduce to 42.4 km/h.

For a vehicle with a mass of 2,100 kg, this means that the kinetic energy in the above mentioned cases would be reduced by 263 kJ (185 kJ respectively) until the collision starts.

In a crash test with an impact speed of 64 km/h (Euro NCAP) the impact energy of the vehicle weighing 2,100 kg is 331 kJ. Once the impact has taken place this energy is transformed into deformation work by the "mechanic crumple zone" in the front of the vehicle and in the deformation element on the barrier. Pre-crash braking has therefore produced an additional "virtual deformation zone". Taking the figures assumed in the example, this "virtual deformation zone" can additionally absorb between 56% and 80% of the energy absorbed by the "mechanical deformation zone".

Figure 2: Reductions in the impact energy of a 2,100 kg vehicle following pre-crash braking with a deceleration of 6.0 m/s² and duration of 1.0 s at different starting speeds.



In order to achieve the same effect using conventional mechanical structures, the vehicle front would need to be considerably longer and / or significantly stiffer. A longer vehicle front would negatively affect the weight, vision and vehicle handling. A stiffer front would negatively affect compatibility with regard to the accident exposures of more vulnerable road users. A "virtual deformation zone" does not have such disadvantages. It is merely necessary to be able to safely recognise an unavoidable collision with pre-crash evaluation of signals received by already existing assembly groups in the vehicle, and then, if the driver fails to react, to trigger an automatic pre-crash braking action before the collision.

Such a procedure has already been implemented for collisions in which a vehicle collides with the rear of another vehicle, as such rear-end collisions can be recognised with a high degree of reliability by already existing sensors.

Other collision scenarios that can also lead to damage of the vehicle front, such as, for example, front-front scenarios or front-side scenarios cannot be handled in the same way at the moment. However, even if the range of applicability is still currently restricted, these systems represent the launch pad for sustained further improvement. The basis must always remain the objective of reducing the number of fatalities, injuries and property damage in real-life accident situations for all those involved.

CRASH TEST

In order to represent the effect of a "virtual crumple zone" in an actual crash test, the DEKRA Crash Test Center in Neumünster carried out a test incorporating this aspect. Planning a test involving an automatically braking vehicle poses two challenges: Firstly, the test facility influences object detection by the vehicle

sensors and, secondly, the test facility sled system must interact with the braked vehicle.

Most modern frontal protection systems detect what is in front of the vehicle on the basis of radar sensors. Several problems arise if these sensors are now to be operated in a hall and the crash block is to be reliably detected as a relevant target object. The radar signal can be reflected from all manner of points in the hall. The hall supports made of reinforced concrete, metal girders for the roof as well as supports and stands for providing the crash area with sufficient lighting all represent additional potential detection targets. The crash block also constitutes an upright obstacle. This means that it cannot always be clearly differentiated from other objects as a relevant sensor target. Multiple reflections in the enclosed hall are likewise possible. To overcome these problems and to conduct a crash test with the vehicle's own environment detection system requires extensive modifications in the vehicle's object detection system.

However, the basic principle on which the object detection system works and the reactions of the entire system in the vehicle should not be altered.

In order to hit the pre-defined impact point on the barrier as accurately as possible the regulated vehicle guidance system of the facility must be engaged for as long as possible. This means that it is not possible to separate the vehicle from the traction trolley at the moment the braking is initiated. Thus the control of the traction cable of the crash facility constitutes a further problem. The desired impact speed is a control variable of crash testing facilities nowadays. If braking is undertaken on the vehicle during the traction phase, the pulling force of the facility is simply increased to attain the previously defined collision speed.

The regulation of the traction cable drive of the facility had to be altered to prevent this. The software of the modified drive control analyses the additional reaction forces measured in the cable. From this the traction force momentarily required is computed to, firstly, ensure the longitudinal guidance of the vehicle and, secondly, to follow the deceleration of the vehicle caused by its autonomous braking system.

The Test Vehicle

The test vehicle was a BMW 530d **Fig 3**. The vehicle was fitted with the currently available active speed regulation system with Stop&Go function including head-on collision warning with braking function. This is a radar-based speed and distance regulation system. The system can also monitor the traffic

environment in front of the vehicle if the speed regulation system is not activated. If a critical head-on situation is detected, the driver is warned in two stages. If the critical nature of a head-on collision situation is very high, a visual-acoustic acute warning is additionally activated that initiates an automatic partial braking with a deceleration of 3 m/s^2 . This means the speed is already being reduced during the driver's reaction time. If the driver reacts, he already encounters a pre-stressed brake and swiftly reaches full deceleration with the aid of the brake assistant.

This equipment, which is currently found on production models, was taken as a basis for the development of a prototype front safety system which finally fulfils the requirements of a test in the hall. This means that it must be first assured that the radar sensor can also reliably detect the target object, in this case the barrier. It is essential that this detection is assured despite the difficult conditions prevailing in the hall. Preliminary tests using the production model object detection system have shown that realistic object detection cannot always be reliably guaranteed in the test conditions. The sensor is normally configured so that it attains its optimum performance in real-life traffic situations. The laboratory crash cannot take into account the real-life traffic environment. This is why the object detection system was subject to tests and modified so that the relevant target can be reliably detected in the hall environment. Testing in the hall can work with restrictions that are not possible in real-life road traffic, e.g. it can be guaranteed in the test in question that the target object travels will continue in a straight line in front of the vehicle and does not carry out any manoeuvres of its own. It must be noted that the constellation used in the hall is not suitable for operating the system in real-life traffic, just as much as the production object detection system is equally unsuitable for operation in the hall.

This alteration in the coordination made it possible to determine the distance to the target object in question, in this case the crash block, as well as the relative speed on the basis of the information provided by the radar sensors of the active speed and distance regulation. It was therefore also possible to trace the entire signal chain from sensor to reaction of the safety systems or to initiation of the automatic emergency braking. Therefore, the safety systems in the test reacted precisely as they would do in a comparable real-life accident scenario.

As the vehicle approached the crash block, different, in part prototype-stage, safety functions were activated, Fig 4. Apart from the ACC radar sensor with special object detection, object identification

and selection, a ABS with prototype function was also necessary to achieve full deceleration. The vehicle was still equipped with electromotive reversible belt retractors for both driver and front passenger. The strategy employed for the driver warning and the initiation of an emergency braking action was also the subject of a prototype design. Finally, a pre-crash deactivation of the fuel pump was also envisioned. The automatic emergency call function after the crash corresponded to the production standard and was likewise employed as part of the test.

In the course of the test the point was eventually reached in which a collision is no longer avoidable by the driver reacting alone (evasion or braking), Fig 5. At this point the automatic emergency braking of the vehicle intervenes and reduces the speed at a maximum deceleration stipulated by the friction coefficient between tyres and road surface.

Figure 3: The test vehicle



Figure 4: Prototype equipment of the test vehicle

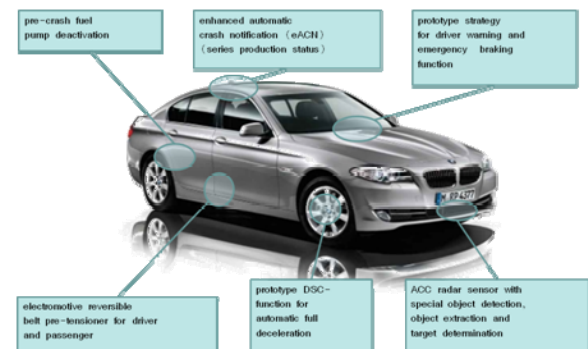
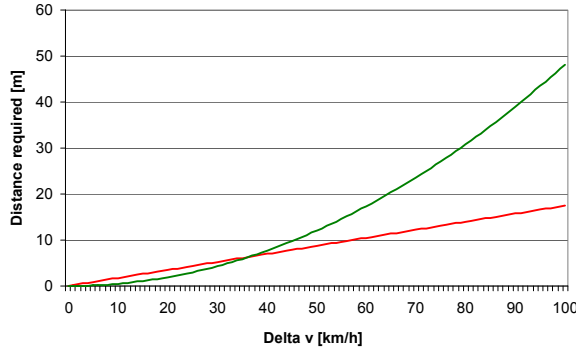


Figure 5: Required distance for an evasive manoeuvre (red curve) and a braking manoeuvre (green curve, $a = 8 \text{ m/s}^2$) to avoid a head-on collision depending on the difference in speed Delta v



As a comparison another BMW 5 series car without front safety system was tested conventionally (i.e. unbraked) using the same configuration.

Test based on the Euro NCAP or IIHS frontal impact test

A starting speed of 64 km/h was chosen for the test. This corresponds to the starting speed of the (unbraked) frontal impact test carried out in accordance with Euro NCAP or IIHS.

The weight of the vehicle in its test condition was 2,164 kg. The vehicle was tested with a running engine so that it could be assured that all the systems were functioning.

As in the Euro NCAP or IIHS test the vehicle overlap was 40%. Driver and front passenger were represented by belted and equipped dummies (Hybrid III 50th percentile male). Children dummies were not used.

In contrast to the normal test procedure in which no pre-crash systems are permitted to be active, they were deliberately activated in this case. Once the vehicle had been accelerated up to test speed, it approached the crash block at a constant speed. At a TTC of 2.1s (TTC = Time To Collision – time that passes until impact if the speed remains constant) the driver is notified by an acoustic warning sound of the impending head-on collision. This warning is effected by a red warning light in the instrument panel and by a warning symbol in the head-up display. It means that the driver sees the symbol directly in front of his field of vision. At the same

time the brake of the vehicle is pre-stressed and the trigger threshold of the brake assistant reduced.

In the system represented here an acoustic warning to the driver is triggered at a TTC of 1.7 s before the impact. At the same time, the system also issues an acoustic alarm in addition to the visual warning. The reversible belt tensioners were activated at a TTC of 1.1 s before impact in order to prevent the occupants from being displaced forward during the braking action. The automatic emergency braking of the vehicle was initiated at 0.9 s before collision. This reduced the speed of the vehicle from 64.8 km/h to 40.4 km/h (-38 %). This corresponds to a reduction of the kinetic energy until collision with the barrier of 61 % from 351 kJ to 136 kJ Fig 6.

The controller of the facility pulling system detected the vehicle deceleration caused by the automatic pre-crash braking and reduced the pulling speed of the drive cable correspondingly.

The lateral deviation of the impact point on the barrier was only 2 mm. The dipping of the vehicle front caused by the braking led to a lowering of the impact point by 35 mm, Fig 7.

The comparison vehicle impacted unbraked at 64 km/h into the barrier.

Figure 6: Alteration of the speed and the kinetic energy of the test vehicle as a consequence of pre-crash braking

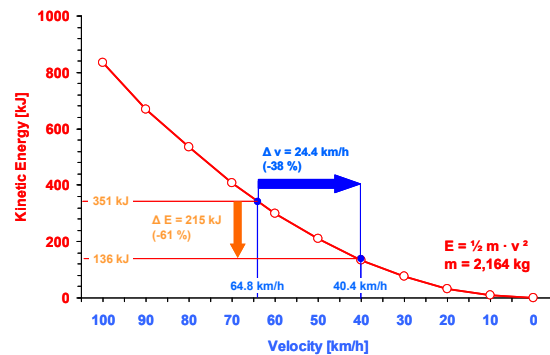


Figure 7: Side view of the braked impact

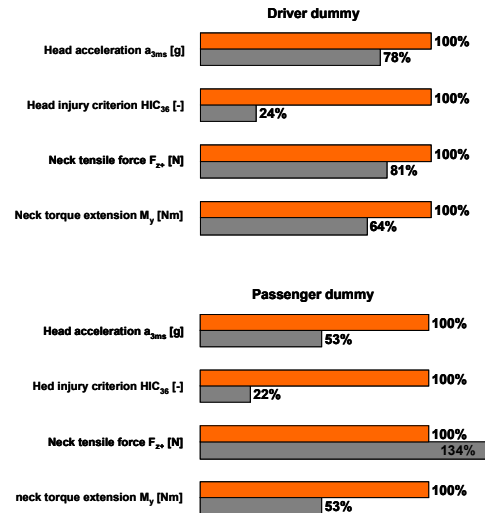


Occupant Load

Even the production model BMW 5 displayed exemplary behaviour in the unbraked crash test. This is underscored by the superb ratings achieved in the US-NCAP, Euro NCAP and IIHS test procedures. As a consequence of the reduced impact speed the measured load on the occupant dummies in comparison to an unbraked crash test at 64 km/h was further reduced by a considerable amount. The relative changes of some key load figures for driver and front passenger dummy are shown in **Fig 8**.

Thus, for example, the head injury criterion HIC36 of the driver dummy in the braked crash test fell by 76% in comparison with the unbraked test. The corresponding reduction for the front passenger dummy was 78 %. The characteristic value for head deceleration a_{3ms} was reduced by 22% for the driver dummy and by 47% for the front passenger dummy.

Figure 8: Comparison of the load figures for the driver and front passenger dummy during the unbraked crash test at an impact speed of 64 km/h (100 % in each case) and in the braked crash test at an impact speed of 40 km/h



Vehicle deformation

The deformed vehicles are shown in **Fig 9**. The area around the front left wheel in particular shows the significantly lower deformation of the vehicle.

Figure 9: Comparison of the deformation of the front of the two test vehicles.



SUPPLEMENTAL FINDINGS FROM REAL-LIFE ACCIDENTS

As various accident research projects and reports in the media show, the risk of car occupants suffering serious or fatal injuries in frontal impacts continues to be very high. About 50% of the seriously injured and

about 40% of the killed vehicle occupants result from a collision at the vehicle front (GIDAS). In about 60% of cases the opponent in the accident was another vehicle (GIDAS) and of these cases a total of 40% are front-rear collisions. This perspective alone is enough to make it sensible to protect the driver in frontal collisions. This is where preventive protection measures offer new possibilities without the disadvantages arising from the mass and dimensions of enlarged or excessively stiffened mechanical deformation zones.

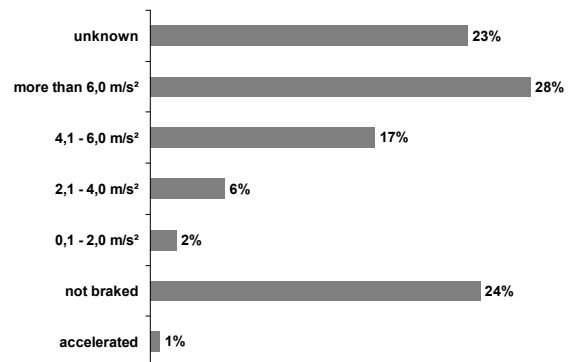
Even so, it must be taken into account that the occupants of the impacting vehicle in a front-rear collision are usually not so greatly endangered. The greatest danger of suffering serious or fatal injuries is in front-front or front-object collisions, the object frequently being a tree. However, modern sensor technology does make it at least possible to detect front-rear collisions and to take corresponding action, which may go as far as automatic emergency braking. Nevertheless, this is an important point of departure for future development. Firstly, however, it is important to identify and utilise suitable sensors, and incorporating them in cooperative systems.

Pedestrians and cyclists are vulnerable road users and are subject to additional risk. Here the protective potential of conventional measures around the car front is already exhausted at impact speeds of 40 km/h (EU directive 78/2009 on pedestrian protection). Preventive safety systems incorporating automatic emergency braking offer additional protection possibilities for this type of vulnerable road user and their efficacy in the real-life traffic environment is potentially even greater than the efficacy of passive protection measures.

In order to estimate the relevant potential benefit it is necessary to know the percentage of the relevant accidents involving car frontal collision in which the car driver in question either failed to apply the brakes in the first place or not with full force.

As part of the vFSS work package "Accident Analyses" Ford studied the GIDAS database with a view to evaluating the corresponding pre-crash braking behaviour, **Fig 10**. In 24 % of the 1,492 cases studied, the cars did not brake. In a further 23% of cases the data contained no information on the braking behaviour. In all other cases the cars were braked before the impact. Of the latter, the deceleration was over 6m/s² in 28% of the cases. An analysis by DEKRA Accident Research confirms these findings.

Figure 10: Frequency distribution of braking deceleration in the pre-crash phase (N = 1,492 front-rear accidents, source: GIDAS)



These findings demonstrate the existence of a significant potential benefit of a preventive frontal protection system. In many cases the time warning would cause the driver to brake, otherwise the emergency braking would be applied automatically. An assisting effect of full braking instead of partial braking (less than 6 m/s²) in the pre-crash phase further increases the potential benefit. Furthermore, it can be assumed that even in accidents in which no information on the braking behaviour in the pre-crash phase is available, a percentage of the vehicles were unbraked or subject to only light braking.

This suggests that forward looking front safety systems can make a considerable contribution to further increasing road safety.

Finally, **Fig 11** shows the development of figures of car occupants, motorcycle riders, pedestrians, cyclists and occupants of trucks over 3.5t killed per year in 15 states of the European Union. For these states the statistics published by CARE (European Road Accident Database) (last update: November 2010) contain a breakdown of the period in question according to the type of road user.

Although the number of killed car occupants fell considerably from 30,799 in 1991 to 12,519 in 2008 by an impressive 59 %, car occupant deaths continue to dominate the figures of road user fatalities. In the pedestrian group over the same period the number of fatalities fell significantly by 57% from 10,022 to 3,813. In the states under consideration killed motorcyclists now make up the second largest group. In the historical development there was a fall here of merely 14% from 5,237 in 1991 to 4,481 in 2008. Cyclists form the fourth largest group of road user fatalities by a clear margin. Their figures have developed from 2,063 fatalities in 1991 to 1,540

fatalities in 2008, corresponding likewise to a significant fall of 50%.

The magnitudes and the trends that these figures clearly suggest that a further successful reduction of the number of road deaths in Europe can only be achieved if

- the number of killed car occupants continues to fall significantly
- the number of pedestrian fatalities likewise continues to fall significantly
- the number of killed two-wheeler road users, in particular motorcyclists, can be significantly reduced.

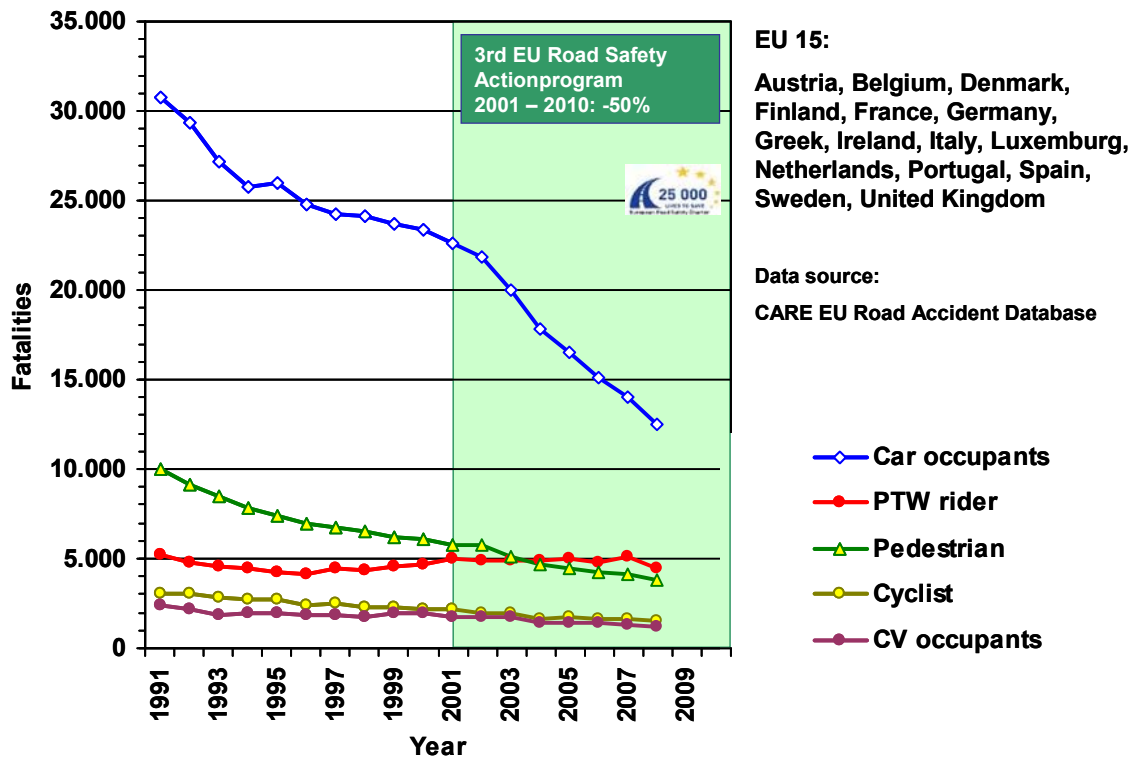
One safety measures that can be particularly effective for car occupants, pedestrians and cyclists is an advanced forward looking frontal safety system like the automatic car emergency braking system outlined in this paper.

The target of further halving the number of road deaths over the period 2011 - 2020 (see Fig 1)

requires the introduction of such systems as fast as possible in as many vehicles as possible. This would create the basis for further development of the systems that, in the end, enable automatic energy dissipation in serious frontal collisions in front-front or front-object scenarios. Current developments have already taken the first steps towards using this future potential.

The precondition for this is detailed definition of the potential benefits depicted and a recognised test procedure with which the performance of the systems can be demonstrated in reproducible form. In this process the evaluation of the systems should not be based on individual dummy figures but on the actual efficacy in real life. To do this, corresponding evaluation procedures and test methods need to be developed. Based on the examples given here, the vFSS group continues to work at pursuing the necessary accident research and development of harmonized test procedures.

Figure 11: Development of the number of car occupants, motorcyclists, pedestrians, cyclists and occupants of trucks over 3.5 t killed on the road per year in 15 states of the European Union from 1991 to 2008



SOURCES

- [1] Sferco, R., Page, Y., Le Coz, J-Y, Fay, P. 2001: Potential Effectiveness of Electronic Stability Programs (ESC) - What European Field Studies Tell Us. Proceedings of the 17th International Technical Conference on the Enhanced Safety of Vehicles (ESV) - Amsterdam, The Netherlands, June 4 - 7, 2001, Paper No. 2001-S2-O-327
- [2] Rieger, G., Scheef, J., Becker, H., Stanzel, M., Zobel, R. 2005: Active Safety Systems Change Accident Environment of Vehicles Significantly - A Challenge für Vehicle Design. Proceedings of the the 19th International Technical Conference on the Enhanced Safety of Vehicles (ESV) - Washington D.C. June 6-9, 2005, Paper No. 05-0053
- [3] Zobel, R., Strutz, T., Scheef, J., 2007: What Accident Analyses Tells About Safety Evolutions of Passenger Vehicles. Proceedings of the 20th International Technical Conference on the Enhanced Safety of Vehicles Conference (ESV) in Lyon, France, June 18-21, 2007, Paper No. 07-0330
- [4] Breuer, J., Faulhaber, A., Frank, P., Gleissner, S. 2007: Real World Safety Benefits of Brake Assistance Systems. Proceedings of the 20th International Technical Conference on the Enhanced Safety of Vehicles Conference (ESV) in Lyon, France, June 18-21, 2007, Paper No.: 07-0103
- [5] Bogenrieder, R., Fehring, M., Bachmann, R.: Pre-Safe in Rear-End Collision Situations. Proceedings of the 21st International Technical Conference on the Enhanced Safety of Vehicles Conference (ESV) - International Congress Center Stuttgart, Germany, June 15–18, 2009, Paper No. 09-0129

STANDARD & INTEGRATED RESTRAINT FIRST ROW SEAT PERFORMANCE IN REAR-IMPACT CRASHES

Nicholas Mango
Elizabeth Garthe

Garthe Associates
United States
Paper Number 11-0381

ABSTRACT

In rear impact crashes, seats provide basic occupant restraint. Using 11 years of NHTSA's NASS CDS data (1997-2007), the performance of first row standard and integrated restraint seats were compiled and contrasted to each other and also to belt restraint performance in frontal crashes. This paper defines integrated restraint (IR) seats as those where the shoulder belt anchor is attached to the seat back frame instead of the vehicle body. IR seats have strengthened frames designed to support the frontal crash belt loads. NHTSA data indicates that more than 500 make/model/year vehicles have an occupant position with an integrated restraint seat. In this study, vehicles with IR seats were identified using NHTSA data and confirmed by individual photographic review.

The median Delta V value for occupants in rear impact crashes was about 20 kph (12 mph); the same as for occupants in frontal crashes. In rear crashes, standard seats deformed or failed (per NHTSA coding) 25% of the time. In frontal crashes, seat belts (which comprise the basic frontal restraint system) failed 0.36% of the time (rate 69 times lower). The median Delta V for all reported seat failures and deformations was 27 kph (16.2 mph). Occupants reached MAIS= 3 (at least one serious injury) at half the Delta V level in rear crashes (19 kph) compared to belted occupants in frontal crashes (38 kph).

The maximum Abbreviated Injury Scale (MAIS) levels were also compiled for integrated versus standard seats. No occupant in an IR seat in a rear crash reached more than MAIS= 1. 50% of all occupants in rear crashes in standard (non-IR) seats experienced injury(s) resulting in MAIS=3 by a Delta V of 19 kph. IR seats were found to significantly reduce the rate of injury (MAIS>0) in rear impact crashes compared to standard seats (p=.05).

INTRODUCTION

In a rear impact crash the primary restraint device is

the occupant's seat.(1) In a front impact crash, the primary restraint device is the 3 point belt (which may be supplemented by an airbag). A literature review indicates that this paper may be the first to compare the effectiveness of Integrated Restraint (IR) and non-IR (standard) seats using contemporary data. This study uses the term "standard" to mean "non-IR seat".

Prior Studies - Prior studies the authors reviewed do not address the focus of this paper. Some of the studies used State, FARS or GES data. None of these datasets contain Delta-V, NASS-AIS injury codes, or seat deformation or failure codes. The injury scaling system used in FARS, GES and State databases is the police KABCO injury system. This system does not reliably identify non-fatally injured occupants with NASS-AIS severity scores of 3 to 6.(2) The papers using the above data sources do not correct for these confounding factors. Several papers do use NASS-CDS (like our study), which does include Delta V, NASS-AIS codes and Seat Deformation/Failure codes. However none of the papers used the available CDS seat Deformation /Failure information. None of the referenced papers used the comprehensive NHTSA list of vehicles with integrated restraint seats. Some of the papers use data that is now up to 28 years old, involved rollovers or were based on experimental data and contained no field data at all.(3,4,5,6,7,8,9,10,11, 12,13,14) At least one study found that standard seats are as effective in reducing injuries in rear crashes as available restraints are in frontal crashes, a premise explored in this paper using more current data. That paper also found that stiffer seats (such as Cab-reinforced) increase injuries in rear impact crashes.(3)

Purpose - This paper employs NHTSA NASS-CDS field data to compare the performance of standard, IR and Cab-reinforced first row outboard occupant seats in rear impact crashes.(15, 16) Cab-reinforced seats are those fitted to pickup trucks where the rear cab bulkhead limits the rearward deflection of the seat back. The performance of these types of seats in rear impact crashes is compared with

occupants protected by standard restraints in equivalent frontal crashes. This same approach was also used in reference (3). The purpose of this paper was to use field data to examine if:

- Standard seats in rear impact crashes offered similar performance to the restraints available in frontal crashes of similar severity.
- IR seats were associated with reduced or increased injury risk in rear impact crashes
- Cab-reinforced (low yielding) seats were associated with reduced or increased injury risk in rear impact crashes.
- Seat performance in terms of deformations or failures varied by Make or Model.

A number of these points are raised in previously published papers.(3,4,5,6,7,8,9,10,11,12,13,14) We examined adult (age >12) front outboard occupants, consistent with NHTSA definitions.(17) We did not include children in this study because of the complexity involved in eliminating the confounding effects of airbag caused injuries involving forward facing and rear facing child seat installations in passenger airbag equipped vehicles.(17)

MAIN BODY

Methodology

We used crash data from eleven recent years (CY 1997-2007) of the National Highway Traffic Safety Administrations' (NHTSA), National Automotive Sampling System (NASS), Crashworthiness Data System (CDS). NASS-CDS is a national probability sample of approximately 4,000 crashes in which a late model year light passenger vehicle sustained sufficient damage to require towing from the scene. Starting in 1996, NHTSA defines "late model year" as the four (+1 / -2) model years around the sampling calendar year.(18)

To identify vehicles with IR seats, we used a NHTSA supplied list of more than 500 make/model/model year vehicles with integrated restraints in one or more seating locations.(19) The vehicles on this list may have front row IR seats, a second or higher row seating position with an IR (such as found in the center seat position in some vehicles with split or fully folding rear seatbacks), or both. The methodology we employed with this list to identify front outboard IR seats is described later in this section.

CDS contains a variable called "Seat Performance" (OA54). In this variable NHTSA coders list which

seats "deformed" or "failed" (NHTSA's terms). We used the NHTSA categories of deformation and failure.

Datasets

Using the 11 years of NASS-CDS data we collected two datasets with similar properties – one for Rear Impacts and one for Frontal Impacts. These datasets were used in all subsequent analyses, and are described below.

Front Impacts Information was collected on vehicles and their occupants that were struck in the front. The vehicles that were impacted in the front included the following. A driver must be present in the vehicle; the Delta V reconstruction must be completed for the vehicle and the Delta V results (in NHTSA's opinion), were reasonable compared to the damage observed on the vehicle (this selection provides the most reliable Delta V data); the vehicle did not rollover or catch fire; the primary general area of damage on the vehicle was the front, and the secondary area of damage was either blank (no 2nd damage) or also the front; the principle direction of force was from the front between 350 and 10 degrees. For the identified crashes and vehicles, the following information was collected: the crash year, primary sampling unit (PSU) and national weighting factor, the vehicle number, make, model, body type and wheelbase. Data was also collected for adult (age >12) occupants in the front row outboard seating positions including; the occupant number, manual and automatic belt use, manual and automatic belt failure data, seat performance data, occupant NASS-AIS MAIS (Maximum Abbreviated Injury Severity), and headrest information. This set of 11 years of data is referred to as the Frontal Impact Dataset.

Rear Impacts Information was collected on vehicles and their occupants that were struck in the rear. The selection criteria used for the vehicles that were impacted in the rear included the following. A driver must be present in the vehicle; the Delta V reconstruction must be completed for the vehicle and the Delta V results (in NHTSA's opinion), were reasonable compared to the damage observed on the vehicle (this selection provides the most reliable Delta V data); the vehicle did not rollover or catch fire; the primary general area of damage on the vehicle was the rear, and the secondary area of damage was either blank (no 2nd damage) or also the rear and the principle direction of force was from the rear between 170 and 190 degrees. For the identified

crashes and vehicles, the following information was collected. The crash year, PSU and national weighting factor, the vehicle number, make, model, body type, wheelbase. Data was also collected for adult (age >12) occupants in the front row outboard seating positions; including the occupant number, manual and automatic belt use, manual and automatic belt failure data, seat performance data, occupant NASS-AIS MAIS, and headrest information. This set of 11 years of data is referred to as the Rear Impact Dataset.

Integrated Seat Restraints A list of the Make / Model / Model years of vehicles in the Rear Impact Dataset was created. We cross-referenced this list with the NHTSA integrated restraint vehicle list to identify the vehicles with one or more IR positions. We then reviewed the NASS-CDS interior first row seat photographs of these vehicles, plus all vehicle Make / Models of MY 2000 or later to identify the vehicles with first row front outboard IR seats. Front row seats where the upper shoulder belt was anchored to the seat frame were considered an integrated restraint (IR) seat. Seats where the shoulder belt passes through a fairlead on the seat but anchors to the vehicle B pillar or similar non-seat structure were not counted as IR seats. We did not include aftermarket retrofit (non-factory installed) seats in the integrated seat group (1 seat identified). All vehicles found to have a factory installed first row outboard IR seat were also found in the NHTSA list, a test that confirmed the validity of the NHTSA list (at least for the vehicles in our rear impact dataset). The finalized front row outboard IR seat vehicle list (validated for vehicles in our Rear Impact Dataset) was used to identify these vehicles in all our analyses. The IR seat occupant group is a subset of the Rear Impact Dataset, so all the criteria enumerated in the Rear Impact Dataset section applies in addition to the IR seat.

Note that it would be difficult to use NASS-CDS photos to confirm the existence of rear IR seating positions. Split or folding rear seats are often an optional equipment item which are both difficult to positively identify in the CDS photographs and unlikely to be decoded using the truncated Vehicle Identification Number (VIN) available in CDS.

Cab Reinforced Seats Using information contained in the vehicle file of NASS-CDS, pickup trucks with short cabs where the first row seatbacks are in close proximity to the cab rear bulkhead face were identified in the Rear Impact Dataset. These are usually the short wheelbase versions of these pickups. The identified group was reviewed using

NASS-CDS case photos to confirm the short cab and the existence of head restraints at each occupant position (older pickup trucks were not required to have head restraints). The Cab-reinforced seat occupant group is a subset of the Rear Impact Dataset, so all the criteria enumerated in the Rear Impact Dataset section applies in addition to the identification of the Cab-reinforced seat.

Analyses

Using the four occupant groups listed above, Frontal Impacts, Rear Impacts, IR and Cab-Reinforced Seats (these latter two being subsets of the Rear Impact Dataset) we performed the analyses listed below. Unless otherwise noted, all results are related to these four occupant groups, and are presented using the weighted (national estimate) values included in NASS-CDS.

Crash Severity Analysis We computed the median Delta-V for each of the occupant groups as a metric to compare the crash severities of the four groups.

MAIS Analysis We computed the Delta V value at which each occupant reached successive Maximum Abbreviated Injury Scale (MAIS) levels.(20) From this we computed the median Delta-V for MAIS=3 (serious) injury for each of the four occupant groups.(21)

Seat and Belt Restraint Performance We examined the performance of seats in rear impacts and manual and automatic restraints in frontal crashes based on the coding of restraint failure or seat deformation and/or failure by NASS-CDS coders. CDS contains a seat performance variable called "Seat Performance" (OA54). This variable indicates which seats "deformed" or "failed" (these are NHTSA defined terms). We used these NHTSA categories of deformation or failure. The determination that a seat or restraint deformed or failed was made by NHTSA's NASS-CDS coders.(1)

Risk of Injury IR versus non IR Seats We computed the risk of any injury for IR and non IR seats and whether the difference was significant or not based on both the national estimate and unweighted (actual count) case values.

Results

Table 1 summarizes the major findings, and includes two NHTSA crash test criteria for reference.(22,23) The median (half above/half below) Delta V value

for the occupants in rear impact crashes is 19.5 kph approximately the same the 19 kph median for restrained occupants in frontal crashes. While not shown in Table 1, the median Delta V for all occupants (restrained and not restrained) in frontal crashes is also similar at 19.5 kph. The rear impact median Delta V was similar for the occupants in IR seats (19 kph) and the occupants in Cab-reinforced seats (19.5 kph). Based on the similarity of these median values, we made direct comparisons of injuries and seat failure / deformation rates.

Rear impact crashes - The median occupant Delta V for a MAIS-3 (at least one serious injury) occurred at 19 kph, half the belted occupant Delta V in frontal crashes (38 kph). At 20 kph Delta V, 56% of occupants in rear impact crashes reached MAIS-3, compared to 6% of restrained occupants in frontal crashes at the same Delta V. Therefore at 20kph (near the median crash severity) more than nine times the percentage (56%/6%) of occupants sustained injury(s) resulting in a MAIS=3 in rear impact crashes relative to restrained occupants in front impact crashes.

Median delta V for seat failure - The median value for failure and deformation for occupied seats in rear impact crashes is 27 kph, about 7 kph above the median crash Delta V. Twenty-three percent (23%) of nation-wide rear impact crashes occurred at or above 27 kph Delta V. Twenty-five percent (25%) of all occupants in the rear impact dataset experienced seat failures or deformations in rear impacts - 69 times the failure rate of belt systems for restrained occupants in frontal crashes (0.36%). IR and Cab-reinforced seats had no seat failures and lower deformation rates of 6% and 1.5% respectively. The higher front outboard seat deformation and failure rates observed with standard seats were associated with a higher percentage of occupants reaching the MAIS=3 (serious) level.

Occupants in an IR seat - No occupant in an IR seat in a rear crash was more than MAIS=1 (no injury above AIS=1) regardless of Delta V. In contrast, 50% of all occupants in rear crashes in standard seats experienced MAIS=3 injury by a Delta V of 19 kph. However, the relatively low number of IR equipped vehicles in rear impact crashes included in NASS-CDS causes the sample size to be relatively low – see Table 1.

Cab Reinforced Seats - One occupant experienced an AIS=3 level injury in a >30 kph Delta V crash and was MAIS=3. No occupant in a Cab-reinforced seat in a rear crash experienced an

injury of AIS=2 and therefore all remaining occupants were MAIS=1 or less. As previously noted, 50% of all occupants in rear crashes in standard seats experienced an injury resulting in MAIS=3 by a Delta V of 19 kph. As with the IR occupant group, there are a relatively low number of short cab pickups in rear impact crashes included in NASS-CDS, and this causes the sample size to be relatively low.

Relative Risk We computed the relative risk of injury for occupants in IR seats relative to standard seats using a Chi-Squared test. As there are no IR seat occupants with MAIS=2 or higher in the NASS-CDS study data, the relative risk for MAIS=2 or higher is mathematically infinitely higher for IR compared to standard seats MAIS>1 levels (division by zero).

Risk of Any Injury We examined the risk of any injury (AIS=1 or higher) for IR versus standard seats. For this test any occupant with MAIS=1 through MAIS=7 (MAIS=7 is “injured but unknown severity”) was considered injured.(10) In this paper, Occupants with MAIS=0 were considered “uninjured” in the context of not having a codeable NASS-AIS injury.(16) We computed the relative risk of injury for occupants in standard seats versus IR seats two different ways to identify differences that might be caused by the sampling nature of NASS-CDS. This is similar to the approach NHTSA used to examine CDS data, and also taught by the authors in their SAE course "Accessing and Analyzing Crash and Injury Data from Online Databases ".(23,24)

National Estimate Using the NASS-CDS national estimates values, the relative risk of any injury for standard (non-IR) versus IR seated occupants was 1.40 times, $p<0.05$. If the IR results are adjusted by two standard errors (an approximation representing a 95% conservative case for the IR group) the relative risk result is 1.90 times relative risk and $p<0.05$.

Random Sample For our second method we treated the NASS-CDS cases as a random sample with all case weights of 1 (no national weighting factor used). The relative risk of any injury for standard (non-IR) seats was 1.41 times that of IR seats, $p=0.07$. Even with the relatively small Integrated Restraint seat group size, the relative risk results meet 93% to 95% confidence levels, depending on which of the above two methods we used.

Table 1.
Summary Information, Adult Front Row Outboard Occupants
Data Source: NASS CDS 1997- 2007

Front Impact Dataset Results			
	kph	mph	
Includes 8,700 Occupants with an equivalent National Estimate of 4,100,000			
Median Delta V, all frontal impacts	19.0	11.4	Restrained Occupants
Belt Restraint Failures	0.36%		Restrained Occupants
Median Delta V for MAIS 3 Serious Injury	38	22.8	Restrained occupants, includes belt failures
NHTSA 30 mph Frontal Test*	48	30	Barrier Speed*
	97.3%		Percentile of national frontal crashes
Rear Impact Dataset Results			
	kph	mph	
Includes 1,250 Occupants with an equivalent National Estimate of 760,000			
Median Delta V, all rear impacts	19.5	11.7	Restrained & Unrestrained Occupants
Median Delta V for Seat Deformation/Failure	27	16.2	Restrained & Unrestrained Occupants
Seat Deformation / Failure Rate	25.1%		Deformation & Failure Rate
	69		Times Risk relative to belt failure in frontals
Median Delta V for MAIS 3 Serious Injury	19	11.4	Belt and no belt, with and without failures
NHTSA 301 Rear Impact Test**	56	35	Delta V**
	98.8%		Percentile of national rear crashes
IR Seat Subset Results			
	kph	mph	
Includes 26 Occupants with an equivalent National Estimate of 5,200			
Median Delta V	19	11.4	Restrained & Unrestrained Occupants
Median MAIS 3 for IR Seats	none		No AIS-3 injuries for IR seats
Median MAIS 2 for IR Seats	none		No AIS-2 injuries for IR seats
Median MAIS 1 for IR Seats	19	11.4	All occupants
IR Seat Deformation Rate	6.2%		Deformation Only (No Failures Recorded)
Cab-Reinforced Seat Subset Results			
	kph	mph	
Includes 24 Occupants with an equivalent National Estimate of 14,000			
Median Delta V	19.5	11.7	All Occupants
Median MAIS 3 for Cab Reinforced Seats	n/a		One AIS 3 injury to one occupant
Median MAIS 2 for Cab Reinforced Seats	none		No AIS-2 injuries
Median MAIS 1 for Cab Reinforced Seats	33	19.8	
Cab-Reinforced Seat Deformation Rate	1.5%		Deformation Only (No Failures Recorded)

Notes: * Barrier approach velocity, Delta V would be higher by about 3mph due to rebound

** 3000lb moving barrier @ 50mph, Delta V varies with target mass

Cab-reinforced seats For Cab-reinforced seats there was one occupant with MAIS=3, no occupants with MAIS>3 and no occupants with MAIS=2. We performed the same injury / no-injury relative risk comparison as outlined above to determine if Cab-reinforced seats were associated with more

injuries than standard seats. Using NASS-CDS national estimates, standard seats were associated with reduced risk of injury - 0.86 at p<0.05. However, the two standard error test reversed this result with standard seats showing 1.3 times higher risk at p<0.05. Results using unit weights (no

national weighting factor used) showed no difference in MAIS=1 and above injuries between standard and Cab-reinforced seats ($p=0.56$). Note that the existence of only one occupant with MAIS=2 or greater means that the above results are primarily driven by MAIS=1 occupants. These occupants have only minor level (AIS=1) injuries and therefore the difference at this low a severity level would require further analyses to determine if it was of practical benefit. Overall, the results indicate that Cab-reinforced seats were associated with a reduction in occupants reaching MAIS-2 and higher, but were not statistically different from standard seats for MAIS=1 level injury. Therefore the data used in this study does not support the conjecture that Cab-reinforced seats are associated with increased occupant injuries in rear impact crashes.

Make & Model We examined the percentage of seat deformation and failures in rear impact crashes by Make and Model. A preliminary analysis did not reveal any Make based differences that were statistically significant. A second analysis by Make and Model showed that seat failures & deformations in rear impact crashes may be associated with specific model lines (or perhaps with specific platforms or seat designs for which we did not have the detailed seat engineering information to statistically investigate). Model level analyses using NASS-CDS is limited by its relatively small sample size and its focus on only late model vehicles.

CONCLUSION

The rate of Non-IR seat failure/deformation in rear impact crashes is 69 times the rate of belt failures in equivalent severity frontal crashes. This is a cause for concern because it was associated with a difference in MAIS=3 injury risk. The median Delta V for all reported seat failures and deformations was 27 kph (16.2 mph). Approximately 25% of occupants in rear impact crashes were in crashes above the Delta V at which 50% of the non-IR seat failure/deformations occurred. Front seat failure could result in injury to children or adults riding in the seat directly behind the failing seat; a factor not included in this study. In a Delta V crash of 20 kph, approximately the median rear impact crash severity, the percentage of occupants in non-IR seats experiencing injuries resulting in MAIS=3 was more than 9 times that of restrained occupants in frontal crashes. Based on this data, standard (non-IR) seats in rear impact crashes did not provide injury protection equivalent to

existing restraints in frontal impacts.

No occupant in an IR seat experienced an injury above AIS=1 (all were MAIS=1 or less). For any injury level, (MAIS>0), occupants in non-IR seats were 1.4 times more likely to be injured than occupants in IR seats ($p<.05$). This result was the same whether weighted (national estimate) or unweighted (raw case) counts were used. The available NASS-CDS injury data for occupants seated in front outboard IR seats indicates that IR seats were associated with fewer occupants (by percentage) reaching any MAIS greater than 1 in rear impact crashes compared to non-IR seats. Stiff (non-yielding) seats, as represented by cab-reinforced seats, were not found to be associated with an increased risk of injury in rear impact crashes, contrary to previously published papers. Only one occupant in a cab-reinforced seat experienced an injury resulting in an MAIS >1. The study data shows that Cab-reinforced seats were associated with fewer occupants (by percentage) reaching MAIS levels 2 and above in rear impact crashes compared to standard seats. The currently available NASS-CDS data for IR seats in rear impact crashes indicates that IR seats were associated with reduced injury rates for all injury levels in rear impact crashes, and that IR seats potentially could provide injury protection comparable to existing restraints in frontal crashes.

REFERENCES

1. National Automotive Sampling System (NASS) Crashworthiness Data System (CDS) Coding Manual, 1997 and 2007
2. Garthe, E. Mango, N. The "AIS-0" Conundrum: The Complexities of Identifying the Uninjured in NASS-CDS Enhanced Safety of Vehicles conference. ESV 2011-0385
3. Prasad P, Kim A, Weerappuli DPV, Robert V, Schneider D. Relationship between passenger seat backs and occupant injury severity in rear end collision: field and laboratory studies. Forty-first Stapp Car Conference; SAE publication no. 973343, pp. 417-449, 1997.
4. Padmanaban J, Burnett RA. Seat integrated and conventional restraints: a study of crash injury/fatality rates in rollovers. Annu Proc Assoc Adv Automot Med. 2008 Oct;52:267-80.

5. Strother CE, James MB. Evaluation of seat back strength and seat belt effectiveness in rear end impacts. Thirty-first Stapp Car Crash Conference; 1987 SAE publication no. 872214.
6. Viano DC. Influence of seat properties on occupant dynamics in severe rear crashes. *Traffic Inj Prev.* 2003 Dec;4(4):324-36.
7. Viano DC. Seat design principles to reduce neck injuries in rear impacts. *Traffic Inj Prev.* 2008 Dec;9(6):552-60.
8. James M, Strother C, Warner C, Decker R, Perl T 1991. Occupant protection in rear-end collisions: I. safety priorities and seat belt effectiveness. SAE. no. 912913. Warrendale, PA: SAE.
9. Molino L 1997. Preliminary assessment of NASS CDS data related to rearward seat collapse and occupant injury. Office of Crashworthiness Standards. National Highway Traffic Safety Administration. US Department of Transportation. Washington, D.C.
10. James M, Strother C, Perl T, Smith G, Warner C. Letter to NHTSA. Docket no. 1998-4064-32. June 11, 2001.
11. Edwards M, Parenteau C, Viano D 2009. Analysis of the seatback incline variable in NASS-CDS. SAE.no. 2009-01-1200. Warrendale, PA: SAE
12. Viano D, Seat Design Principles to Reduce Neck Injuries in Rear impacts, *Traffic Injury Prevention*, 2008, 9552-560
13. Warner C, James M, Strother C, Decker R, Perl T 1991. Occupant protection in rear-end collisions: II: The role of Seat Back Deformation in Injury Reduction SAE. no. 912914. Warrendale, PA: SAE
14. Bensen B, Smith G., Kent R., Monson C, Effect of Seat Stiffness in Out-of-Position Occupant Response in Rear-End Collisions. SAE. no. 962434 Warrendale, PA: SAE
15. US Department of Transportation, National Highway Traffic Safety Administration. National Automotive Sampling System, Crashworthiness Data System (NASS-CDS) data base. Washington, D.C
16. US Department of Transportation, National Highway Traffic Safety Administration. National Automotive Sampling System, Crashworthiness Data System (NASS-CDS) description (on-line). Washington, D.C.
http://www.nhtsa.dot.gov/people/ncsa/nass_cds.html
17. Kindelberger JC, Chidester AB, Ferguson E: Air bag crash investigations. Paper presented at the Enhanced Safety of Vehicles conference. ESV Paper Number 299. pp. 2.
18. National Automotive Sampling System (NASS) Crashworthiness Data System (CDS) Analytic User's Guide, 1996 thru 2006
19. US Department of Transportation, National Highway Traffic Safety Administration. Integrated seats/all belts to seat list. (On-line list downloaded August 2008) Washington, D.C.
ftp://ftp.nhtsa.dot.gov/NCAP_Select:NCAPdb.mdb
20. US Department of Transportation, National Highway Traffic Safety Administration. 2000 NASS Injury Coding Manual, Editors, 2000 edition: Veridian Engineering. Authors, 1990 edition (1998 Revision, 1998 Update), Association for the Advancement of Automotive Medicine. Washington, D.C.
21. Association for the Advancement of Automotive Medicine. The Abbreviated Injury Scale, 1990 Revision, Update 98. (Description of MAIS on pg. viii) Des Plaines, Illinois.
22. US Department of Transportation, National Highway Traffic Safety Administration. NHTSA Publishes Upgraded Vehicle Standard For Fire Protection in Rear Impact Crashes - press release Tuesday, November 25, 2003 by Tim Hurd, (202) 366-9550 NHTSA 51-03.
23. Stucki SL, Hollowell WT, Fessahaie O: Determination of frontal offset test conditions based on crash data. Paper presented at the Enhanced Safety of Vehicles conference. ESV Paper Number 98-S1-O-02. pp. 1-2.
24. SAE Course Garthe E, Mango N, "Accessing and Analyzing Crash and Injury Data from Online Databases".

SEAT HEADREST DEVELOPMENT TO DETECT THE HEAD POSITION OF PASSENGER

Su Hwan, Hwang
Eun Sue, Kim
Gil Joo, Kim
Bong Jun, Lee
Hyundai Motors
South Korea

ABSTRACT

It is the essential technique to percept the position of passenger's head before rear collision to pre-crash headrest for minimizing the one's neck damage. This research introduces the technique of perception of head using the electrostatic capacity sensor in the head rest.

When the distance between the head rest and passenger's head is measured, pre-crash headrest could be adjusted to most proper position for Whiplash protection. It will improve safety technology.

INTRODUCTION

The research of the latest vehicle accidents show that 25% were caused by the rear-end collisions where 80% injuries were to the neck. As a result, the headrest that minimizes passenger's neck injury preceding the rear-end collision is necessary and the number of mechanical/electronic neck injury prevention systems were introduced and being applied.

However, the focus of this study is on developing the system that takes precautions against the possible neck injuries by automatically realizing an optimal safety positioning preceding the rear-end collision. To accomplish this, the passenger head location detection technology is crucial. In this study, the electrostatic capacity styled sensor technology is mounted in the headrest to detect passenger's head location to boost the neck-injury prevention performances by reducing passenger's head and the headrest's Backset in rear-end collision and to address the passenger's comfort by naturally maintaining passenger's head and headrest's distance in daily use. The electrostatic capacity sensor has no directionality in receptive fields and has expansive measurement ranges which makes favorable for the head detection.

SYSTEM CONFIGURATION

The system is configured for headrest to operate the motor by actually configuring an electrostatic capacity styled sensor to seat's headrest which controls the relative distances between the head and the headrest.

System is configured with the sensor module which processes frequencies detected from electrode areas of electrostatic capacity sensor & head, and the seat ECU which controls headrest's forward and backward operations; the seat ECU is configures with the radar to detect rear approaching vehicles.

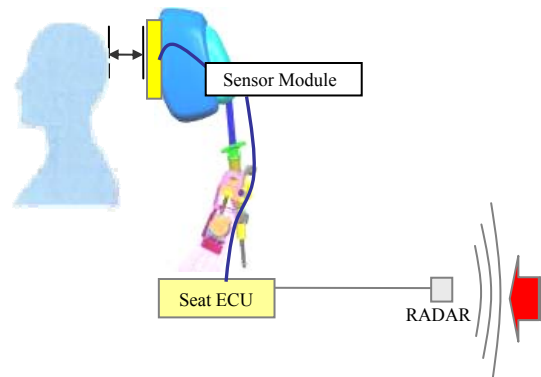


Figure 1. Head Detection Seat Schematic.

Sensor module & controller converts head's electricity quantum frequency to digital value to extract the distance information then transmits the information to seat ECU for the control of headrest operation commending motor. As the first operation of a sequence, moves the headrest forward/upward by detecting the collision warning signal thru rear radar and stops the motor to maintain 10mm Backset between passenger's head and headrest to minimize the neck injury in rear-ends collision, then moves the headrest to its original position at the end to restore the passenger programmed comfort location.

Fig.2 is the block diagram for sensor module.

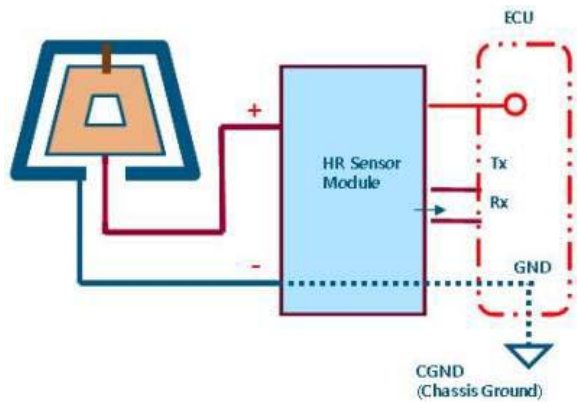


Figure 2. Sensor Module Block Diagram

The system is operated by the logic, Fig.3.

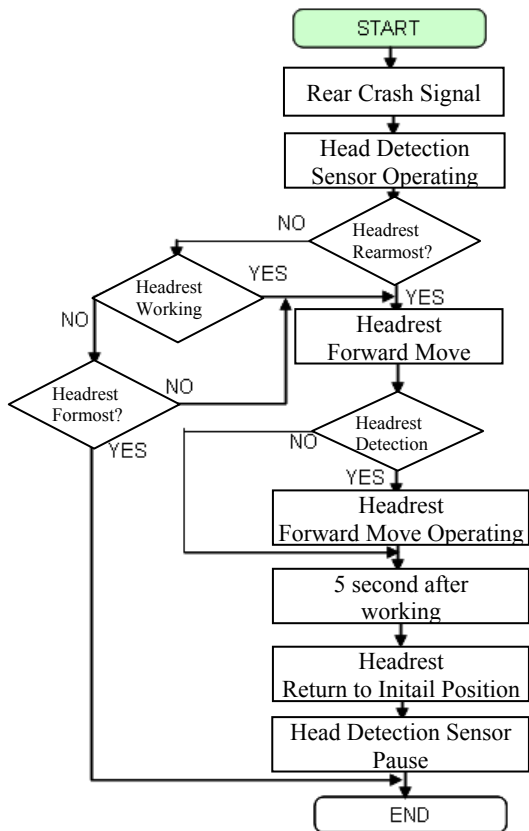


Figure 3. System Control Logic



Figure 4. TEST JIG

Type Specific Experiments of Electrostatic Capacity Sensors

The experiment is conducted to identify the favorable head sensing materials by measuring 4 forms of electrostatic capacity variations. The silver and copper were chosen for its high conductivity which is favorable for detecting the electrostatic capacity variations. For a detection target, a case containing water that is dielectric constancy favorable with the head were used in an experiment.

On Fig. 4, the distance corresponding electrostatic capacity variations is detected while moving the water pouch forward and backward directions from the front of seat's headrest. Detected electrostatic capacity is shown as a frequency and distance corresponding frequency variations were measured for the distance measurement.

Table 1. Sample Specific Grouping

Classifications	Shapes	Electrode Quality
SAMPLE 1		Silver
SAMPLE 2		Silver + Copper
SAMPLE 3		Copper (Trapezoid)
SAMPLE 4		Copper (Circular)

Test Results & Evaluations

Conducted the experiments on 4 samples and obtained the result shown on Fig. 3. Fig. 5 shows the data value of 4 experimental samples. The frequency values from oscillator circuits are measured in accordance to the distances for the experiment value.

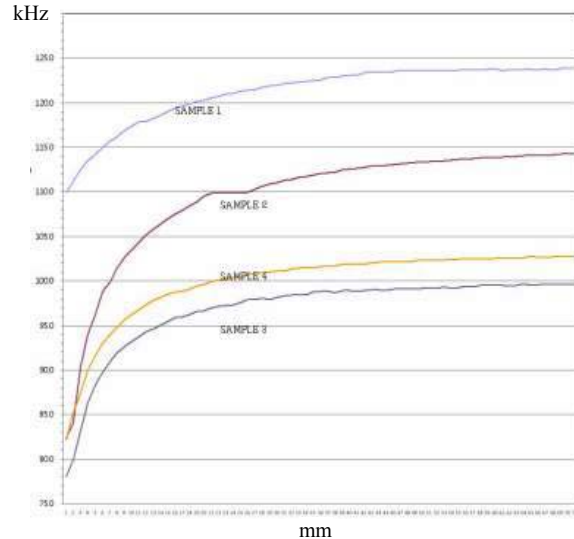


Figure 5. Frequency Value of Sample Specific Distance

SAMPLES 1, the frequency values per distances are mild.

This represents the frequency value for the headrest and the head's distance of 10mm. The case of frequency value's variation error on areas outside the 10mm boundaries, it shows that there can be a greater range of error from the headrest operation halt distance. SAMPLE 2 has about 1 KHz greater frequency displacement volumes for each 1mm at 10mm distance of Fig. 5. Therefore, it can be seen that the halt location establishment is more effective for the existing silver with the copper plate additions compared to other SAMPLES by 0.5 KHz per each 1mm. SAMPLE 3 & SAMPLE 4 show a favorable frequency displacement values which indicates insignificant effect of shape changes. After setting the initial frequency value to where the distance between the head & headrest are 70mm and final frequency value at 0mm, SAMPLE 3 has large variation volumes as shown on Table 2. Also, to effectively detect the electrostatic capacities of human body's dielectric constancy, high electric conductive material should be used. Electrostatic capacity, larger the accumulated electricity quantum is longer the detection distance is. A highly conductive and wider sized material for the pole plate or high dielectric constancy substances increases the electrostatic capacity.

Table 2. Frequency Variation Value

Classifications	70mm~0mm Block			Remarks
	Initial Values	Final Values	Variation Values	
SAMPLE1	123.93	109.97	13.96	Small
SAMPLE2	114.24	82.31	31.93	Large
SAMPLE3	99.60	78.00	21.6	Medium
SAMPLE4	102.74	82.17	20.57	Medium

Over time, there are insignificant fluctuations to frequency values as shown on Fig. 6.

The assurance of stability is indicated since the reliable resulting values were obtained due to minimal volatilities of the initial value.

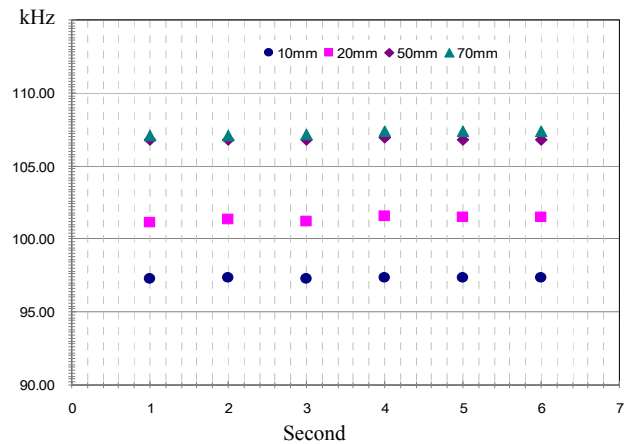


Figure 6. Time Specific Displacement Values of the Frequencies

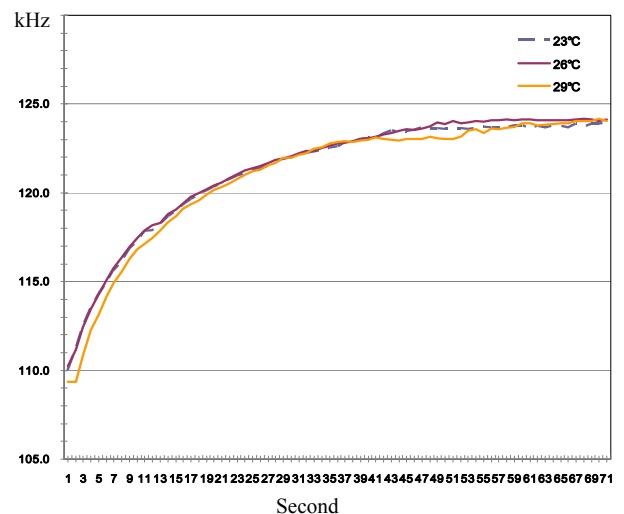


Figure 7. Temperature Specific Displacement Values of Frequencies

Fig. 7 shows the resulting values for the temperature change corresponding frequency values. The same specifications as SAMPLE 1 was repeatedly measured at 23°C, 26°C, 29°C for the temperature displacement measurement and has error range of 1Khz, ±3mm; the effect of temperature displacement is less at upper temperature.

CONCLUSIONS

In this study, the sensor module is developed to graft the electrostatic capacity sensor technology onto the seat's headrest for the extraction of distance information and TEST JIG was utilized to conduct basic system performance evaluation of the sensor module's pole plate samples which supplies crucial variables. Able to select the useful electrostatic capacity sensor pole plate for the seat's headrest by understanding electrode sample specific characteristics and able to validate the usefulness in acquiring the distance information as the electrostatic capacity fluctuates according to the electricity quantum variations of the distances.

The characteristics of frequency values were verified through the basic performance evaluations, however execution of improvements are crucial from additional environmental tests.

REFERENCES

- [1] Chi, G. H., Kim B H., Kim, H. Y. and Chang, I. B., 2003 "The development of punch-die aligning algorithm in micro punch system with using the total capacitance," J. of KSPE, Vol. 20, No. 7, pp. 114-119.
- [2] Ahn H. J., Chang, I. B., and Han, D. C., 1997 "A study on a capacitive displacement sensor for the ultraprecision measurement," J. of KSPE, Vol. 14, No. 11, pp. 110-117.
- [3] Restagno. F., Crassous, J., Charlaix. E. and Monchanin, M., 2001 "A new capacitive sensor for displacement measurement in a surface-force apparatus." Meas. Sci. Technol., Vol. 12, No. 1, pp. 16-22.
- [4] Doebelin, E. O., 1990 "Measurement Systems: Application and Design," McGraw Hill.
- [5] Maxim, 2005 "MAX038: High-Frequency Waveform Generator," Maxim.
- [6] Analog Devices, 2005 "AD637: High Precision, Wideband RMS-to-DC Converter," Analog Devices.
- [7] Analog Devices, 2000"AD633: Low Cost Analog Multiplier," Analog Devices.
- [8] Wu, C. M., Su, C. S.and Peng, G. S., 1996 "Correction of nonlinearity in one-frequency optical

interferometry," Meas, Sci. Technol., Vol. 7, No. 4, pp. 520-524.

[9] JongAhn Kim, JaeWan Kim, GaeBong Um, JooShik Kang, "Electrostatic Capacity Shape Displacement Sensor Module Circuit Development & Performance Evaluations" Journal of the Korean society for precision engineering, Article 24, No.

REDUCING NECK INJURIES BY CONTROLLING SEAT BACK DYNAMIC MOVEMENT

Dongwoo, Jeong

GilJoo, Kim

Bongjun, Lee

Seat system design engineering team/Hyundai motor Company

South Korea

Johan Svard

Peter Axelsson

Sweden Autoliv Safety Center/Autoliv

Sweden

Paper Number 11-0278

ABSTRACT

Neck injuries caused by rear-end collision are the most common injury type in motor vehicle accidents. The exact mechanism that causes whiplash is still not agreed upon. What has been agreed upon is that reducing relative movement between head and torso reduces neck injury. There are two ways to reduce relative movement between head and torso. One is supporting the passenger's head as fast as possible. Head acceleration is increased, reducing the relative acceleration between head and torso. This approach is the most common way to prevent whiplash injuries. The other way is to reduce torso acceleration by controlling the seat back and reducing the relative acceleration between head and torso. Based on benchmark test results, the second approach is an easy and robust way to handle the newly enhanced KNCAP test protocol. This study addresses a neck injury protection device to deal with enhanced neck injury rating systems in KNCAP & EURONCAP by controlling seat back frame movement. The device has been built, simulated, and tested.

INTRODUCTION

The perception that frontal and side collision has a direct relationship to passenger safety in a vehicle collision has caused continuous interest and research on this topic. Therefore, there have been active developments related to the regulations/product property evaluations and systems that deal with this type of collision. Rear-end collisions are less likely to be fatal to passengers than frontal and side collisions, but occur at a higher frequency. This has caused a gradual increase in interest due to the raised societal expenses. In order to regulate this, product

property evaluation has been progressing centered around insurance institutes. Since 2004, both IIHS & THATCHAM have conducted static and dynamic assessments and released the results.

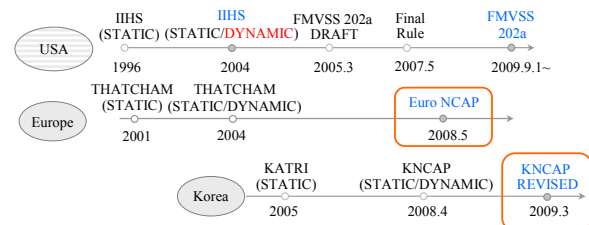


Figure 1. Regional specific neck injury assessments/product property status

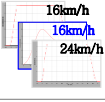
As shown on Figure 1, EURONCAP has developed new evaluation criteria and has been conducting assessments for rear-end collision neck injuries since 2008. They have done so by adding supplements to the existing IIHS. KNCAP imported EURONCAP evaluation criteria and adjusted them to Korea circumstances. KNCAP has been conducting assessments since 2008, and enhanced injury criterion will be enforced in 2009. EURONCAP and KNCAP use combined ratings system for frontal, side, and rear-end collisions. They report the assessment results, with each category separately evaluated and recorded. This research supplements the existing IIHS criteria, identifies the enhanced EURONCAP and KNCAP injury criterion regarding seat characteristics, and introduces developments of improved system.

Regional neck injury property evaluation status

IIHS's existing dynamic performance evaluation factors of Fx, Fz, T1, HRCT are not enough to

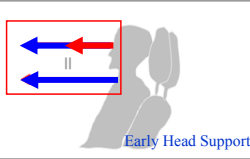
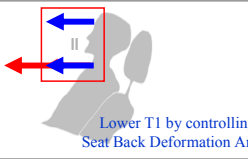
represent actual neck injuries in rear-end collisions. To supplement, Euroncap & Kncap added 3 criteria as shown on Table 1: NIC, Nkm, HRV.

Table 1.
Product property evaluation status

	IIHS (North)	KNCAP	EURO NCAP
Dynamic Injury Criteria	<ul style="list-style-type: none"> Fx Fz T1 HRCT 	<ul style="list-style-type: none"> Fx Fz T1 HRCT NIC Nkm HRV 	<ul style="list-style-type: none"> Fx Fz T1 HRCT NIC Nkm HRV 
Rating	<ul style="list-style-type: none"> GOOD ACCEPTABLE MARGINAL POOR 	<ul style="list-style-type: none"> 4.9-6 4.0-4.9 3.1-4.0 2.2-3.1 0-2.2 	<ul style="list-style-type: none"> GOOD 3.00-4.00 MARGINAL 1.50-2.99 POOR 0.00-1.49

The general concept for neck injury reduction, currently used in most of the models, utilizes forward protrusion of the headrest structure upon collision. This provides head support and creates affinity between torso acceleration and head acceleration by raising the head's acceleration, as shown on Table 2. This system generally has superior HRCT(HeadRest Contact Time) but has the tendency to show unfavorable T1 accelerations. Although the system introduced by the other concept is somewhat slower to support the head, the head's acceleration is matched by lowering the torso's acceleration. This case shows superior T1 but has the tendency to show unfavorable HRCT.

Table 2.
Basic concept of neck injury reduction

Increase Head acceleration	Reduce Torso Acceleration
 <p>Early Head Support</p>	 <p>Lower T1 by controlling Seat Back Deformation Angle</p>
<ul style="list-style-type: none"> Increase head acceleration to reduce relative acceleration differences between head and torso 	<ul style="list-style-type: none"> Reduce Torso acceleration to reduce relative acceleration differences between head and torso
<ul style="list-style-type: none"> Most of Current Re-active H/rest system 	<ul style="list-style-type: none"> AUTOLIV whips

METHOD

Competition-Car Evaluation Study

Analysis of Table 3, the competition-car evaluation result, shows T1 and HRV(Head rebound velocity) values to be most unfavorable among the 7 dynamic

injury criteria. Since the dynamic performance factor is derived by selecting a superior score between T1 and HRCT and then totaling up that score with the rest of the 5 categories in neck injury assessment, improvement to the HRV value is the most important.

Table 3.
KNCAP neck injury evaluation status of competition-car

	SEAT	Dynamic							STATIC + DYNAMIC (%)	RATING	
		NIC	Nkm	HRV	FX	FZ	OR				Total
						T1	HRCT				
1	NON AHR	1.13	1.27	0.87	1.5	1.5	0	1.5	7.77	83.7	5★
2	Whips	1.5	1.5	1.5	1.5	1.5	1.5	0	9	99.6	5★
3	ACTIVE	0.85	0.67	0.58	1.2	1.18	0.55	1.32	5.8	68	4★
4	NON AHR	1.5	1.16	1.14	1.5	1.11	1.35	1.5	7.91	85	5★
5	ACTIVE	0.83	0.9	0.82	1.5	1.5	0	1.5	7.05	79.3	4★
6	NON AHR	1.27	0.82	0.4	1.14	1.11	0.13	1.38	6.12	71.2	4★
AVERAGE		1.18	1.05	0.89	1.39	1.32	0.59	1.20	7.03	78.6	4★

Table 4.
KNCAP evaluation status of tested seats

	SEAT	Dynamic							STATIC + DYNAMIC (%)	RATING	
		NIC	Nkm	HRV	FX	FZ	OR				Total
						T1	HRCT				
1	AHR	0.69	1.31	0.72	1.5	1.5	1.5	1.5	7.22	82.2	5★
2	AHR	1	1.08	0.74	1.5	1.5	1.38	1.5	7.32	83.2	5★
3	Non AHR	1.39	1.16	0.71	1.5	1.5	1.24	1.5	7.76	84.3	5★
4	Non AHR	1.29	1.05	0.86	1.5	1.5	0.9	1.5	7.7	82.9	5★
5	AHR	1.39	1.08	0.67	1.5	1.5	0.91	1.5	7.36	83.8	5★
6	AHR	1.24	1.23	0.75	1.48	1.5	0.39	1.5	7.7	82.6	5★
AVERAGE		1.18	1.21	0.66	1.48	1.46	0.82	1.47	7.44	83.1	5★

As shown on Table 4, evaluation results of HMC models show weak HRV and an insufficient margin, although 5★ has been obtained. To obtain the above results, numerous tests were performed to each model. It can be confirmed that the best way to improve neck injury assessment is to boost the HRV value and back frame deformation characteristics, which can be verified through competitive analysis of a superior HRV valued vehicle.

HRV (Head Rebound Velocity) value generally occurs when the elastic strain energy stored in seat is converted to kinetic energy in the dummy after maximum acceleration of sled has been achieved. Maximum restitution rate generally occurs at the point where the dummy's head and headrest separate, or immediately after. To improve the HRV value: thicken the seat's pad, since the seat absorbs the dummy's inertial force; widen the seat back's frame;

increase the headrest's stay strength; induce plastic deformation in the seat back to remove elastic energy. Figure 2, below, shows HRV value obtained through the evaluation of HMC & competitors' seats. All of the seats have similar HRV values except "A seat."

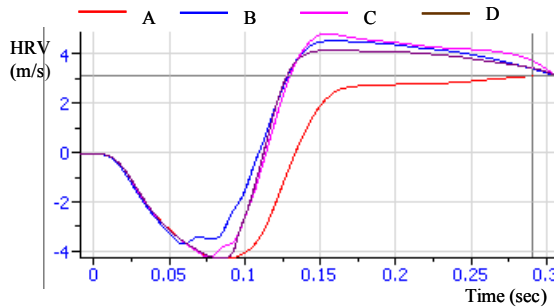


Figure 2. HRV Evaluation Graph

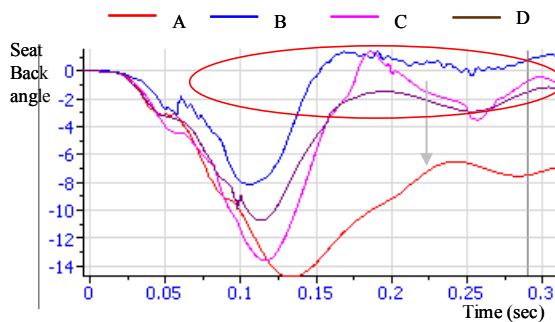


Figure 3. Deformation angle of seat back

	A	B	C	D	Average seat
Max Deform Angle	14.6	8.2	13.8	10.7	11±1°
Deformation Angle at 300ms	7.24	0	0.5	1.2	0-1°
System	Whips	Passive	Re active	Passive	-
HRV (3.2m/s-4.8m/s)	3.2	4.3	4.8	4.2	4.13

Table 5. Benchmarking test results

Analysis of Figure 3 and Table 5 shows the notable differences are from the seat back angle's displacement volume. "A Seat" had the largest seat back displacement along with higher permanent displacements for the seat-back. This shows the use of a structural system that absorbs the dummy's energy using plastic deformation of the seat back upon collision.

System Design

The development of a structural system that can control the seat back's deformation in a rear-end collision is necessary. This system should also meet HMC's seat mountable conditions. As shown on Figure 4 and Figure 5, the system operates only in collisions and is in a locked position during general operation.

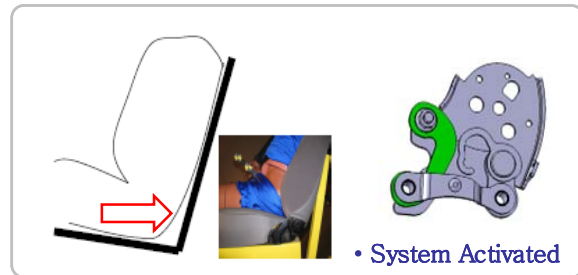


Figure 4. System activated in rear-end collision

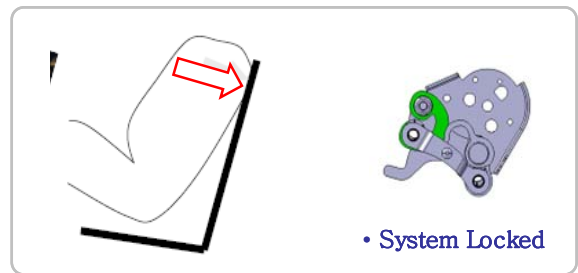


Figure 5. System locked in general conditions

Design model improvements were executed during phase 4 in considerations of package conditions, collision conditions, general usage conditions, and optional applications on current frames, et cetera. The final Design Model specification drawing has been released as shown on Table 6.

Table 6. Revised model of Reduction System

Current	1 st	2 nd	3 rd	4 th (Final Model)

The system(Whips: Whiplash Injury Protectin System) should work as below in figure 6. The corresponding detachable side cover for the system operations is also shown.

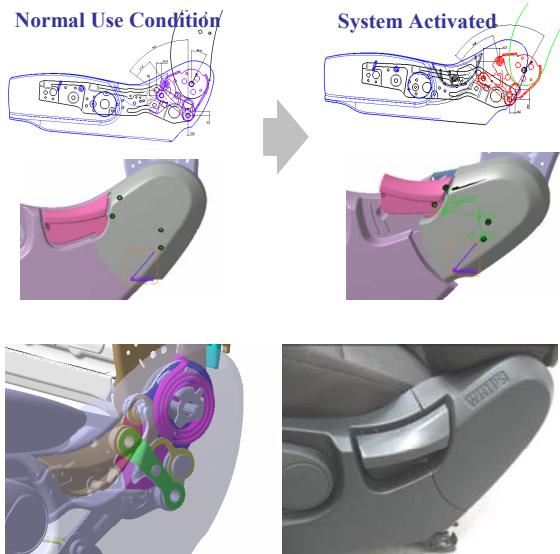


Figure 6. Detachable side cover concept & actual sample for Whips

System Analysis

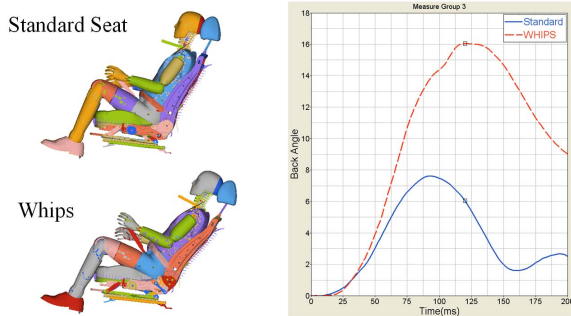


Figure 7. Seat Back's Maximum Displacement in Rear-End Collision with Whips & Standard seat

The designed model was used for the neck injury analysis. The system's parts were adjusted, as it wasn't functioning during the analysis phase 1. The system was functioning well, however, during the analysis phase 2 with some modification. As shown in Figure 7, the following were confirmed: the seat back's rearward maximum displacement with Whips exceeded the standard seat deformation angle by 8 degrees. As shown in Figure 8, HRV improved by 0.75 points compared to the existing value because of induced plastic deformation within the system, and the dynamic performance improved by 0.95 points, 4.5 □ → 5.0 □ (0.5 □ ↑).

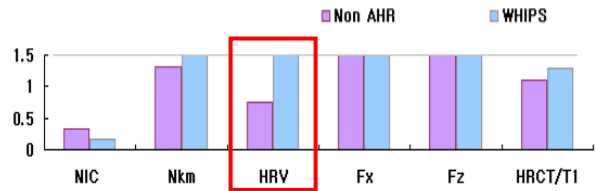


Figure 8. Analysis result with Standard seat and Whips

Evaluation Result

The improved model, which is based on the analysis results of the Whips application, was used as a final evaluation. An evaluation was conducted, and the system operated normally, as shown in Table 7.

Table 7. System condition of Before/After crash

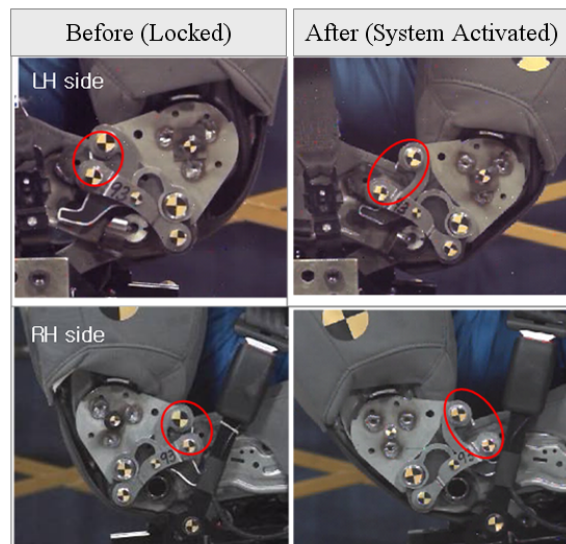


Table 8. Evaluation results of KNCAP Whips

		HRV	FZ	%	Rating
Current standard seat	-	0.71	1.5	84	5.0★
Current standard seat with conventional active headrest	Active Headrest	0.72	1.5	82	5.1★
Whips system Test 1	Whips system applied	1.5	0.95	83	5.4★
Whips system Test 2	Volvo Headrest Was applied	1.5	1.5	95	5.6★
Whips system Test 3	Headrest blower modified	1.5	1.5	96	5.7★

Table 8. shows the evaluation result of the Whips application. On the first evaluation, HRV value improved but Fz value worsened. Contrasted with the existing standard seat, the head's tensile force increased and the seat back's displacement value

came close to 16 degrees when the Whips system was applied. Whips applied HRV's characteristic curves are shown in Figure 9. Definite differences can be confirmed when compared to the standard (passive system) seat.

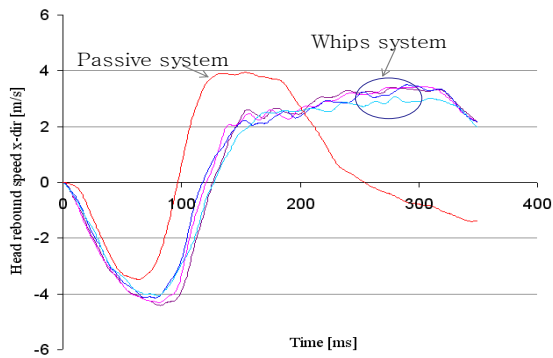


Figure 9. Evaluation result of HRV with standard seat and Whips

The result was a worse value for Fz because the Whips system has a greater seat back deformation angle than the standard seat, as shown in Figure 10.

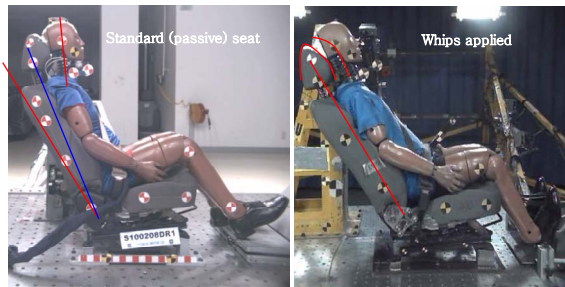


Figure 10. Standard vs Whips applied dummy motion

Next, a trend validation test was performed using the Volvo headrest. The result was a good score. It can be deduced from this second result that an improvement to Fz value is possible if using the appropriate headrest shape, internal structure shape, stays, et cetera.

For the third test, as shown in Figure 11, the shape of the headrest's blower area was improved. The original round shape was flattened out and the stay strength was increased.

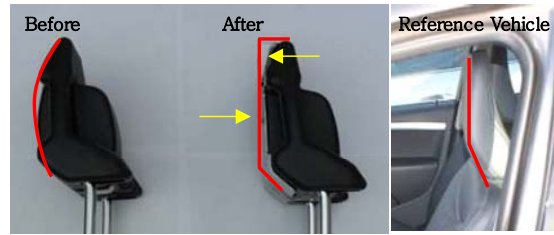


Figure 11. Headrest inner part shape improved

Additional validation is planned such as severe rear crash, frontal crash, luggage block retention, et cetera.

CONCLUSIONS

This research was a study on the fundamental approaches to neck injury reduction. Minimization of the head and torso's relative motion is the basis of neck-injury reduction. Two basic systems were studied: a system that creates forward protuberance of the headrest to increase the head's acceleration and minimize the torso acceleration variances, and a system that minimizes the torso acceleration and minimizes the head acceleration variances.

Frame behavior characteristics and HRV correlation analysis were conducted by analyzing the evaluation results of HMC seats and competition-car seats. The most influential factor on HRV value improvement was the seat's capacity to absorb the dummy's collision energy, especially the frame's ability to absorb energy was founded to be critical.

Development of a system that induces plastic deformation to absorb collision energy, therefore improving HRV, was confirmed. A robust system was designed by applying a Reduction System that can respond to the new injury criteria of KNCAP and EURO NCAP for HRV, Nkm, NIC, et cetera.

REFERENCES

- [1] RCAR (Research Council for Automobile Repairs), "A Procedure for Evaluating Motor Vehicle Head Restraint (Issue3)", 2008.
- [2] RCAR-IIWPG (International Insurance Whiplash Prevention Group), "Sear/Head Restraint Evaluation Protocol (version3)", 2008.

[3] Euroncap (EURO New Car Assessment Program, “The Dynamic Assessment of Car Seats for Neck Injury Protection test Protocol (Version2.8)”, 2008.

[4] Ministry of Land, Transport and Maritime Affairs “Vehicle Safety Evaluation Test and Related Regulations”

[5] Association of British Insurers(2008), “Motor Insurance Claims Data”, London, UK, Association of British Insurers.

[6] Klaus Bortenschlager, “Detailed Analysis Of Biorid-II Response Variations In Hardware And Simulation”, PDB, Daimler AG, DYNAmore GmbH, ESV 09-0492, 2009

[7] LS-DYNA KEYWORD USER’S MANUAL – Version 971